

Edit Lengyel

**Antiferromagnetism and Superconductivity
in Ce-based
Heavy-Fermion Systems**



Cuvillier Verlag Göttingen

**Antiferromagnetism and Superconductivity in Ce-based
Heavy-Fermion Systems**

Dissertation

zur Erlangung des akademischen Grades

Doctor rerum naturalium

(Dr. rer. nat.)

vorgelegt

der Fakultät Mathematik und Naturwissenschaften
der Technischen Universität Dresden

von

Edit Lengyel

geboren am 05. August 1974 in Deva, Rumänien

MAX-PLANCK-INSTITUT FÜR CHEMISCHE PHYSIK FESTER STOFFE
DRESDEN, 2007

Bibliografische Information der Deutschen Nationalbibliothek

Die Deutsche Nationalbibliothek verzeichnet diese Publikation in der Deutschen Nationalbibliografie; detaillierte bibliografische Daten sind im Internet über <http://dnb.ddb.de> abrufbar.

1. Aufl. - Göttingen : Cuvillier, 2008

Zugl.: (TU) Dresden, Univ., Diss., 2007

978-3-86727-696-2

Gutachter:

Prof. Dr. Frank Steglich

Prof. Dr. Joachim Wosnitza

Prof. Dr. Joe D. Thompson

Tag der mündlichen Prüfung: 07. September 2007

© CUVILLIER VERLAG, Göttingen 2008

Nonnenstieg 8, 37075 Göttingen

Telefon: 0551-54724-0

Telefax: 0551-54724-21

www.cuvillier.de

Alle Rechte vorbehalten. Ohne ausdrückliche Genehmigung des Verlages ist es nicht gestattet, das Buch oder Teile daraus auf fotomechanischem Weg (Fotokopie, Mikrokopie) zu vervielfältigen.

1. Auflage, 2008

Gedruckt auf säurefreiem Papier

978-3-86727-696-2

Table of Contents

List of symbols and abbreviations	iii
Introduction	1
1 Theoretical concepts	5
1.1 Introduction to heavy-fermion systems	5
1.1.1 The Kondo effect	5
1.1.2 Kondo lattice and magnetism in heavy-fermion systems	8
1.1.3 Heavy-fermion and intermediate-valence systems	10
1.2 Superconductivity in heavy-fermion systems	11
1.2.1 Conventional versus unconventional superconductivity	11
1.2.2 Unconventional superconductivity mediated by electrons in heavy-fermion systems	16
a. Magnetically mediated superconductivity	17
b. Valence-fluctuation mediated superconductivity	18
1.3 Non-Fermi-liquid behavior in heavy-fermion systems	20
1.3.1 The Landau-Fermi-liquid state	20
1.3.2 Non-Fermi-liquid behavior	22
1.3.3 Quantum critical phenomena	22
2 Experimental methods	25
2.1 General concepts about heat capacity	25
2.2 The quasiadiabatic heat-pulse technique used for measurements of heat capacity under high pressure and at low temperatures	26
2.2.1 Compensated quasiadiabatic heat-pulse technique	27
2.2.2 High pressure	29
2.3 Measurements under hydrostatic pressure and data analysis	32
2.3.1 Experimental setup	32
2.3.2 Measurement techniques	33

2.4	Measurements in a Quantum Design PPMS	41
3	Ce_nT_mIn_{3n+2m} (T: Co, Rh, Ir) family of heavy-fermion systems	43
3.1	Introduction	43
	CeCoIn₅	46
3.2	Effect of pressure on the heavy-fermion superconductor CeCoIn ₅ . . .	46
3.2.1	Physical properties of CeCoIn ₅	46
3.2.2	Experimental results - CeCoIn ₅	52
3.2.3	Discussion - CeCoIn ₅	73
	Ce₂RhIn₈	76
3.3	Effect of pressure on the heavy-fermion antiferromagnet Ce ₂ RhIn ₈ . .	76
3.3.1	Physical properties of Ce ₂ RhIn ₈	76
3.3.2	Experimental results - Ce ₂ RhIn ₈	80
3.3.3	Discussion - Ce ₂ RhIn ₈	95
4	The heavy-fermion antiferromagnet and superconductor CeCu₂Si₂	97
4.1	Short overview	97
4.2	Physical properties	98
4.3	Experimental results	109
4.3.1	Interplay of antiferromagnetism and superconductivity in CeCu ₂ Si ₂	111
	a. A/S-type CeCu ₂ Si ₂ at ambient pressure	121
	b. A/S-type CeCu ₂ Si ₂ at low pressures	126
4.3.2	Superconductivity in the high-pressure range	142
4.3.3	Comparison of the evolution of the superconducting properties in the different pressure regimes	152
4.4	Discussion	178
5	Summary	183
	Bibliography	187
	Acknowledgments	199
	Author's declaration	201
	Versicherung	203

List of symbols and abbreviations

a.c.	alternating current
AFM	antiferromagnetic, antiferromagnetism, antiferromagnetically
ARPES	angle resolved photo-emission spectroscopy
B	magnetic field
BCS	J. Bardeen, L. Cooper and R. Schrieffer (authors of a microscopic theory of superconductivity from 1957)
C	specific heat
C_{el}	electronic specific heat
CDW	charge-density-wave
CEF	crystalline electric field
CuBe	copper-beryllium alloy
dHvA	de Haas-van Alphen
DOS	density of states
E_F	Fermi energy
FFLO	Fulde-Ferrell-Larkin-Ovchinnikov
FM	ferromagnetic, ferromagnetism, ferromagnetically
FS	Fermi surface
HF	heavy-fermion
IC	incommensurate
IV	intermediate valence, intermediate valent
k	wave vector
k_F	Fermi wave vector
l_{tr}	carriers mean-free path
LFL	Landau-Fermi-liquid

m^*	effective mass
p	pressure
MP35N	Co-Ni-Cr-Mo alloy
NFL	non-Fermi-liquid
NQR	nuclear quadrupole resonance
NRG	numerical renormalization group
PM	paramagnetic, paramagnetism
PPMS	Physical Properties Measurement System
QCP	quantum critical point
QP	quasiparticle
QPT	quantum phase transition
R	universal gas constant, $R = 8.314472 \text{ J}/(\text{molK})$
RKKY	Ruderman-Kittel-Kasuya-Yoshida
SC	superconductor, superconductivity, superconducting
SCES	strongly correlated electron systems
SDW	spin-density-wave
T	temperature
T_c	superconducting transition temperature
T_K	Kondo temperature
T_N	Néel temperature
T_{coh}, T^*, T_1^{max}	coherence temperature
v_F	Fermi velocity
v_s	velocity of sound in a solid
γ	electronic specific-heat coefficient
$\Delta(k), \Delta_k$	k -dependent energy gap function
θ_D	Debye temperature
μ_B	Bohr magneton
ξ_0	coherence length
ρ	electrical resistivity
χ	magnetic susceptibility

Introduction

Within the last three decades various intermetallic compounds have been found to possess “heavy” electrons. Known under the name of heavy-fermion (HF) materials, they cover an important research area in the field of solid state physics. HF systems usually contain rare-earth elements such as Ce, Yb or actinides like U. Ce-based HF systems are the most numerous among rare-earth-based HF systems. In this case Ce is known to be in the Ce^{3+} valence state with one $4f$ electron. Depending on the occupation number of the $4f$ state of Ce, a multitude of different ground states can be expected for these compounds. In order to tune a Ce-based system through the several different ground states, pressure can be considered the cleanest available tool. With increasing pressure the interaction between the conduction electrons and the $4f$ electron of Ce is gradually increasing. The Kondo interaction, considered to be the basic ingredient in the formation of a HF state, seems to play an important role in the region where the $4f$ electron of Ce is slightly interacting with the conduction electrons. As a result of the competition between the Ruderman-Kittel-Kasuya-Yosida (RKKY) interaction, leading to the formation of a magnetic ground state, and the Kondo interaction, leading to the formation of a non-magnetic singlet ground state, an antiferromagnetically (AFM) ordered state usually occurs at low temperatures in this low hybridization state. At pressures high enough to lead to the transition of the $4f$ electron of Ce into the conduction band a state, called intermediate-valence (IV) state, is formed. Superconductivity (SC), found to be unconventional and most likely mediated by the different fluctuations associated to the specific instabilities present nearby, exists in many of the Ce-based compounds. AFM spin fluctuations are supposed to mediate the formation of SC in the vicinity of the AFM ordered state, while strong valence fluctuations, related to the delocalization of the $4f$ electron of Ce, are considered responsible for the SC state existing in the proximity of a valence instability of Ce.

In this work we have studied the effect of pressure on three different tetragonal Ce-based systems. All three compounds are, at ambient pressure, in a HF state. CeCoIn_5 , a HF SC at ambient pressure [Petrovic 2001a], is located in the close vicinity

of an AFM instability. Though never detected in CeCoIn_5 , an AFM ordered state is expected to exist at a slightly negative pressure. Application of pressure moves CeCoIn_5 even further away from the AFM ordered state. Ce_2RhIn_8 , a compound belonging to the same family of $\text{Ce}_n\text{T}_m\text{In}_{3n+2m}$ (T: Co, Rh, Ir) HF compounds as CeCoIn_5 , orders AFM at ambient pressure [Thompson 2001]. Application of pressure continuously suppresses the AFM phase transition temperature. The appearance of pressure-induced SC is expected in this material. The third investigated compound, the *A/S*-type CeCu_2Si_2 , already at ambient pressure offers the possibility to study the intimate interaction between AFM and SC [Steglich 1979]. The AFM ordered state, present above the temperature where SC is formed, is gradually suppressed by application of pressure, while the SC state is stabilized upon increasing pressure. With further increasing pressure, CeCu_2Si_2 approaches the region where the degeneracy of the $4f$ state is increased by a collapse of the crystalline electric field (CEF) splitting and a transition to an IV state takes place. However, SC survives in the system over a very broad pressure range. While the role of the AFM order in the formation of a SC state is relatively easy to study in a large number of Ce-based HF systems, the influence of the unstable $4f$ state of Ce on the formation of a SC state is still a problem difficult to approach experimentally. CeCu_2Si_2 is nearly unique among Ce-based HF compounds by the fact that SC is present at low temperatures over a wide pressure range and typical instabilities, such as AFM and valence, are both accessible by application of moderate pressure and are in the same time sufficiently separated in pressure to be distinguishable.

Most of this thesis is based on results obtained from low-temperature ($0.26 \text{ K} \leq T \leq 7 \text{ K}$) heat-capacity measurements under hydrostatic pressure ($p < 2.1 \text{ GPa}$) and in magnetic field ($B \leq 8 \text{ T}$). In addition, results from pressure-dependent low-temperature ($T \geq 0.26 \text{ K}$) a.c.-susceptibility and magnetocaloric measurements are presented. Even though difficult to measure under extreme conditions as high pressure and low temperatures, the specific heat represents the thermodynamic property of matter which gives important information about bulk properties. Application of pressure can produce structural, electronic or other kind of phase transitions in matter. Compared to other control parameters, such as chemical doping or magnetic field, pressure is the cleanest tool to tune a system by only reducing its unit-cell volume.

The SC state, when present, and its interplay with the AFM instability was investigated in the three compounds studied in this work. Predictions of the AFM spin-fluctuation theory, as well as of theories promoting magnetic-fluctuation mediated SC in HF systems, have been probed by our measurements. The influence of a possible valence instability on the high-pressure SC state of CeCu_2Si_2 has been

studied as well. The possible existence of quantum critical points (QCPs) in regions where different types of instabilities are suppressed to $T = 0$ K was also addressed in this work. Landau-Fermi-liquid (LFL) type behavior at low temperatures, suited to describe the normal state of certain HF materials, is not expected to be observed in systems located in the vicinity of a QCP. Therefore, deviations from the predictions of the LFL theory, e.g. a logarithmic divergence of the low-temperature electronic specific-heat coefficient, were used to verify the proximity of a system to a QCP.

The thesis is divided into six chapters. Theoretical concepts, related to the different physical phenomena observed in the studied materials and considered necessary for the understanding of the experimental results, are contained in the first chapter. Chapter 2 describes the experimental techniques employed in this thesis. An important issue addressed in this chapter is related to the way accurate specific-heat data can be obtained by measuring under extreme conditions as high pressures and low temperatures. Therefore, a new type of pressure cell, used to achieve higher pressures, developed during this thesis is as well described. The way the experimental data were analyzed and an estimation of the errors implied in the obtained results are also included in this chapter. Chapters 3 and 4 present the experimental results. In Chapter 3 results obtained on two members of the $Ce_nT_mIn_{3n+2m}$ (T: Co, Rh, Ir) family of HF compounds, $CeCoIn_5$ and Ce_2RhIn_8 , are described. Presenting a layered structure, similar to the structure of high- T_c cuprate SCs, the $Ce_nT_mIn_{3n+2m}$ (T: Co, Rh, Ir) family of HF compounds are suited to study the supposed role of electronic dimensionality in the formation of a magnetically mediated SC state. A brief description of the $Ce_nT_mIn_{3n+2m}$ (T: Co, Rh, Ir) family of HF compounds is given at the beginning of Chapter 3. The remaining of this chapter is divided in two parts. The effect of pressure on the HF SC $CeCoIn_5$ is presented in the first part, while the second part describes the evolution under pressure of the HF AFM Ce_2RhIn_8 . Both parts end with a discussion. Chapter 4 is devoted to A/S -type $CeCu_2Si_2$ under pressure. Accurate low-temperature heat-capacity data up to $p < 2.1$ GPa, obtained for the first time on A/S -type single-crystalline $CeCu_2Si_2$, are presented. A detailed study in the low-pressure range, while slowly increasing pressure, helped to carefully analyze the peculiar interplay of AFM and SC in A/S -type $CeCu_2Si_2$. With increasing pressure, we were able by our measurements to distinguish between two different SC regions: SC at low pressures, in the vicinity of an AFM QCP, and SC at high pressures, in a region located close to a possible valence transition of Ce. Moreover, we have observed evidence for different SC order parameters in the two distinct SC regions. Support in favor of the suggestion that different mechanisms (AFM spin fluctuations in the low-pressure SC region and valence fluctuations in the high-pressure

SC region) are implied in the formation of the two SC states has been found. At the end, Chapter 5 summarizes the thesis.

Chapter 1

Theoretical concepts

1.1 Introduction to heavy-fermion systems

Low-temperature physical properties of matter are connected to the low-entropy states and therefore to a small number of degrees of freedom. Knowledge about the ground-state properties of matter stays at the basis of understanding any physical properties which appear at higher temperatures. Additional degrees of freedom can be taken into account in the study of a system only when the ground-state properties are elucidated. HF systems are especially suited to study the ground-state properties of matter due to the increased values of their measurable physical properties at low temperatures. With their usual transition temperatures of about 10 K or below, the HF systems are unlikely to lead to immediate applications but they may help to find out and to solve the insufficiencies of the existing theories in order to better understand condensed matter physics at higher temperatures.

1.1.1 The Kondo effect

The Kondo effect arises from the interaction between a single magnetic ion, such as iron, and the conduction electrons in an otherwise non-magnetic metal (e.g. Fe in Au). When embedded in a sea of conduction electrons, the spin of this magnetic impurity interacts with the conduction electrons. As a result of this interaction, a logarithmic increase of the electrical resistivity of the metal when the temperature is decreased, $\Delta\rho(T) \propto -\ln T$, and a minimum in $\rho(T)$ right before $\rho(T)$ starts to logarithmically increase, is found. In 1964, it was shown by Kondo that this low-temperature increase of the resistivity is due to the electronic scattering from the magnetic ion which interacts with the conduction electrons, while the observed minimum in $\rho(T)$ derives from an interplay between the monotonically decreasing phonon resis-

tivity, usually $\Delta\rho_{phonon}(T) \propto T^5$, and the logarithmically increasing spin-dependent contribution [Kondo 1964]. However, though the high-temperature properties were very well reproduced, this first theoretical estimation made by Kondo was leading to the unphysical prediction that the resistance would be infinite at $T = 0$ K. Due to the extremely strong coupling at low temperatures between the impurity spin and the conduction electrons, the perturbation theory used by Kondo in solving this problem was breaking down. Known as the ‘Kondo problem’, the behavior at low temperatures remained unsolved for a while. Ten years later, under the name of ‘single-impurity Kondo model’, a new theory based on the numerical renormalization group (NRG), accounting for the low-temperature properties of the metallic systems with a low amount of magnetic impurities, was elaborated [Wilson 1975]. Replacing the perturbation theory used by Kondo by the NRG theory, Wilson has obtained ground-state and low-temperature results for the case of the isolated magnetic impurity with spin $S = 1/2$. As a result of an antiparallel type of interaction, at low temperatures, the impurity spin is completely compensated by the spins of the conduction electrons, leading to the formation of a Kondo singlet. The exchange hamiltonian can be written as: $H = -JSs$, with S representing the spin of the magnetic impurity, s the spin of a conduction electron and J the coupling. The coupling J depends on the hybridization matrix element, V , between the impurity spin and the conduction electrons as $J \propto V^2$. For a negative coupling J , typical for the antiparallel interaction, it was shown that the exact solution at $T = 0$ K consists of a non-magnetic singlet. Following the work of Wilson, exact results for the low-temperature thermodynamic properties by using the Bethe-Ansatz were obtained [Andrei 1980, Desgranges 1982]. Triggered by the experimental results, orbital degeneracy (spin-orbit coupling) and CEF splitting effects were later added to these models (by using the Coqblin-Schrieffer model [Coqblin 1969] and the N -fold degenerate Anderson model [Anderson 1981, Bickers 1987]), leading to relatively good agreement between the experimental findings and the theoretical estimates [Rajan 1983, Desgranges 1985, Desgranges 1987]. Those theoretical results are especially suited to describe Ce and Yb impurities with $N = 2j + 1$, where j is the total angular-momentum quantum number associated with the degenerate ground-state multiplet of the impurity ion. The main results of the single-impurity Kondo model can be summarized as following:

1. At $T = 0$ K the properties are characteristic of a spin-singlet state (non-magnetic). The magnetic susceptibility, χ , and the electronic specific-heat coefficient, γ , are greatly enhanced and the electrical resistivity approaches the unitarity limit ρ_0 . The low-temperature ($T \ll T_K$, for T_K cf. no. 3) behavior is characteristic of a local LFL state, with strongly enhanced values of χ and γ .

2. At very low temperatures ($T \ll T_K$), the electrical resistivity shows a $\rho(T) = \rho_0 - AT^2$ dependence, again typical for a local LFL state, while $\Delta\rho(T) = \rho(T) - \rho_0 \propto -\ln T$ at elevated temperatures.
3. There exists a characteristic Kondo temperature, T_K , which defines a very smooth transition from the LFL behavior to the free ion behavior at high temperatures. The Kondo temperature is determined by:
 $k_B T_K \propto \frac{1}{N(E_F)} \exp\left(-\frac{1}{|JN(E_F)|}\right)$, where $N(E_F)$ represents the electronic density of states (DOS) at the Fermi level, E_F .
4. The local DOS of the magnetic impurity at $T = 0$ K shows two peaks, one broad peak centered at the position of the singly occupied impurity level (e.g. $3d$ or $4f$ level), below E_F , and a very narrow peak located at E_F . The latter one, known as the Kondo or Abrikosov-Suhl resonance peak, has a width of the order of T_K and accounts for the low-temperature behavior.

Depending on the relative distance of the impurity level, ε_d (or ε_f), to E_F four different regimes can be distinguished. The transition through different regimes can be obtained for example by application of pressure or by chemical doping. Considering U as representing the Coulomb interaction between the electrons in the impurity ion state, the different regimes are as following:

1. $2\varepsilon_d + U \ll E_F$ - the impurity level, ε_d , lies deep below the Fermi level. In this case the magnetic moment of the impurity does not form.
2. $\varepsilon_d \ll E_F \ll 2\varepsilon_d + U$ - the impurity level approaches the Fermi level. In this case the magnetic moment of the impurity forms and the Kondo effect takes place.
3. $\varepsilon_d \approx E_F$ or $2\varepsilon_d + U \approx E_F$ - the impurity level lies in the vicinity of the Fermi level. In this case an IV regime is achieved. No separate charge and Kondo peaks are obtained, the two peaks being merged.
4. $\varepsilon_d \gg E_F$ - the impurity level is located far above the Fermi level. This situation is known as the empty orbital regime. The impurity level is predominantly in the state with no electrons, with the average occupancy of the level being well below integer. Neither the magnetic moment of the impurity nor the Kondo resonance form.

It is worth noting that in the case of a magnetic impurity embedded in a metallic host, the value of U depends on the hybridization between the open core shell of the

impurity and the conduction electrons. Moreover, in the case of rare-earth impurities with $4f$ electrons, due to the fact that the $4f$ wavefunction is more localized and closer to the nucleus, the values of U are expected to be higher than in the case of $3d$ impurities. In the case of Ce as magnetic impurity, application of pressure leads to the gradual shift of the impurity level, ε_f , towards the Fermi level, E_F , and a gradual transition through the above-described states, from no. 1 to 4, is expected.

1.1.2 Kondo lattice and magnetism in heavy-fermion systems

In the Kondo lattice, the Kondo ions form a dense, periodic array. Contrary to the relatively simple model of the single-impurity Kondo problem, the Kondo-lattice problem, although relatively well understood, is not completely solved analytically at present. However, treatment of the Kondo lattice is usually based upon the single-impurity Kondo model. While the single-impurity Kondo model handles the situation where the concentration of impurities is low enough that one impurity does not ‘feel’ the influence of its nearest neighbor, in the case of Kondo-lattice compounds, the magnetic impurities are located close enough to manifest inter-site interactions. The impurity spins interact with each other via the conduction electrons through the so-called Ruderman-Kittel-Kasuya-Yoshida (RKKY) interaction. This interaction couples the impurity spins, leading to the formation of a magnetically ordered state (AFM, FM or both because the RKKY interaction extends beyond nearest-neighbor pairs). The energy associated with the RKKY interaction is: $k_B T_{RKKY} \propto J^2 N(E_F)$, with J and $N(E_F)$ defined in the previous section.

The Kondo effect only arises when the total spin of the ion embedded in the metal is non-zero (magnetic). Therefore, the behavior associated with the Kondo effect can also occur in compounds with $4f$ impurities as Ce. Because the spatial extension of the $4f$ wavefunction in Ce is rather small, the concentration of Ce ions in a non-magnetic host can be surprisingly large (of order of 1 at.%) without violating the conditions necessary for the single-impurity Kondo effect to appear. In the case of Ce-based Kondo lattices, when the $4f$ level is located not too far from the Fermi level, the ground-state properties of the system are determined by the competition between the Kondo effect and the RKKY interaction. While the former one tries to compensate the local moment of Ce leading to the formation of a non-magnetic singlet at low temperatures, the RKKY interaction leads to the formation of a magnetic ground state. Since both energies, $k_B T_{RKKY}$ and $k_B T_K$, strongly depend on the coupling J between the impurity spins and the conduction electrons, a unified qualitative phase diagram, taking into account both interactions, was established by Doniach for the case of AFM inter-site interactions on a chain of Kondo ions (see figure 1.1)

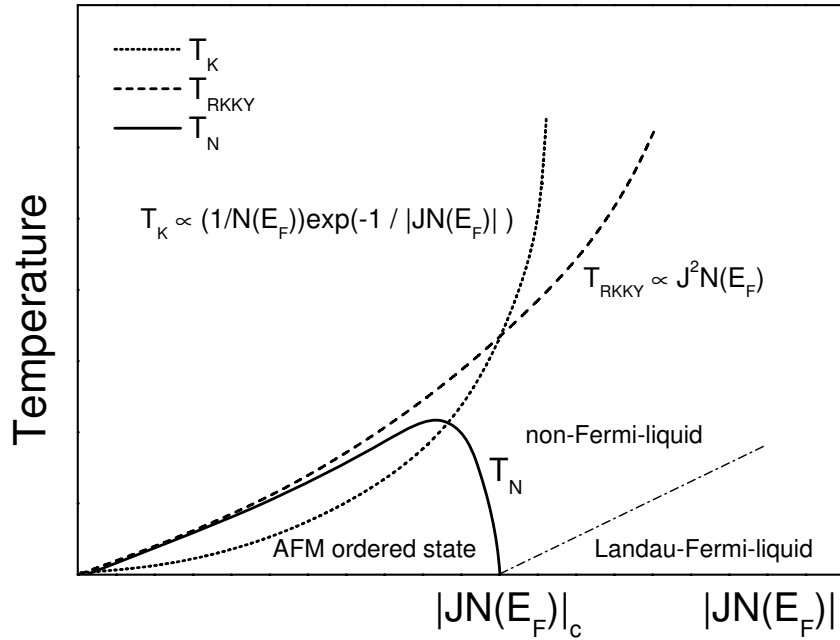


Figure 1.1: Doniach phase diagram for AFM HF systems.

[Doniach 1977]. For small $|J|$, the RKKY interaction dominates and the system orders magnetically. For the strong-coupling case (large values of $|J|$), the Kondo energy dominates and the system is non-magnetic. The real ordering temperature, T_N , therefore increases initially with increasing $|J|$, then passes through a maximum and approaches zero at a critical value, $|JN(E_F)|_c$.

On the magnetically ordered side of the Doniach phase diagram ($|JN(E_F)| < |JN(E_F)|_c$ in figure 1.1) the system is characterized by a weak AFM state. Due to partial Kondo compensation, the ordered moment in this state is relatively small.

On the non-magnetic side of $|JN(E_F)|_c$ ($|JN(E_F)| > |JN(E_F)|_c$ in figure 1.1), where the Kondo regime dominates, the observed properties at high temperatures ($T > T_K$) can be described within the calculations emerging from the single-impurity Kondo picture, while strong deviations from that situation appear at low temperatures. Because of the periodicity in a Kondo lattice the ground state of the system is of coherent nature leading to a low-temperature behavior well explained within the LFL theory. Due to the coherent scattering of the conduction electrons on the magnetic impurities, at low temperatures ($T \rightarrow 0$ K), the resistivity, $\rho(T)$, of a Kondo-lattice system is characterized by a steep drop, contrary to the single-impurity case, where the resistivity at $T \rightarrow 0$ K tends to a large value, ρ_0 . When at each impurity site a Kondo singlet ground state is formed, those states will scatter electrons. Due to the periodicity of these sites in a lattice, the resonant elastic scattering at each site

will form a highly renormalized band of width $\sim T_K$. As a result, a heavy-electron state is formed, with the quasiparticles (QPs) exhibiting strongly enhanced values of the effective masses, m^* . Therefore, large values of the magnetic susceptibility and of the electronic specific-heat coefficient are observed at low temperatures. The formed heavy QPs show LFL behavior at low temperatures. The observed values of m^* are usually about $100 \div 1000$ times larger than in simple metals (e.g. Cu).

In the case of the electrical resistivity, the transition from the high-temperature logarithmic temperature dependence of ρ ($\Delta\rho(T) \propto -\ln T$) to the low-resistance coherent state, characterized by LFL behavior ($\Delta\rho(T) \propto T^2$), in the Kondo-lattice systems, happens through a maximum in the $\rho(T)$ curve. The maximum is associated to the coherence temperature, T_{coh} . Therefore, T_{coh} is often used as a rough estimate for T_K ($T_{coh} \propto T_K$).

Even though at the moment is still an unsolved theoretical issue, the Kondo-lattice effect may explain the formation of heavy QPs in rare-earth-based HF systems. The formation of the bound states between the local moments and the conduction electrons is an effect local in space but non-local in time. An analogy between the formation of heavy-electron bound states in HF systems and the formation of Cooper pairs in SCs was also suggested [Coleman 2002].

1.1.3 Heavy-fermion and intermediate-valence systems

In the case of rare-earth-based intermetallic compounds, the electronic configuration of the rare earth is $[\text{Xe}]4f^n 5d^1 6s^2$, with n integer from 0 to 14. Therefore, rare earths are usually characterized by a trivalent state corresponding to the $4f^n$ configuration. Ce, Sm, Eu, Tm and Yb are known to be outstanding among rare-earth elements. Their anomalous behavior consists in the fact that at different conditions (e.g. different compounds, pressure), a departure from the $4f^n$ ionic configuration with n being integer has been found. Depending on the strength of the hybridization between the conduction electrons and the $4f$ electrons of the rare earth, V , the $4f^n$ and $4f^{n-1}$ states have a non-zero occupation probability. In the case of Ce, a Ce^{3+} ionic configuration, with $4f^n$, $n = 1$ is expected. For Ce-based compounds, a deviation from the integer $n = 1$ value (where n is averaged over the Ce-based lattice compound) can lead to different situations:

1. $4f^n$, $n = 1$, stable $4f$ shell, in most cases long-range magnetic order occurs, localized $4f$ electrons;
2. $4f^n$, $n \approx 1 - \epsilon$, with $\epsilon > 0$, $\epsilon \rightarrow 0$, Kondo regime, HF systems, $4f$ electrons almost localized;

3. $4f^n$, $n \approx 1 - \epsilon$, with $\epsilon > 0$, IV regime, $4f$ electrons delocalize, the HF state breaks down.

Application of pressure or appropriate chemical doping can shift Ce-based compounds from the integer $n = 1$ valence to the IV regime. The above-mentioned regimes are qualitatively described by the Doniach phase diagram presented in figure 1.1, with the IV regime for Ce-based compounds being located on the right side of the phase diagram. In the case of Ce compounds, increasing pressure induces an increasing hybridization strength between the $4f$ electrons of Ce and the conduction electrons, i.e. increases the value of $|JN(E_F)|$. Around the region where long-range magnetic order disappears, it was experimentally observed that, in some of the HF compounds, SC sets in at low temperatures.

1.2 Superconductivity in heavy-fermion systems

1.2.1 Conventional versus unconventional superconductivity

Superconductivity (SC), at the time of its discovery by H. Kamerlingh Onnes in 1911 in mercury [Kamerlingh 1911], was defined as the complete absence of resistance to electric current below a certain temperature T_c , called the SC transition temperature. Until 1933, when the Meissner effect was discovered [Meissner 1933], it was considered that the absence of electrical resistance is the only property which makes a SC to differ from a non-superconducting material. The discovery of the Meissner effect, as the property of a SC to expel the magnetic field from its interior, has shown that the SC state is a true, reversible, thermodynamic state. A microscopic theory of SC was developed in 1957 by J. Bardeen, L. N. Cooper and J. R. Schrieffer, known today as the BCS theory [Bardeen 1957]. According to this theory, below T_c , the electrons are forming paired states (named Cooper pairs) due to the interaction with the crystal lattice.

In matter in general, at microscopic level, forces between particles are transmitted by the exchange of small energy packets, called quanta. When electrons in a metal exchange these quanta of attractive energies they can overcome their electrostatic repulsion and they can form a new bound state. These new electronic bound states in a SC are called Cooper pairs and they are the basic ingredients for a SC state in matter. The Cooper pairs are characterized by an integer spin (in units of \hbar), 0 or 1, therefore they behave like bosons. In the conventional BCS type SC the electrons are paired by the exchange of the quanta of lattice vibrations, called phonons. This kind of pairing favors the formation of s -wave pairs - spin singlets ($S = 0$) with an angular

momentum $l = 0$. The so formed Cooper pairs are scattering on magnetic impurities existing in the SC matter. Only a tiny amount of magnetic impurities (< 1 at.%) leads to a full suppression of the SC state. HF SCs are showing two major differences compared to classical BCS type SCs: i) the existing charge carriers in HFs are heavy QPs with large effective masses m_{HF}^* and ii) HF SCs contain a dense array of magnetic ions which need to be non-pair-breaking (otherwise SC would not appear in HF systems). Therefore, the Cooper pairs in HF SCs are formed by heavy QPs and the attractive binding force is most likely non-phononic in origin. The latter is suggested by the fact that the existing large m_{HF}^* signals a correspondingly small Fermi velocity (v_{HF}) of the charge carriers, which is approximately of the same order of magnitude as the sound velocity (v_s) in the HF systems. In a normal metal, the Fermi velocity of electrons, v_{el} , is about three orders of magnitude larger than the velocity of sound, v_s . This retardation of the electron-phonon interaction in normal metals is the necessary condition in the BCS theory of SC to avoid the Coulomb repulsion between the charge carriers forming the Cooper pair. Consequently, phonon mediated BCS-like SC is very unlikely to exist in HF SCs. Furthermore, in the last three decades, many experimental evidences of anisotropic pairing states appeared not only in the case of HF systems (e.g. CeCu₂Si₂ [Steglich 1979], UBe₁₃ [Ott 1983], UPt₃ [Stewart 1984], CeIrIn₅ [Petrovic 2001b], CeCoIn₅ [Petrovic 2001a]), but also in the high- T_c cuprate SCs (e.g. La_{1.85}Ba_{0.15}CuO₄ [Bednorz 1986], (Hg_{0.8}Tl_{0.2})Ba₂Ca₂Cu₃O_{8.33} [Sun 1994]) or in the ruthenates (e.g. Sr₂RuO₄ [Maeno 1994]), demonstrating the non-*s*-wave, unconventional, character of the Cooper pairs.

Taking into account that up to now there exist several classes of SC materials and that there are some experimentally proven evidences for physical properties in the SC state of those materials which are in contradiction with the predictions of the conventional BCS theory (see table 1.1), it is expected that new mechanisms and, therefore, new theories have to be worked out for the explanation of those unconventional SC properties. The very first question arising in this problem is related to the provenience of the binding force needed for the formation of Cooper pairs. The existing differences suggest that the mechanism of attraction does not have to do much with phonons but might be purely or mainly electronic in origin. Along the past decade, fluctuations associated to different types of instabilities, like spin fluctuations, valence fluctuations, orbital fluctuations, etc., were proposed as ingredients for the formation of Cooper pairs in unconventional SCs. However, guided by the experimental observations, good theoretical estimations have been obtained for the case of spin-, respective, valence-fluctuation mediated SC [Monthoux 1999, Onishi 2000, Monthoux 2001, Monthoux 2004]. The pressure in-

duced unconventional SC in Ce-based HF materials like CePd₂Si₂, CeIn₃, CeCu₂Si₂, CeCu₂Ge₂ [Mathur 1998, Yuan 2003] is very well described within the theoretical framework of electron spin- or electron charge-density-fluctuation mediated SC. However, the first clear experimental prove for magnetically mediated SC became available in the case of the U-based HF SC, UPd₂Al₃, by tunneling conductivity and inelastic neutron-scattering experiments [Jourdan 1999, Sato 2001].

In conventional SCs, the binding of electrons in Cooper pairs is described by the emission and absorption of phonons (waves of lattice density). For the above-mentioned models for the formation of unconventional SC one can similarly imagine the binding of electrons via emission and absorption of waves of electron spin-, respectively, charge-density.

Looking back to the evolution in time, the appearance of SC in HF systems close to a magnetic instability has brought scientists to the idea that SC could be related to the existing magnetic instability. The unusual behavior of SC under pressure in CeCu₂Si₂ and CeCu₂Ge₂ [Bellarbi 1984, Thomas 1993, Thomas 1996, Jaccard 1999] did, however, not fit into this picture, due to the extension of the SC phase far beyond the existence of the magnetic instability. Therefore, it was supposed that the pronounced increase of the SC transition temperature in the high-pressure range in the above-mentioned HF systems has to be connected to a possible valence transition of Ce (in analogy with the isostructural $\gamma - \alpha$ transition existing in metallic Ce [Koskenmaki 1978]). However, the theory for magnetically mediated SC proposed by Monthoux and Lonzarich [Monthoux 1999] could not explain the “unusual” SC phase diagram of CeCu₂(Si,Ge)₂. Onishi and Miyake have tried to approach this “unusual” phase diagram by a model where they have considered valence fluctuations to be involved in the sharp increase of the SC transition temperature under pressure. In their model they have used the extended periodic Anderson model with Coulomb repulsion potential between f and conduction electrons [Onishi 2000]. The theoretical model has been convincing to some extent, but the existence of the magnetic fluctuations around the AFM QCP has been neglected. Later on, experimental evidence for the existence of two separated SC domes under pressure in CeCu₂(Si_{1-x}Ge_x)₂ ($x \neq 0, 1$), which merge in the case of the stoichiometric compounds CeCu₂Si₂ and CeCu₂Ge₂ into one extended SC region [Yuan 2003], has eliminated part of the mysteries concerning the unusual phase diagram. A similar approach, like the one for the spin-fluctuation mediated SC, has been made for the valence-fluctuation mediated pairing as well [Monthoux 2004], in this way shedding more light to the SC anomalies seen so far in HF materials. In the following part we will briefly describe these two most popular theoretical models existing up to now for SC in HF systems.

Table 1.1: Conventional and unconventional SC. Some important similarities and differences (part of the content was taken from [Leggett 1997]).

Conventional SC (BCS)	Unconventional SC	Comments
Cooper pairs: - formed by renormalized band electrons around the Fermi level (from light QPs with small m_{el}^*)	Cooper pairs: - formed by heavy QPs around the Fermi energy (from heavy QPs with large m_{HF}^*)	- in the case of HF SC, $\frac{\Delta C}{\gamma_{HF} T_c} \Big _{T=T_c} \approx 1 \div 2$ or higher, but it is never much smaller than 1; $m_{HF}^* \approx 1000 m_{el}^*$
- phonon mediated pairing; - high Fermi velocity: $v_{F_{el}} \approx 1000 v_s \Rightarrow$ the retarded electron-phonon interaction avoids Coulomb repulsion	- non-phonon mediated pairing; $v_{F_{HF}} \approx v_s$; electron mediated pairing?	$k_{F_{HF}} \approx k_{F_{el}}$; $(k_F = m^* v_F / \hbar)$ $v_{F_{HF}} \approx v_s \approx v_{F_{el}} / 1000$
s - wave pairing; isotropic pairing; $S = 0, l = 0$ (singlet); - energy gap: $\Delta(k) = const., \forall k$ - phonon-induced interaction is not very sensitive to the momentum transfer, therefore the simplest possible pairing ($S = 0, l = 0$) is favored	p - or d - wave pairing (also f - wave); anisotropic pairing; $S = 1, l = 1$ (triplet); $S = 0, l = 2$ (singlet); - energy gap: $\Delta(k) \neq const.$; $\exists k$ for which $\Delta(k) = 0$ (nodes of the gap function) - momentum transfer might be very important	- HF SC: CeCoIn ₅ - most likely $d_{x^2-y^2}$ singlet pairing (or d_{xy}); evidence from thermal-conductivity (κ) and angle-dependent specific-heat measurements; - high- T_c cuprate SCs: $d_{x^2-y^2}$ singlet pairing; supported by ARPES, SQUID measurements; - Sr ₂ RuO ₄ : p - wave triplet pairing; - ³ He: p - wave triplet pairing;
- only gauge symmetry is broken	- gauge symmetry + additional symmetries (one or more) are broken	- e.g. - additional broken symmetry could be the inversion symmetry in unconventional SCs (e.g. superfluidity in ³ He; CePt ₃ Si)

Conventional SC (BCS)	Unconventional SC	Comments
- $C(T)$, for $T \ll T_c$, shows an exponential decay: $C(T) \propto \exp(-\frac{\Delta}{k_B T})$	- $C(T)$, for $T \ll T_c$, shows a non-exponential behavior (power law): $C(T) \propto T^n$	- existence of nodes on the FS ($\exists k$ for which $\Delta(k) = 0$) in unconventional SC leads to power-law T dependencies of the specific heat at low T
- normal-state properties: → LFL behavior	- anomalous normal-state properties can be often seen: → NFL behavior	- NFL behavior is seen in the normal state of many HF SCs ($\Delta\rho(T) \propto T^n, n \neq 2$), as well in high- T_c SCs ($\Delta\rho(T) \propto T$)
- coherence length: $\xi_0 \approx 10^4 \text{Å}$	- coherence length: HF SC: - $\xi_0 \approx (50 \div 100) \text{Å}$ high- T_c cuprate SC: - $\xi_0 \approx (10 \div 30) \text{Å}$	- coherence length (ξ_0) represents the radius of the Cooper pairs in a SC; $\xi_0 \sim \frac{\hbar v_F}{ \Delta }$ for a SC, independent of the type
- magnetic impurities destroy SC - paramagnetic impurities are not strongly pair-breaking, due to isotropic pairing - SC does not coexist with magnetic order	- magnetic impurities do not destroy SC, they even might favor SC - paramagnetic impurities are strongly pair-breaking, due to anisotropic pairing - SC can often coexist with magnetic order	- HF SC: - doping with non-magnetic La on Ce site in CeCu_2Si_2 destroys SC: CeCu_2Si_2 is SC $\text{Ce}_{(1-x)}\text{La}_x\text{Cu}_2\text{Si}_2$ - for $x \geq 0.1$ does not SC; - in many cases unconventional SC appears around magnetically ordered phases (e.g. HF-AFM-SC, HF-FM-SC, high- T_c cuprate SC, etc.); - CeCu_2Si_2 , UGe_2 , YBCO, etc.
- high purity samples are not essentially required for occurrence of SC, only magnetic impurities have strong pair-breaking effect	- unconventional SC appears usually in very high purity materials	

Conventional SC (BCS)	Unconventional SC	Comments
<p>- T_c is connected to the size of the energy gap by: $2\Delta(T = 0\text{ K}) \approx 3.5k_B T_c$; $\Delta(T = 0\text{ K}) \approx (0.1 \div 1)\text{ meV} \approx 10^{-(4\div 5)} E_F$</p>	<p>- prediction of the BCS theory like: $2\Delta(T = 0\text{ K}) \approx 3.5k_B T_c$ is not valid in high-T_c SCs, where: $2\Delta(T = 0\text{ K}) \gg 3.5k_B T_c$ $(2\Delta(T = 0\text{ K}) \approx 60\text{ meV})$</p>	
<p>- singlet SC: $B_{c2}^{orbital}(0\text{ K}) \ll B_{Pauli}(0\text{ K})$, therefore, the Pauli limit is irrelevant</p>	<p>- triplet SC: - Pauli limiting is not existing, only orbital limiting must be taken into account - singlet SC (e.g. HF SC): - $B_{c2}^{orbital}(0\text{ K})$ and $B_{Pauli}(0\text{ K})$ might be of the same order of magnitude, therefore, they both might affect the upper critical field, B_{c2}</p>	<p>- SC in magnetic field implies: - orbital effects: $B_{c2}^{orbital}(0\text{ K}) \sim m^* T_c$ - Pauli limit: $B_{Pauli}(0\text{ K}) \approx (1.8\text{ T/K}) T_c$; both effects are pair-breaking, reducing the upper critical field, B_{c2}</p>
<p>- BCS theory predicts for the highest transition temperature 30 K: $T_c \lesssim 30\text{ K}$</p>	<p>- high-T_c SCs have high SC transition temperatures: $70\text{ K} \lesssim T_c \lesssim 150\text{ K}$</p>	<p>- maximum observed T_c at ambient pressure of $T_c \approx 138\text{ K}$ in $(\text{Hg}_{0.8}\text{Tl}_{0.2})\text{Ba}_2\text{Ca}_2\text{Cu}_3\text{O}_{8.33}$</p>
<p>- phonon mediated interaction: → local in space, → non-local in time</p>	<p>- spin (valence, etc.)-fluctuation mediated interaction: → non-local in space, → non-local in time</p>	<p>(see theoretical approach of Monthoux and Lonzarich [Monthoux 2004])</p>
<p>- Coulomb repulsion is not favorable for the formation of SC</p>	<p>- Coulomb repulsion helps the formation of p - wave triplet paired state in the case of FM-fluctuation mediated SC</p>	<p>- in the context of magnetically mediated SC, repulsive channel might help the formation of Cooper pairs [Monthoux 2004]</p>

1.2.2 Unconventional superconductivity mediated by electrons in heavy-fermion systems

Electron spin-, respectively, charge-density-fluctuation mediated SC was studied theoretically by using the mean-field theory of SC for metallic systems on the border of a magnetic, respectively, charge-density instability [Monthoux 1999, Monthoux 2001]

[Monthoux 2004]. The calculations were done for cubic (3D) and tetragonal (2D) lattices, as well as for AFM, FM, respectively, charge fluctuations. One of the major differences between the conventional phonon mediated and the unconventional magnetically or charge-density-fluctuation mediated SC consists in the fact that the former one is usually taken to be local in space but non-local in time, while the two latter ones are non-local in both space and time. The non-locality in space leads to anisotropic pairing states, typical for the unconventional type of SC found in HF systems. The calculations are based on the parametrization of an effective interaction arising from the exchange of spin-density, respectively, charge-density fluctuations.

Magnetically mediated superconductivity

In the vicinity of a continuous magnetic quantum phase transition (QPT) or QCP, the susceptibility of the system could become divergent and thus the interactions become rather strong. Therefore, slow spin fluctuations with large amplitudes are existing around a magnetic QCP. The charge carriers possessing their own spin, in their movement along the crystal, are feeling these strong fluctuations and they communicate via emitting and absorbing some energy from the environment. If the conditions are favorable to overcome the repulsive interaction existing among them, the electrons form Cooper pairs. An important aspect of the magnetic interaction is the vector nature of the spin. The longitudinal and transverse spin fluctuations can be seen in a similar way like the longitudinal and transverse phonons that mediate the conventional pairing. However, the important difference is coming from the fact that while the phonon-mediated interaction does not take into account the relative orientation of the spins of the interacting particles, the magnetically mediated interaction strongly depends on it. One obtains the SC transition temperature T_c from the solutions of the Eliashberg equations (McMillan type of formula) [Millis 1988, Lonzarich 1997, Mathur 1998]:

$$T_c \sim T_{sf} \left[1 - \left(\frac{\xi_0}{l_{tr}} \right)^2 \right] \theta e^{-\frac{1+\lambda'}{g\lambda'}}, \quad (1.1)$$

where T_{sf} represents the spin-fluctuation temperature, analogous to the Debye temperature in the BCS theory, and is associated with the bandwidth of the spectrum Γ_q which describes the relaxation rates of spin fluctuations at a wave vector q . T_{sf} sets the overall energy scale for spin-fluctuation mediated SC in a system. λ' represents the enhancement of the QP mass due to magnetic interactions and it is proportional to the q -space average of $1/\Gamma_q$. At a magnetic QCP λ' diverges, while away from the magnetic QCP it becomes small and therefore T_c is strongly suppressed. g measures the

relative strength of the interaction in the given pair states. The factor θ depends on the form of Γ_q and partly represents damping due to incoherent inelastic scattering. $\left[1 - \left(\frac{\xi_0}{l_{tr}}\right)^2\right]$ measures damping due to scattering from impurities, either magnetic impurities or non-magnetic ones for the case of anisotropic pairing. It defines the condition for the appearance of unconventional SC, namely that the charge carriers' mean-free path, l_{tr} , must exceed the coherence length, ξ_0 , also suggesting that unconventional SC is more stable in systems with small ξ_0 (e.g. HF systems and high- T_c SCs). The most important results of the above-described model can be summarized in a few important conclusions (no. 1-5 from [Monthoux 1999, Monthoux 2001] and no. 6 from [Hertz 1976, Millis 1993, Moriya 1995, Nakamura 1996, Lonzarich 1997]):

1. magnetically mediated SC is more robust in quasi-2D rather than in 3D electronic structures; furthermore, in the quasi-2D case SC can be observed in a wider region at the border of the magnetic instability than in the case of 3D;
2. the appearance of magnetically mediated SC is more favored in the case of the AFM order as compared to the FM order;
3. the most robust pairing is obtained for the spin-singlet $d_{x^2-y^2}$ Cooper pair state;
4. for the $d_{x^2-y^2}$ Cooper pair state, the most robust pairing is expected to appear for the magnetic fluctuations at q_0 near $[\pi, \pi]$;
5. high SC transition temperatures can be obtained in systems with high spin-fluctuation temperatures T_{sf} ;
6. in the vicinity of an AFM instability, the maximum value of T_c is obtained around the critical concentration where $T_N \rightarrow 0$ K, n_c (or critical pressure, p_c , respectively). The magnetic transition temperature vanishes as $T_{N\acute{e}el, Curie} \propto |p - p_c|^\gamma$ at the critical pressure p_c , with: $\gamma = 3/4$ for a 3D FM, $\gamma = 2/3$ for a 3D AFM and $\gamma = 1$ for a 2D AFM and a 2D FM.

Valence-fluctuation mediated superconductivity

Analogous to the model of spin-fluctuation mediated SC where the magnetic susceptibility of the system is supposed to diverge at a magnetic QCP, Monthoux and Lonzarich have considered the possibility of pairing near instabilities produced by the divergence of the particle-density response function [Monthoux 2004]. In this situation one could include structural instabilities, characterized by the softening of phonons in some regions of the Brillouin zone. Similar to the situation described in

the previous paragraph, the induced interaction produced by those soft phonons, in contrast to the conventional phonons, is non-local in space. Typical situations where one could expect a density response function to be strongly enhanced are the border of a charge-density-wave transition, a stripe instability or a valence instability (a transition where the structure of the unit cell remains the same, but its volume changes, e.g. the $\gamma - \alpha$ transition in metallic Ce). If the charge-density transition is strongly first order, the charge-density response function is not sufficiently enhanced and, therefore, the QP interaction is not strong enough to lead to SC. The isostructural $\gamma - \alpha$ transition of Ce, which could take place in many Ce-based HF systems, is a typical case where the transition is of first order, except at the critical end point. Therefore, for the appearance of charge-density-fluctuation mediated SC there are two major conditions to be fulfilled:

- i) the critical end point of the density transition must be in the same temperature range where the SC pairing is expected;
- ii) the critical end point must be at low enough temperature in order that thermal fluctuations are not strong enough to destroy the SC pairs.

The theoretical model assumes for the density response function a similar form like the one assumed for the magnetic susceptibility in the model of magnetically mediated SC. The main results of the model can be summarized as follows [Monthoux 2004]:

1. the increase of the lattice anisotropy from 3D to 2D increases the robustness of charge-density-fluctuation mediated SC;
2. weakening the first-order character of the valence transition enhances the density fluctuations and, therefore, enhances the SC transition temperature;
3. the critical end point of the valence transition must be at low enough temperature in order to achieve the SC state;
4. the most robust pairing is obtained in the spin-singlet $d_{x^2-y^2}$ Cooper pair state;
5. for the $d_{x^2-y^2}$ Cooper pair state, the most robust pairing is expected to appear for the charge-density fluctuations with small wave vector q_0 , near the center of the Brillouin zone.

A comparison of the two models, treating a magnetic, respectively, a valence instability in order to obtain SC, leads to the conclusion that in both models the most robust SC is obtained for the $d_{x^2-y^2}$ Cooper pair state, but with the most enhanced response function obtained for different wave vectors. Magnetic pairing gives the

highest T_c for the wave vector, q_0 , near $[\pi, \pi]$, while the charge-density-fluctuation mediated pairing for a wave vector close to the center of the Brillouin zone. This observation could be very important for the SC in the Ce-based HF systems which show an AFM QCP (at p_c) and a low-temperature critical end point (at p_v) for the valence transition of Ce. When the two mentioned key transitions appear at the same critical pressure ($p_c \approx p_v$), both pairing mechanism could reinforce each other, giving rise to a more robust SC state. When the two transitions are well separated on the pressure scale ($p_c < p_v$), one expects two separated SC domes, one located in the vicinity of the AFM QCP (p_c) and the second one located close to the valence instability region (p_v). The $\text{CeCu}_2(\text{Si}_{1-x}\text{Ge}_x)_2$ family of HFs can be taken as a very good example where the system under pressure passes through both phase transitions, a magnetic and a valence transition. Atomic disorder in unconventional SCs usually reduces the SC transition temperature, as well as the width of the region where SC is present. Consequently, the low Ge containing systems in this family, due to the atomic disorder introduced by doping, show two well separated SC domes located around the two critical pressures, p_c , respectively, p_v ($p_c < p_v$), while the stoichiometric compounds, where the atomic disorder is substantially smaller, show a very broad SC region under pressure as a result of the overlapping of the two distinct extended SC domes.

1.3 Non-Fermi-liquid behavior in heavy-fermion systems

1.3.1 The Landau-Fermi-liquid state

The Landau-Fermi-liquid (LFL) theory dates back to 1956 and it is related to the work of Landau, who has shown that a system of interacting fermions, under certain conditions, can be described within the picture of a non-interacting fermionic system (Fermi gas) [Landau 1956, Landau 1957, Landau 1959]. An important aspect of this similarity consists in the fact that it is valid only for low excitation energies and temperatures. The interacting fermions are treated as QPs, carrying the same spin, charge and momentum as the original particles, but being “dressed” by the excitations coming from the environment. With these conditions fulfilled, a one to one correspondence between the QPs and the non-interacting fermions can be usually done. As a consequence, simple metals, if they are not in a magnetic or SC state, at low temperatures, $k_B T \ll E_F$, can be described within the free-electron picture, replacing the electrons by QPs, the latter containing information about the environ-

ment, such as lattice vibrations, spin fluctuations, electronic interactions, etc. The effective mass of the QPs, m^* , is therefore renormalized and displays values higher than that of the bare electron mass, m_0 . The renormalization factor can be defined as:

$$\frac{m^*}{m_0} = 1 + \frac{F_1^s}{3}, \quad (1.2)$$

where F_1^s is a symmetric Landau parameter. In the case of HF systems this renormalization factor has very large values, leading to heavy QPs with values of the effective masses, m_{HF}^* , up to 1000 times larger than m_0 .

The low-temperature thermodynamic and transport properties of a LFL system, described within the free-electron picture, are modified as a direct consequence of the effective mass renormalization. In the following, some of the physical properties of metals, predicted within the LFL theory for $T \rightarrow 0$ K are presented:

- The density of states at the Fermi energy is given by:

$$N(E_F) = \frac{m^* k_F}{\pi^2 \hbar^2}. \quad (1.3)$$

- The temperature-independent Pauli susceptibility is defined by:

$$\chi = \frac{\mu_0 \mu_B^2 m^* k_F}{\pi^2 \hbar^2} \frac{1}{1 + F_0^a}, \quad (1.4)$$

with F_0^a being the antisymmetric Landau parameter.

- The electronic specific heat behaves as:

$$\frac{C}{T} = \gamma = \frac{m^* k_F k_B^2}{3 \hbar^2}. \quad (1.5)$$

- The Wilson ratio is defined as:

$$R_W = \frac{\pi^2 k_B^2}{3 \mu_0 \mu_B^2} \frac{\chi}{\gamma} = \frac{1}{1 + F_0^a}. \quad (1.6)$$

- The electrical resistivity varies as:

$$\rho(T) = \rho_0 + AT^2, \quad (1.7)$$

where ρ_0 is the residual resistivity and the A coefficient reflects the cross-section of the QP-QP scattering, $A \propto \gamma^2 \propto N(E_F)^2$.

As in the case of normal metals, the low-temperature properties of certain HF systems can usually be described within the LFL theory. Therefore, the above-listed formulas also apply in the case of HF systems, with the corresponding mass renormalization.

1.3.2 Non-Fermi-liquid behavior

While certain HF systems can be described as Fermi-liquids down to sufficiently low temperatures, remarkable deviations in the thermodynamic and transport properties have been observed in a growing number of systems. The systems showing deviations from the predictions of the LFL theory are usually called non-Fermi-liquid (NFL) systems. In order to understand the unusual physical properties in these systems, several routes leading to the NFL state have been proposed. Among them one can mention the QCP scenario, the multichannel Kondo-impurity effect or the Kondo-disorder model. The main features related to NFL behavior ($T \rightarrow 0$ K) include (see also table 1.2):

- $\Delta\rho(T) \propto \pm T^n, n < 2$ - non-quadratic temperature dependence of the electrical resistivity;
- e.g. $\gamma(T) \propto -\log(T/T_0)$, $\gamma(T) \propto \gamma_0 - aT^{1/2}$ - strongly temperature-dependent specific-heat coefficient, γ ;
- e.g. $\chi(T) \propto -\log(T/T_0)$, $\chi(T) \propto bT^\beta$ ($\beta = \pm 3/2, -4/3, -1$) - divergent magnetic susceptibility, χ .

The low-temperature divergence of γ indicates the divergence of the effective mass and points towards a breakdown of the LFL theory.

As quantum critical phenomena are the most significant in the case of the Ce-based systems presented in this work, in the following part we will give an overview to some of the basic concepts related to QCPs.

1.3.3 Quantum critical phenomena

Quantum phase transitions (QPTs) are phase transitions taking place at zero temperature. The critical point related to a continuous QPT is known as a quantum critical point (QCP). Therefore, a QCP is a zero-temperature instability between two phases of matter where quantum fluctuations develop long-range correlations in both space and time [Sachdev 1999]. The difference from the case of a finite-temperature critical point consists in the fact that the thermal fluctuations of the order parameter are replaced by quantum fluctuations in the case of a QCP. In the case of a finite-temperature critical point, the coherence of quantum fluctuations is destroyed on a time scale longer than $\tau \sim \hbar/k_B T$, therefore the role of quantum fluctuations is negligible, while in the case of a QCP their role becomes significant. Classical and quantum phase transitions are both characterized by divergent correlation lengths

and correlation times but with irrelevant dynamical critical behavior in the case of classical transitions (only spatial correlations being relevant) and coupled dynamical and static critical behavior in the case of continuous QPTs. A d -dimensional quantum system can be viewed as a $d + z$ -dimensional classical system, with z being the dynamical scaling exponent. Although experimentally unusual behaviors of the physical properties of systems around a QCP have been found in many cases, a complete theoretical understanding is still missing. The large values of several physical properties of HF systems at low temperatures made this family of materials especially suited for the study of quantum critical phenomena. The ground state in rare-earth-based HF systems is usually determined by the interplay between the Kondo effect and the RKKY interaction, the latter one leading to formation of magnetic order. Therefore, in many of these systems, the magnetic transition temperature can be continuously tuned to zero temperature by an external control parameter like pressure, chemical doping or magnetic field, leading to the appearance of a magnetic QCP.

There are two main routes to look at the quantum critical behavior in HF systems. The first approach is treating the QCP within the itinerant scenario [Hertz 1976, Millis 1993, Moriya 1995, Lonzarich 1997], while the failure of its predictions in the case of some HF compounds (e.g. CeCu_{6-x}Au_x [Löhneysen 1994, Schröder 2000], YbRh₂(Si_{1-x}Ge_x)₂ [Trovarelli 2000, Gegenwart 2002]) has guided theorists to a new concept, namely the “locally critical” scenario.

Within the itinerant scenario (also called spin-density-wave (SDW) scenario), based on the role of spin fluctuations at a QCP, the behavior of the physical properties of a system close to a magnetic QCP have been theoretically estimated [Hertz 1976, Millis 1993, Moriya 1995, Lonzarich 1997]. Strong deviations from the typical LFL behavior have been found for the systems located around a QCP. The main predictions of these theories for the physical properties in the vicinity of a magnetic QCP, such as the electronic specific heat, $C(T)/T$, magnetic susceptibility, $\chi(T)$, and electrical resistivity, $\rho(T)$, together with the corresponding references, are summarized in table 1.2. Experimental findings have shown that several HF systems in the vicinity of a magnetic QCP can be described within this scenario.

Unusual properties around a QCP, such as E/T and H/T scaling and an effective charge-carrier mass which is diverging stronger than logarithmically, found in HF systems as CeCu_{6-x}Au_x [Löhneysen 1994, Schröder 2000] and YbRh₂(Si_{1-x}Ge_x)₂ [Trovarelli 2000, Gegenwart 2002] cannot be described within the itinerant scenario. In order to understand these “unconventional” properties, Si *et al.* [Si 2001] and Coleman *et al.* [Coleman 2001, Coleman 2002] have proposed the locally quantum critical scenario. In their theory, vestiges of local moments remain as local critical modes

theory	physical quantity	AFM - $z = 2$ $d = 3$	AFM - $z = 2$ $d = 2$	FM - $z = 3$ $d = 3$	FM - $z = 3$ $d = 2$
(a)	$C(T)/T$	$\gamma_0 - aT^{1/2}$	$\log(T_0/T)$	$\log(T_0/T)$	$T^{-1/3}$
	$\Delta\chi(T)$	$T^{3/2}$	$\chi_0 - dT$	-	-
	$\Delta\rho(T)$	$T^{3/2}$	T	T	-
(b)	$C(T)/T$	$\gamma_0 - aT^{1/2}$	$\log(T_0/T)$	$\log(T_0/T)$	$T^{-1/3}$
	$\Delta\chi(T)$	$T^{-3/2}$	$(-\log T)/T$	$T^{-4/3}$	$-1/(T \log T)$
	$\Delta\rho(T)$	$T^{3/2}$	T	$T^{5/3}$	$T^{4/3}$
(c)	$C(T)/T$	$\gamma_0 + T^{1/2}$	-	$\log(T_0/T)$	$T^{-1/3}$
	$\Delta\chi(T)$	$T^{-3/2}$	-	$T^{-4/3}$	T^{-1}
	$\Delta\rho(T)$	$T^{3/2}$	-	$T^{5/3}$	$T^{4/3}$

Table 1.2: Predictions for the temperature dependencies of the specific heat, C/T , susceptibility, χ , and resistivity, ρ , at low temperatures, in the NFL regime, as obtained from spin-fluctuation theories. The different theories are indicated by (a), (b) and (c). The corresponding references are: (a)-[Hertz 1976], [Millis 1993] (b)-[Moriya 1995], (c)-[Lonzarich 1997] (table taken from [Stewart 2001]).

which coexist with the long-wavelength critical fluctuations of the order parameter at the QCP.

A large reconstruction of the FS across the magnetic QCP, from a small FS on the AFM side to a large FS on the paramagnetic side of the QCP, not detectable in the case of the SDW scenario, is expected in the case of a local QCP. Different from the mean-field type of quantum critical behavior in the vicinity of a SDW type QCP, destruction of the Kondo screening or/and breaking-up of the heavy QPs into their components, conduction electrons and local $4f$ moments, was predicted. It was proposed by Si *et al.* [Si 2001] that 2D magnetic fluctuations may lead to a local type of quantum critical behavior.

Based on the experimental findings, it is believed that the existence of a SDW type of QCP in HF systems favors the appearance of a SC state around the QCP, while in the HF systems, displaying around a magnetic QCP the properties corresponding to a local type of QCP, a SC state has not been observed yet.

Chapter 2

Experimental methods

2.1 General concepts about heat capacity

The heat capacity (C) of a material is defined as the amount of heat required to change its temperature by one degree. It is an extensive variable and has units of energy per degree Kelvin,

$$C(T) = \frac{\delta Q}{dT} = T \frac{dS}{dT} \left(\frac{\text{J}}{\text{K}} \right). \quad (2.1)$$

In spite of its simple definition, the heat capacity is a complex physical property of a system, containing a global information about the constituents of the system and about the manner in which the internal energy is distributed among them. In statistical mechanics, the entropy of a system, S , is defined as:

$$S = - \left(\frac{\partial F}{\partial T} \right)_V, \quad (2.2)$$

where F represents the Helmholtz free energy. The free energy, F , is defined as:

$$F = - \frac{k_B T}{\ln Z}, \quad (2.3)$$

Z being the partition function of the system:

$$Z = \sum_i \exp \left(\frac{-E_i}{k_B T} \right), \quad (2.4)$$

where the summation is over all the allowed states of the system. Since all different modes in a system (electronic, translational, vibrational, rotational, etc.) contribute additively to the energy of a state, the partition function can be expressed as a product of the partition functions corresponding to each different mode. Therefore,

it is obvious that the heat capacity of the system is a sum of all the contributions from these different modes and its variation with temperature depends on the particular temperature dependence of each of these modes. With simple models one can estimate the contribution to the heat capacity of the system of each of the existing modes and in this way, by fitting the experimental data, one can get information about different properties of the system.

The principle of heat-capacity measurements is quite simple and follows from its definition (see equation 2.1). An accurate knowledge of the energy input to the system (δQ) and of the resulting change in temperature (dT), in the conditions where the system is adiabatically isolated, gives the value of the heat capacity of the system. This method, called “adiabatic calorimetry”, was introduced by Nernst and Eucken in 1910 and it was the most used technique until the mid 1960’s when other techniques became available. Nowadays, among the most developed techniques for measuring heat capacity, one should mention the alternating current method (a.c. method), the relaxation-time technique, continuous heating method, the differential calorimetry and the quasiadiabatic heat-pulse technique. Each of these methods has different advantages and disadvantages, depending mainly on the temperature range of interest, on the thermal conductivity of the sample and on the sample mass. Measurements of the heat capacity become more difficult in the case of extreme conditions like very low temperatures or high pressures. In the following we will focus on low-temperature heat-capacity measurements under high pressure. For this purpose two main techniques were developed:

- i) the quasiadiabatic heat-pulse technique, available for $0.05 \text{ K} \leq T \leq 10 \text{ K}$ and $p \leq 4 \text{ GPa}$;
- ii) the a.c. calorimetry, available for $0.05 \text{ K} \leq T \leq 10 \text{ K}$ and $p \leq 30 \text{ GPa}$.

The latter one has the advantage of a broader pressure range but it does not give accurate absolute values of $C(T, p, B)$. In the next part we will describe the quasiadiabatic heat-pulse technique in the case of heat-capacity measurements under pressure.

2.2 The quasiadiabatic heat-pulse technique used for measurements of heat capacity under high pressure and at low temperatures

Most of the heat-capacity measurements presented in this work have been performed by using the compensated quasiadiabatic heat-pulse technique implemented

for low-temperature heat-capacity measurements under high pressure. This technique is meant to be used mainly to investigate the effect of pressure on the heat capacity of HF materials, where it is well known that the effective mass of the QPs, m_{QP}^* , which is proportional to $C(T)/T$ at low temperatures, is of the order of $m_{QP}^* \approx (100 \div 1000)m_{el}^*$, where m_{el}^* represents the effective mass of an electron in a simple metal such as Cu. At the basis of these measurements stays the quasiadiabatic heat-pulse technique but implemented for usage in the case of high sample masses. In order to obtain heat-capacity data under pressure, the studied samples have to be enclosed and pressurized in a pressure cell before the heat capacity of the loaded pressure cell can be measured. The heat capacity of the studied material is then obtained by measuring the heat capacity of the complete pressure cell loaded with $m \approx (0.3 \div 0.5)$ g of sample from which is subtracted the heat capacity of the empty pressure cell measured under the same conditions. Because of the large heat capacity of the empty pressure cell, to achieve good accuracy in the obtained results, only materials having a high heat capacity, such as HF systems, are suited for these measurements.

As mentioned earlier, the heat capacity of a material is an extensive variable and therefore depends on the quantity of the material measured. The corresponding intensive variable is the specific heat (C). Unlike the heat capacity, the specific heat is a physical property which does not depend on the measured quantity. The units for specific heat are J/(kgK) or J/(molK).

2.2.1 Compensated quasiadiabatic heat-pulse technique

The quasiadiabatic heat-pulse technique is based on the principle of the adiabatic calorimetry. The studied system is isolated adiabatically from the environment. At a certain temperature, T , a well-known heat pulse δQ is applied to the system and the resulting increase in temperature, dT , is accurately measured. The heat capacity of the system is then computed as $C(T + dT/2) = \delta Q/dT$. The difference between the basic technique and the compensated quasiadiabatic heat-pulse technique consists in the fact that, in the case of the latter, the temperature of the environment is kept always constant at a lower temperature than the studied sample and, due to the quasiadiabatic conditions, the losses from the sample to the bath during the entire measurement are evaluated and compensated. A schematic description of the compensated quasiadiabatic heat-pulse technique is presented in figure 2.1. A data point is taken between each two consecutive steps, k and $k + 1$. One step consists of a heating time (Δt), waiting time and a short computing time. At each step k , a heat pulse of $Q^k = P_0^k \Delta t$ (P_0^k - applied power, Δt - heating time) is given to the sample and the temperature increase ΔT^k is measured. Between application of two

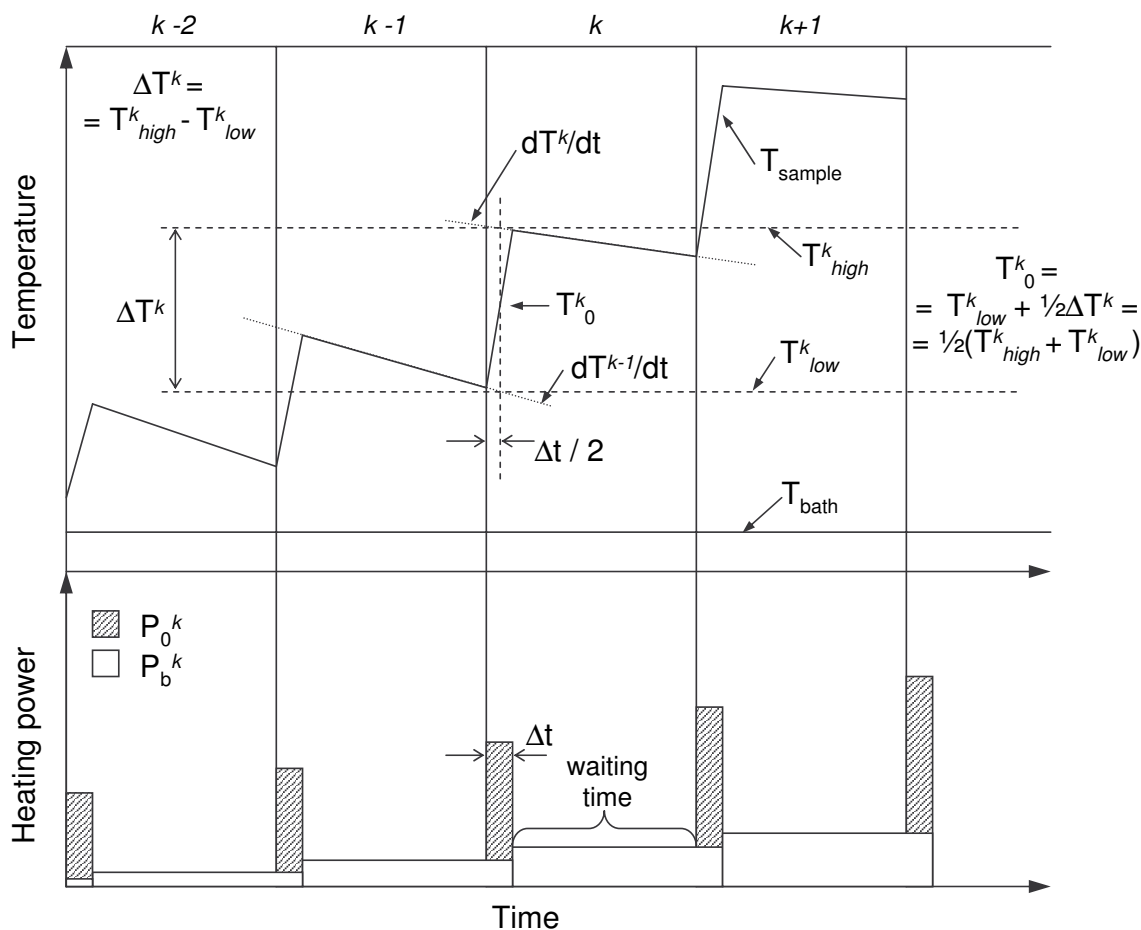


Figure 2.1: Schematic description of the compensated quasiadiabatic heat-pulse technique. P_0^k and P_b^k represent the applied power (heat pulse) and the background power, respectively.

consecutive heat pulses, in the waiting time, the evolution of the sample temperature in time, $T^k(t)$, is monitored. The bath temperature T_{bath} is maintained constant over the entire measurement. Placing a quasiadiabatically isolated sample in a colder environment ($T_{bath} < T_{sample}$) is leading to a continuous heat flow from the sample to the bath. Therefore, instead of a constant $T^k(t)$ dependence of the sample temperature after each heat pulse Q^k expected in adiabatic conditions ($dT^k/dt = 0$), a relaxation of the sample temperature towards the bath temperature is detected ($dT^k/dt \leq 0$). For each step k , from the decay of T^k in the waiting time (dT^k/dt), the background power, P_b^k , needed to compensate the losses to the bath (to obtain $dT^k/dt \approx 0$) is iteratively estimated and applied to the sample. A fit to the $T^k(t)$ data starting from a certain $t^* > \Delta t$ is done in order to extrapolate the dependence of the sample temperature, T^k , in the time interval outside of the waiting time. A linear fit to the $T^k(t)$ data is usually used. As described in the figure 2.1, the temper-

ature increase, ΔT^k , is evaluated at half of the heating interval Δt , by extrapolating the detected $T^k(t)$ and $T^{k-1}(t)$ behaviors, by using the parameters from the above-mentioned linear fits, dT^k/dt and dT^{k-1}/dt , to the corresponding values at $\Delta t/2$, T_{high}^k and T_{low}^k ($\Delta T^k = T_{high}^k - T_{low}^k$). The value of the heat capacity is then computed for T_0^k , as $C^k(T_0^k)$, where T_0^k represents the sample temperature estimated as $T_0^k = T_{low}^k + 1/2\Delta T^k = 1/2(T_{low}^k + T_{high}^k)$ (see figure 2.1). In order to compensate the heat flow from the sample to the bath, the background power, P_b^k , is applied to the sample over the entire duration of a step (including heating, waiting and computing time), but in calculating $C^k(T)$ is not taken into account as a heat source for the obtained ΔT^k . A more detailed description of the computing of the specific heat in the case of the compensated quasiadiabatic heat-pulse technique is given in [Hellmann 1993].

2.2.2 High pressure

Pressure is one of the most important control parameters in the field of solid state physics. The application of pressure can produce structural, electronic or other kinds of phase transitions reducing the interatomic spaces in a material in a clean and controllable way. Compared to other control parameters such as chemical doping, which introduces additional atomic disorder, or application of a magnetic field, breaking the time-reversal symmetry, hydrostatic pressure offers the chance to tune a system through phase transitions only by reducing its volume, in this way helping in the understanding of the underlying phenomena. Particularly, the field of strongly correlated electron systems requires the use of high pressure in combination with low temperatures and high magnetic fields. Therefore, measurements of the heat capacity under such conditions are very demanding. Pressure cells must be prepared from special hard materials which are non-magnetic, are maintaining their good mechanical properties from room temperature down to low temperatures and do not become brittle upon cooling. As we have already mentioned at the beginning of this chapter, two different types of measurement techniques are available for heat-capacity measurements under high pressure and at low temperatures. While the quasiadiabatic heat-pulse technique requires the usage of piston-cylinder type pressure cells, the a.c. method can be used in combination with different high-pressure techniques, such as piston-cylinder type pressure cells or anvil type pressure cells. However, the a.c. technique has the disadvantage of measuring the heat capacity of the system only in arbitrary units, while the quasiadiabatic heat-pulse technique offers a good accuracy in obtaining the absolute values of the heat capacity. The anvil type pressure cells, being used only in combination with the a.c. calorimetry, have the advantage



Figure 2.2: Piston-cylinder type pressure cells used for specific-heat measurements at low temperatures. Left photo (a): double-layer pressure cell (type II - Ni-Cr-Al inner layer, CuBe outer jacket); right photo (b): mono-layer pressure cell (type I - CuBe). The different components of the cells are indicated by numbers from 1 to 9. 1: locking nut (CuBe); 2: blocking disc (*a* - tungsten carbide (WC), *b* - CuBe); 3: piston (WC); 4: sealing ring (CuBe); 5: POM capsule (sample space); 6: plug (*a* - WC, *b* - CuBe); 7: main body of the pressure cell; 8: blocking disc (*a* - Ni-Cr-Al); 9: locking nut (CuBe).

of a relatively large pressure range ($p \leq 30$ GPa) and large temperature range, but the heat capacity is obtained only in arbitrary units. The piston-cylinder type cells, when used together with the quasiadiabatic heat-pulse technique, offer a very good accuracy in the absolute values of the heat capacity, but have a much lower limit for the highest achievable pressure ($p \leq 4$ GPa) [Eremets 1996]. In this study, for the measurements of specific heat under pressure, we have used piston-cylinder type

pressure cells combined with the compensated quasiadiabatic heat-pulse technique. Good materials for this type of pressure cells are the non-magnetic alloys, as copper-beryllium alloy (CuBe) [Fujiwara 1980], the Ni-Cr-Al alloy [Uwatoko 2002] and the Co-Ni-Cr-Mo alloy (MP35N) [Walker 1999]. Experiments show that the pressure limit for piston-cylinder type cells is about 4 GPa. Pressure cells made out of mono-layer CuBe can reach at low temperatures a maximum value of 2 GPa, while double-layer type cells, using an inner layer of either Ni-Cr-Al or MP35N and an outer layer of CuBe can reach at low temperatures pressures up to about $(3.5 \div 4)$ GPa. Unfortunately, due to its large heat capacity at low temperatures, the MP35N alloy cannot be used for heat-capacity measurements at low temperatures. Therefore, in this work we have used two types of piston-cylinder pressure cells, one for the lower pressure range ($p \leq 1.6$ GPa), made from a mono-layer of CuBe (type I), and a double-layer type pressure cell (type II), made from an inner cylinder of Ni-Cr-Al and an outer jacket of CuBe, for the higher pressure range ($1.6 \text{ GPa} \leq p \leq 2.1$ GPa). Even though the Ni-Cr-Al alloy is known since the late 70's [Eremets 1996], it is available on the market only since 2001 [Uwatoko 2002]. Therefore, to our knowledge, the double-layer type pressure cell, with the inner layer made from the Ni-Cr-Al alloy, was developed and used in this thesis for the first time to measure the specific heat under hydrostatic pressure. Figure 2.2 shows photos of the unloaded pressure cells used in this work. The components of the pressure cells are indicated in the figure by numbers and are described in the figure caption. The CuBe and the Ni-Cr-Al alloy used for the pressure cells have been undergoing special thermal treatment in order to achieve the hardness needed to reach high pressures. The pressure is applied at room temperature (from top, as viewed in figure 2.2) and clamped by the locking nut. A total sample mass of about $(300 \div 500)$ mg, is placed in the POM (polyoxymethylene) capsule. A small piece of In or Sn, placed next to the sample inside of the POM capsule serves as pressure sensor, while a second piece is placed outside of the cell as reference sample for ambient pressure. The pressure in the cell is detected at low temperature, in the same range of temperature as the measurements of the specific heat are carried out. A more detailed description about the estimation of pressure will be given later. The POM capsule is then filled up with the pressure transmitting medium and sealed by a plug. For heat-capacity measurements under pressure, at low temperatures and in high magnetic fields, the pressure transmitting medium, as well as other materials used in the construction of the pressure cell, is required to be non-magnetic, to exhibit at low temperatures a good thermal conductivity and a low heat capacity, as well as a low pressure dependence of its heat capacity. In addition, the pressure transmitting medium needs to be chemically inactive and to

not solidify at room temperature in the used pressure range. In our measurements, we have used fluorinert FC72 as pressure transmitting medium, a liquid which offers good quasi-hydrostatic conditions. Teflon, a material often used in pressure cells, has been also tested for preparing capsules. Despite of its good mechanical properties at high pressures, it is softer than POM and, therefore, it is more difficult to use it for sealing volatile liquids (such as fluorinert FC72) in order to prevent them from escaping. Moreover, the heat capacity of a capsule prepared from POM is smaller than that of one made from teflon. Therefore, we have used capsules of POM in our experiments. The available sample volume in both types of our pressure cells is similar, while the total mass, as well as the total heat capacity, of the type I cell is smaller. The mono-layer cell is weighing about 65 g in comparison to about 82 g in the case of the double-walled pressure cell.

2.3 Measurements under hydrostatic pressure and data analysis

2.3.1 Experimental setup

Heat-capacity, $C(T, B, p)$, measurements under pressure were done in a single-shot ^3He evaporation cryostat equipped with a SC magnet providing a magnetic field up to $B = 8$ T. The temperature range of the measurements is $0.35 \text{ K} \leq T \leq 7 \text{ K}$, but temperatures down to $T \approx 0.26 \text{ K}$ were also obtained by using adiabatic demagnetization of the magnetic moments of the Cu contained in the pressure cells. A compensated-coil system attached to the equipment allows us, in addition to the $C(T)$ measurements, to detect SC phase transitions by a.c.-susceptibility ($\chi_{a.c.}(T)$) measurements. Unfortunately, the resolution of the coil is not high enough for the detection of AFM phase transitions. The coil is therefore used for the detection of SC phase transitions of any sample studied under pressure, as well as to determine the pressure in the cell by measuring the pressure-induced shift of the SC transition temperature of Sn or In. During the measurements, the pressure cell is fixed in the cryostat in the center of the SC magnet, as well as inside of the compensated coil, by attaching it to a silver rod. In order to obtain a good thermal insulation of the pressure cell from the environment, the silver rod is fixed to the ^3He system by nylon wires. On the upper end of the silver rod, in the compensated region of the magnet, two thermometers are mounted. To assure a heat flow to the thermometers through the sample when a heat pulse is given to the measured assembly, a heater is attached to the bottom of the pressure cell. In order to cool down the pressure cell,

a mechanical switch operated at room temperature from the top of the cryostat is used to connect the pressure cell to the ^3He bath. To isolate the pressure cell from the environment during the measurements, the contact to the ^3He bath is opened. A more detailed description of the system, as well as of the electronic setup used for the measurements, is contained in [Hellmann 1993].

2.3.2 Measurement techniques

Heat-capacity measurements - $C(T, B, p)$

The heat-capacity measurements under pressure were performed by employing the compensated quasiadiabatic heat-pulse technique. The measured ensemble consists of the pressure cell, the silver rod used to fix the cell, two thermometers mounted on the silver rod and a heater attached to the pressure cell. The studied sample is loaded in the pressure cell. In order to get the heat capacity of the sample, measurements of the heat capacity of the pressure cell without sample inside (addenda) have to be performed. The sample heat capacity is then calculated by subtracting the measured addenda from the total heat capacity obtained with the sample included. Special attention must be paid to the pressure and magnetic-field dependence of the measured addenda. Therefore, the addenda must be measured in all the different magnetic fields and at different pressures. The variation with pressure of the addenda is caused by the pressure-dependent heat capacity of the POM, flourinert FC72 and In (or Sn) used in the pressure cell. The components of the pressure cell made out of hard materials, as CuBe, WC, Ni-Cr-Al, do not show any significant pressure-dependent but rather a magnetic-field-dependent heat capacity in the temperature and pressure range of our measurements.

In this work we have used 4 pressure cells, 3 of type I and one type II pressure cell. The addenda of each pressure cell was measured for all magnetic fields used later in the heat-capacity measurements of the different samples. For the pressure dependence of the specific heat of POM and flourinert FC72 one of the pressure cells, without sample but containing the POM capsule and the pressure transmitting medium, flourinert FC72, was pressurized and its heat capacity was measured at 4 different pressures. The obtained data were then interpolated in order to derive the data for the complete pressure range.

Figures 2.3 and 2.4 show, as examples, the temperature dependencies of the contribution to the total measured heat capacity (C_{total}) of the different components, such as sample (C_{sample}), POM capsule ($C_{POM\ capsule}$), pressure sensor (In or Sn) ($C_{Sn-inside\ the\ cell}$), pressure transmitting medium ($C_{Flourinert\ FC72}$) and the pressure

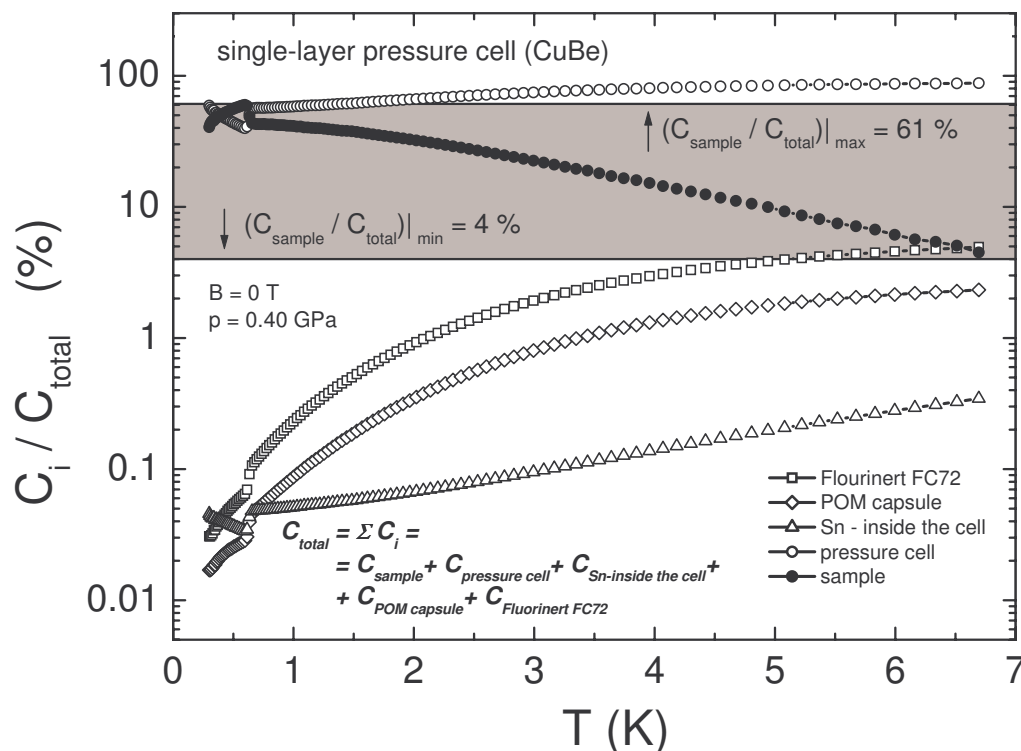


Figure 2.3: Contribution of the different components of the pressure cell to the total measured heat capacity, C_i/C_{total} , as function of temperature, obtained for the case of measurements of $CeCu_2Si_2$ at $p \approx 0.40$ GPa, performed in a mono-layer (type I) pressure cell. The different components, i , are indicated in the figure. $C_{pressure\ cell}$ refers to the total heat capacity of the pressure cell containing only the metallic parts (except the pressure sensor (Sn in this case) from inside the cell), silver rod, thermometers and heater. The full symbols indicate the sample contribution to the total heat capacity. The hatched area marks the region where the C_{sample}/C_{total} is located at different temperatures.

cell ($C_{pressure\ cell}$), used in one measurement of specific heat under pressure. In these plots, we have included in $C_{pressure\ cell}$ the heat capacity of the silver rod, thermometers and heater used in the experiment, as well as the heat capacity of the bare pressure cell without POM capsule, pressure transmitting medium and pressure sensor. The different contributions to the total measured heat capacity, C_i/C_{total} , are presented in percentage (%) and are shown in a logarithmic scale. The magnetic field and pressure are indicated in the figures. The hatched region in both figures is marking the region where the contribution of the measured sample is located. The minimum and maximum values are indicated in the figures. In figure 2.3, where a mono-layer (type I) pressure cell was used, the contribution of the sample to C_{total} is,

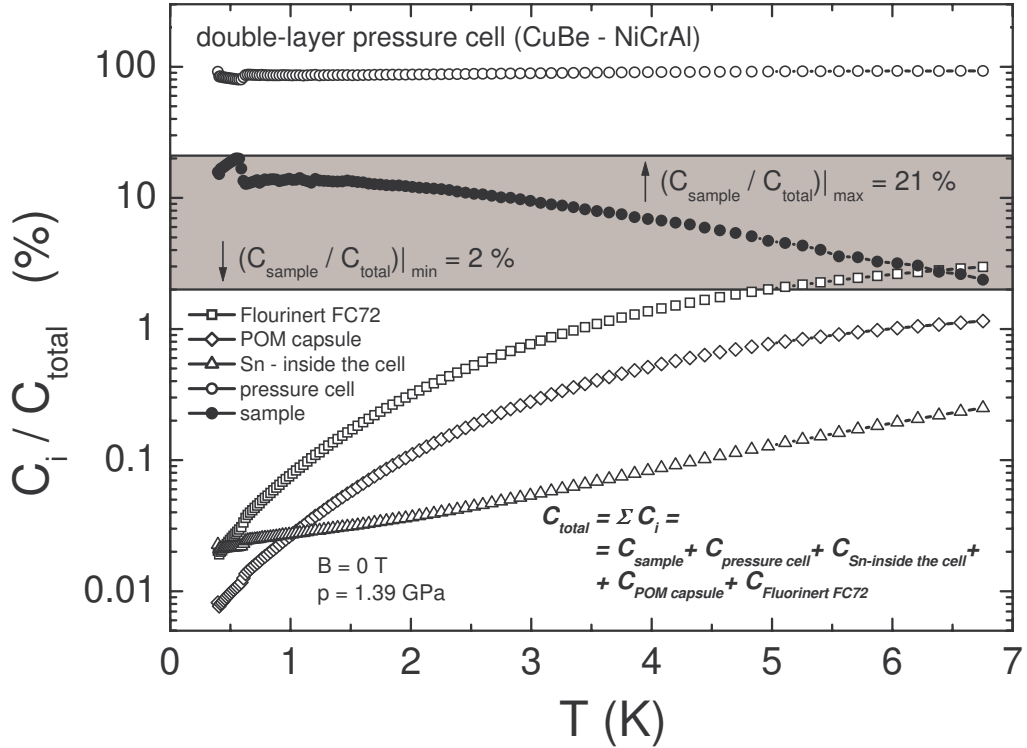


Figure 2.4: Contribution of the different components of the pressure cell to the total measured heat capacity, C_i/C_{total} , as function of temperature, obtained for the case of measurements of $CeCu_2Si_2$ at $p \approx 1.39$ GPa, performed in a double-layer (type II) pressure cell. The different components, i , are indicated in the figure. $C_{pressure\ cell}$ refers to the total heat capacity of the pressure cell containing only the metallic parts (except the pressure sensor (Sn in this case) from inside the cell), silver rod, thermometers and heater. The full symbols indicate the sample contribution to the total heat capacity. The hatched area marks the region where the C_{sample}/C_{total} is located at different temperatures.

at low temperatures, about 40% to 60%, while at higher temperatures this value is strongly decreasing, reaching at about $T \approx 7$ K only 4%. In the case of the double-layer (type II) pressure cell the resolution in measuring a sample is strongly reduced due to the much larger heat capacity of the pressure cell. However, as seen in figure 2.4, good values as C_{sample}/C_{total} from 2% to 21% can be obtained. As seen in the presented examples, the largest contribution to C_{total} is coming either from the pressure cell or from the measured sample. However, the pressure transmitting medium, the POM capsule and the pressure sensor are also having remarkable contributions to C_{total} , C_i/C_{total} reaching at high temperatures ($T \approx 7$ K) values up to 5% (see, e.g. figure 2.3).

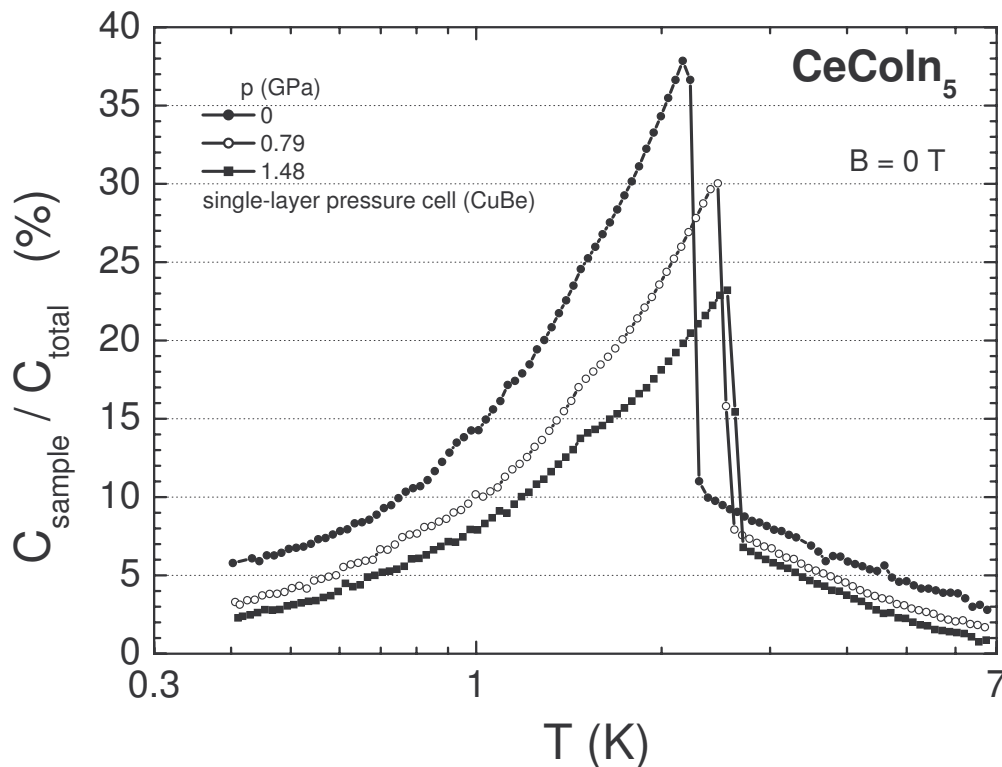


Figure 2.5: $C_{\text{sample}}/C_{\text{total}}$ versus T for different pressures, estimated in the case of heat-capacity measurements under pressure on CeCoIn_5 . A mono-layer type pressure cell (type I) was used for the measurements. The pressure interval shown in the figure covers the complete pressure and temperature range presented in this work.

In order to estimate the accuracy of the measurements of the heat capacity under pressure presented in this work we have summarized the pressure and temperature dependencies of $C_{\text{sample}}/C_{\text{total}}$ in figures 2.5, 2.6 and 2.7. Each figure corresponds to measurements done on a specific compound, CeCoIn_5 in figure 2.5, Ce_2RhIn_8 in figure 2.6 and CeCu_2Si_2 in figure 2.7. The pressure values, as well as the type of the pressure cell used in the respective pressure range, are indicated in the figures. For each compound, the whole pressure and temperature range presented in this work is covered.

Estimation of the transition temperatures from $C(T)$ data

In order to determine the transition temperatures from the measured specific-heat data, the entropy-balance technique was employed. A second-order phase transition is usually characterized by a finite jump in the specific-heat value right at the

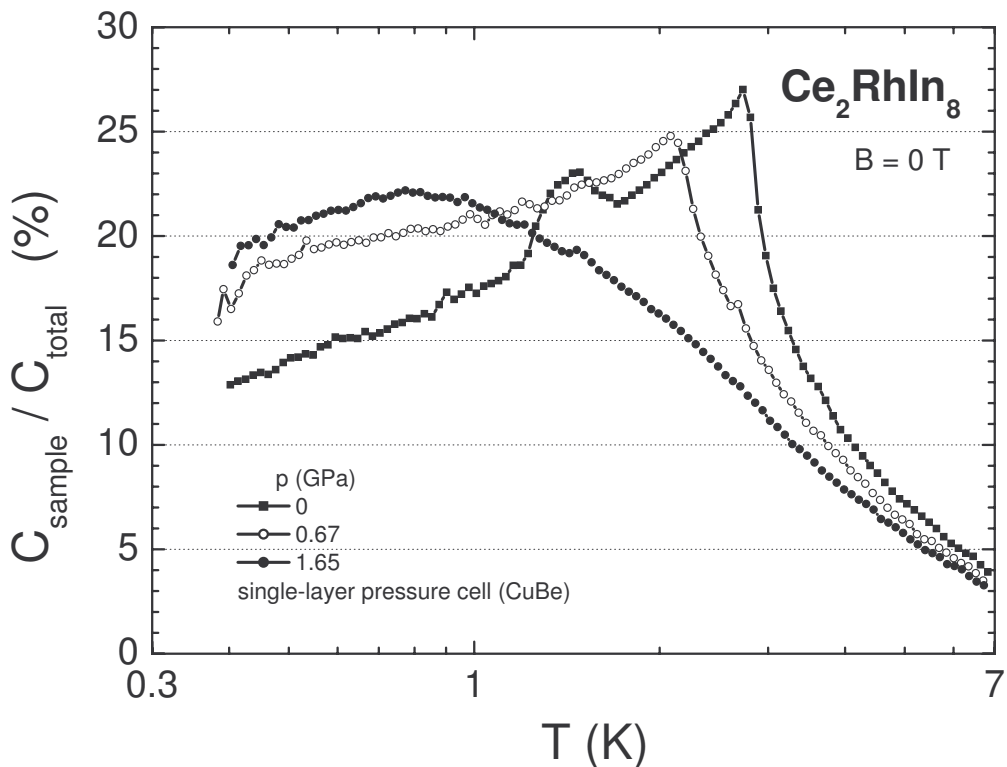


Figure 2.6: $C_{\text{sample}}/C_{\text{total}}$ versus T for different pressures, estimated in the case of heat-capacity measurements under pressure on Ce_2RhIn_8 . A mono-layer type pressure cell (type I) was used for the measurements. The pressure interval shown in the figure covers the complete pressure and temperature range presented in this work.

transition temperature ($\Delta S = 0$). In real measurements, the detected anomaly has a tendency of broadening and the jump in $C(T)$ does not take place right at the transition temperature but extends over a wider temperature range (around the transition temperature). Therefore, in the entropy-balance method, the shape of the anomaly seen in specific heat at any kind of second-order phase transition is idealized in order to reconstruct the sharp transition expected theoretically. Figure 2.8 depicts how this method is used. The shape of the anomaly seen in $C(T)/T$, shown by open circles, is idealized by extrapolating the data of $C(T)/T$ before and after the phase transition (see the two continuous lines extending the data). As known, the area enclosed by $C(T)/T$ versus T corresponds to entropy,

$$\Delta S \Big|_{T_1}^{T_2} = \int_{T_1}^{T_2} \frac{C(T)}{T} dT. \quad (2.5)$$

As suggested by the name of the method, the transition temperature, labeled T_c , is taken right at the temperature where the entropy lost by the broadening of the tran-

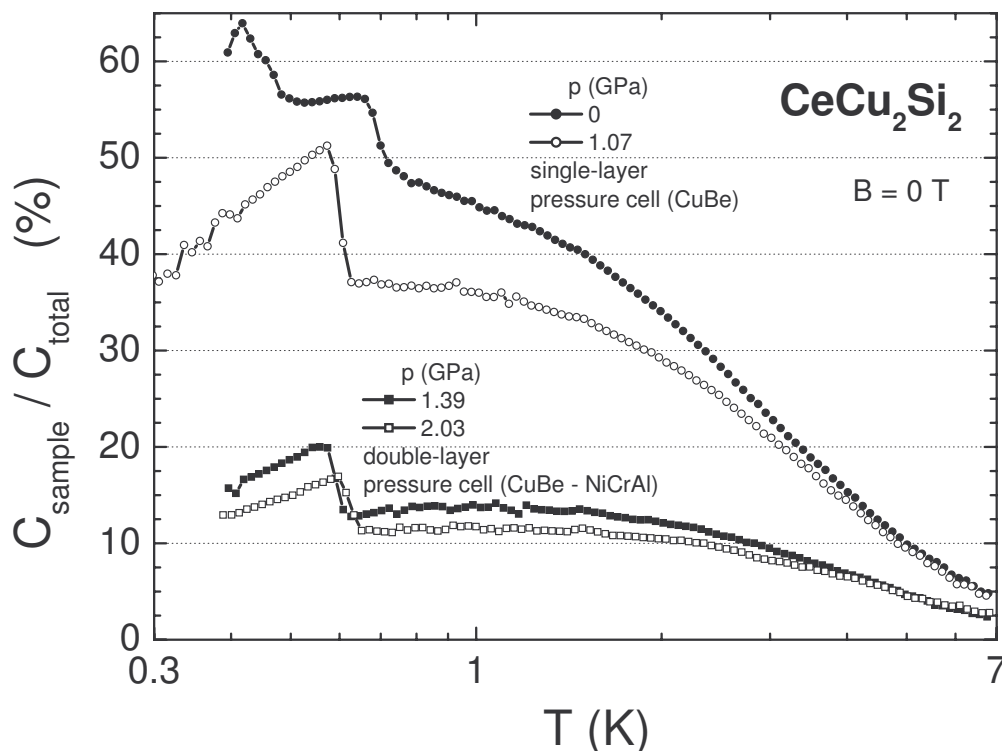


Figure 2.7: $C_{\text{sample}}/C_{\text{total}}$ versus T for different pressures, estimated in the case of heat-capacity measurements under pressure on CeCu_2Si_2 . A mono-layer type pressure cell (type I) was used for the measurements between $0 \text{ GPa} \leq p \leq 1.07 \text{ GPa}$, while for the pressure range $1.39 \text{ GPa} \leq p \leq 2.03 \text{ GPa}$ a double-layer (type II) pressure cell was employed. The complete pressure and temperature range presented in this work is covered by the data shown in the figure.

sition, A_1 , is recovered at temperatures right above T_c , A_2 . In figure 2.8, the hatched regions depict A_1 and A_2 , while the vertical line, marking T_c is taken in such a way that $A_1 = A_2$. Also described in the figure, the ratio of $\Delta C/(\gamma_n T_c)|_{T=T_c}$, characterizing the phase transition, is estimated by using the values of $C_n(T_c)/T_c = \gamma_n$ and $C_s(T_c)/T_c = \gamma_s$ obtained from the idealized phase transition. The indices n , respectively s , correspond to the normal state (n , $T > T_c$) and to the ordered/superconducting state (s , $T \leq T_c$).

Determination of pressure

The estimation of pressure has been done in the same temperature range as the measurements were performed. The SC transition temperature of our pressure sensor (In or Sn), placed in the pressure cell under the same conditions as the samples,

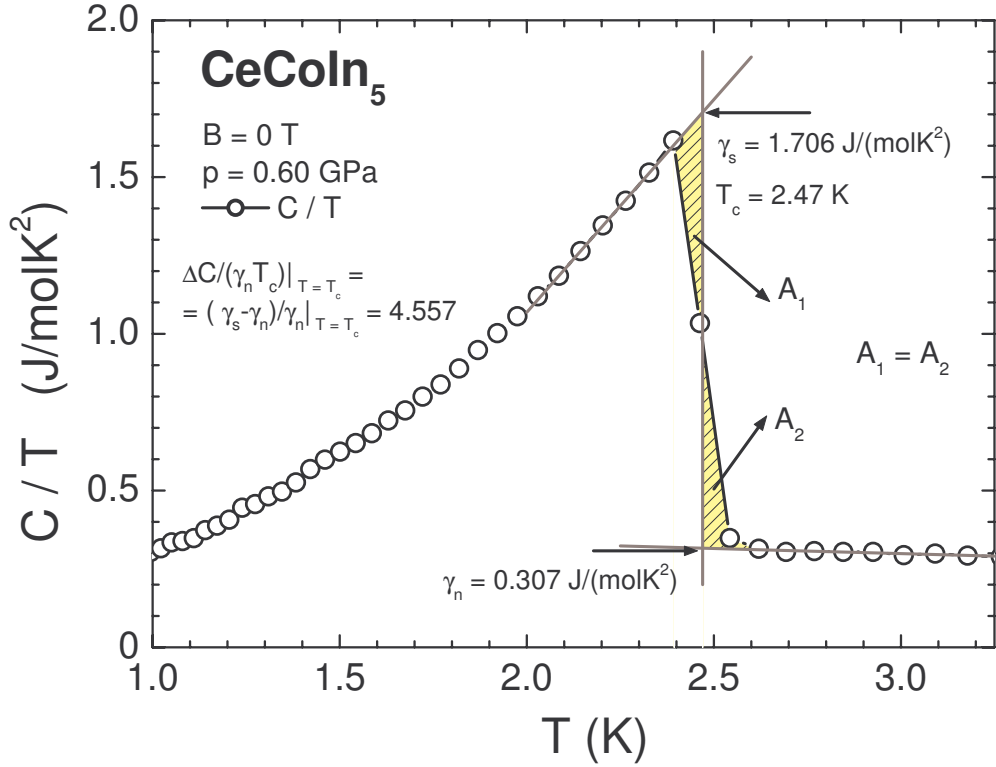


Figure 2.8: Description of the entropy-balance technique used to estimate the transition temperature from the anomaly seen at a second-order phase transition in specific-heat data. Open symbols represent the measured C/T data, while the two continuous lines on top of the data are representing the extrapolation of the measured $C(T)/T$ below and above the transition temperature, T_c . The vertical line marks the value of T_c . The area of the hatched regions, A_1 and A_2 , are corresponding to entropy. T_c is defined by the condition: $A_1 = A_2$. The index n is used for *normal state*, while s refers to the *ordered/superconducting state*. (Superconducting transition of CeCoIn_5 at $p \approx 0.60 \text{ GPa}$, $B = 0 \text{ T}$, as an example.)

is detected by $\chi_{a.c.}(T)$ measurements. In the case of In or Sn, the evolution of T_c with pressure is well established in literature [Eiling 1981]. In order to obtain the reference T_c at ambient pressure, a similar piece of In, respectively Sn, as used in the pressure cell, is fixed outside of the cell. Figure 2.9 exemplifies the $\chi_{a.c.}(T)$ signal as function of T obtained from the two pieces of Sn (inside and outside of the pressure cell) used to monitor the pressure in our experiments. The values of T_c obtained from the differently placed pieces of Sn are indicated in the figure by arrows. The SC transition at higher T is coming from the Sn placed outside of the pressure cell, always at ambient pressure, while at lower T the SC transition of the pressurized Sn,

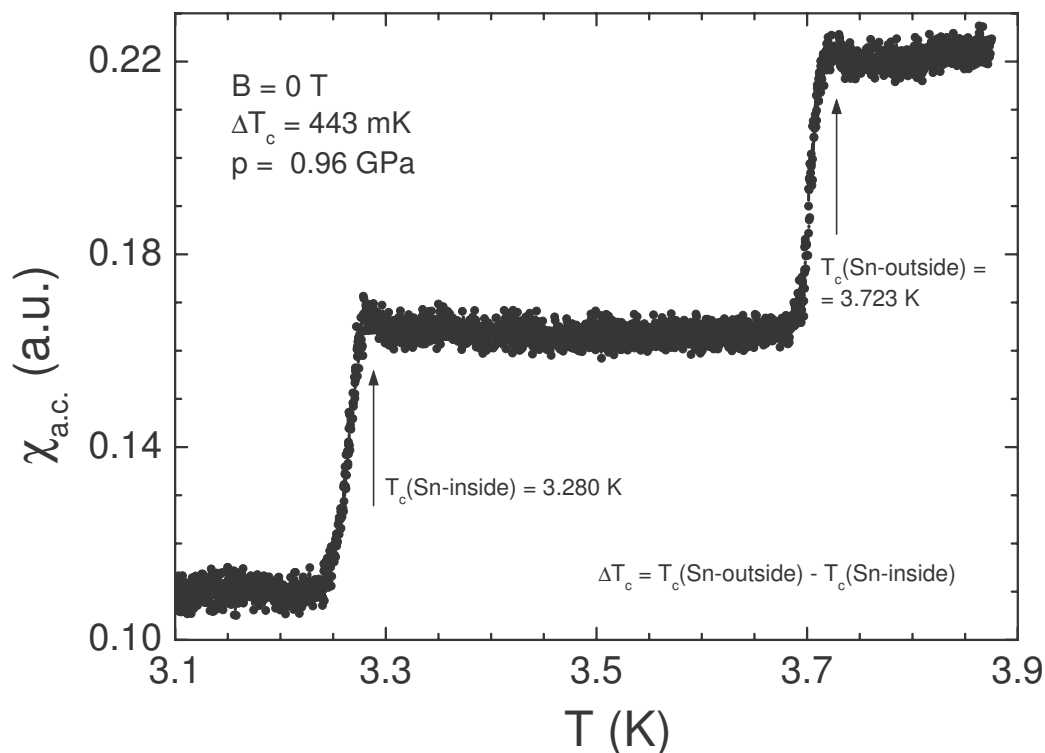


Figure 2.9: $\chi_{a.c.}(T)$ versus T showing the SC phase transitions of the two Sn samples used to monitor the pressure in the pressure cell. The SC transition at higher T is used as reference and corresponds to the piece of Sn at ambient pressure, placed outside of the pressure cell ($T_c(\text{Sn} - \text{outside})$), while at lower T , the SC transition of the pressurized piece of Sn, located in the pressure cell ($T_c(\text{Sn} - \text{inside})$), can be seen. The pressure is estimated from the difference of the two transition temperatures, ΔT_c , conform to a dependence known from literature [Eiling 1981].

located in the pressure cell, can be seen. In accordance to [Eiling 1981], the obtained $\Delta T_c \approx 0.443$ K corresponds, in the case of Sn, to a pressure of $p \approx 0.96$ GPa. Up to the highest pressure of our measurements, the width of the detected SC phase transition is narrow and stays within the same limits for both pieces of Sn, independent of their location, inside or outside of the pressure cell, showing the good hydrostatic conditions achieved in our experiments.

A.c.-susceptibility measurements - $\chi_{a.c.}(T, B, p)$

A.c.-susceptibility measurements in different magnetic fields, $\chi_{a.c.}(T, B, p)$, for detection of the SC phase transitions have been performed parallel to the specific-heat measurements under pressure. The compensated-coil system, also used for detecting

the SC transition of the pressure sensor placed in the pressure cell, was used to reveal the diamagnetic signal from the SC samples. The SC transition temperature, T_c , was determined as being the temperature where 50% of the transition was reached. The width of the transition was estimated from the temperature where the onset of the transition is detected, T_c^+ , to the temperature where the transition is fully developed, T_c^- . As error bars for T_c we have taken the distances from T_c to T_c^+ and T_c^- , respectively.

Magnetocaloric measurements - $T(B, p)$

Quasiadiabatic $T(B)$ scans have been carried out at different pressures. The same configuration, as used for the specific-heat measurements under pressure, has also been used for monitoring the temperature variation of the adiabatically isolated pressure cell loaded with samples, while the magnetic field was slowly swept. The system was thermally disconnected from the bath and the bath temperature was kept constant during the measurements. The obtained data represent not only the temperature change of the sample due to the change of B but the temperature variation of the complete system including the pressure cell, mounting rod, thermometers and heater. The obtained $T(B)$ data were used to detect transition temperatures. In order to obtain reliable data, in the temperature and magnetic-field range where measurements with samples were performed, the same experiment was carried out on the empty pressure cell. More details about the way we have processed our $T(B)$ data are contained in the section 4.3.3.

2.4 Measurements in a Quantum Design PPMS

Several measurements of the specific heat ($C(T, B)$) and electrical resistivity ($\rho(T)$) at ambient pressure have been conducted in a Quantum Design PPMS equipped with a ^3He unit. For the heat-capacity measurements, a relaxation-time technique was employed. In comparison to the quasiadiabatic heat-pulse technique, where measurements can be performed only while heating the system, the relaxation-time technique allows measurements to be done both while cooling and while warming the system. Hysteretic behavior between the data taken on warming respectively on cooling the system helps to identify the first-order character of a phase transition. The electrical-resistivity measurements were performed by a standard a.c. four-point technique. The SC transition temperature in the case of electrical-resistivity measurements was taken at the temperature where the resistivity is reaching the value of $\rho = 0 \mu\Omega\text{cm}$.

Chapter 3

$Ce_n T_m In_{3n+2m}$ (T: Co, Rh, Ir) family of heavy-fermion systems

3.1 Introduction

The discovery of SC in the HF compound $CeCu_2Si_2$ in 1979 [Steglich 1979] has motivated scientists to search for other Ce-based HF compounds displaying SC either at ambient pressure or under application of pressure. However, for the following 20 years, the tetragonal 122 compounds, similar to $CeCu_2Si_2$, crystallizing in the $ThCr_2Si_2$ structure were in the focus of research. The only other Ce-based HF compound known to form in a different crystal structure and showing pressure-induced SC was the cubic $CeIn_3$ ($T_c \approx 0.25$ K at $p \approx 2.6$ GPa) [Walker 1997]. The discovery of the $Ce_n T_m In_{3n+2m}$ (T: transition metal) family of HF compounds, opened a new route in the history of HF SC. Based on the cubic $CeIn_3$ ($m = 0, n = \infty$), the $Ce_n T_m In_{3n+2m}$ ($n = 1, 2, m = 1$) compounds are known to form with Co, Rh or Ir as transition metals (T). All but one of the members of this family either show SC at ambient pressure or they become SC when they are subject to high pressure. Ce_2IrIn_8 ($m = 1, n = 2, T = Ir$) is the only exception where until now, neither bulk SC nor magnetic order was observed down to $T \approx 50$ mK [Thompson 2001]. $CeCoIn_5$ ($m = 1, n = 1, T = Co$), an ambient-pressure HF SC, displays SC below a transition temperature of $T_c \approx 2.3$ K [Petrovic 2001a]. This transition temperature is known to be the highest among all ambient-pressure Ce-based HF SCs. Its bi-layer relative, Ce_2CoIn_8 ($m = 1, n = 2, T = Co$), as well as $CeIrIn_5$ ($m = 1, n = 1, T = Ir$), exhibits SC at ambient pressure [Thompson 2001, Petrovic 2001b]. The compounds having Rh as transition metal, $CeRhIn_5$ ($m = 1, n = 1$) and Ce_2RhIn_8 ($m = 1, n = 2$) are both ambient-pressure AFMs and become SCs under application

of pressure [Hegger 2000, Thompson 2001, Nicklas 2003]. Therefore, not only the SC state, but also the presence of strong magnetic fluctuations in these materials offer a good chance to study the interplay of magnetism and SC and the origin of the unconventional SC state in HF systems.

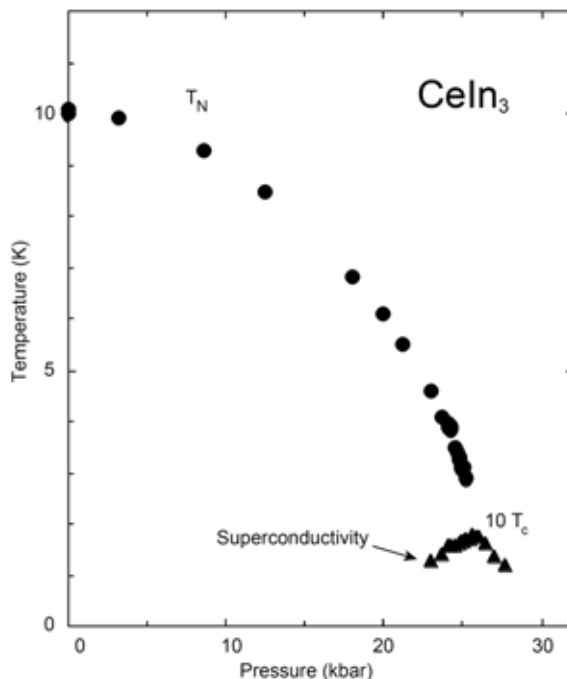


Figure 3.1: $T - p$ phase diagram obtained by resistivity measurements under pressure on single-crystalline $CeIn_3$. For the SC region, the values of T_c are scaled by a factor of ten. Figure taken from [Mathur 1998].

As mentioned earlier, the family of $Ce_nT_mIn_{3n+2m}$ ($n = 1, 2$ or ∞ , $m = 0$ or 1) compounds is based on $CeIn_3$ (cubic structure, $m = 0$, $n = \infty$), a HF AFM at ambient pressure ($T_N \approx 10.1$ K) which becomes SC upon application of pressure, displaying a maximum $T_c \approx 0.25$ K at $p \approx 2.6$ GPa [Walker 1997]. The $T - p$ phase diagram of $CeIn_3$, presented in figure 3.1 [Walker 1997, Mathur 1998], can be considered as a generic phase diagram for many HF materials. The magnetic order is suppressed in the system by application of pressure (or chemical doping in some cases), while the SC state emerges from a region where strong long-range magnetic interactions are present. The SC region in the $T - p$ diagram displays a dome-like shape, with its maximum transition temperature located in the pressure region where magnetism is completely suppressed in the system, $T_N \rightarrow 0$ K. The $Ce_nT_mIn_{3n+2m}$ compounds have a tetragonal unit cell. The structure of these compounds can be viewed as n consecutive layers of $CeIn_3$ alternating with m layers of TIn_2 . The crystal structure of these compounds is presented in figure 3.2. Apart from the cubic $CeIn_3$ ($m = 0$,

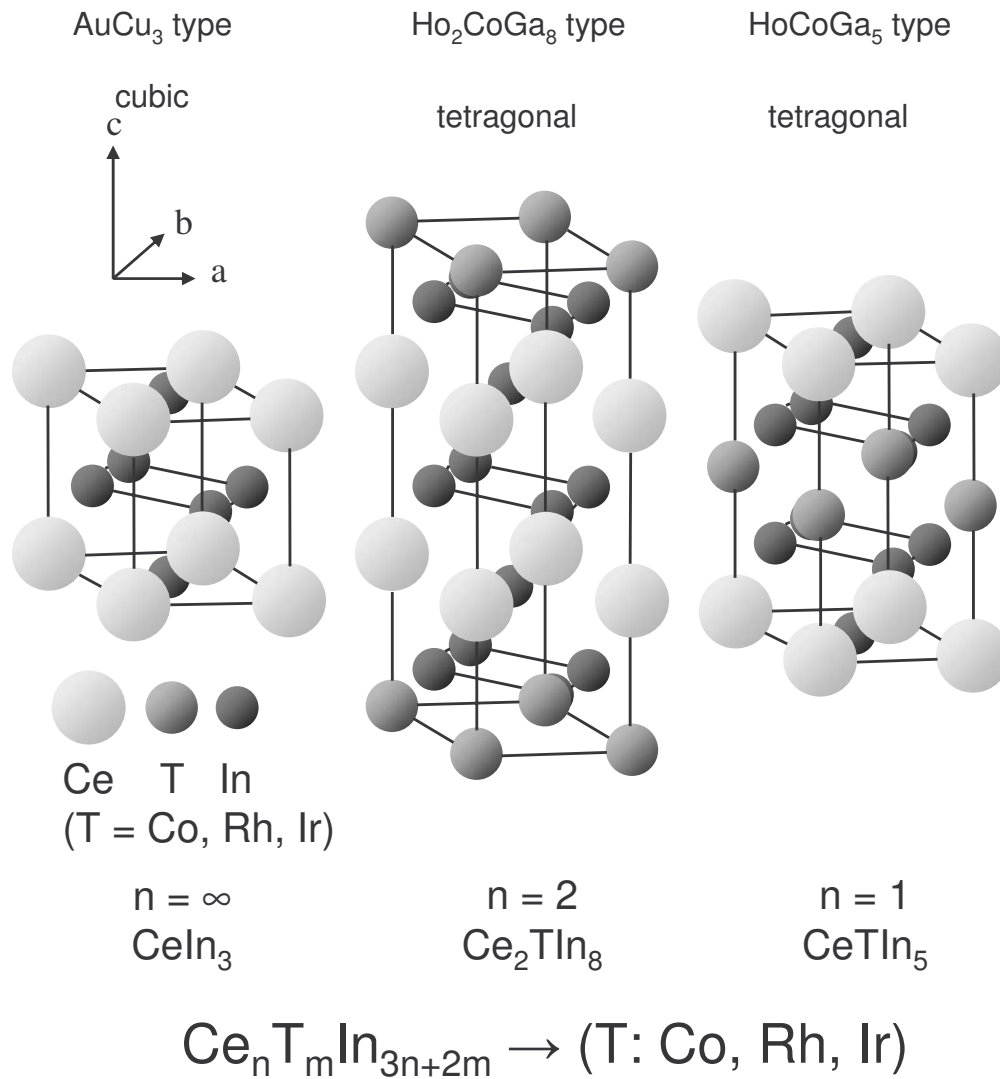


Figure 3.2: Schematic view of the crystal structure of the $\text{Ce}_n\text{T}_m\text{In}_{3n+2m}$ ($n = 1, 2$ or ∞ , $m = 0$ or 1 , T: Co, Rh, Ir) family of compounds. Left side: - parent compound CeIn_3 - $n = \infty$, $m = 0$; middle: - bi-layer compounds Ce_2TIn_8 - $n = 2$, $m = 1$; right side: mono-layer compounds CeTIn_5 - $n = 1$, $m = 1$. Above each subfamily of materials the corresponding structure type is indicated.

$n = \infty$), considered as the infinite-layer compound (∞ consecutive CeIn_3 layers), two distinct tetragonal structures can be distinguished, the so-called mono-layer structure, CeTIn_5 ($m = 1$, $n = 1$), and the bi-layer, Ce_2TIn_8 ($m = 1$, $n = 2$), structure. The successive layers of TIn_2 can be considered as spacers between the CeIn_3 layers and they are meant to gradually increase the anisotropy in the system from the isotropic CeIn_3 to Ce_2TIn_8 and finally to the most anisotropic system, CeTIn_5 . The layered structure of these materials can also be regarded in analogy with the structure of the cuprate SCs.

Similar to $CeIn_3$, many HF compounds are known to date which reveal long-range AFM order at ambient pressure but adopt a SC ground state at pressures close to a critical pressure, p_c , necessary to completely suppress long-range magnetic order, $T_N \rightarrow 0$ K (e.g. $CeCu_2Ge_2$ [Jaccard 1999], $CePd_2Si_2$ [Grosche 1996]). The occurrence of SC in the vicinity of a zero-temperature magnetic instability (quantum phase transition) supports theories in which the Cooper pairs form through the exchange of magnetic spin fluctuations carried by itinerant heavy QPs [Monthoux 1999, Monthoux 2001]. In conformity with these theories, favorable conditions for SC are [Monthoux 2001]:

1. closeness to a QCP;
2. the existence of a quasi-two-dimensional (2D) electronic structure with AFM interactions;
3. d -wave pairing state;
4. high spin-fluctuation temperature T_{sf} ($T_{sf} \propto k_F^2/m^*$).

A more detailed description of the theory of spin-fluctuation mediated SC is contained in section 1.2.2. In order to test the relevance of the spin-fluctuation mediated SC scenario and in particular the effect of electronic dimensionality on the SC state, the recently discovered family of HF compounds $Ce_nT_mIn_{3n+2m}$ (T: Co, Rh or Ir) is particularly suited, since the coupling between the $CeIn_3$ layers can be adjusted through the introduction of TIn_2 layers. In this work we have done hydrostatic-pressure studies on two members of this family of HF materials, namely the ambient-pressure SC $CeCoIn_5$ and the bi-layer HF AFM compound Ce_2RhIn_8 . For each compound, a short overview of the main physical properties is followed by the presentation of our pressure results and a short discussion.

3.2 Effect of pressure on the heavy-fermion superconductor $CeCoIn_5$

3.2.1 Physical properties of $CeCoIn_5$

The layered compound $CeCoIn_5$ is an ambient-pressure HF SC, presenting the highest SC transition temperature of $T_c \approx 2.3$ K among Ce-based HF SCs [Petrovic 2001a]. Although it belongs to the family of tetragonal $HoCoGa_5$ structure, discovered more than 20 years ago [Grin 1979], $CeCoIn_5$ has received special attention

only after the discovery of its SC properties at low temperatures [Petrovic 2001a]. Its layered crystal structure, resembling the structure of the high- T_c cuprate SCs, has motivated scientists to explore the physical properties of CeCoIn₅, as well as of its relative compounds CeRhIn₅ and CeIrIn₅. Although the isoelectronic substitution of Co by Rh, respectively Ir in the CeTIn₅ (T: Co, Rh, Ir) series leads to a continuous increase of the volume of the unit cell, from Co to Rh and further to Ir, the SC properties are not directly related to this volume change, hinting to the fact that mechanisms other than only the compression of the unit cell play a role in producing SC. While CeCoIn₅ and CeIrIn₅ are HF SCs at ambient pressure with $T_c \approx 2.3$ K [Petrovic 2001a] and $T_c \approx 0.4$ K [Petrovic 2001b], respectively, CeRhIn₅ is a HF AFM at ambient pressure becoming SC at finite pressure (at $p \approx 1.63$ GPa, $T_c \approx 2$ K) [Hegger 2000]. However, when gradually substituting the transition metal Co by Rh and by Ir in CeCoIn₅, despite of the gradual increase of the unit-cell volume, V_0 , the lattice parameters show quite a different behavior, c decreasing and a increasing in the direction Co \rightarrow Rh \rightarrow Ir [Petrovic 2001a, Hegger 2000, Petrovic 2001b]. High-pressure X-ray diffraction measurements have revealed that for the CeTIn₅ (T: Co, Rh, Ir) family of compounds the most significant hybridization element V_{pf} , between the $4f$ electrons of Ce and the $5p$ electrons of In, does increase in the same direction as T_c is increasing, namely from Rh \rightarrow Ir \rightarrow Co [Kumar 2004]. Moreover, in the three mentioned compounds, V_{pf} reaches the same value at the pressures (p_{max}) where $T_c(p)$ of each compound is attaining its maximum value, hinting at the importance of the value of V_{pf} in generating SC [Kumar 2004] (see table 3.1).

The Kondo temperature of a system is known to depend as $k_B T_K \propto \frac{1}{N(E_F)} \exp\left(\frac{-1}{N(E_F)V^2}\right)$, where k_B is the Boltzmann constant, $N(E_F)$ represents the electronic DOS at the Fermi level E_F and V is the hybridization matrix element between the f electrons and the conduction electrons (for details see section 1.1.1). Additionally, T_K is known to be proportional to the electronic specific-heat coefficient, γ , of the system and therefore proportional to the spin-fluctuation temperature, T_{sf} , $T_K \propto \frac{1}{\gamma} \propto T_{sf}$ [Moriya 1995, Monthoux 1999]. The theory of magnetically mediated SC predicts a SC transition temperature, T_c , directly proportional to T_{sf} , a dependence presented in the first chapter of this work in equation 1.1. Therefore, the detected dependence of V_{pf} , the dominant hybridization in the CeTIn₅ (T: Co, Rh, Ir) family of materials, seems to be directly related to the variation of T_c in these compounds [Kumar 2004]. As already mentioned, it is therefore likely that the hybridization between the $4f$ electrons of Ce and the $5p$ electrons of In is mostly responsible for SC in this family of compounds, while the transition-metal atoms, T, are mainly serving as spacers in the crystal lattice [Kumar 2004]. Moreover, a

compound	at $p = 0$ GPa	T_c (K)	V_0 (\AA^3)	a (\AA)	c (\AA)	$V_{pf}(0 \text{ GPa})$ (eV)	p_{max} (GPa)	$V_{pf}(p_{max})$ (eV)
CeCoIn ₅	HF SC	2.3 [1]	160.774 [1]	4.614 [1]	7.552 [1]	2.066 [4]	1.4 [5],[6]	2.130 [4]
CeRhIn ₅	HF AFM	- ($T_c \approx 2$ K at $p \approx 1.63$ GPa) ^[2]	163.217 [2]	4.652 [2]	7.542 [2]	2.030 [4]	2.4 [2]	2.136 [4]
CeIrIn ₅	HF SC	0.4 [3]	163.754 [3]	4.668 [3]	7.515 [3]	2.031 [4]	2.9 [7]	2.135 [4]

Table 3.1: Physical properties of CeTIn₅ (T: Co, Rh, Ir) family of compounds. The used symbols are representing: T_c - SC transition temperature at ambient pressure, V_0 - unit-cell volume at room temperature and at ambient pressure, a, c - lattice parameters at room temperature and at ambient pressure, $V_{pf}(0 \text{ GPa})$ - hybridization element at ambient pressure (see text for details), p_{max} - the pressure where T_c is reaching its maximum value, $V_{pf}(p_{max})$ - hybridization element estimated at p_{max} (see text for details). References are indicated in brackets bellow each value and they correspond to: [1]-[Petrovic 2001a], [2]-[Hegger 2000], [3]-[Petrovic 2001b], [4]-[Kumar 2004], [5]-this work, [6]-[Sidorov 2002], [7]-[Muramatsu 2003].

magnetically mediated pairing mechanism might be considered as a source for the formation of SC in these compounds. The mentioned parameters, T_c , a , c , V_0 and V_{pf} , and their dependence on the transition metal, T, in the CeTIn₅ (T: Co, Rh, Ir) family of compounds are presented in table 3.1.

SC in CeCoIn₅ does not only set in at a relatively high temperature, but also bears unusual properties. There is strong evidence that SC in CeCoIn₅, as well as in the relative compounds from the CeTIn₅ (T: Co, Rh, Ir) family of materials, is unconventional. A remarkably large value of the ratio $\Delta C/(\gamma_n T_c)|_{T=T_c} \approx 5$ is found when entering the SC state in CeCoIn₅ at ambient pressure. This value confirms that Cooper pairs are formed by the heavy QPs and points towards very strong coupling in this compound (the value expected for weak-coupling SC, based on the BCS theory is $\Delta C/(\gamma_n T_c)|_{T=T_c} \approx 1.43$). Moreover, at temperatures below T_c a non-exponential decrease of $C(T)/T$ with decreasing temperature is found. At very low temperatures, deep in the SC state, $\Delta C(T)/T \propto T$ was detected [Movshovich 2001]. Also speaking in favor of an unconventional SC state in CeCoIn₅ are thermal-conductivity, κ , and spin-lattice relaxation rate, $1/T_1$, data. These show, at ambient pressure, in the SC state unusual temperature dependencies like: $\kappa(T) \propto T^{3.37}$ at very low temperatures ($0.033 \text{ K} \leq T \leq 0.1 \text{ K}$) [Movshovich 2001], respectively $1/T_1(T) \propto T^3$ [Kohori 2001].

These power-law temperature dependencies point to a SC order parameter with line nodes and, together with measurements of the Knight shift [Kohori 2001], suggest unconventional spin-singlet SC in CeCoIn₅. Angular-dependent thermal-conductivity, κ , measurements found a prominent four-fold modulation in κ as the magnetic field was rotated in the basal plane, with the amplitude of the four-fold term increasing at low temperatures by an order of magnitude compared to the normal state [Izawa 2001]. The magnitude and location of maxima in the angle-dependent κ are consistent with a SC order parameter having $d_{x^2-y^2}$ symmetry [Izawa 2001]. However, the angular dependence of the zero-energy DOS determined by specific-heat measurements points to a d_{xy} symmetry [Aoki 2004].

At ambient pressure, the HF character of CeCoIn₅ is reflected not only by the heavy mass detected by the large C/T coefficient measured at $B = 0$ T at a temperature right above the transition temperature, $C/T|_{T=3\text{K}} \approx 0.353$ J/(molK²), but also by the large values of the upper critical fields, $B_{c2}(0)$, necessary to completely suppress SC, $B_{c2}(0)|_{B\parallel c} \approx 4.9$ T [Petrovic 2001a] and $B_{c2}(0)|_{B\parallel(ab)} \approx 11.6$ T [Bianchi 2003a]. The large anisotropy seen in the values of $B_{c2}(0)$, together with a strongly direction-dependent effective mass and a quasi-2D FS dominated by nearly cylindrical sheets detected by dHvA measurements [Settai 2001, Shishido 2002], is another interesting characteristic which affects the physical properties of CeCoIn₅. Moreover, the experimentally observed FS of CeCoIn₅ was well explained theoretically by including the Ce $4f$ states as itinerant electrons in the FS volume [Maehira 2003]. Related to the role of the hybridization between the Ce $4f$ and the In $5p$ electrons, V_{pf} , to the electronic structure of CeCoIn₅ (as well as to the occurrence of SC in CeCoIn₅), it was shown by Maehira and coworkers that the large hybridization between the $4f$ electrons of Ce and the $5p$ electrons of In occurs in the vicinity of the Fermi level and, therefore, the main, quasi-2D, Fermi surfaces are constructed from the band having the Ce $4f$ and the In $5p$ states [Maehira 2003].

The SC phase transition in CeCoIn₅ at ambient pressure changes from second to first order when the magnetic field is increased and $T_c(B)$ is lowered below a characteristic temperature, T_0 , for both directions of the applied magnetic field ($B \parallel c$ and $B \parallel (ab)$), with $T_0 \approx 0.3T_c$ (where T_c represents the SC transition temperature at $B = 0$ T) [Tayama 2002, Bianchi 2002, Bianchi 2003a]. As was predicted theoretically in the mid 1960's [Sarma 1963, Maki 1964], this effect is due to Pauli limiting in a type II SC, in the case when the orbital effect as pair-breaking mechanism can be neglected relative to the Pauli paramagnetism. Subsequent theoretical studies predicted that in the case of clean-limit SC ($l_{tr} \gg \xi_0$, where l_{tr} symbolizes the QP mean-free path and ξ_0 the SC coherence length) on increasing the magnetic field close

to $B_{c2}(0)$, a phase transition from the mixed (vortex) state to the so-called Fulde-Ferrell-Larkin-Ovchinnikov (FFLO) state occurs [Fulde 1964, Larkin 1965], before the system turns into the normal state. The FFLO state consists of an inhomogeneous SC phase with an order parameter being periodically modulated along the magnetic field [Fulde 1964, Larkin 1965]. Nevertheless, the theoretical prediction of a first-order SC phase transition close to $B_{c2}(0)$ was for the first time found experimentally in $CeCoIn_5$. Additionally, $CeCoIn_5$ satisfies the requirements for the formation of the FFLO state and indeed, it was found that signatures of a possible FFLO state appear close to $B_{c2}(0)$, for the case when B is applied parallel to the (ab) plane [Bianchi 2003a]. However, the origin of the anomaly detected in the SC phase of $CeCoIn_5$, close to $B_{c2}(0)$, for $B \parallel (ab)$, and ascribed to the FFLO state, is controversial. It is known that $CeCoIn_5$ at ambient pressure is located in the vicinity of an AFM instability. Therefore, magnetism as possible origin for the observed high-field anomaly in the SC state could not be ruled out. However, recent pressure studies on $CeCoIn_5$ have found that both, the change to first-order character of the SC phase transition in the vicinity of $B_{c2}(0)$ [Tayama 2005, Miclea 2006a], as well as the phase transition attributed to the formation of the FFLO state [Miclea 2006a], are persisting upon increasing pressure, while the system is driven away from the magnetic fluctuations. Moreover, the region in the $B - T$ plane where the FFLO state is detected is expanding upon increasing pressure, eliminating the possibility of magnetism being responsible for the appearance of this new phase in the SC state [Miclea 2006a]. However, the appearance of the FFLO state for the case when the magnetic field is applied perpendicular to the basal plane is not yet clarified.

The ambient-pressure magnetic susceptibility, χ , of $CeCoIn_5$ is anisotropic, with χ being larger for a magnetic field applied along the tetragonal c axis [Petrovic 2001a]. The high-temperature effective moment, obtained from a polycrystalline average of χ data above $T = 200$ K, is $\mu_{eff} \approx 2.59\mu_B$ per Ce, close enough to the Hund's rule value of $\mu_{eff} = 2.54\mu_B$ per Ce^{3+} known for the $J = 5/2$ Ce multiplet [Petrovic 2001a]. The high-temperature electrical resistivity, $\rho(T)$, of $CeCoIn_5$ at ambient pressure exhibits a behavior typical for HF systems, with a broad maximum seen around a characteristic temperature $T^* \approx 50$ K [Petrovic 2001a]. This temperature marks the continuous transition from incoherent scattering of electrons (with $\Delta\rho(T) \propto -\ln T$) at high temperatures to the coherent scattering existing in the low-temperature region. The mentioned $\rho(T)$ dependence indicates that the low-temperature properties of $CeCoIn_5$ are dominated by Kondo renormalization. Studies of the CEF excitations in $CeCoIn_5$ have shown that the CEF level splitting in this compound is similar to that found for its Rh and Ir homologues and can be regarded as derived from the cubic parent com-

pound CeIn₃ [Christianson 2004]. While the doublet Γ_7^1 represents the ground state, the four-fold degenerate Γ_8 excited state of CeIn₃ is split into two doublets, Γ_7^2 and Γ_6 , in the tetragonal crystal symmetry of CeTIn₅ (with T: Co, Rh or Ir). Therefore, in the presence of the tetragonal environment of the CeTIn₅ family of compounds, the Ce³⁺ $J = 5/2$ multiplet splits into three Kramers doublets, Γ_7^1 - ground state, Γ_7^2 - first excited state and Γ_6 - highest-lying excited state [Christianson 2004]. It should be noted that the distinction between the Γ_7^1 and Γ_7^2 states is a matter of convention. Therefore, in the work of Christianson *et al.* [Christianson 2004], the Γ_7^1 was chosen as ground state.

At ambient pressure, the SC transition in CeCoIn₅ emerges from a NFL-like normal state. The low-temperature normal-state electrical resistivity, $\rho(T)$, of CeCoIn₅ at ambient pressure shows a linear temperature dependence ($\Delta\rho(T) \propto T$) over an extended temperature range, $T_c < T < 20$ K [Petrovic 2001a, Paglione 2003]. This dependence is characteristic of a NFL state. The electronic specific heat of CeCoIn₅, measured at ambient pressure for $B \parallel c$, at $B = 5$ T, a magnetic field high enough to completely suppress the SC state ($B_{c2}(0) \approx 4.9$ T for $B \parallel c$), reveals a logarithmic increase of $C(T)/T$ with decreasing temperature, over more than one decade in temperature, $\Delta C(T)/T \propto -\ln T$ [Petrovic 2001a, Bianchi 2003b]. Additionally, ¹¹⁵In NQR measurements on CeCoIn₅ in the normal state reveal a nuclear spin-lattice relaxation rate $1/T_1(T) \propto T^{1/4}$ [Kohori 2001], strongly deviating from the Korringa behavior of a LFL, $1/T_1(T) \propto T$. These unusual dependencies persisting over an extended temperature range show that the ambient-pressure properties of CeCoIn₅ deviate from that known for a LFL state. Moreover, similar NFL properties are also observed around the pressure-induced SC state in the related compound CeRhIn₅ [Thompson 2003].

Electrical-resistivity measurements show that application of pressure leads to a slight increase of the SC transition temperature of CeCoIn₅ up to $p \approx 1.4$ GPa. Upon further increasing pressure T_c decreases [Nicklas 2001, Sidorov 2002]. Moreover, the residual resistivity, ρ_0 , in the pressure range $0 \text{ GPa} \leq p \leq 1.4 \text{ GPa}$ is continuously decreasing upon increasing pressure, remaining nearly constant with further increasing pressure ($1.4 \text{ GPa} \leq p \leq 4 \text{ GPa}$) [Nicklas 2001, Sidorov 2002]. High-pressure studies on the HF AFM and pressure-induced SC CeRhIn₅, together with the pressure studies on CeCoIn₅, reveal very similar $p - T$ phase diagrams for these two compounds [Knebel 2004, Nicklas priv. comm., Sidorov 2002]. The SC dome appearing in both compounds can be overlapped by shifting the pressure axis of CeRhIn₅ by $\Delta p \approx -1.5$ GPa [Knebel 2004, Nicklas priv. comm., Sidorov 2002], suggesting that CeCoIn₅ at ambient pressure is located just at the border to an AFM instability.

The NFL behavior seen in CeCoIn₅ at ambient pressure, as well as the steep decrease of ρ_0 with increasing pressure ($0 \text{ GPa} \leq p \leq 1.4 \text{ GPa}$), is also suggesting the presence of strong magnetic fluctuations in CeCoIn₅ at ambient pressure. Nevertheless, magnetic order was so far not detected in CeCoIn₅. However, recent studies of Cd-doped CeCoIn₅ (CeCo(In_{1-x}Cd_x)₅), where Cd replaces In leading to the increase of the volume of the unit cell, found AFM order coexisting with SC already at small Cd concentrations [Pham 2006], supporting the fact that CeCoIn₅ at ambient pressure must be located close to an AFM instability. AFM spin fluctuations are supposed to mediate Cooper pairing in the unconventional SC state of CeCoIn₅, as well as in the relative SC compounds from the $Ce_nT_mIn_{3n+2m}$ (T: Co, Rh, Ir) family of HFs.

3.2.2 Experimental results - CeCoIn₅

The HF SC CeCoIn₅ crystallizes in the tetragonal HoCoGa₅ structure with the lattice parameters $a = 0.4614 \text{ nm}$ and $c = 0.7552 \text{ nm}$ at room temperature [Petrovic 2001a]. As already mentioned in the introductory part of this chapter, the crystal structure of CeCoIn₅ (shown in figure 3.2, right side), the same as in the case of the relative compounds CeTIn₅ with transition metal T being Rh or Ir, can be regarded as alternating layers of CeIn₃ and CoIn₂ (respectively TIn₂). The single crystals of CeCoIn₅ were synthesized from In flux by combining stoichiometric amounts of Ce and Co with excess In in an alumina crucible and encapsulating the crucible in an evacuated quartz ampoule. At temperatures of about 450°C the excess In flux is removed with a centrifuge [Petrovic 2001a]. The obtained single crystals have platelet-like forms with characteristic dimensions of $3 \text{ mm} \times 3 \text{ mm} \times 0.1 \text{ mm}$ [Petrovic 2001a]. The proper tetragonal HoCoGa₅ structure was confirmed by powder X-ray diffraction patterns obtained on crushed single crystals [Petrovic 2001a].

We have studied the low-temperature ($0.35 \text{ K} \leq T \leq 7 \text{ K}$) heat capacity of single-crystalline CeCoIn₅ under hydrostatic pressure ($0 \text{ GPa} \leq p \leq 1.5 \text{ GPa}$) and in magnetic field ($0 \text{ T} \leq B \leq 8 \text{ T}$). The single crystals of CeCoIn₅ used in our measurements have been prepared by P. G. Pagliuso in the group of J. L. Sarrao at Los Alamos National Laboratory, USA. The heat-capacity measurements under hydrostatic pressure have been performed by the compensated quasiadiabatic heat-pulse technique in a single-shot ³He evaporation cryostat equipped with a SC magnet. To achieve hydrostatic pressure, a CuBe piston-cylinder type pressure cell with Fluorinert FC72 as pressure transmitting medium was used. To monitor the pressure at low temperatures, the SC transition temperatures of two small pieces of In, one fixed outside and the second placed inside of the pressure cell, were inductively detected. The outer In sample served as reference for ambient pressure, while the In placed

inside, next to the samples, was used for detecting the pressure in the cell. Several single crystals, with a total sample mass of about 0.3 g, were used to perform the measurements under pressure. The single crystals used for the measurements were not all orientated in the same direction with respect to the direction of the applied magnetic field. Due to their thin platelet shapes, most of the crystals were placed in the pressure cell with $B \parallel c$, while the remaining samples were arranged with $B \parallel (ab)$. Over the entire measured pressure range, the crystals did not change their orientations relative to the direction of the applied magnetic field. Parallel to specific-heat measurements under pressure the SC transition of CeCoIn₅ was also monitored by a.c.-susceptibility measurements by using the same coil as used for detecting the SC transition of the pressure sensor. A more detailed description of the performed experiments is contained in Chapter 2. To estimate the magnitude of the errors implied in our specific-heat data under pressure on CeCoIn₅ presented in this section, the relative contribution of the heat capacity of the total amount of measured sample to the total measured heat capacity, C_{sample}/C_{total} , for the entire temperature and pressure range of our experiment is shown in figure 2.5. In order to obtain the electronic specific heat (C_{el}) of CeCoIn₅, the contribution of the lattice to the specific heat, $C_{lattice}$, is needed to be subtracted. $C_{lattice}(T)$, as well as its pressure dependence, can be taken from the pressure-dependent specific heat of the isostructural non-magnetic reference compound, LaCoIn₅. Unfortunately, the several data sets of ambient-pressure specific heat of LaCoIn₅ known to us from different single- or polycrystalline samples (data from [Thompson priv. comm.]) are showing a large sample dependence. However, the average Debye temperature, θ_D , obtained from the existing data is relatively low (in metals at low temperatures: $C(T) \approx \gamma T + (const./\theta_D^3)T^3$, γ - Sommerfeld coefficient, the first term being attributed to the charge carriers and the second one to the lattice). Therefore, at relatively high temperatures ($3 \text{ K} \leq T \leq 7 \text{ K}$ in our case), the contribution of the lattice to the total specific heat of CeCoIn₅ seems to become significant. A large lattice specific heat may then also lead to a strong pressure dependence of $C_{lattice}(T)$ ($3 \text{ K} \leq T \leq 7 \text{ K}$). It is worth mentioning that, to our knowledge, specific-heat data of LaCoIn₅ under pressure are not available. Due to these uncertainties, over the entire measured pressure range we do not subtract the lattice contribution to $C(T)$ from our data for CeCoIn₅. Thus, one should keep in mind that the data for $C(T)$ of CeCoIn₅ presented in this chapter include $C_{lattice}(T)$. The results affected by this approach are mentioned in the text and they should be regarded with care. The nuclear Schottky contributions of Co and In to the specific heat of CeCoIn₅ were not subtracted from the data either, since they are considered negligible in the temperature and magnetic-field range of our measurements ($T \geq 0.35 \text{ K}$, $B \leq 8 \text{ T}$).

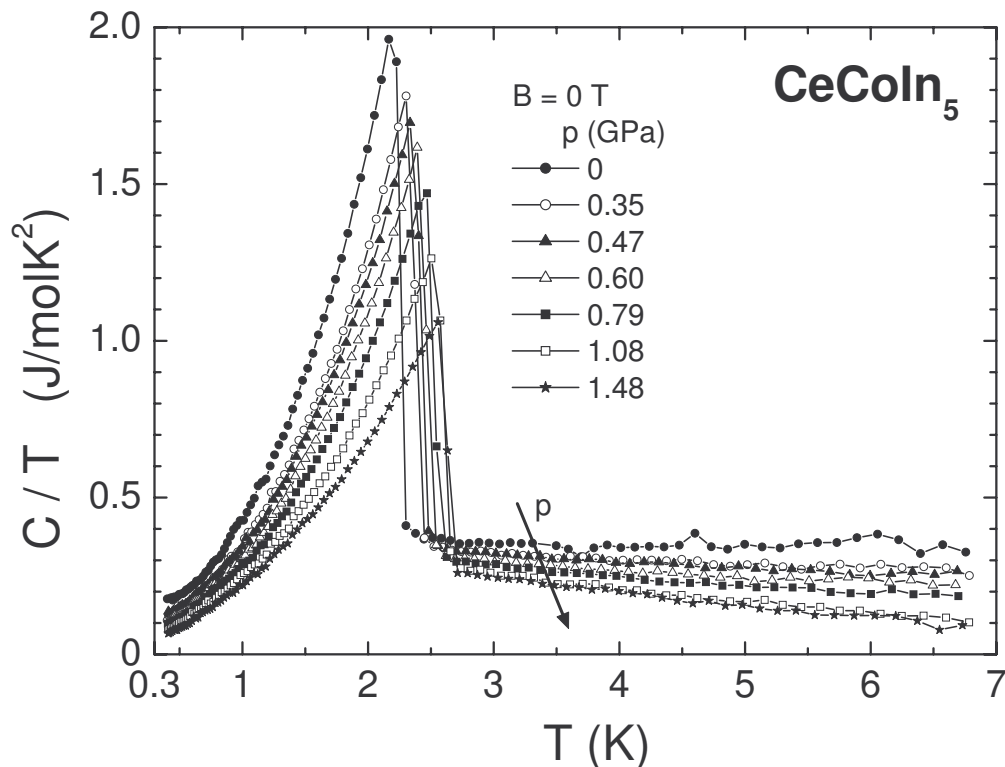


Figure 3.3: Low-temperature specific heat of $CeCoIn_5$ as $C(T)/T$ versus T at $B = 0$ T for pressures as indicated in the figure. The arrow marks the direction of increasing pressure.

The low-temperature ($0.35 \text{ K} \leq T \leq 7 \text{ K}$) specific heat of $CeCoIn_5$ and its pressure dependence ($0 \text{ GPa} \leq p \leq 1.5 \text{ GPa}$) in zero magnetic field is shown in figure 3.3. At ambient pressure, a transition into a SC state is emphasized by the large jump in $C(T)/T$ at the transition temperature $T_c \approx 2.26 \text{ K}$. The SC state, as well as the high jump in $C(T)/T$, is persisting with increasing pressure. A transition temperature of $T_c \approx 2.63 \text{ K}$ is detected at the highest pressure of our experiment, $p \approx 1.48 \text{ GPa}$. Application of pressure leads to an increase of the SC transition temperature with an initial slope of $dT_c/dp \approx 0.34 \text{ K/GPa}$, a value in good agreement with results obtained from measurements of thermal expansion [Oeschler 2003] and electrical resistivity under pressure [Nicklas 2001]. The increase of $T_c(p)$ under application of pressure deviates from its initial linear trend at pressures above $p \approx 0.7 \text{ GPa}$ and gradually becomes less pronounced when approaching $p \approx 1.5 \text{ GPa}$ (see figure 3.5a). The evolution of T_c with increasing pressure obtained by our measurements agrees very well with that observed by electrical-resistivity measurements under pressure [Nicklas 2001], where it was shown that $T_c(p)$ is reaching a maximum value at

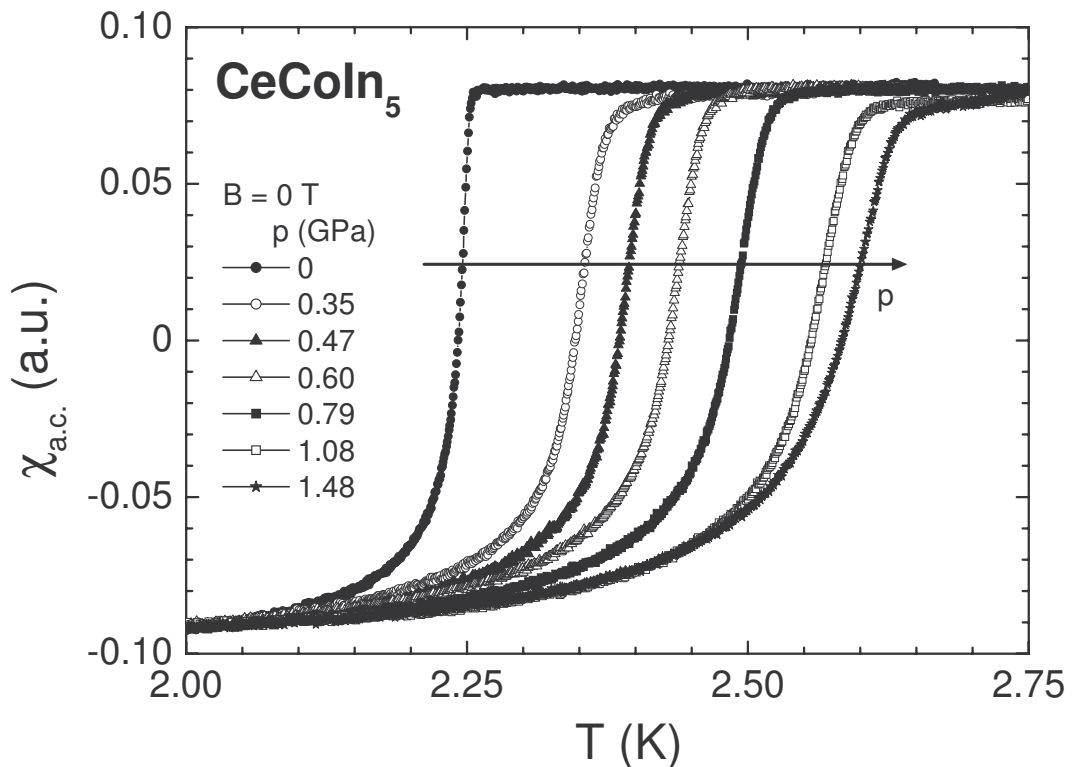


Figure 3.4: Evolution of the $\chi_{a.c.}(T)$ of CeCoIn_5 through the SC phase transition at $B = 0$ T and at different applied pressures. The symbols for different pressures are indicated in the figure and are maintained the same for each pressure in the three figures 3.3, 3.4 and 3.6. The arrow is indicating the direction of increasing pressure.

$p \approx 1.4$ GPa. The SC phase transition in CeCoIn_5 , seen by the anomaly in the specific heat, is accompanied by a diamagnetic signal in the a.c.-susceptibility measurements performed simultaneously to the measurements of specific heat. Figure 3.4 shows the evolution of the SC transition under pressure as detected by a.c.-susceptibility measurements. The SC transition temperatures, as well as the width of the phase transitions, detected by both, specific-heat and $\chi_{a.c.}(T)$ measurements, are in good agreement. Additionally, the width of the phase transition stays constant with increasing pressure over the entire measured pressure range, $p \leq 1.5$ GPa, proving also the good hydrostatic conditions in our measurements.

As an overall phase diagram obtained from our specific-heat measurements under pressure at $B = 0$ T, the obtained pressure dependencies of the physical properties, such as the SC transition temperature, T_c , specific-heat coefficient, $C/T|_{T=3\text{K}}$, residual specific-heat coefficient in the SC phase at $T = 0$ K, $C/T|_{T=0\text{K}}$, and the $\Delta C/(\gamma_n T_c)|_{T=T_c}$ ratio, are shown in figure 3.5.

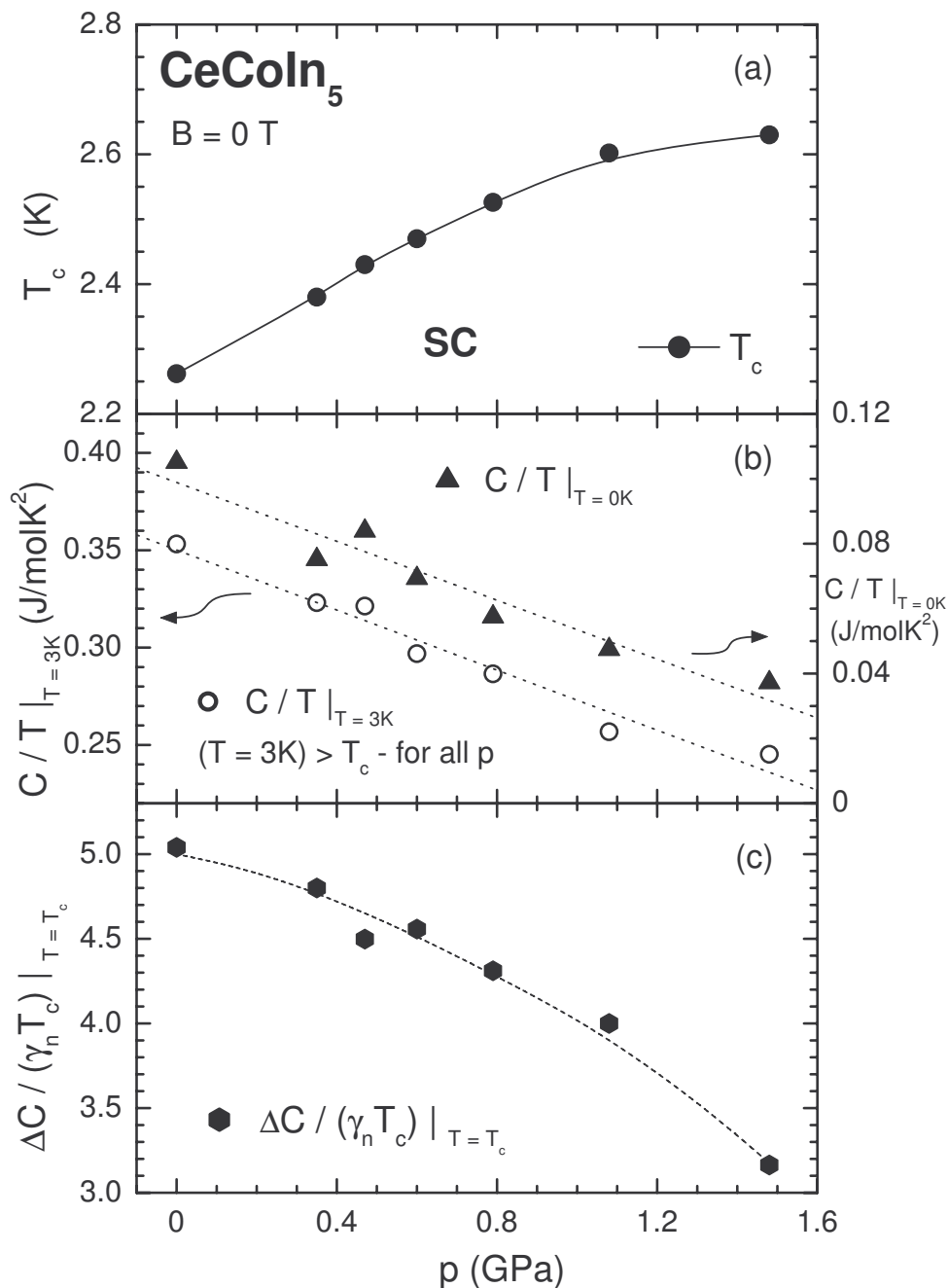


Figure 3.5: Pressure ($p \leq 1.5$ GPa) dependence of different physical properties of $CeCoIn_5$ obtained for $B = 0$ T. (a) T_c versus pressure, as obtained from our specific-heat data (by using the entropy-balance technique). (b) Left axis: $C/T|_{T=3K}$ versus pressure (open circles); right axis: $C/T|_{T=0K}$ (in the SC state) versus pressure (full triangles) (see text for describing the way we have estimated our data). The lines are representing the linear fits to the corresponding data. (c) $\Delta C / (\gamma_n T_c)|_{T=T_c}$ versus pressure.

As seen in panel (b) of figure 3.5 (left axis), the specific-heat coefficient C/T taken at $T = 3$ K, a temperature situated above T_c over the whole pressure range of our measurements, shows at ambient pressure a value of $C/T|_{T=3\text{K}} \approx 0.353$ J/(molK²) and decreases gradually with increasing pressure with a rate of $d \ln(C/T|_{T=3\text{K}})/dp \approx -0.263$ /GPa. Due to the SC state existing below T_c , ($T_c < 3$ K for $p \leq 1.5$ GPa), we take $C/T|_{T=3\text{K}}$ as an estimate for the Sommerfeld coefficient, γ . The large value of $C/T|_{T=3\text{K}}$ at ambient pressure shows the HF character of CeCoIn₅ ($C/T|_{T=3\text{K}} \approx \gamma \propto m^*$). Measurements in magnetic fields high enough to suppress the SC phase transition at ambient pressure show an increase of the electronic specific-heat coefficient with decreasing temperature ($B \parallel c$) [Petrovic 2001a], suggesting the possibility that the HF state is not yet completely formed at such an elevated temperature as $T = 3$ K, continuing to develop down to lower temperatures. However, the mentioned increase of the electronic specific-heat coefficient is often interpreted as due to NFL behavior characteristic to the vicinity of a QCP. Therefore, it can be possible that the $C/T|_{T=3\text{K}}$ is not accurately reflecting the HF character of the system.

With increasing pressure, the decrease of $C/T|_{T=3\text{K}}$ (estimate for the Sommerfeld coefficient, γ) is in good agreement with the behavior seen in Ce-based HF compounds, where the application of pressure leads to the increase of the hybridization strength between the $4f$ electrons of Ce and the conduction electrons, manifested by the increase of the Kondo temperature and by the reduction of the effective QP mass, m^* . Moreover, in the framework of the spin-fluctuation theory, the decrease of the effective QP mass indicates an increase of the characteristic spin-fluctuation temperature T_{sf} ($T_{sf} \propto k_F^2/m^*$) [Moriya 1995]. As already presented in section 1.2.2, in the context of the above-mentioned theory the variation of the spin-fluctuation temperature is supposed to be responsible for the variation of T_c in the system (see also equation 1.1 in section 1.2.2) [Millis 1988, Lonzarich 1997, Mathur 1998, Monthoux 1999]. Therefore, the decrease of the effective QP mass in CeCoIn₅ under pressure reflects an increase of the spin-fluctuation temperature, T_{sf} . Along with the observed increase of T_c , this is strongly hinting at magnetically mediated Cooper pairing in this HF SC ($T_c \propto T_{sf} \propto 1/m^*$). Moreover, a tendency to saturation of the γ coefficient of CeCoIn₅ under pressure is observed right in the pressure range where the increase of T_c is becoming less pronounced ($p \geq 0.7$ GPa) and $T_c(p)$ is reaching its maximum value, further supporting the prediction of the theory of magnetically mediated SC where $T_c \propto T_{sf} \propto 1/m^*$.

A measure of the SC coupling strength, the $\Delta C/(\gamma_n T_c)|_{T=T_c}$ ratio presented in figure 3.5c decreases with increasing pressure and shows values between $\Delta C/(\gamma_n T_c)|_{T=T_c} \approx 5$ and $\Delta C/(\gamma_n T_c)|_{T=T_c} \approx 3$. These values are extremely large

compared to the BCS value of $\Delta C/(\gamma_n T_c)|_{T=T_c} \approx 1.43$ known for a weak-coupling SC. The large values of $\Delta C/(\gamma_n T_c)|_{T=T_c}$ hint to the fact that Cooper pairs in the SC state of CeCoIn₅ are formed by strongly coupled heavy QPs. However, the aforementioned possible interpretations related to the increase of the electronic specific-heat coefficient with decreasing temperatures observed in magnetic fields high enough to suppress SC might also affect the obtained values of $\Delta C/(\gamma_n T_c)|_{T=T_c}$, leading to the possibility of a somewhat weaker coupling in SC CeCoIn₅.

We have estimated the low-temperature dependence of C/T of CeCoIn₅ ($B = 0$ T) in the SC state at temperatures well below T_c , by fitting the data of $C(T)/T$ in the temperature range $0.4 \text{ K} \leq T \leq 1 \text{ K}$ (down to the lowest temperature of our measurements). In the respective temperature interval, the data show a $C(T)/T = \gamma_0 + bT^2$ dependence for the entire pressure range of the experiment ($p \leq 1.5 \text{ GPa}$). As an estimate for the value of C/T at $T = 0 \text{ K}$ in the SC state, $C/T|_{T=0\text{K}}$, the residual specific-heat coefficient, γ_0 , obtained from the above-mentioned fitting was taken. The pressure dependence of $C/T|_{T=0\text{K}}$ is shown in figure 3.5b (right axis). A gradual decrease of $C/T|_{T=0\text{K}}$ with increasing pressure, with a rate of $d(C/T|_{T=0\text{K}})/dp \approx -0.045 \text{ J}/(\text{molK}^2\text{GPa})$, can be observed, from $C/T|_{T=0\text{K}} \approx 0.105 \text{ J}/(\text{molK}^2)$ at ambient pressure to $C/T|_{T=0\text{K}} \approx 0.037 \text{ J}/(\text{molK}^2)$ at the highest pressure of our experiment, $p \approx 1.48 \text{ GPa}$. At ambient pressure and $B = 0 \text{ T}$, a linear temperature dependence of the low-temperature $C(T)/T$ of CeCoIn₅ in the SC state was reported for $0.095 \text{ K} \leq T \leq 0.4 \text{ K}$ [Movshovich 2001]. Since our measurements were not performed down to such low temperatures, in the case when the $\Delta C(T)/T \propto T^2$ dependence observed by our measurements down to only $T \approx 0.4 \text{ K}$ indeed changes to the $\Delta C(T)/T \propto T$ behavior reported for temperatures below $T = 0.4 \text{ K}$ [Movshovich 2001], it is possible that our values of $C/T|_{T=0\text{K}}$ are slightly overestimated. However, the overall pressure dependence of $C/T|_{T=0\text{K}}$, as well as the non-exponential low-temperature behavior of $C(T)/T$ in the SC state, is precisely determined. The power-law dependence of $C(T)/T$ at low temperatures, deep in the SC state, suggests the unconventional character of the SC state in CeCoIn₅ over the entire pressure range measured ($p \leq 1.5 \text{ GPa}$). It is worth noting that $C/T|_{T=0\text{K}}$ shows low, but non-zero values at ambient and finite pressure ($p \leq 1.5 \text{ GPa}$).

The ratio of $(C/T|_{T=0\text{K}})/(C/T|_{T=3\text{K}})$ can be considered an estimate of the amount of the FS which does not show a SC gap. In CeCoIn₅ $(C/T|_{T=0\text{K}})/(C/T|_{T=3\text{K}})$ decreases gradually with increasing pressure from $(C/T|_{T=0\text{K}})/(C/T|_{T=3\text{K}}) \approx 0.3$ at ambient pressure to $(C/T|_{T=0\text{K}})/(C/T|_{T=3\text{K}}) \approx 0.14$ at $p \approx 1.48 \text{ GPa}$, suggesting a gradual increase of the fraction of the FS implied in SC from about 70% at $p = 0 \text{ GPa}$

to about 86% at $p \approx 1.48$ GPa. It is known that at ambient pressure CeCoIn₅ is located in the vicinity of an AFM instability, while application of pressure leads to moving the system away from it. The observed increase of the fraction of the FS implied in SC with increasing pressure suggests that application of pressure on CeCoIn₅ leads to gradual suppression of the AFM order (expected at a slightly negative pressure) in favor of the SC state. The competition of the two phenomena suggests a common mechanism for the formation of both states (AFM, at a slightly negative pressure, and SC) in CeCoIn₅. The numbers given for $(C/T|_{T=0\text{K}})/(C/T|_{T=3\text{K}})$ might well be affected by the uncertainties in determining $C/T|_{T=0\text{K}}$ and by the fact that the Sommerfeld coefficient is estimated by C/T at $T = 3$ K. However, even if the numbers would slightly change, the overall pressure dependence and, therefore, the above-presented interpretation should remain valid.

The temperature dependence of the $B = 0$ T low-temperature entropy of CeCoIn₅ and its variation with increasing pressure are shown in figure 3.6. The same symbols are used for the different pressure values in the three figures 3.3, 3.4 and 3.6. As seen in figure 3.6, over the whole measured temperature range ($0.35 \text{ K} \leq T \leq 7 \text{ K}$) the entropy is continuously decreasing with increasing pressure. At ambient pressure, right above the SC phase transition, the entropy of CeCoIn₅ is reaching the value of $S(T_c, p = 0 \text{ GPa}) \approx 0.28R \ln 2$, while with increasing pressure this value is gradually decreasing. At the highest pressure of our experiment the entropy at T_c amounts $S(T_c, p \approx 1.48 \text{ GPa}) \approx 0.18R \ln 2$ only. This gradual decrease of the entropy with increasing pressure, on both temperature sides of the SC phase transition, reflects the increase of the hybridization strength of the $4f$ electrons of Ce with the conduction electrons associated with an increase of the Kondo temperature, T_K . The pressure dependence of T_K in CeCoIn₅ is shown in the inset of figure 3.6. The Kondo temperature is obtained according to the results of the single-impurity Kondo model ($S = 1/2$), in which T_K is defined as about twice the temperature where the entropy of the system is reaching the value of $S(T_K/2) = 0.5R \ln 2$ [Desgranges 1982]. In order to estimate T_K at those pressures where for $T \leq 7$ K the entropy does not reach the mentioned value of $0.5R \ln 2$, the data at temperatures up to $T = 7$ K were extrapolated to higher temperatures. Therefore, one should keep in mind that the error bars in determining T_K are gradually increasing with increasing pressure. In addition, the fact that the lattice contribution to the specific heat of CeCoIn₅ was not subtracted from the data is leading to an overestimation of the entropy at higher temperatures and correspondingly to an underestimation of T_K over the whole measured pressure range. However, at sufficiently low temperatures, the contribution of the lattice to the specific heat, defined as $C_{\text{lattice}}(T) = \beta T^3 = (\text{const.}/\theta_D^3)T^3$, is decreasing with in-

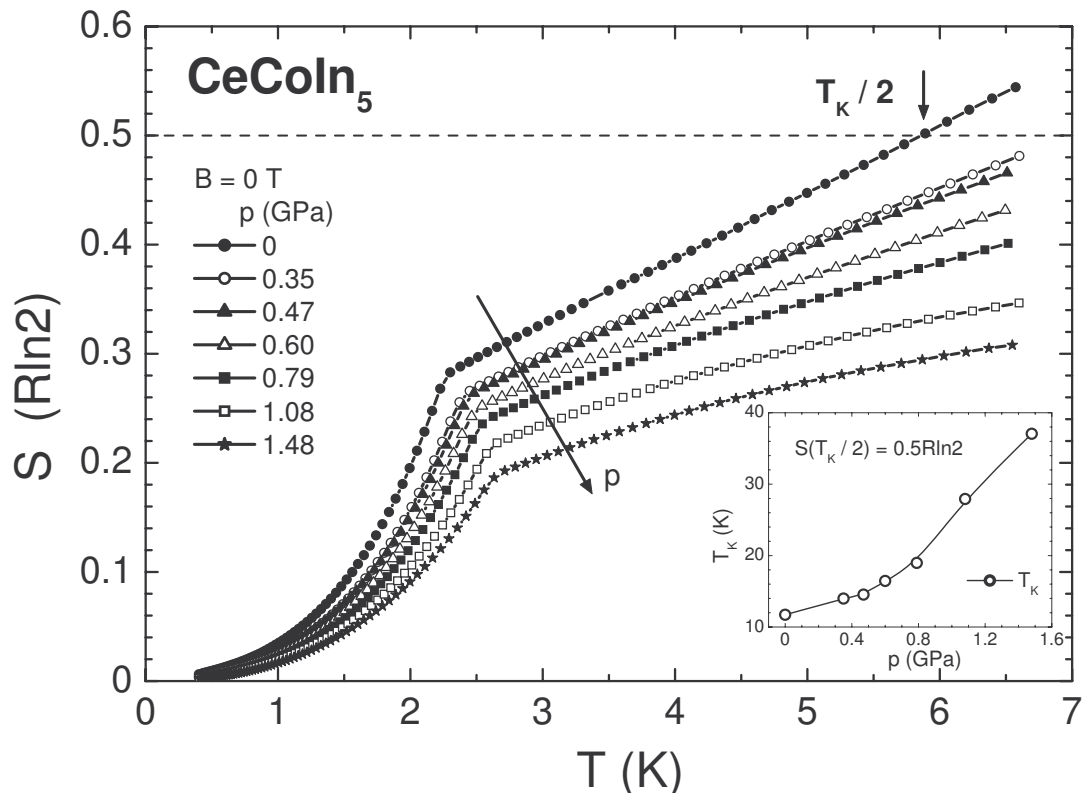


Figure 3.6: Temperature and pressure dependence of the low-temperature entropy of $CeCoIn_5$ at $B = 0$ T. The different pressures are indicated in the figure. The different symbols in the figure, used for different values of p , are consequent with the symbols used in the previous figures 3.3 and 3.4. The dashed line marks the entropy of $0.5R \ln 2$, a value which according to the single-impurity Kondo model is reached by a system ($S = 1/2$) at the temperature equal to about $T_K/2$ [Desgranges 1982]. The pressure dependence of T_K , obtained corresponding to the above-mentioned model - $S(T_K/2) = 0.5R \ln 2$ - is contained in the inset.

creasing pressure. Therefore, the errors in the absolute values of the specific heat (and automatically of the high-temperature entropy and T_K) are decreasing with increasing pressure. With these sources of errors, affecting our specific-heat data on $CeCoIn_5$ mainly in the temperature range of $3 \text{ K} \leq T \leq 7 \text{ K}$, the experimentally determined values for the high-temperature entropy and T_K should be regarded with care, but their general pressure dependencies may be considered reliable. Nevertheless, the increase of T_K with increasing pressure ($dT_K/dp \approx 18 \text{ K/GPa}$), as well as the absolute values of T_K (e.g. $T_K|_{p=0\text{GPa}} \approx 12 \text{ K}$) obtained by our specific-heat measurements, shows a relatively good agreement with the results obtained from electrical-resistivity measurements under pressure [Nicklas 2001], where the temperature at which the re-

sistivity is reaching its maximum value (T^*) is taken as an estimate for the Kondo temperature of the system (from resistivity: $dT^*/dp \approx 28$ K/GPa; $T^*|_{p=0\text{GPa}} \approx 53$ K [Nicklas 2001]).

Application of a magnetic field to $CeCoIn_5$ is leading to a gradual shift of the SC phase transition to lower temperatures. At ambient pressure, the system exhibits a relatively strong anisotropy. The upper critical field necessary to completely suppress SC, $B_{c2}(0)$, is $B_{c2}(0)|_{B\parallel c} \approx 4.9$ T for $B \parallel c$ [Petrovic 2001a], while it is more than twice larger for $B \parallel (ab)$, $B_{c2}(0)|_{B\parallel(ab)} \approx 11.6$ T [Bianchi 2003a]. This large anisotropy is well explained also by dHvA measurements, which show that the FS is mainly consisting of nearly cylindrical sheets, hinting to a quasi-2D electronic structure in this compound [Settai 2001, Shishido 2002]. Our measurements of the heat capacity in magnetic field were performed on a system formed by a collection of more than 50 pieces of $CeCoIn_5$. Therefore, the precise orientation of the samples with respect to the magnetic field was difficult to achieve. However, the samples were assembled in the pressure cell in the way that some of them were oriented with $B \parallel c$, while the remaining samples were placed with $B \parallel (ab)$. Over the entire pressure range the orientation of the samples with respect to the magnetic field was remaining the same. Therefore, our specific-heat data under pressure and in magnetic field ($B \leq 8$ T) show the transitions for both main orientations of the magnetic field. Moreover, the accuracy of the absolute values of the specific heat in magnetic field, below T_c , is affected by the fact that the data were normalized to the total sample mass, without taking into account the different amounts of differently oriented samples. However, the transition temperatures for the two different orientations of the magnetic field ($B \parallel c$ and $B \parallel (ab)$) can be accurately estimated. Figure 3.7 shows the evolution, as function of magnetic field, of the low-temperature $C(T)/T$ of $CeCoIn_5$ for three different values of pressure: $p = 0$ GPa in panel (a), $p \approx 0.79$ GPa in panel (b) and $p \approx 1.48$ GPa in panel (c). For low values of B (e.g. $B = 1$ T) the detection of the two distinct phase transitions corresponding to the two different orientations of the magnetic field is impossible within the resolution of our measurements, but at higher values of B ($B \geq 3$ T) the two transitions are well separated. At $B = 1$ T, the two phase transitions corresponding to $B \parallel c$ and $B \parallel (ab)$ are very close in temperature, giving rise to a single anomaly, the obtained transition temperature being overestimated for the direction $B \parallel c$ and underestimated for $B \parallel (ab)$. Due to the much smaller value of $B_{c2}(0)|_{B\parallel c}$ than that of $B_{c2}(0)|_{B\parallel(ab)}$, for $B \leq 5$ T, the phase transitions at lower temperatures are corresponding to $B \parallel c$, while the transitions at higher values of T are associated to $B \parallel (ab)$. As an example, in panel (c) of figure 3.7 the two distinct SC phase transitions (at $B = 3$ T) for the two different

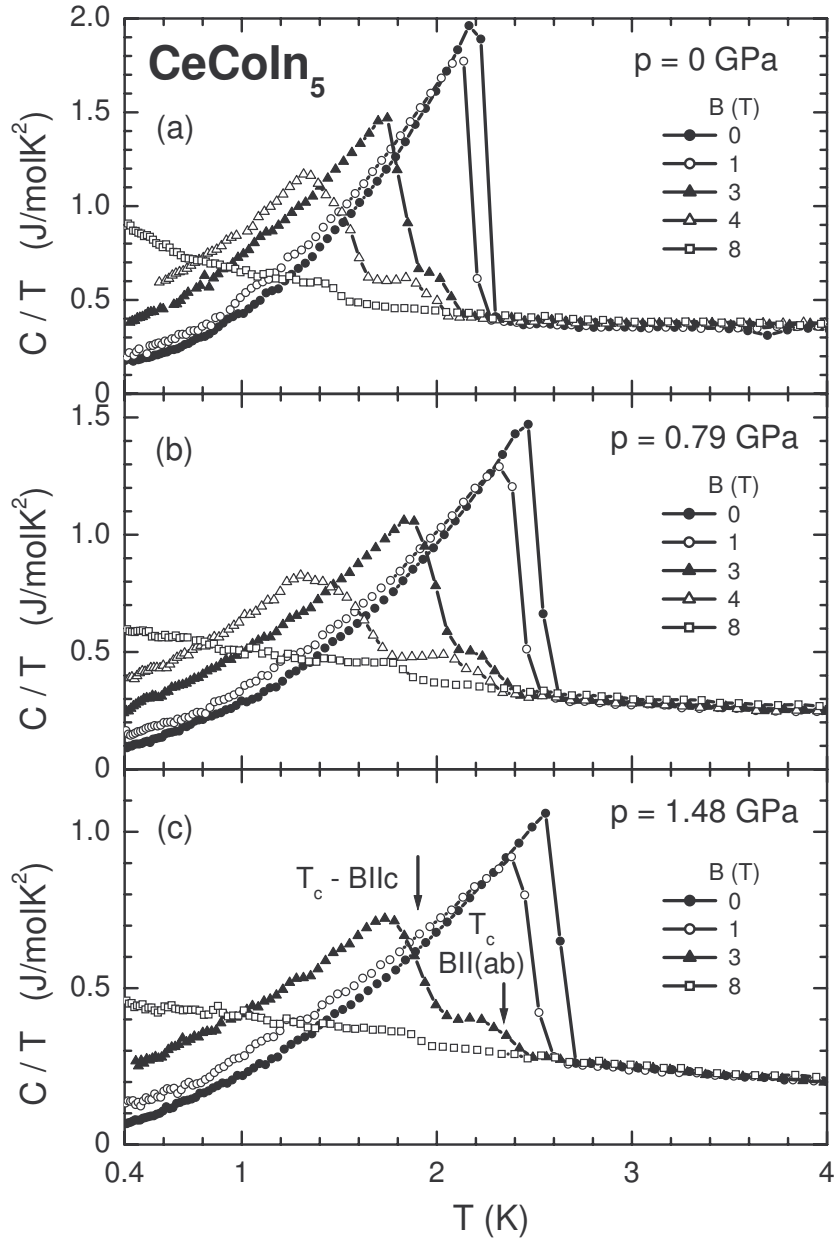


Figure 3.7: Effect of magnetic field ($B \leq 8$ T) on the low-temperature $C(T)/T$ of $CeCoIn_5$ for three different pressures: $p = 0$ GPa - (a), $p \approx 0.79$ GPa - (b) and $p \approx 1.48$ GPa - (c). The symbols used for each value of B are the same in the three panels and are mentioned in the figure. Due to the mixed orientation of samples with respect to the direction of the applied magnetic field, two phase transitions are detectable in magnetic field, each of them corresponding either to $B \parallel c$ (transition lower in temperature) or to $B \parallel (ab)$ (the transition at higher T) (see for example the arrows in panel (c) indicating the positions of the different T_c -s). The SC phase transitions at $B = 8$ T are corresponding to $B \parallel (ab)$.

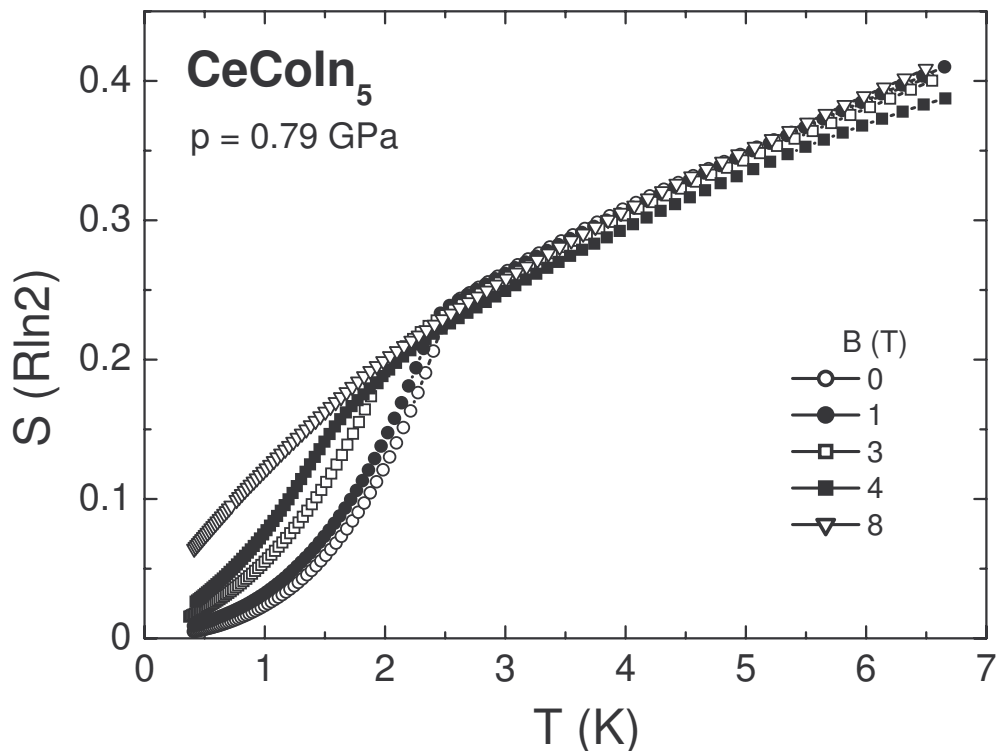


Figure 3.8: Evolution of the low-temperature entropy of CeCoIn_5 in different magnetic fields (see symbols in the figure) for $p \approx 0.79$ GPa. The complete amount of samples measured in the pressure cell are oriented with respect to the direction of the applied magnetic field in both directions, $B \parallel c$ and $B \parallel (ab)$.

field orientations are indicated by arrows. At $B = 8$ T, only one SC phase transition can be detected, the transition corresponding to $B \parallel (ab)$. The evolution of the low-temperature entropy of CeCoIn_5 with increasing magnetic field is presented in figure 3.8 for $p \approx 0.79$ GPa. The $C(T)/T$ data obtained at this pressure, and also presented in figure 3.7b, were used to estimate the low-temperature entropy shown in figure 3.8. In order to evaluate the low-temperature entropy of the system at values of T below the limit of our measurements of $T \approx 0.35$ K, the measured data were extrapolated to $T = 0$ K. Due to the fact that at $B \leq 5$ T the temperature dependence of C/T below T_c could be well fitted with $C(T)/T|_{T < T_c} = \gamma_0 + bT^2$, the low-temperature extrapolation of the data measured for $B \leq 5$ T was done according to the above-mentioned equation, with the parameters γ_0 and b taken from fitting the experimental data. For $B = 8$ T, where the SC phase transition for $B \parallel c$ is completely suppressed, the extrapolation to $T = 0$ K was done by following to low temperatures the $\Delta C(T)/T \propto -\ln T$ dependence detected at higher temperatures (for $T \leq 1$ K \leq

$T_c|_{B=8T}$ for all p ; $p \leq 1.5$ GPa). As seen in the figure 3.8, at temperatures $T \leq T_c$ (T_c being the SC transition temperature at $B = 0$ T and $p \approx 0.79$ GPa), the entropy of the system is gradually increasing with increasing magnetic field. Independent of the value of B , the same value of entropy is attained at $T = T_c$. At $T > T_c$, $S(T, B)$ follows a single curve for all values of B . The same behavior, consisting in the magnetic-field-independent normal-state entropy (conservation of the entropy between the normal and SC state), can be detected in CeCoIn₅ over the entire pressure range of our measurements, $p \leq 1.48$ GPa. This finding might imply that the developing of the HF state, expected to take place continuously down to low temperatures (below T_c for $B = 0$ T), is interrupted and replaced by the SC state in CeCoIn₅.

The obtained $B - T$ phase diagram of CeCoIn₅ and its evolution with increasing pressure is presented in figures 3.9a, for $B \parallel (ab)$, and 3.10a, for $B \parallel c$. The evolution of T_c with increasing pressure for different values of the applied magnetic field is shown in figures 3.9b and 3.10b, for $B \parallel (ab)$ and $B \parallel c$, respectively.

When the magnetic field is applied in the basal plane ($B \parallel (ab)$), the highest value of $B = 8$ T applied in our measurements is not sufficient to completely suppress the SC state in CeCoIn₅ for the entire range of pressure, $p \leq 1.48$ GPa. However, as seen in figure 3.9a, with increasing pressure up to $p \approx 1.48$ GPa, an increase of the upper critical field $B_{c2}(0)|_{B \parallel (ab)}$, as well as a strong decrease of the initial slope of the $B_{c2}(T)$ curve at T_c , can be observed from our measurements (for $B \parallel (ab)$). The observed pressure-induced increase of $B_{c2}(0)|_{B \parallel (ab)}$ is in good agreement with results obtained by more precise measurements performed at low temperatures and in high magnetic fields by means of magnetization [Tayama 2005] and specific-heat measurements under pressure [Miclea 2006a]. From the former an increase from $B_{c2}(0)|_{B \parallel (ab)} = 11.6$ T at ambient pressure to $B_{c2}(0)|_{B \parallel (ab)} = 14.5$ T at $p = 1.38$ GPa [Tayama 2005] was obtained, while the low-temperature specific-heat measurements under pressure of Miclea *et al.* [Miclea 2006a] show for the upper critical field ($B \parallel (ab)$) values of $B_{c2}(0)|_{B \parallel (ab)} = 11.6$ T at ambient pressure and $B_{c2}(0)|_{B \parallel (ab)} = 14.3$ T at $p = 1.34$ GPa. The initial slope of the upper critical field, $dB_{c2}(T)/dT|_{T=T_c}$, for $B \parallel (ab)$, is decreasing upon increasing pressure, from $dB_{c2}(T)/dT|_{T=T_c; B \parallel (ab)} \approx -14.85$ T/K at ambient pressure to $dB_{c2}(T)/dT|_{T=T_c; B \parallel (ab)} \approx -10.03$ T/K at $p \approx 1.48$ GPa. These values are as well in relatively good agreement with $dB_{c2}(T)/dT|_{T=T_c; B \parallel (ab)} \approx -30.5$ T/K at $p = 0$ GPa and $dB_{c2}(T)/dT|_{T=T_c; B \parallel (ab)} \approx -16.4$ T/K at $p = 1.34$ GPa obtained from the specific-heat measurements of Miclea *et al.* [Miclea 2006a]. The discrepancy in the absolute values comes from the fact that we have estimated the initial slope of the upper critical field from the values of T_c between $B = 0$ T and $B = 3$ T, a way which is leading to a strong underestimation of $dB_{c2}(T)/dT|_{T=T_c}$.

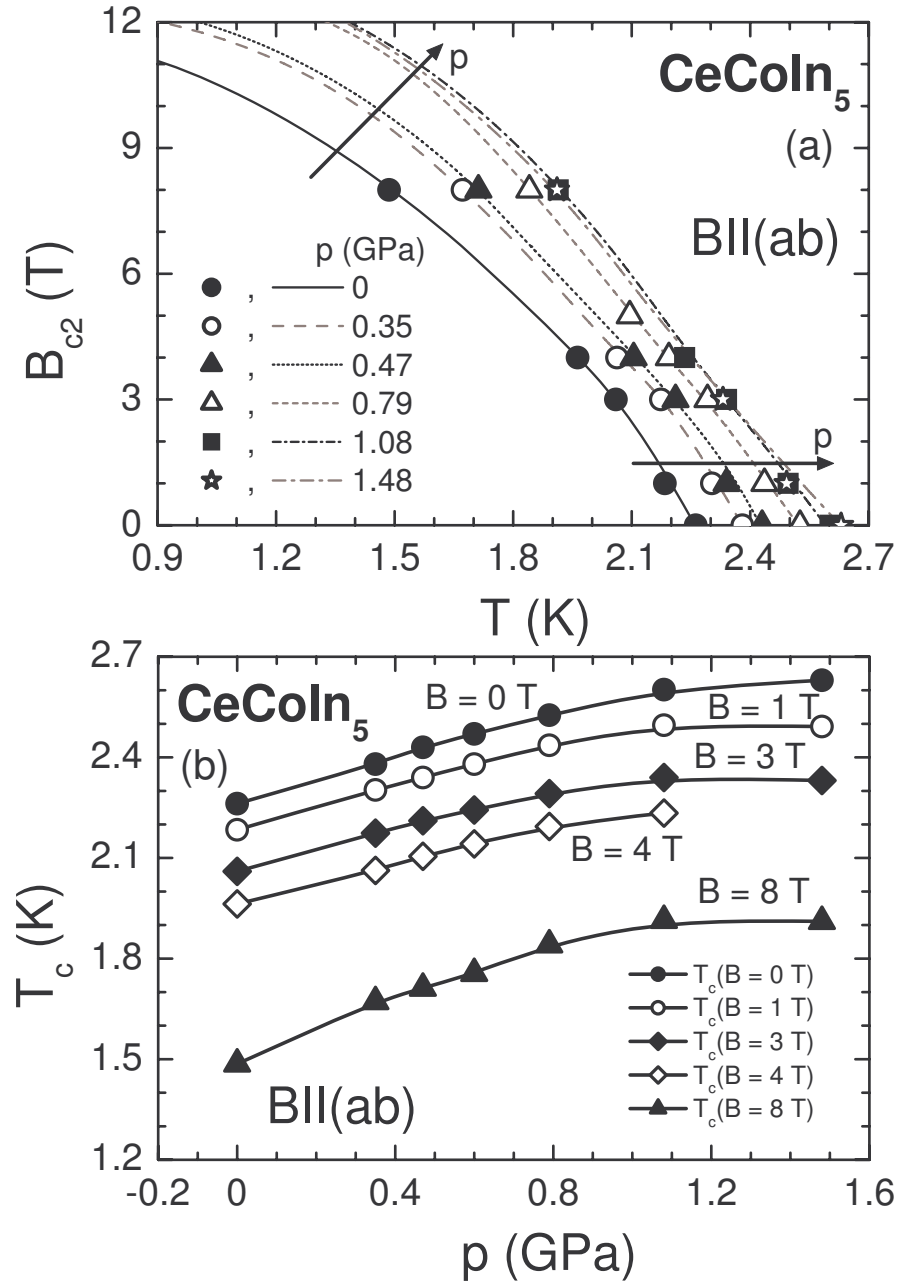


Figure 3.9: (a) $B - T$ phase diagram of the SC phase transition in CeCoIn_5 obtained for different pressures, for $B \parallel (ab)$. Symbols for different pressures are indicated in the figure. The different lines are guides to the eyes. The arrows indicate the direction how pressure is increasing. (b) $T - p$ phase diagram of CeCoIn_5 obtained for different values of the applied magnetic field ($B \leq 8$ T), for $B \parallel (ab)$. The values of B and the corresponding symbols are indicated in the figure.

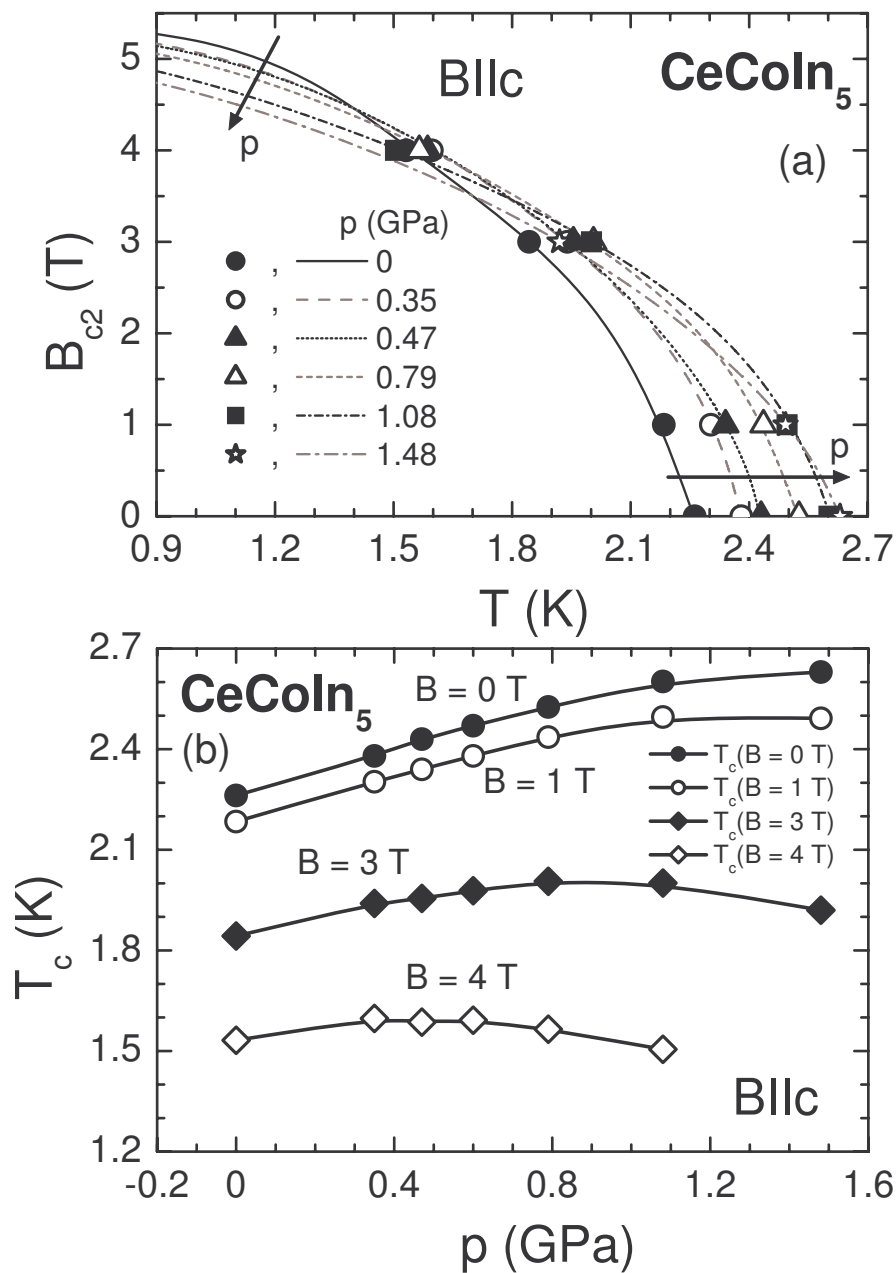


Figure 3.10: (a) $B-T$ phase diagram of the SC phase transition in CeCoIn₅ obtained for different pressures, for $B \parallel c$. Symbols for different pressures are indicated in the figure. The different lines are guides to the eyes. The arrows are indicating the direction how pressure is increasing. (b) $T-p$ phase diagram of CeCoIn₅ obtained for different values of the applied magnetic field, for $B \parallel c$. The values of B and the corresponding symbols are indicated in the figure.

The application of a magnetic field parallel to the c direction is leading to a different behavior than that seen in the case of $B \parallel (ab)$. The initial slope of the upper critical field, $\mathrm{d}B_{c2}(T)/\mathrm{d}T|_{T=T_c; B \parallel c}$, as well as the value of the upper critical field at $T = 0$ K, $B_{c2}(0)|_{B \parallel c}$, is decreasing upon increasing pressure (see figure 3.10a). Together with the results for $B \parallel (ab)$, this emphasizes an increase of the anisotropy in CeCoIn₅ with increasing pressure. A good agreement with results obtained by pressure-dependent low-temperature magnetization [Tayama 2005] and specific-heat measurements [Miclea 2006b] is found in the case of $B \parallel c$ too. A reduction of $\mathrm{d}B_{c2}(T)/\mathrm{d}T|_{T=T_c}$ for $B \parallel c$, from $\mathrm{d}B_{c2}(T)/\mathrm{d}T|_{T=T_c; B \parallel c} \approx -12.82$ T/K at ambient pressure to $\mathrm{d}B_{c2}(T)/\mathrm{d}T|_{T=T_c; B \parallel c} \approx -7.25$ T/K at $p \approx 1.48$ GPa is obtained by our measurements, values determined by using the difference between T_c obtained at $B = 0$ T and $B = 1$ T. The values reported in literature of $\mathrm{d}B_{c2}(T)/\mathrm{d}T|_{T=T_c; B \parallel c} \approx -10.8$ T/K for $p = 0$ GPa and $\mathrm{d}B_{c2}(T)/\mathrm{d}T|_{T=T_c; B \parallel c} \approx -6.5$ T/K for $p = 1.34$ GPa [Miclea 2006b] are supporting our results. Despite a pressure-induced increase of T_c in CeCoIn₅, the upper critical field for $B \parallel c$ decreases from its ambient-pressure value of $B_{c2}(0)|_{B \parallel c} = 4.9$ T [Miclea 2006b] ($B_{c2}(0)|_{B \parallel c} = 4.95$ T [Tayama 2005]) to $B_{c2}(0)|_{B \parallel c} = 4.2$ T at $p = 1.34$ GPa [Miclea 2006b] ($B_{c2}(0)|_{B \parallel c} = 3.8$ T at $p = 1.5$ GPa [Tayama 2005]), a tendency also displayed by our measurements (see figure 3.10a).

Interestingly, as seen in the lower panel of figure 3.10, the pressure where $T_c(p)$ for a certain value of the magnetic field is reaching its maximum value, $p_{max}(B)$, is gradually decreasing with increasing B (for $B \parallel c$). Theoretical predictions for the AFM spin-fluctuation mediated SC suggest that for $B = 0$ T a maximum value of $T_c(p)$ is obtained at the critical pressure p_c (respectively critical concentration, n_c) where $T_N(p)$ is suppressed to $T_N = 0$ K [Millis 1993, Nakamura 1996, Lonzarich 1997, Mathur 1998, Monthoux 1999] (see section 1.2.2 for more details). Accordingly, at $B = 0$ T, the existence of an AFM QCP is expected close to the pressure $p_{max}(0)$, where $T_c(p)$ for $B = 0$ T is reaching its maximum value. From the $T_c(p)$ dependence obtained for different values of B ($B \parallel c$) presented in figure 3.10b we have estimated the pressures, $p_{max}(B)$, where the corresponding $T_c(p)$ attains its maximum value. The magnetic-field dependence of p_{max} is shown in figure 3.11. In addition, the pressure dependence of the upper critical field, $B_{c2}(0)|_{B \parallel c}$, taken from magnetization measurements under pressure [Tayama 2005] is also depicted in figure 3.11 (open symbols). The gray area indicates the region where at $T = 0$ K CeCoIn₅ is in the SC state ($B \parallel c$). By means of electrical-resistivity measurements under pressure and in magnetic field on CeCoIn₅, Ronning *et al.* [Ronning 2006] have estimated, for $B \parallel c$, the pressure dependence of the critical field, $B_{crit}(p)$. For each pressure, B_{crit} was obtained from the magnetic-field dependence of the A coefficient of the T^2 term in the

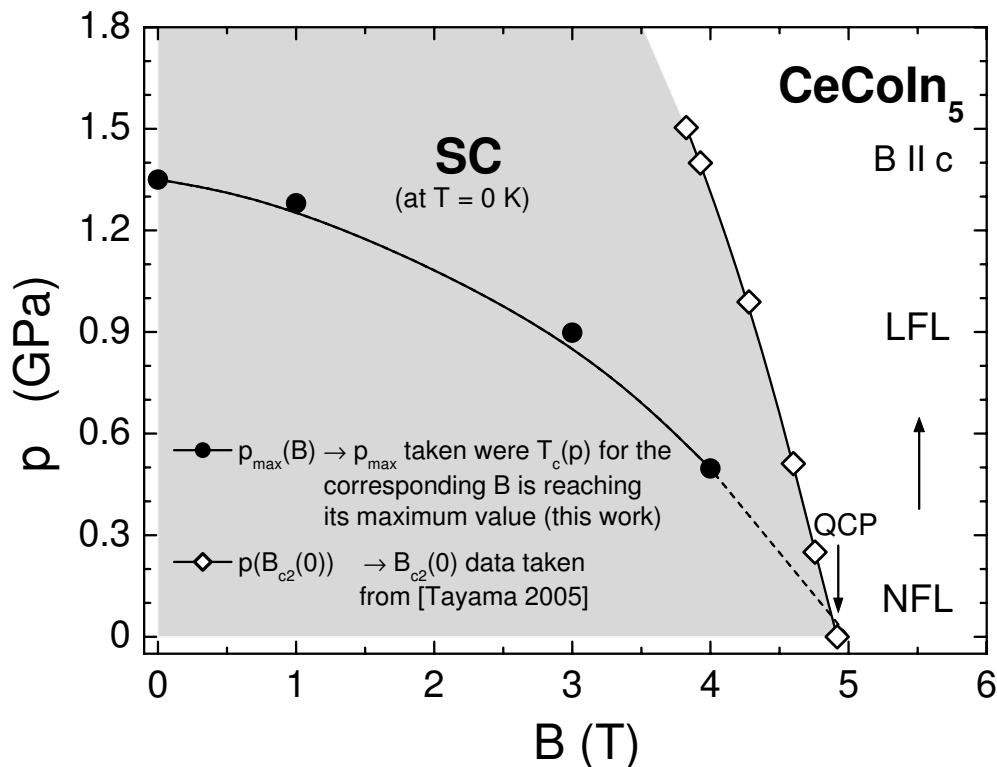


Figure 3.11: Data in the $p - B$ plane obtained for $CeCoIn_5$ ($B \parallel c$). Closed symbols represent the pressure, p_{max} , where for each specific value of B the corresponding $T_c(p)$ (see figure 3.10a) is attaining its maximum value. The open symbols show the pressure dependence of the upper critical field, $B_{c2}(0)|_{B \parallel c}$, as $p(B_{c2}(0))$. The $p(B_{c2}(0))$ data are taken from the work of Tayama *et al.* [Tayama 2005]. The gray area in the figure indicates the region where, at $T = 0$ K, $CeCoIn_5$ is in a SC state ($B \parallel c$).

resistivity ($\rho(T) = \rho_0 + AT^2$) [Ronning 2006]. As a measure of the effective mass of the QPs, the A coefficient ($A \propto m^{*2}$) is expected to diverge at a QCP. In order to obtain B_{crit} , the magnetic-field dependence of the A coefficient was fitted corresponding to $A = A_0(B - B_{crit})^{-1.37}$. Close to the obtained B_{crit} , NFL behavior was detected by the temperature dependence of the resistivity [Ronning 2006]. Surprisingly, our $p_{max}(B)$ ($B \parallel c$) dependence follows the $p(B_{crit})$ line obtained by Ronning *et al.* [Ronning 2006], suggesting that $p_{max}(B)$, shown by closed symbols in figure 3.11, follows the line of expected QCPs in $CeCoIn_5$ ($B \parallel c$). In consequence, the $p_{max}(B)$ values can be considered as critical values where magnetic-field and pressure-tuned QCPs are expected in $CeCoIn_5$ when $B \parallel c$ and figure 3.11 can be viewed as a phase diagram obtained in the $p - B$ plane at $T = 0$ K. The dashed line in figure 3.11

represents the extrapolation of the obtained $p_{max}(B)$. These results show that the maximum value of $T_c(p)$ of CeCoIn₅ is obtained at the critical pressure where a QCP is expected, independent of the value of the applied magnetic field ($B \parallel c$). As mentioned earlier, AFM spin-fluctuation theory predicts that at zero magnetic field a maximum value of $T_c(p)$ is obtained at the critical pressure where the AFM QCP is expected ($T_N \rightarrow 0$ K). Therefore, our results suggest that, in the case of CeCoIn₅, for $B \parallel c$, the afore-mentioned theoretical prediction is valid not only for zero magnetic field, but also for $B \neq 0$ T.

As seen in figure 3.11, the magnetic-field dependence of p_{max} extrapolated to $p_{max} = 0$ GPa yields a value of $B \approx 5$ T, in good agreement with the value of B where a magnetic-field-induced QCP was reported at ambient pressure for $B \parallel c$ [Paglione 2003, Bianchi 2003b]. The detected value of $B \approx 5$ T is close to the upper critical field, $B_{c2}(0)|_{B \parallel c}$. Therefore, it was speculated that the magnetic-field-induced QCP in CeCoIn₅ at ambient pressure ($B \approx 5$ T) could have SC fluctuations as origin [Paglione 2003]. However, based on experimental findings, several arguments exist against a possible SC origin of the magnetic-field-induced QCP. (i) It was found that in CeCoIn₅ at ambient pressure the SC phase transition for $B \parallel c$ at temperatures below a crossover temperature, T_0 , is a first-order phase transition [Bianchi 2002]. Therefore, the SC fluctuations do not become critical. Moreover, the first-order type of the SC transition at $T \leq T_0$ is persisting with increasing pressure (with a pressure-dependent T_0) [Tayama 2005]. (ii) CeRhIn₅, having a larger volume of the unit cell than CeCoIn₅ and presenting AFM order at ambient pressure, as well as pressure-induced SC at higher values of p , displays a $T - p$ phase diagram very similar to that found in the case of CeCoIn₅. A shift of the pressure axis of CeRhIn₅ by $\Delta p \approx -1.5$ GPa leads to an overlap of the $B = 0$ T $T - p$ phase diagram of the two compounds [Knebel 2004, Nicklas priv. comm., Sidorov 2002], suggesting that at ambient pressure CeCoIn₅ is close to an AFM instability. Moreover, dHvA measurements under pressure on CeRhIn₅ reveal a reconstruction of the FS, right at the critical pressure where $T_c(p)$ is reaching its maximum value [Shishido 2005]. The observed change of the FS and the seeming divergence of the cyclotron mass at the critical pressure lead to the speculation that a crossover from the localized to the itinerant state of the $4f$ electron of Ce is taking place at this pressure [Shishido 2005]. However, neither long-range AFM order nor a valence change of Ce was detected in CeCoIn₅. Therefore, the first-order SC phase transition in the vicinity of $B_{c2}(0)$ for $B \parallel c$ in CeCoIn₅ and the closeness to an AFM instability at ambient pressure suggest that the magnetic-field-induced QCP seen at $B \approx B_{c2}(0) \approx 5$ T is more likely due to critical AFM fluctuations than due to SC fluctuations. Our results depicted

in figure 3.11, together with the findings from electrical-resistivity measurements of Ronning *et al.* [Ronning 2006], show that the $p_{max}(B)$ curve, namely the line of expected QCPs, is existing over a broad field and pressure region, $0 \text{ T} \leq B \leq 5 \text{ T}$ and $1.4 \text{ GPa} \geq p_{max} \geq 0 \text{ GPa}$, respectively. Moreover, these results are also suggesting that the magnetic-field-induced QCPs are moving to lower magnetic fields with increasing pressure with a much stronger pressure dependence than $B_{c2}(0)|_{B \parallel c}$, leading to $p_{max} \approx 1.4 \text{ GPa}$ at $B = 0 \text{ T}$, while $B_{c2}(0) \approx 4 \text{ T}$ for $p \approx 1.4 \text{ GPa}$. Therefore, though the critical field almost coincides with $B_{c2}(0)$ at ambient pressure, their evolutions with increasing pressure are completely different, the $p_{max}(B)$ and $p(B_{c2}(0))$ lines departing from each other upon increasing pressure, ruling out SC fluctuations being at the origin of the possible QCPs. In conclusion, these results help to rule out a SC origin of the magnetic-field-induced QCP found in CeCoIn₅ at ambient pressure in the region of $B \approx B_{c2}(0) \approx 5 \text{ T}$ and rather support its possible AFM origin. Moreover, the possibility of existence of a line of QCPs in the $p - B$ phase diagram of CeCoIn₅ at $T = 0 \text{ K}$ ($B \parallel c$) is also suggested, QCPs which probably have their origin in AFM quantum critical fluctuations. The possible existence of AFM QCPs right in the pressure region, $p_{max}(B)$, where $T_c(p)$ for the respective B is reaching its maximum value, independent of the value of B , is suggested. However, the possibility of a valence-fluctuating regime in the close vicinity of the AFM instability in both compounds, CeRhIn₅ and CeCoIn₅, should not be neglected.

Unfortunately, as seen in figure 3.9b, due to the experimental limitations of our setup, mainly consisting in a too small available magnetic field, a similar study for the case of $B \parallel (ab)$ was not possible. However, magnetic-field-dependent specific-heat and resistivity measurements on CeCoIn₅ at ambient pressure have shown that for $B \parallel (ab)$ also exists a magnetic-field-tuned QCP close to the upper critical field, $B_{c2}(0)|_{B \parallel (ab)}$ [Ronning 2005]. Moreover, the magnetic field is less effective in suppressing the critical fluctuations and restoring the FL behavior for $B \parallel (ab)$ as compared to $B \parallel c$ [Ronning 2005]. Therefore, it is expected that the relative closeness to the QCP in CeCoIn₅ strongly depends on the orientation of the magnetic field, the NFL behavior and the fluctuations responsible for the observed quantum critical phenomena being more robust when the magnetic field is applied in the plane ($B \parallel (ab)$) [Ronning 2005].

As seen in figure 3.11, the $p_{max}(B)$ ($B \parallel c$) line where magnetic-field and pressure-induced QCPs are expected in CeCoIn₅ is located in the region where at $T = 0 \text{ K}$ the system is in a SC state (gray area). Therefore, detection of a QCP in the SC state, as well as of the NFL behavior characteristic for the normal state in the close vicinity of a QCP, is not possible, except for $B \approx 5 \text{ T}$, $p = 0 \text{ GPa}$ (indicated by

an arrow and labeled “QCP” in figure 3.11). Indeed, as mentioned earlier, a QCP, suggested by strong deviations of the measured physical properties from a behavior characteristic to a LFL state, has been observed right at this point ($B \approx 5$ T, $p_{max} = 0$ GPa) [Paglione 2003, Bianchi 2003b]. By assuming SC fluctuations at the origin of this observed QCP one would expect that these SC fluctuations also lead to a QCP once the pressure is increased. Since $B_{c2}(0)|_{B\parallel c}$ only slightly increases with increasing pressure one expects that for a certain value of B , $B \gtrsim 5$ T, the NFL behavior observed at ambient pressure should also not change with increasing pressure (at least the NFL behavior should track the pressure dependence of $B_{c2}(0)|_{B\parallel c}$). On the other hand, if the QCP observed at ambient pressure is related to the $p_{max}(B)$ line, at a fixed value of B , $B \gtrsim 5$ T, a change from NFL to LFL behavior is expected upon increasing pressure. This issue is nicely elucidated by our pressure and magnetic-field-dependent specific-heat data on CeCoIn₅. Indeed, the specific-heat data for $B = 8$ T presented in figure 3.12 clearly show a gradual transition from NFL to LFL behavior with increasing pressure. Therefore, it is becoming evident that the observed NFL behavior is related to the $p_{max}(B)$ line. In conclusion, these results help to rule out SC fluctuations being at the origin of the QCP seen in CeCoIn₅, suggesting that the observed quantum critical behavior is most likely related to a yet undetected AFM instability in CeCoIn₅.

In the vicinity of a QCP, a system is known to show deviations from LFL behavior. The low-temperature electronic specific heat of a system is characterized by a linear T dependence in the LFL region, while the NFL regime shows a $\Delta C(T)/T \propto -\ln T$ dependence for 2D and a $\Delta C(T)/T \propto -\sqrt{T}$ dependence for 3D critical AFM spin fluctuations [Moriya 1995] (for details see table 1.2). Due to the fact that a SC phase transition is detected in our specific-heat measurements on CeCoIn₅ over the entire measured pressure range at a relatively high temperature (e.g. $T_c|_{p=0\text{GPa}} \approx 2.3$ K), the examination of the normal-state properties of the system at temperatures $T > T_c$ is very difficult (since there is a relatively narrow temperature range available at $T > T_c$ and, additionally, we did not remove the lattice contribution to the specific heat, which is non-negligible in this temperature range). Application of magnetic field leads to the suppression of the SC phase and therefore helps to access the low-temperature normal-state properties of a system. However, in the case of CeCoIn₅ the magnetic field necessary to destroy the SC state is rather high, making the study of CeCoIn₅ more difficult. Moreover, as previously described, in our measurements part of the samples were oriented in the direction $B \parallel c$, while the remaining part were placed corresponding to $B \parallel (ab)$, leading to the detection of the SC phase transitions corresponding to both orientations. Therefore, the complete suppression

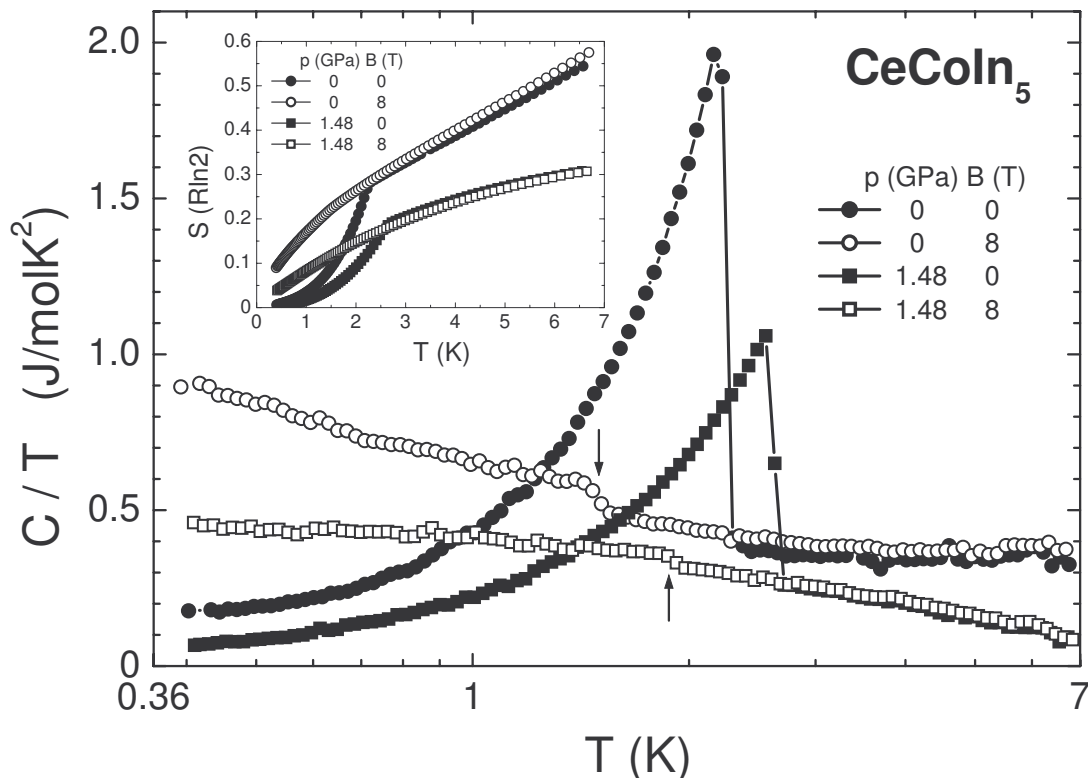


Figure 3.12: Specific heat of $CeCoIn_5$ as $C(T)/T$ versus $\log T$ at $p = 0$ GPa (circles) and $p \approx 1.48$ GPa (squares), both at $B = 0$ T (full symbols) and $B = 8$ T (open symbols). Arrows indicate the SC phase transition anomalies at $B = 8$ T for $B \parallel (ab)$. Inset: calculated entropy as function of T for the specific-heat curves shown in the main figure. The symbols are the same as in the main plot.

of the SC phase transition anomaly in our data is not achieved for the entire pressure and magnetic-field range of our measurements ($p \leq 1.48$ GPa, $B \leq 8$ T), causing an uncertainty in the temperature dependence of the low-temperature C/T in the normal state of $CeCoIn_5$. $C(T)/T$ of $CeCoIn_5$ on a logarithmic temperature scale is presented in figure 3.12 for ambient pressure and for the highest pressure of our measurements of $p \approx 1.48$ GPa, at $B = 0$ T and $B = 8$ T. Apart from the sharp SC phase transition seen at $B = 0$ T, at $B = 8$ T a tiny anomaly (marked by arrows) is visible at about $T \approx 1.48$ K ($p = 0$ GPa) and $T \approx 1.91$ K ($p \approx 1.48$ GPa), corresponding to the SC phase transition of those crystals placed with $B \parallel (ab)$. Below the SC phase transition at $B = 8$ T, at temperatures $T \leq 1$ K, the ambient-pressure $C(T)/T$ data increase as $-\ln T$ upon cooling, clearly indicating NFL behavior. In contrast, for $p \approx 1.48$ GPa a nearly constant $C(T)/T$ is detected for $T \leq 1$ K, a dependence expected for a LFL.

The gradual pressure-induced change from a logarithmic temperature dependence of $C(T)/T$ to a nearly constant $C(T)/T$ at low temperatures suggests that CeCoIn₅ at $B = 8$ T ($B \parallel c$) is tuned by application of pressure from a NFL to a LFL state. These findings suggest that CeCoIn₅ at $p = 0$ GPa and $B = 8$ T ($B \parallel c$) is located close to a QCP, while by application of pressure is shifted away from it. This supports our data presented in figure 3.11, where the $p_{max}(B)$ line was suggested to be a line of QCPs.

In addition, the $B = 0$ T data in figure 3.12 illustrate that the SC coupling strength, measured by the ratio of $\Delta C/(\gamma_n T_c)|_{T=T_c}$, is decreasing upon increasing pressure. The strong reduction of the low-temperature entropy with increasing pressure, as well as the recovery of the entropy in the normal state, independent of the value of B , over the entire pressure range of our experiment ($p \leq 1.48$ GPa), is exemplified in the inset of figure 3.12.

3.2.3 Discussion - CeCoIn₅

We have studied the pressure ($p \leq 1.5$ GPa) and magnetic-field ($B \leq 8$ T) dependence of the low-temperature (0.35 K $\leq T \leq 7$ K) specific heat of the HF SC CeCoIn₅. At $B = 0$ T, the SC transition temperature, T_c , is increasing with increasing pressure from $T_c \approx 2.26$ K at $p = 0$ GPa to a maximum value of about $T_c \approx 2.63$ K at $p \approx 1.4$ GPa, from where it starts to decrease upon further increasing the pressure. Due to the SC state in CeCoIn₅ at low temperatures, as an estimate for the Sommerfeld coefficient, γ , we used the value of the specific-heat coefficient at $T = 3$ K ($C/T|_{T=3K}$), a temperature which exceeds T_c in the entire pressure range of our experiment. Since the Sommerfeld coefficient is directly proportional to the effective QP mass, m^* , ($\gamma \propto m^*$) we consider $C/T|_{T=3K}$ as a direct measure of m^* . The HF character of CeCoIn₅ is suggested by the large values of $C/T|_{T=3K}$ obtained over the entire pressure range of our experiment (e.g. $C/T|_{T=3K} \approx 0.353$ J/(molK²) at $p = 0$ GPa). It was shown that the effective QP mass in CeCoIn₅ decreases continuously with increasing pressure, with $d \ln(C/T|_{T=3K})/dp \approx -0.263$ /GPa. In good agreement with the pressure dependence of m^* , the Kondo temperature, T_K , continuously increases with increasing pressure, both dependencies suggesting the expected increase with pressure of the strength of the hybridization between the Ce $4f$ and the conduction electrons in CeCoIn₅. Moreover, for the entire measured pressure range, $1/m^* \propto T_c$ is found in CeCoIn₅. This supports the prediction of the theory of spin-fluctuation mediated SC ($T_c \propto T_{sf} \propto 1/m^*$) [Millis 1988, Lonzarich 1997, Mathur 1998] and suggests that the SC state in CeCoIn₅ is likely to be mediated by strong magnetic fluctuations.

A $\Delta C(T)/T \propto T^2$ dependence in the SC state of CeCoIn₅, in the low-temperature range of $0.4 \text{ K} \leq T \leq 1 \text{ K}$, has been detected over the entire measured pressure range ($p \leq 1.5 \text{ GPa}$), hinting at the unconventional nature of the SC state in CeCoIn₅. Moreover, the $\Delta C/(\gamma_n T_c)|_{T=T_c}$ ratio, a measure of the SC coupling strength, decreases with increasing pressure and shows, over the entire pressure range of our experiment, extremely high values, suggesting that Cooper pairs in the SC state of CeCoIn₅ are formed by strongly coupled heavy QPs.

The estimated residual specific-heat coefficient (at $T \rightarrow 0 \text{ K}$), in the $B = 0 \text{ T}$ SC state of CeCoIn₅, $C/T|_{T=0\text{K}}$, displays non-zero values and gradually decreases with increasing pressure. The ratio between the residual specific-heat coefficient and the Sommerfeld coefficient in the normal state, $(C/T|_{T=0\text{K}})/(C/T|_{T=3\text{K}})$, decreases upon increasing pressure, hinting at a gradual increase of the fraction of the FS implied in the SC state with increasing pressure. These results clearly suggest the gradual shift of CeCoIn₅ from a SC state in the vicinity of an AFM instability at ambient pressure to a SC state at finite pressure, where the influence of the AFM fluctuations is much less perceptible. A common mechanism implied in both phenomena, long-range AFM order expected at a slightly negative pressure and SC, appears therefore likely.

The low-temperature entropy of CeCoIn₅ at $B = 0 \text{ T}$, over the whole measured temperature range, is continuously decreasing with increasing pressure. At $T = 6 \text{ K}$, the value of $S(p = 0 \text{ GPa})|_{T=6\text{K}} \approx 0.5 R \ln 2$ obtained at ambient pressure is gradually reduced to $S(p \approx 1.48 \text{ GPa})|_{T=6\text{K}} \approx 0.3 R \ln 2$ at the highest pressure of our experiment. Consequently, the Kondo temperature of the system is increasing from $T_K \approx 12 \text{ K}$ at $p = 0 \text{ GPa}$ to $T_K \approx 37 \text{ K}$ at $p \approx 1.48 \text{ GPa}$. The observed results are consistent with the well-known behavior of Ce-based HF systems and are due to a pressure-induced increase of the strength of the hybridization between the $4f$ electrons of Ce and the conduction electrons.

The large values of the upper critical field observed at ambient pressure, characteristic to HF systems, are persisting with increasing pressure in CeCoIn₅. Furthermore, the anisotropy of the SC state found to be large already at ambient pressure further increases with increasing pressure ($p \leq 1.5 \text{ GPa}$): $B_{c2}(0)|_{B\parallel c}$ decreases, while $B_{c2}(0)|_{B\parallel(ab)}$ increases upon increasing pressure.

Our experiments have shown that over the entire pressure range $p \leq 1.5 \text{ GPa}$, the total entropy achieved in the normal state is independent of the value of the external magnetic field (for $B \leq 8 \text{ T}$). This conservation of entropy suggests that the formation of the HF state, expected to take place continuously down to lower temperatures (below T_c for $B = 0 \text{ T}$), is interrupted and replaced by the SC state in CeCoIn₅.

AFM spin-fluctuation theory suggests that at $B = 0$ T the critical pressure (p_c) where T_N is suppressed to $T_N = 0$ K is located in the pressure region where the SC transition temperature $T_c(p)$ reaches its maximum value [Millis 1993, Nakamura 1996, Lonzarich 1997, Mathur 1998, Monthoux 1999]. Since for $B = 0$ T the maximum value of $T_c(p)$ for CeCoIn₅ is obtained at $p_c \approx 1.4$ GPa, we would expect the presence of an AFM QCP in CeCoIn₅ at this pressure. However, detection of this QCP is difficult because of the SC state. Application of a magnetic field helps to suppress the SC state. By defining $p_{max}(B)$ as the pressure where, for the case of $B \parallel c$, the $T_c(p)$ corresponding to each value of B is reaching its maximum value, we have shown that there exists the possibility to have at $p_{max}(B)$ a line of QCPs (see figure 3.11). We have seen that the $p_{max}(B)$ curve obtained by our measurements is located right where the line of QCPs has been detected by the resistivity measurements under pressure and in magnetic field ($B \parallel c$) of Ronning *et al.* [Ronning 2006]. Therefore, we suggest that the above-mentioned prediction of the AFM spin-fluctuation theory is valid in the case of CeCoIn₅ also for magnetic fields $B \neq 0$ T ($B \parallel c$). Due to the fact that the presumable line of QCPs is almost completely located in the region where the SC phase is present, observation of the QCPs is unlikely. The extrapolation of the $p_{max}(B)$ curve to $p_{max} = 0$ GPa leads to a value of the magnetic field of about $B \approx 5$ T. Since at $T = 0$ K, the $B \approx 5$ T, $p_{max} = 0$ GPa point is located right at the border of the SC state, the presence of a QCP can be expected for CeCoIn₅ at ambient pressure and at $B \approx 5$ T ($B \parallel c$). Several experiments performed at ambient pressure and at low temperatures indeed hint at the existence of a QCP at $B \approx 5$ T ($B \parallel c$). Since this value of B nearly coincides with the value of the upper critical field necessary to completely suppress SC, $B_{c2}(0)|_{B \parallel c}$, the possibility of a SC origin of the observed QCP cannot be excluded. However, we have shown that our data help to eliminate the possibility of SC fluctuations as a source for the observed magnetic-field-induced QCP in the ambient-pressure CeCoIn₅ and suggest that the observed QCP is of AFM origin. Ambient-pressure measurements in high magnetic fields and at low temperatures by Ronning *et al.* have shown that there also exists a magnetic-field-induced QCP for $B \parallel (ab)$ and the value of the critical field also coincides with the upper critical field for $B \parallel (ab)$ [Ronning 2005]. Therefore, it seems that the magnetic anisotropy of the SC state in CeCoIn₅ is strongly linked to the AFM fluctuations. These results also suggest that the same mechanism is implied in the formation of both states in CeCoIn₅, AFM (at a slightly negative pressure) and SC, and speak in favor of the magnetic-fluctuation mediated SC state in CeCoIn₅.

The predicted line of QCPs, $p_{max}(B)$ ($B \parallel c$), nearly completely hidden in the SC state of CeCoIn₅, exhibits a much stronger pressure dependence compared to

the upper critical field of SC, $B_{c2}(0)|_{B\parallel c}$. Our pressure-dependent low-temperature specific-heat data at a fixed value of B , $B \gtrsim 5$ T, show a clear shift from NFL behavior at ambient pressure to LFL behavior at higher pressures, suggesting that by increasing the pressure (at $B \gtrsim 5$ T) one is moving away from the quantum critical region (respectively, line of QCPs) in CeCoIn₅. Since in the pressure range of our experiment $B_{c2}(0)|_{B\parallel c}$ decreases only slightly with increasing pressure and the $p_{max}(B)$ line shifts to very low values of B upon increasing pressure, it is obvious that the observed pressure-induced change from a NFL to a LFL behavior is not related to SC, instead it is most probably linked to the $p_{max}(B)$ line. Therefore, it is supposed that AFM critical fluctuations are most likely responsible for the observed magnetic-field-induced QCP at ambient pressure, as well as for the line of expected QCPs hidden by the SC state of CeCoIn₅. Whether these QCPs, predicted to be located in the SC state, really exist or not is still an open question. Though CeCoIn₅ is apparently located very close to an AFM instability at ambient pressure, it is worth noting that no long-range magnetic order has been detected in CeCoIn₅ so far. Moreover, a possible pressure-induced valence transition (at p_v) in CeCoIn₅, not very far from the AFM instability (at p_c ; $p_c \leq p_v$), though not yet observed, should not be neglected. However, regarding the SC state in CeCoIn₅ for $p \leq 1.5$ GPa, we have provided strong evidence that this is an unconventional SC state and that the mechanism mediating the formation of the Cooper pairs is most likely electronic in origin, an AFM spin-fluctuation mediated SC state being strongly suggested.

3.3 Effect of pressure on the heavy-fermion anti-ferromagnet Ce₂RhIn₈

3.3.1 Physical properties of Ce₂RhIn₈

Ce₂RhIn₈ belongs to the subfamily of $Ce_nRh_mIn_{3n+2m}$ compounds ($n = 2, m = 1$) derived from the HF AFM CeIn₃ (cubic structure, $n = \infty, m = 0, T_N \approx 10.1$ K) which becomes a SC with a maximum $T_c \approx 0.25$ K at $p \approx 2.6$ GPa [Walker 1997]. CeRhIn₅ ($n = 1, m = 1, T_N \approx 3.8$ K) can be described as a layered structure, consisting of alternating layers of CeIn₃ and RhIn₂ along the c axis [Hegger 2000]. CeRhIn₅ under pressure becomes a SC with a maximum $T_c \approx 2.1$ K at $p_c \approx 2.1$ GPa [Fisher 2002] being one order of magnitude larger than that of CeIn₃. The compound presented here, Ce₂RhIn₈ ($n = 2, m = 1, T_N \approx 3$ K), crystallizes in the tetragonal Ho₂CoGa₈ structure (shown in figure 3.2, middle) consisting of alternating bi-layers of CeIn₃ and one layer of RhIn₂ [Thompson 2001]. Due to its crystal structure Ce₂RhIn₈

can be regarded as a magnetic hybrid between $CeIn_3$ and $CeRhIn_5$. Therefore, one expects the physical properties of Ce_2RhIn_8 to be located somewhere in between those of $CeIn_3$ and $CeRhIn_5$.

Similar to the $n = \infty$ and $n = 1$ compounds, $CeIn_3$ and $CeRhIn_5$, the physical properties of Ce_2RhIn_8 result from the competition between magnetic exchange interaction and Kondo effect. In addition, the effect of CEFs has to be considered. At ambient pressure, Ce_2RhIn_8 is a HF AFM with a Néel temperature $T_N \approx 3$ K. Susceptibility data above $T = 200$ K show that the high-temperature effective magnetic moment exhibits a small anisotropy, but is almost equal to the Hund's rule value of $\mu_{eff} = 2.54 \mu_B$ per Ce^{3+} expected for the $J = 5/2$ Ce multiplet ($\mu_{eff} = 2.53 \mu_B$ per Ce for $B \parallel (ab)$ and $\mu_{eff} = 2.47 \mu_B$ per Ce for $B \parallel c$) [Malinowski 2003]. Consistent with the single-impurity Kondo behavior, the resistivity in the temperature interval $55 \text{ K} \leq T \leq 130 \text{ K}$ follows a $\Delta\rho(T) \propto -\ln T$ dependence [Malinowski 2003]. A maximum in the resistivity, indicating the onset of coherent Kondo scattering, is seen at $T^* \approx 4.5$ K [Nicklas 2003]. The Sommerfeld coefficient, estimated from $C_{el}(T)$ at a temperature slightly above the AFM phase transition, of $\gamma \approx 0.5 \text{ J}/(\text{K}^2\text{mol-Ce})$ proves the HF nature of Ce_2RhIn_8 and is similar to the value of $\gamma \approx 0.4 \text{ J}/(\text{molK}^2)$ found for $CeRhIn_5$ [Hegger 2000], but higher than the value of $\gamma \approx 0.12 \text{ J}/(\text{molK}^2)$ for $CeIn_3$ [Sato 1993]. The Kondo temperature of Ce_2RhIn_8 , estimated from specific-heat measurements to be $T_K \approx 10$ K, similar to the situation in $CeRhIn_5$, is of the same order of magnitude as the Néel temperature, $T_K \sim T_N$, leading to interesting physical properties in both compounds. Contrasting with the similarities between Ce_2RhIn_8 and $CeRhIn_5$ seen in the Sommerfeld coefficient, T_N and T_K , the low-temperature ordered moment of Ce_2RhIn_8 of $\mu_{ord} \approx 0.55 \mu_B$ per Ce [Bao 2001] is very close to that for the $n = \infty$ compound $CeIn_3$ ($\mu_{ord} \approx 0.48 \mu_B$ per Ce [Benoit 1980], $\mu_{ord} \approx 0.65 \mu_B$ per Ce [Lawrence 1980]), while the ordered moment of $CeRhIn_5$ has a higher value ($\mu_{ord} \approx (0.75 - 0.80) \mu_B$ per Ce [Bao 2000, Llobet 2004]). The higher value of μ_{ord} in $CeRhIn_5$ suggests the possibility that Kondo screening is more effective in the more 3D-like systems. It was found that the low-temperature magnetic moment of Ce_2RhIn_8 points 52° from the (ab) plane [Bao 2001], while in the case of $CeRhIn_5$ the moments rotate in the (ab) plane showing a helical magnetic structure along the c axis [Bao 2000]. To our knowledge, the direction of the magnetic moment for the $n = \infty$ member $CeIn_3$ has not yet been determined [Benoit 1980, Lawrence 1980].

As already mentioned, the thermodynamic properties of Ce_2RhIn_8 at low temperatures are dominated by the interplay of Kondo and RKKY interactions with the Kondo temperature being of the same order of magnitude as the AFM ordering temperature T_N . The partially Kondo-compensated magnetic state in Ce_2RhIn_8 is

reflected by the reduced ordered moment. Moreover, the magnetic entropy released at the ordering temperature, $S_{el}(T_N)$, represents only $\approx 34\%$ of the full entropy $R \ln 2$ associated with the CEF doublet ground state. The full entropy of $R \ln 2$ is achieved at $T \approx 20$ K, similar to what was found for $CeRhIn_5$ ($n = 1$) [Cornelius 2001]. At temperatures $T < T_N$ the ambient-pressure specific-heat measurements at $B = 0$ T show for the case of $CeRhIn_5$ ($n = 1$) the existence of an anisotropic SDW gap opening on the FS, while in the case of the more 3D compound Ce_2RhIn_8 ($n = 2$) a behavior consistent with a simple AFM magnon is detected [Cornelius 2001]. From fitting the $B = 0$ T specific-heat data at $T < T_N$, a relatively large residual specific-heat coefficient at $T = 0$ K of $\gamma_0 \approx 0.37$ J/(K²mol-Ce) was extracted for Ce_2RhIn_8 in comparison to only $\gamma_0 \approx 0.056$ J/(molK²) for the case of $CeRhIn_5$ [Cornelius 2001]. It was therefore estimated that approximately 92% of the FS remains ungapped below T_N for Ce_2RhIn_8 in comparison to only $\approx 12\%$ for the case of $CeRhIn_5$ [Cornelius 2001]. This behavior hints at the more 2D-like electronic structure in the case of the $n = 1$ member of this family, $CeRhIn_5$, in comparison to the $n = 2$ member, Ce_2RhIn_8 [Cornelius 2001]. The RKKY interaction in Ce_2RhIn_8 gives rise to the AFM ordered state below $T_N \approx 3$ K, as well as to a very rich $B - T$ phase diagram [Cornelius 2001]. For the magnetic field $B \parallel c$, Ce_2RhIn_8 , similar to $CeRhIn_5$, shows a typical behavior for an AFM as T_N decreases with increasing magnetic field. The situation appears to be different for $B \parallel a$, where in both compounds several magnetic-field-induced phase transitions occur at temperatures below T_N [Cornelius 2001]. However, pointing to a less anisotropic situation in the case of Ce_2RhIn_8 ($n = 2$), for $B \parallel a$ T_N also decreases with increasing magnetic field in a manner similar to the case of $B \parallel c$, while in $CeRhIn_5$ ($n = 1$) for $B \parallel a$ T_N slightly increases with increasing magnetic field [Cornelius 2001]. In figure 3.13 the ambient-pressure $B - T$ phase diagram of Ce_2RhIn_8 is shown for $B \parallel a$, as taken from Cornelius *et al.* [Cornelius 2001]. The nature of the phase transitions which occur below T_N in external magnetic field $B \parallel a$ in both Ce_2RhIn_8 and $CeRhIn_5$, as well as the order of the phase transitions, has not yet been elucidated [Cornelius 2001]. However, despite of the similar $B - T$ phase diagrams for $CeRhIn_5$ ($n = 1$) and Ce_2RhIn_8 ($n = 2$) for both field orientations, $B \parallel a$ and $B \parallel c$, suggesting a similarity in the electronic dimensionality of the two systems, a clear discrepancy is visible in the anisotropy of $T_N(B)$. While in $CeRhIn_5$ upon increasing B T_N shows a slight increase for $B \parallel a$ and decreases for $B \parallel c$, in the case of Ce_2RhIn_8 almost no anisotropy of $T_N(B)$ can be observed, T_N decreasing slightly with increasing B for both field orientations. This feature might suggest the more 3D character of Ce_2RhIn_8 .

At temperatures below $T \approx 20$ K, C_{el}/T and the thermal-expansion coefficient

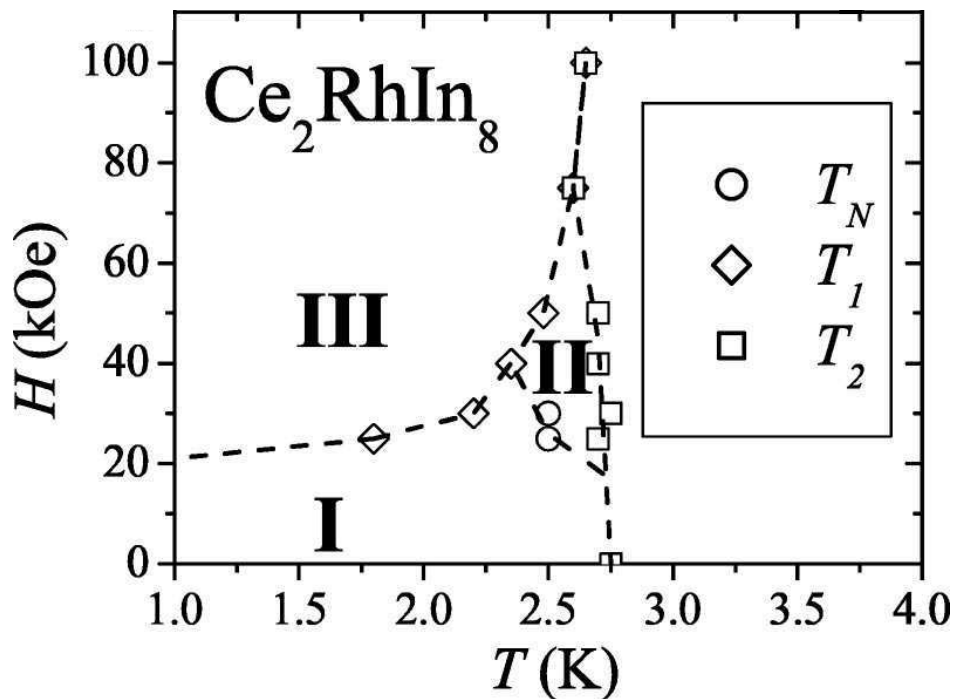


Figure 3.13: $B-T$ phase diagram of Ce_2RhIn_8 for $B \parallel a$ ($p = 0$ GPa). T_N corresponds to the AFM phase transition, while T_1 and T_2 mark the magnetic-field-induced transitions. The dashed lines are guides to the eyes. The nature of the phase transitions at T_1 and T_2 is not yet known. Figure taken from [Cornelius 2001].

divided by temperature, α/T , grow with decreasing temperature [Malinowski 2003], a behavior consistent with the Kondo renormalization. Above $T \approx 20$ K the thermodynamic properties of Ce_2RhIn_8 are not dictated anymore by magnetic order or by Kondo renormalization, but are dominated by CEF effects [Malinowski 2003]. In the presence of tetragonal crystal symmetry the Ce^{3+} $J = 5/2$ multiplet splits into three doublets: $\Gamma_7^{(2)}$ - ground state, $\Gamma_7^{(1)}$ - first excited state situated at Δ_1 above the ground state and Γ_6 - highest-lying state at Δ_2 above the ground state ($\Delta_1 \approx (71 \pm 6)$ K and $\Delta_2 \approx (195 \pm 10)$ K for Ce_2RhIn_8) [Malinowski 2003]. The CEF level scheme for the three members of the $Ce_nRh_mIn_{3n+2m}$ family is similar. The ground state is the $\Gamma_7^{(2)}$ doublet while the four-fold degenerate Γ_8 excited state of the cubic $CeIn_3$ is split into two doublets, $\Gamma_7^{(1)}$ and Γ_6 , in the tetragonal crystal symmetry, with a similar value of Δ_1 in the two tetragonal compounds $CeRhIn_5$ and Ce_2RhIn_8 , but with a Δ_2 approximately 40% higher in the case of the more anisotropic, 2D-like, $CeRhIn_5$ [Malinowski 2003].

Measurements of the electrical resistivity of Ce_2RhIn_8 under pressure revealed a monotonic reduction of T_N upon increasing pressure up to $p \approx 1.6$ GPa. The observed $T_N(p)$ dependence extrapolated to $T_N = 0$ K yields a critical pressure of $p_c \approx 3$ GPa

[Nicklas 2003]. At $p \geq 1.6$ GPa SC was shown to be established in Ce_2RhIn_8 , with a maximum resistive onset $T_c(onset) \approx 2$ K at $p \approx 2.3$ GPa [Nicklas 2003]. The SC phase transition detected by resistivity measurements is very broad in temperature. For $p \approx 1.63$ GPa, the onset of SC appears already at $T_c(onset) \approx 1.1$ K, while the zero-resistance state, accompanied by the onset of the diamagnetic response seen in a.c. susceptibility, sets in at $T_c \approx 0.6$ K [Nicklas 2003]. Unfortunately, due to limitations in temperature and pressure, the zero-resistance state was not possible to be followed over the whole pressure range presented in the work of Nicklas and coworkers [Nicklas 2003]. The detected maximum in the resistive SC onset temperature of $T_c(onset) \approx 2$ K, together with the broad SC phase transition observed in $\rho(T)$, leads to the conclusion that the maximum bulk T_c in Ce_2RhIn_8 should be at temperatures lower than $T = 2$ K. Therefore, comparing the maximum values of T_c obtained in the three members of the $Ce_nRh_mIn_{3n+2m}$ family suggests that the bi-layer compound, Ce_2RhIn_8 , is indeed situated somewhere in between the $n = 1$ and $n = \infty$ members, in agreement with the theory of magnetically mediated SC. This theory predicts that T_c for the magnetic-fluctuation mediated SC should increase upon reducing the dimensionality of the system [Monthoux 2001]. However, the large residual resistivity in Ce_2RhIn_8 , $\rho_0 \approx 65 \mu\Omega\text{cm}$ [Nicklas 2003], two orders of magnitude larger than compared to those in $CeRhIn_5$ and $CeIn_3$, where $\rho_0 \approx 1 \mu\Omega\text{cm}$ [Hegger 2000, Mathur 1998], makes the comparison more difficult. dHvA measurements together with LDA (local density approximation) calculations have revealed that the topology of the FS at ambient pressure, mainly consisting of cylindrical FS sheets, hints at an anisotropic, quasi-2D, electronic structure in Ce_2RhIn_8 [Ueda 2004]. The main physical properties presented above for the three members of the $Ce_nRh_mIn_{3n+2m}$ family are summarized in table 3.2. In the following part we will present a pressure study on the low-temperature specific heat of Ce_2RhIn_8 . The interplay of Kondo interaction, AFM order and SC, as well as the role of dimensionality on the possibly magnetically mediated SC in the $Ce_nRh_mIn_{3n+2m}$ family, will be studied in more detail.

3.3.2 Experimental results - Ce_2RhIn_8

We have performed low-temperature ($0.35 \text{ K} \leq T \leq 7 \text{ K}$) heat-capacity measurements on single-crystalline Ce_2RhIn_8 under hydrostatic pressure ($0 \text{ GPa} \leq p \leq 1.65 \text{ GPa}$) and in magnetic field ($0 \text{ T} \leq B \leq 8 \text{ T}$). The single-crystalline samples of Ce_2RhIn_8 used in our experiments were prepared by N. O. Moreno in the group of J. L. Sarrao at Los Alamos National Laboratory, USA. The Ce_2RhIn_8 single crystals were grown from In flux. Powder X-ray diffraction patterns obtained on crushed single

compound	n	γ (J/(K ² mol-Ce))	T_N (K)	p_c (GPa)	maximum T_c (K)	μ_{ord} (μ_B per Ce)	q (h,k,l)	ρ_0 ($\mu\Omega\text{cm}$)
CeRhIn ₅ ($m = 1$)	1	0.40 [1]	3.8 [1]	2.1 [2]	2.1 [2]	0.75 - 0.80 [3],[4]	($\frac{1}{2}, \frac{1}{2}, 0.297$) [3]	1 [1]
Ce ₂ RhIn ₈ ($m = 1$)	2	0.50 [5]	3.0 [5]	3 [6]	2 (onset of T_c) [6]	0.55 [7]	($\frac{1}{2}, \frac{1}{2}, 0$) [7]	65 [6]
CeIn ₃ ($m = 0$)	∞	0.12 [8]	10.1 [9]	2.6 [9]	0.25 [9]	0.48; 0.65 [10],[11]	($\frac{1}{2}, \frac{1}{2}, \frac{1}{2}$) [10],[11]	1 [9]

Table 3.2: Physical properties of the $Ce_nRh_mIn_{3n+2m}$ compounds. The used symbols are representing: γ - Sommerfeld coefficient, T_N - Néel temperature, p_c - critical pressure where $T_N \rightarrow 0$ K, T_c - SC transition temperature, μ_{ord} - low-temperature ordered moment, q - AFM propagation vector and ρ_0 - residual resistivity. References are indicated in brackets below each value and they correspond to: [1]-[Hegger 2000], [2]-[Fisher 2002], [3]-[Bao 2000], [4]-[Llobet 2004], [5]-this work, [6]-[Nicklas 2003], [7]-[Bao 2001], [8]-[Sato 1993], [9]-[Walker 1997], [10]-[Benoit 1980], [11]-[Lawrence 1980].

crystals confirmed the proper tetragonal Ho_2CoGa_8 structure (crystal structure shown in figure 3.2, middle) with lattice parameters $a = 0.4665(1)$ nm and $c = 1.2244(5)$ nm at room temperature [Thompson 2001]. The heat-capacity measurements under hydrostatic pressure have been performed by the compensated quasiadiabatic heat-pulse technique in a single-shot 3He evaporation cryostat equipped with a SC magnet. To achieve hydrostatic pressure, a CuBe piston-cylinder type pressure cell with Fluorinert FC72 as pressure transmitting medium was used. To monitor the pressure at low temperatures, the SC transition temperatures of two small pieces of Sn, one fixed outside and the second placed inside of the pressure cell, were inductively detected. The outer Sn sample served as reference for ambient pressure, while the Sn placed inside, next to the samples, was used for detecting the pressure in the cell. A more detailed description of the experimental setup used for our measurements is contained in Chapter 2. Several single crystals, with a total sample mass of about 0.4 g, were used to perform the measurements under pressure. The different pieces had two specific orientations with respect to the direction of the applied magnetic field, most of them being placed with $B \parallel c$ and only a few with $B \parallel (ab)$. Concerning the quality of the samples, small amounts of In inclusions remaining from the flux and accounting for approximately 4% of the total sample mass could be detected by a.c.-susceptibility measurements. The heat capacity of the included In is negligible in comparison to the heat capacity of the measured samples and therefore does not need to be subtracted.

However, due to the correction to the total sample mass, a shift to higher absolute values (by $\approx 4\%$) of the determined specific heat of Ce_2RhIn_8 could be regarded as error bar. The total amount of samples measured in the pressure cell contributes only partly to the total measured heat capacity. Therefore, to estimate the accuracy of the absolute values of $C(T)$ of Ce_2RhIn_8 obtained by our measurements we have represented in figure 2.6 the relative contribution of the heat capacity of the samples to the total heat capacity (C_{sample}/C_{total}) over the entire pressure and temperature range of our experiment. One can see that values of C_{sample}/C_{total} ranging from about 4% to 28% are obtained for the measured temperature and pressure interval. These values are relatively good for this type of heat-capacity measurements under hydrostatic pressure. Measurements of the low-temperature ($0.5\text{ K} \leq T \leq 4\text{ K}$) specific heat at ambient pressure and in applied magnetic field ($B \leq 3\text{ T}$, $B \parallel (ab)$) on a sample prepared from the same batch as the samples used in the pressure cell have been carried out in a Quantum Design PPMS with a ^3He option by employing the relaxation-time technique. In order to check for the appearance of pressure-induced SC at low temperatures, measurements of a.c. susceptibility were also performed. For temperatures down to $T = 260\text{ mK}$ the ^3He evaporation cryostat (combined with adiabatic demagnetization of the magnetic moments of Cu from the pressure cell) was used, while for temperatures down to $T = 50\text{ mK}$ a Kelvinox 100 dilution refrigerator was employed. For the complete pressure range, the electronic contribution to the specific heat (C_{el}) of Ce_2RhIn_8 was obtained by subtracting the lattice specific heat obtained at ambient pressure from the isostructural non-magnetic reference compound La_2RhIn_8 [Malinowski 2003]. The relatively small variation of the specific heat of La_2RhIn_8 with pressure, in the temperature and pressure range of our experiment ($0.35\text{ K} \leq T \leq 7\text{ K}$, $p \leq 1.65\text{ GPa}$), was neglected. The nuclear Schottky contribution of In to the specific heat of Ce_2RhIn_8 was not subtracted from the data since it is considered small enough to be neglected in the temperature and magnetic-field range of our measurements ($T \geq 0.35\text{ K}$, $B \leq 8\text{ T}$).

The low-temperature electronic contribution to the specific heat ($C_{el}(T)$) and the electrical resistivity ($\rho(T)$) of Ce_2RhIn_8 at ambient pressure and zero external magnetic field are shown in figure 3.14. The specific-heat data are taken from the present pressure experiment (with the samples placed in the pressure cell but without an applied pressure), while the resistivity data are taken from the work of Nicklas *et al.* [Nicklas 2003]. A pronounced anomaly in the specific heat is observed, indicating the transition to an AFM ordered state at $T_N \approx 2.99\text{ K}$. When further lowering the temperature a second anomaly is found at $T_{NL} \approx 1.53\text{ K}$ which most likely marks the transition from an incommensurate to a commensurate magnetically ordered state

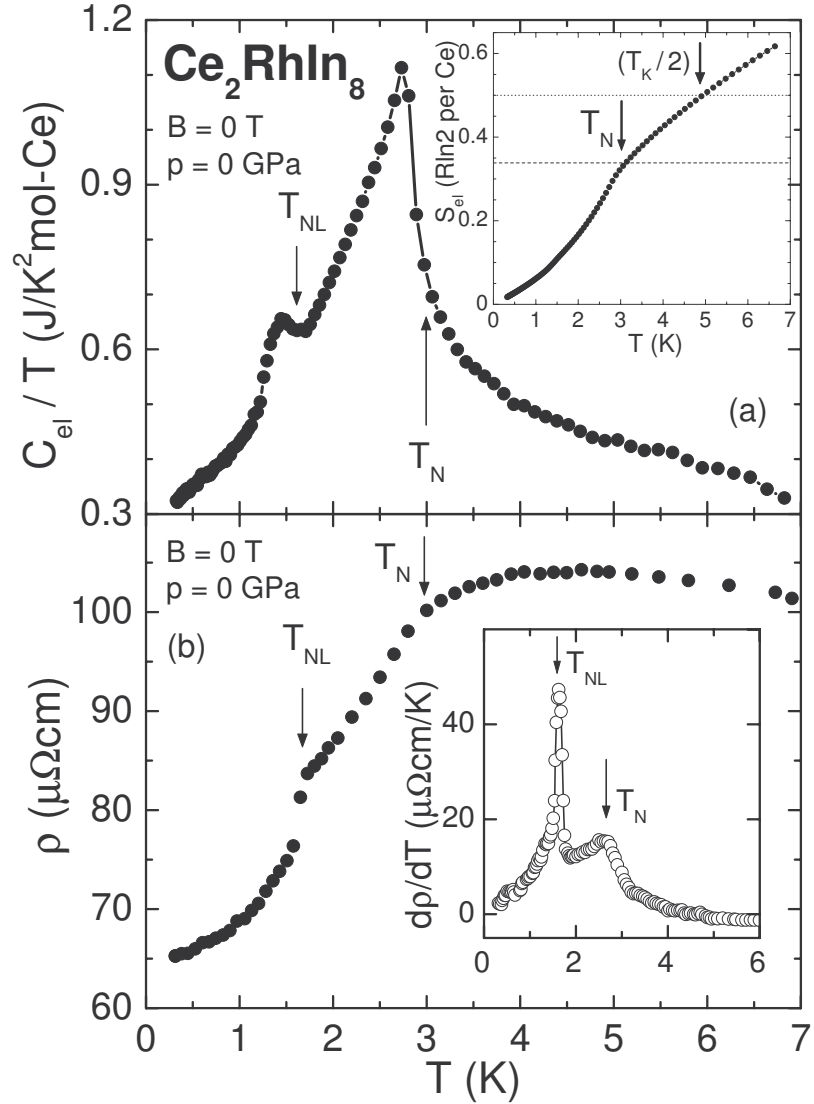


Figure 3.14: (a) Ambient-pressure electronic specific heat of Ce_2RhIn_8 as $C_{el}(T)/T$ versus T for $B = 0$ T. The inset shows the obtained ambient-pressure magnetic entropy as $S_{el}(T)$ versus T . The dashed line marks the value of the entropy ($S_{el}(T_N) \approx 0.34R \ln 2$) reached at T_N , while the dotted line indicates the value of $S_{el}(T_K/2) = 0.5R \ln 2$ ($S = 1/2$) [Desgranges 1982]. (b) Low-temperature resistivity of Ce_2RhIn_8 versus T obtained at ambient pressure and at $B = 0$ T [Nicklas 2003]. The corresponding derivative of the resistivity, as $d\rho(T)/dT$ versus T , is shown in the inset [Nicklas 2003]. In both panels arrows indicate the transition temperatures, T_N and T_{NL} .

[Llobet unpublished]. Due to the magnetic order in the system, the Sommerfeld coefficient of Ce_2RhIn_8 cannot be easily determined, but the value of C_{el}/T taken

at $T = 4$ K, right above the AFM transition, is considered a good approximation. At ambient pressure, Ce_2RhIn_8 exhibits $C_{el}/T|_{T=4K} \approx 0.5$ J/(K²mol-Ce), a value which proves the HF nature of Ce_2RhIn_8 . The electronic contribution to the low-temperature entropy is reaching a value of $S_{el}(T_N) \approx 0.34R \ln 2/\text{Ce}$ at T_N (see dashed line in the inset of figure 3.14a), the remaining entropy up to $S_{el} = R \ln 2/\text{Ce}$ being recovered only at $T \approx 20$ K [Cornelius 2001]. The low value of the entropy at the AFM transition is showing that the full moment of Ce of about $2.54 \mu_B$ is strongly reduced at low temperatures due to Kondo screening. The Kondo temperature of the system is determined from specific-heat measurements according to the single-impurity Kondo model [Desgranges 1982]. There it is estimated that at $T \approx T_K/2$ the entropy should reach half of the complete entropy of $R \ln 2$ per Ce atom (for spin 1/2) ($S_{el}(T_K/2) = 0.5R \ln 2$, see dotted line in the inset of figure 3.14a). The value of $T_K \approx 10$ K obtained from our heat-capacity measurements agrees satisfactorily with $T^* \approx 4.5$ K determined from the maximum in the electrical resistivity (see figure 3.14b) [Nicklas 2003].

As already mentioned in the previous section, the ambient-pressure low-temperature $B - T$ phase diagram of Ce_2RhIn_8 is very complex, similar to the case of the $n = 1$ relative, $CeRhIn_5$. For $B \parallel c$, however, the phase diagram is relatively simple, with the AFM transition gradually shifting to lower temperatures upon increasing the magnetic field [Cornelius 2001]. In the case of $B \parallel a$ the situation is more complicated, additional transitions showing up at finite magnetic fields [Cornelius 2001] (see figure 3.13). Figure 3.15 displays the evolution of $C_{el}(T)/T$ versus T for different applied magnetic fields as detected from measurements in the pressure cell. As seen in this figure, the high-temperature anomaly indicating T_N is slightly shifted to lower temperatures upon increasing magnetic field, while the lower magnetic transition at T_{NL} is shifted to higher temperatures with increasing magnetic field. Due to the specific orientation of the samples (as described previously), we probably detect in our measurements transitions from both directions, $B \parallel c$ and $B \parallel (ab)$. However, as seen in [Cornelius 2001], for $B \parallel c$ only T_N is detected in magnetic field, while for $B \parallel a$ other transitions can be seen as well. Moreover, as indicated by the data of Cornelius *et al.* [Cornelius 2001], the anisotropy of T_N versus B is very small. Therefore, we can assume that for magnetic fields $B \leq 8$ T, no difference of T_N versus B for the two different orientations of the magnetic field would be detected by our measurements. Consequently, we suppose that the transitions observed in addition to that at T_N are most probably corresponding to $B \parallel (ab)$. The phase transition at T_{NL} is not only shifting to higher temperatures, but also sharpens with increasing B , becoming more first-order like. Moreover, the field-induced magnetic transitions detected in

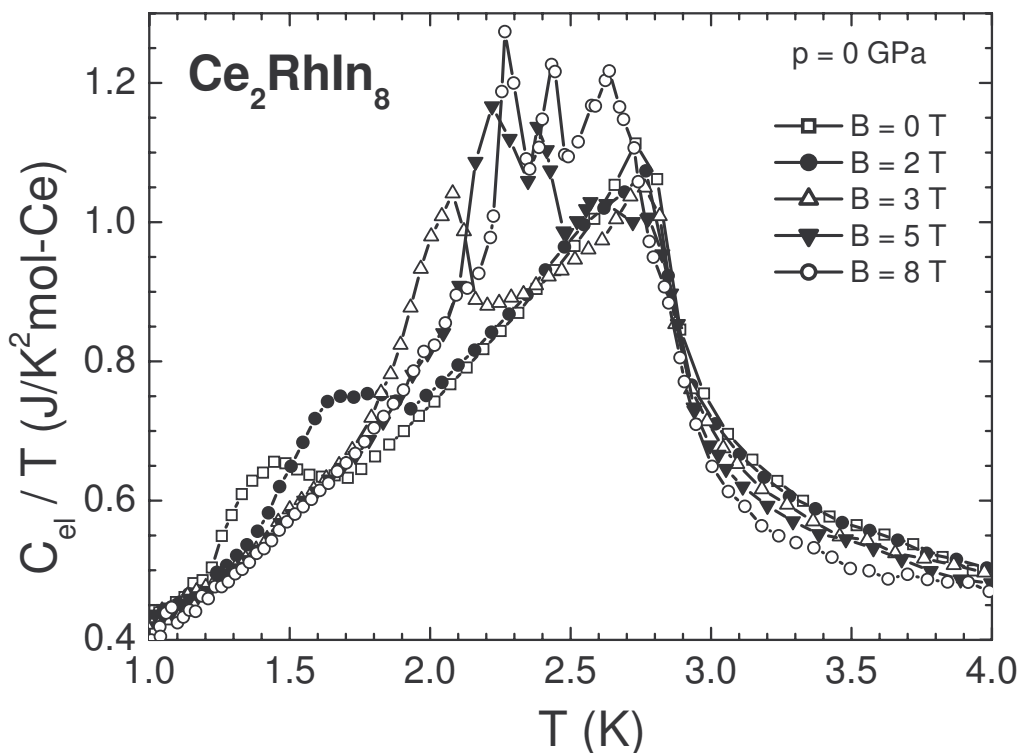


Figure 3.15: $C_{el}(T)/T$ versus T of Ce_2RhIn_8 at ambient pressure and in different magnetic fields, with the values of B indicated in the figure. The data were taken in the pressure cell (using our pressure setup but without applying pressure), with part of the samples oriented with $B \parallel (ab)$, while the others were oriented with $B \parallel c$ (as described in the text).

our measurements also seem to sharpen with increasing magnetic field, their shape at high B suggesting a first-order character of these phase transitions too.

Measurements of the specific heat at ambient pressure and in magnetic field $B \parallel (ab)$ on Ce_2RhIn_8 , carried out in a Quantum Design PPMS, reveal hysteresis for the lower magnetic transition at T_{NL} between the data taken upon warming and cooling, respectively. Figure 3.16 presents the respective $C_{el}(T)/T$ curves taken on increasing and on decreasing the temperature, for $B = (0, 1, 2, 3)$ T ($B \parallel (ab)$). The hysteretic behavior is more pronounced in the low-magnetic-field region ($B = 0$ T and $B = 1$ T) where the transition is broader in temperature and its shape does not hint at a first-order character of the transition. At $B = 3$ T, the shape of the anomaly at T_{NL} suggests a first-order nature of the phase transition though no hysteresis can be resolved by our measurements, probably due to narrowing and sharpening of the phase transition anomaly. However, as seen in many HF AFMs, the first-order

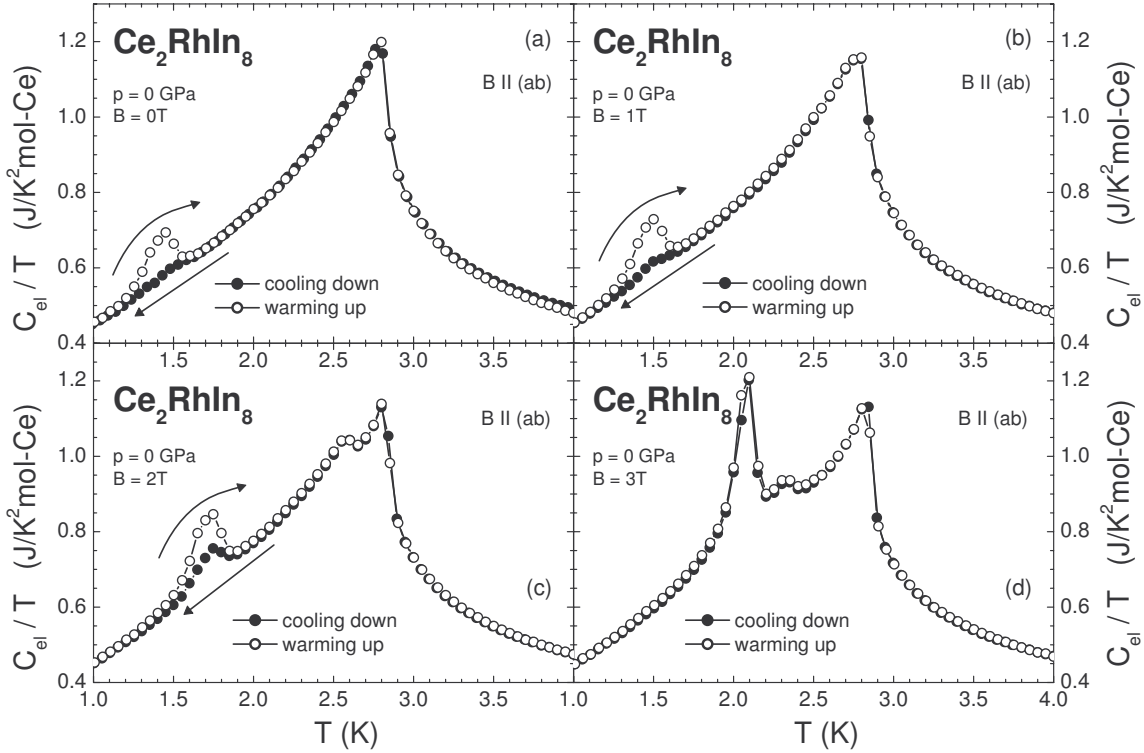


Figure 3.16: $C_{el}(T)/T$ versus T of Ce_2RhIn_8 at ambient pressure and in different magnetic fields ($B \parallel (ab)$). The four panels, in order from (a) to (d), show data for $B = 0$ T, $B = 1$ T, $B = 2$ T and $B = 3$ T, respectively. Data were measured in a Quantum Design PPMS in two directions, on warming (open symbols) and on cooling (full symbols). In all panels, the transition seen at higher temperatures (at $T \approx 3$ K) corresponds to the AFM transition (T_N), while the transition at lower temperatures (ranging from $T \approx 1.5$ K in (a) to $T \approx 2.1$ K in (d)) represents the magnetic transition at T_{NL} . The intermediate phase transitions are induced by magnetic field. Arrows indicate the hysteretic behavior at the lower magnetic transition, T_{NL} , between warming, respectively, cooling the system.

character of the phase transition at T_{NL} , a transition from an incommensurate to a commensurate magnetic order, would not be surprising. A phase diagram obtained from our specific-heat measurements at ambient pressure is shown in figure 3.17.

The electronic contribution to the specific heat of Ce_2RhIn_8 (C_{el}) at different pressures up to $p \approx 1.65$ GPa and at zero magnetic field is shown as $C_{el}(T)/T$ versus T in figure 3.18. With increasing pressure, T_N decreases monotonically with an initial slope of $dT_N/dp \approx -1.09$ K/GPa (see dashed line in figure 3.19), a slope slightly larger than inferred from both, resistivity ($dT_N/dp|_{\text{from } \rho(T)} \approx -0.76$ K/GPa) [Nicklas 2003] and thermal-expansion ($dT_N/dp|_{\text{from } \alpha(T)} \approx (-0.73 \pm 0.17)$ K/GPa) [Malinowski 2003] measurements. At higher pressures ($p > 1.3$ GPa), T_N starts to decrease even more

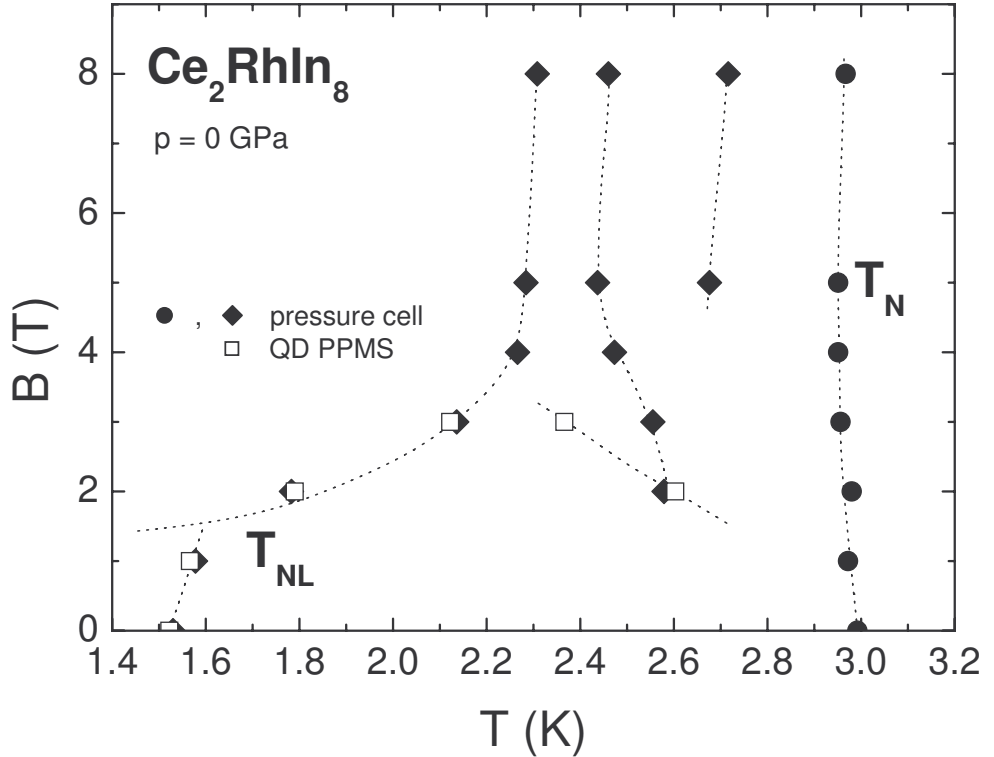


Figure 3.17: $B - T$ phase diagram obtained at ambient pressure on Ce_2RhIn_8 . Full symbols are representing data measured in the pressure cell, while the data shown by open squares are obtained from specific-heat measurements in a Quantum Design PPMS. The dotted lines are used for guidance. For the measurements performed in the Quantum Design PPMS the orientation of magnetic field was $B \parallel (ab)$. For the experiments in the pressure cell the data were taken on a group of samples with the magnetic field oriented either $B \parallel c$ or $B \parallel (ab)$. The anisotropy of $T_N(B)$ between $B \parallel (ab)$ and $B \parallel c$ is known to be very small [Cornelius 2001], therefore, the $T_N(B)$ data can be associated to either of the field directions and the additional phase transitions at $T < T_N$ are very probably corresponding to $B \parallel (ab)$ (see text for details).

rapidly. In accordance with the predictions of the spin-fluctuation theory for an itinerant AFM QCP, T_N should vanish in the vicinity of the critical pressure, p_c , as $T_N(p) \propto |p - p_c|^\gamma$ with $\gamma = 2/3$ for a 3D AFM [Millis 1993] (see details in section 1.2.2). A fit to the measured $T_N(p)$ data with the above-mentioned function ($\gamma = 2/3$) is shown by the dotted line in figure 3.19. The extrapolation of $T_N(p)$ to $T_N \rightarrow 0$ K, adopting $T_N(p) \propto |p - p_c|^{2/3}$ (see dotted line in figure 3.19), leads to $p_c \approx 2.03$ GPa. The obtained p_c is slightly lower than the value of $p_{c|\text{from } \rho(T)} \approx 3$ GPa extrapolated from resistivity measurements under pressure, where an exponent $\gamma = 1$ ($T_N(p) \propto |p - p_c|^\gamma$)

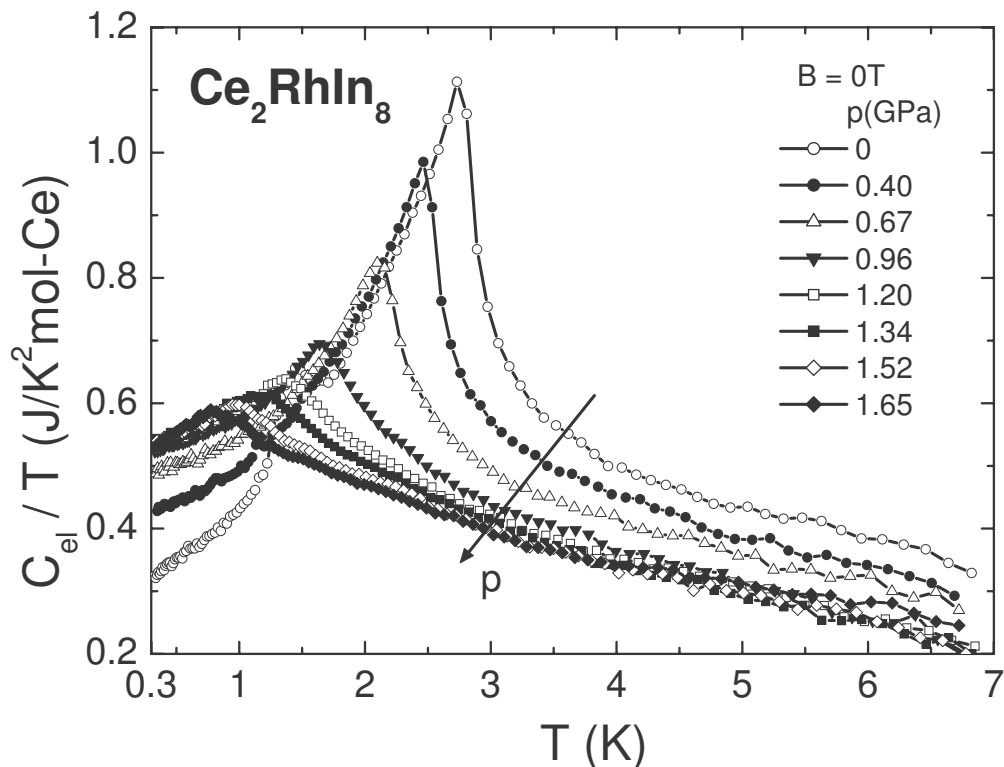


Figure 3.18: Specific heat at $B = 0$ T of Ce_2RhIn_8 , as $C_{el}(T)/T$ versus T , for pressures as indicated in the figure. The arrow indicates the direction of increasing pressure.

attributed to a 2D AFM [Millis 1993] was used to extrapolate the data to $T_N = 0$ K [Nicklas 2003]. However, due to the relatively high distance from our last measured data point to the critical pressure at which $T_N \rightarrow 0$ K, the obtained value of p_c should be regarded with caution. In contrast to the behavior observed for $T_N(p)$, T_{NL} is decreasing drastically upon increasing pressure. Within the temperature limit of our cryostat ($T_{min} = 0.35$ K), no second anomaly can be resolved already at $p \geq 0.4$ GPa for $B = 0$ T. The obtained $T - p$ phase diagram, including the above-mentioned extrapolation of $T_N(p)$ to $T_N = 0$ K indicated by the dotted line, is shown in figure 3.19.

Application of pressure on Ce_2RhIn_8 also leads to the appearance of a region in temperature, above T_N (the upper temperature limit is fixed by our experimental setup to $T = 7$ K), where $\Delta C_{el}(T)/T \propto -\sqrt{T}$, characteristic for NFL behavior (for details see table 1.2 for 3D AFM). Moreover, with increasing pressure, this temperature region, where a \sqrt{T} type increase of $C_{el}(T)/T$ with decreasing temperature is detected, is broadening, suggesting that the system is approaching an AFM QCP.

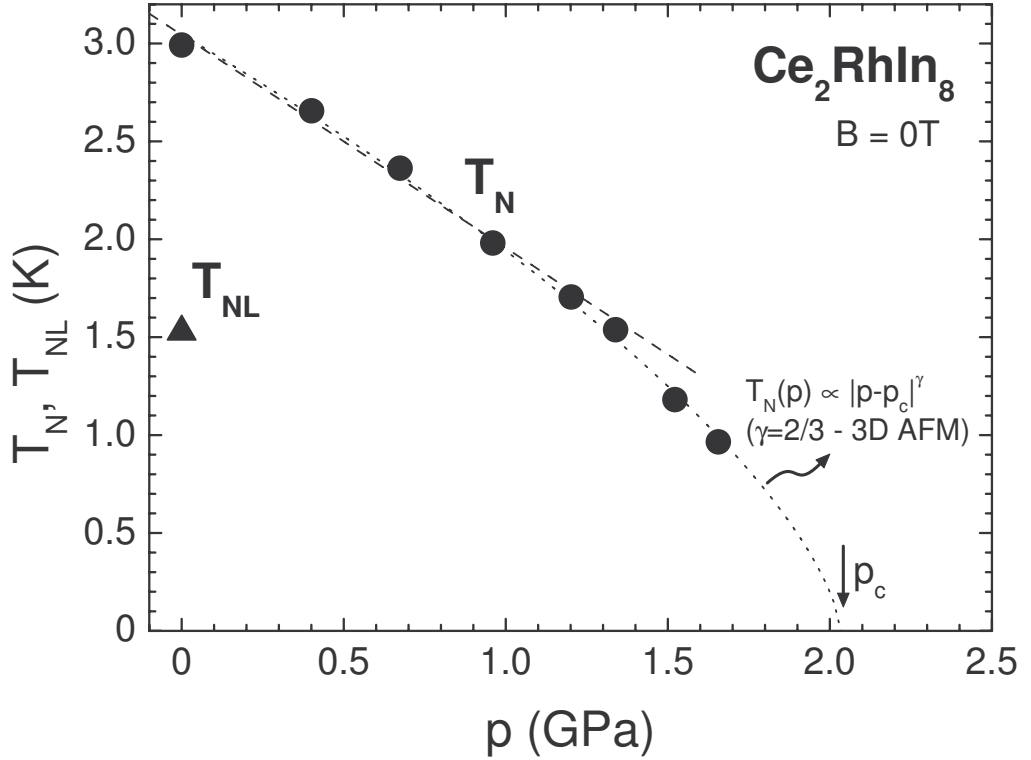


Figure 3.19: T_N versus p of Ce_2RhIn_8 ($B = 0$ T). The dashed line represents the initial slope $dT_N/dp \approx -1.09$ K/GPa. The dotted line corresponds to a fit to the data with $T_N(p) \propto |p - p_c|^{2/3}$. The obtained fit was used at low temperatures to extrapolate $T_N(p)$ to $T_N = 0$ K. The obtained critical pressure - p_c - is indicated by the arrow.

Further on, application of magnetic field up to $B = 8$ T does not change the observed \sqrt{T} dependence of $C_{el}(T)/T$ over the whole measured pressure range. This behavior is as expected, since in this range of magnetic field ($B \leq 8$ T) T_N is nearly unchanged by the application of magnetic field. It should be mentioned that no considerable difference between the $\Delta C_{el}(T)/T \propto -\sqrt{T}$ (3D AFM) and $\Delta C_{el}(T)/T \propto -\ln T$ (2D AFM) dependencies of $C_{el}(T)/T$ at $T > T_N$ can be observed in our pressure-dependent measurements. Therefore, in our specific-heat data on Ce_2RhIn_8 we observe NFL behavior, but to distinguish between the NFL type dependencies typical for 3D or 2D AFMs is not possible (for details about NFL behavior see table 1.2).

The pressure dependence of the magnetic entropy is presented in figure 3.20. The temperature at which the entropy, taken at different pressures, reaches the value of $S_{el} = 0.5R \ln 2$ per Ce, indicated by the horizontal line in figure 3.20, represents about half of the characteristic temperature $T_K(p)$ of the system ($S(T_K/2) = 0.5R \ln 2$

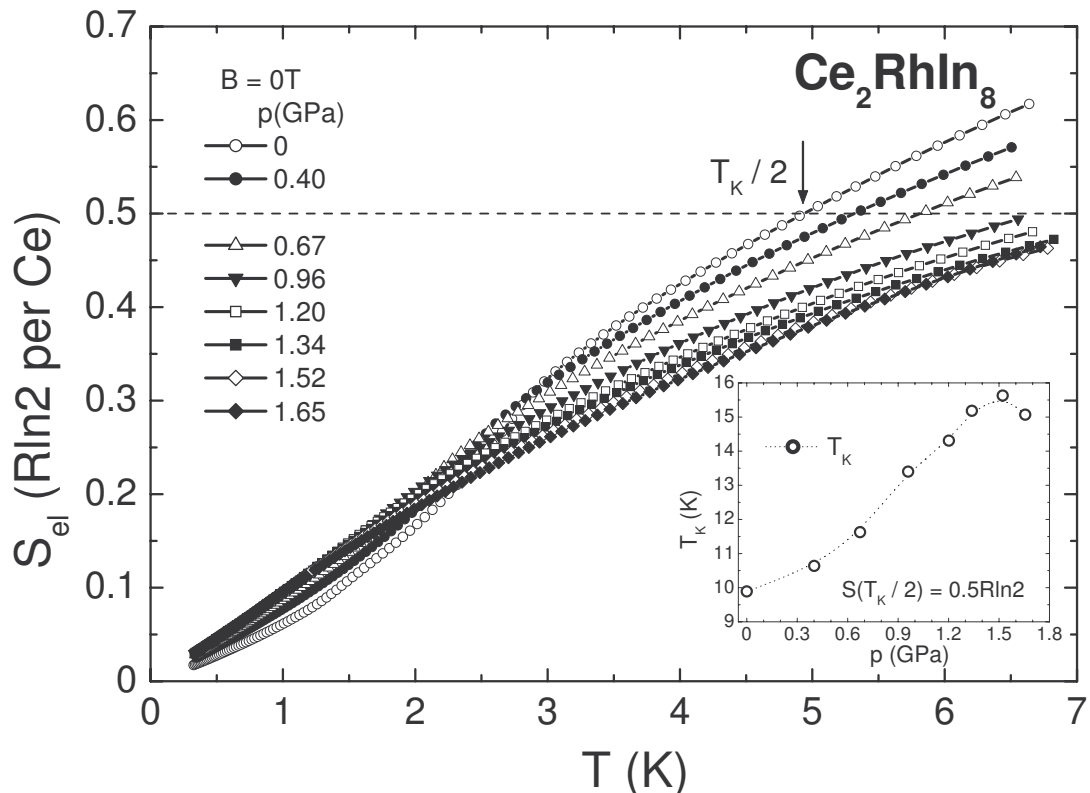


Figure 3.20: Evolution of the magnetic entropy of Ce_2RhIn_8 with increasing pressure, as $S_{el}(T)$ versus T , for different pressures indicated in the figure. The dashed line, at $S_{el} = 0.5R \ln 2$ per Ce, marks the value of entropy which should be reached at about $T_K/2$ according to the single-impurity Kondo model (for $S = 1/2$) [Desgranges 1982]. The inset shows the variation with pressure of the obtained Kondo temperature, T_K .

according to the single-impurity Kondo model - $S = 1/2$ -) [Desgranges 1982]. The inset of figure 3.20 shows the estimated T_K versus p . In order to obtain T_K at higher pressures, where the system does not reach the entropy value of $S_{el} = 0.5R \ln 2$ per Ce in the measured temperature range up to $T = 7$ K, the data were linearly extrapolated to higher temperatures. As expected for Ce-based HF systems, T_K increases with increasing pressure from $T_K \approx 10$ K at ambient pressure to $T_K \approx 16$ K at the highest pressure of our experiment of $p \approx 1.65$ GPa. The increase of T_K at lower pressures is relatively uniform with increasing pressure and a tendency to saturation is visible at $p \geq 1.3$ GPa. However, the slight decrease of T_K at very low pressures ($p < 0.5$ GPa) prior to a gradual increase upon increasing pressure, as detected by resistivity measurements [Nicklas 2003], is not seen in our data. At temperatures above T_N , the total entropy of the system is decreasing with increasing pressure. The

magnetic entropy obtained right at the AFM phase transition is gradually shifted to lower temperatures with increasing pressure and its value of $S_{el}(T_N) \approx 0.34R \ln 2$ per Ce atom obtained at ambient pressure is continuously reduced upon increasing pressure to a value of $S_{el}(T_N) \approx 0.1R \ln 2$ per Ce atom at $p \approx 1.65$ GPa. This effect of pressure is typical for Ce-based HF systems and is resulting from the reduction of the low-temperature magnetic moment of Ce under pressure due to the increase of the Kondo screening of the f electrons by the conduction electrons.

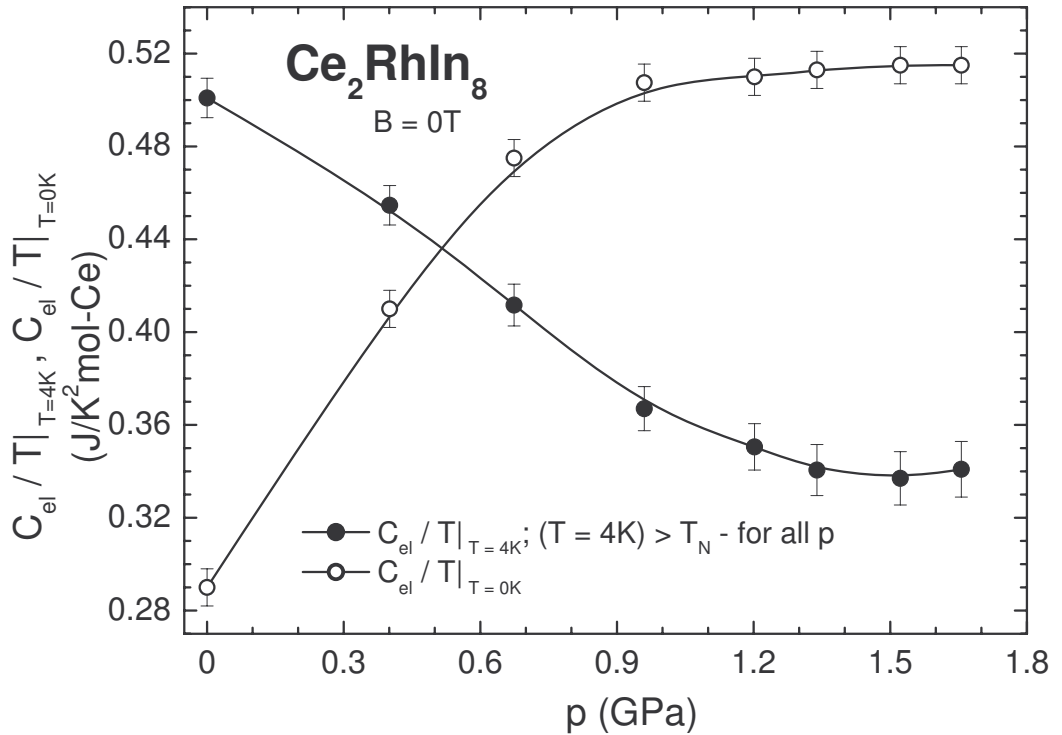


Figure 3.21: Pressure dependence of C_{el}/T taken at $T = 4$ K (full symbols), a temperature which is greater than T_N over the whole measured pressure range, and C_{el}/T obtained by extrapolation of $C_{el}(T)/T$ at $T < T_N$ to $T = 0$ K (open symbols) obtained for Ce_2RhIn_8 ($B = 0$ T).

Due to the presence of the AFM phase transition at low temperatures in Ce_2RhIn_8 and due to its robustness against the external magnetic field for $B \leq 8$ T, the values of C_{el}/T at a temperature above T_N (e.g. $T = 4$ K) were taken as an approximate measure of the Sommerfeld coefficient. As shown in figure 3.21 (full symbols), C_{el}/T taken at $T = 4$ K, a temperature higher than T_N over the whole pressure range, also decreases with increasing pressure at an initial rate of $d(C_{el}/T|_{T=4K})/dp \approx -0.139$ J/(K²mol-CeGPa). Qualitatively, this is attributed to

the increasing hybridization between the Ce 4f and the conduction electrons. However, at $p \geq 0.95$ GPa, the pressure-induced decrease of $C_{el}/T|_{T=4K}$ deviates from the almost linear behavior and becomes less pronounced, leading above $p \approx 1.3$ GPa to a nearly pressure-independent $C_{el}/T|_{T=4K}$ up to our highest pressure of $p \approx 1.65$ GPa. Spin-fluctuation theory suggests that the spin-fluctuation temperature, T_{sf} , increases as the effective mass of the QPs decreases in the system, $T_{sf} \propto 1/m^*$ [Moriya 1995]. Moreover, it was proposed that the appearance of magnetically mediated SC in the vicinity of an AFM instability leads to a SC transition temperature $T_c \propto T_{sf}$ (see for details section 1.2.2 and equation 1.1) [Millis 1988, Lonzarich 1997, Mathur 1998]. In the case of Ce_2RhIn_8 , pressure-induced SC is shown to set in at about $p \approx 1.6$ GPa, with T_c initially increasing with increasing pressure [Nicklas 2003]. Therefore, the nearly pressure-independent value of $C_{el}/T|_{T=4K}$ obtained from our measurements at high pressures ($C_{el}/T|_{T=4K} \approx \gamma \propto m^*$), in the pressure range where T_c is supposed to increase, may leave an open question with regard to the theory of magnetically mediated SC. However, as shown in figure 3.18, the suppression of the AFM phase transition by pressure gives way to a \sqrt{T} -like increase of $C_{el}(T)/T$ upon cooling in the paramagnetic state, typical for NFL behavior. The enlargement of the temperature region in which $C_{el}(T)/T$ deviates from the behavior of a LFL upon increasing pressure can be interpreted as getting closer to a QCP. Therefore, NFL behavior at $T > T_N$, appearing at high pressures while approaching an AFM QCP, could be taken as an explanation for the slight increase of $C_{el}/T|_{T=4K}$ above $p \approx 1.5$ GPa. As seen in figure 3.18, concomitant to the decrease of T_N with increasing pressure, the height of the anomaly in $C_{el}(T)/T$ at the AFM phase transition also decreases and the phase transition becomes broader in temperature. The ratio of $\Delta C/(\gamma T_N)$, measured at the AFM phase transition, decreases monotonically upon increasing pressure from a value of $\Delta C/(\gamma T_N)|_{T=T_N} \approx 1.16$ at $p = 0$ GPa to $\Delta C/(\gamma T_N)|_{T=T_N} \approx 0.114$ at $p \approx 1.65$ GPa. $C_{el}(T)/T$ data of Ce_2RhIn_8 at $B = 0$ T show a $C_{el}(T)/T = \gamma_0 + bT^2$ dependence for $T < T_N$. The residual electronic specific-heat coefficient at $T = 0$ K in the AFM state and at $B = 0$ T, $C_{el}/T|_{T=0K}$, was obtained for each pressure by extrapolating the detected $C_{el}(T)/T = \gamma_0 + bT^2$ dependence to $T = 0$ K ($C_{el}/T|_{T=0K} = \gamma_0$). The pressure evolution of $C_{el}/T|_{T=0K}$ is shown in figure 3.21 (open symbols). A step increase of $C_{el}/T|_{T=0K}$ with increasing pressure is visible for low pressures, while at higher pressures ($0.95 \text{ GPa} \leq p \leq 1.65 \text{ GPa}$) a nearly pressure-independent value of $C_{el}/T|_{T=0K}$ can be detected. Both curves presented in figure 3.21 suggest that the system is approaching an AFM QCP upon increasing pressure.

As seen in many Ce-based AFM HF systems, like in the $n = \infty$, $CeIn_3$, [Walker 1997] and $n = 1$, $CeRhIn_5$, [Hegger 2000] members of the $Ce_nRh_mIn_{3n+2m}$

family, SC appears in a region around the critical pressure at which T_N is suppressed to $T_N = 0$ K. Indeed, electrical-resistivity measurements under pressure on Ce_2RhIn_8 revealed the appearance of the SC state in the vicinity of the AFM instability [Nicklas 2003]. At $p \approx 1.6$ GPa, a state with zero resistance was found below $T \approx 0.6$ K, a temperature where also a.c.-susceptibility measurements showed the entrance into a diamagnetic state [Nicklas 2003]. Upon further increasing pressure, T_c was found to increase, but the determination of its accurate pressure dependence was not possible due to the fact that data were not taken at low enough temperatures [Nicklas 2003]. Nevertheless, guided by the onset of the SC phase transition in resistivity data, a maximum value of $T_c(p)$ could be detected for $p \approx 2.3$ GPa [Nicklas 2003]. This pressure is close to the estimated critical pressure where AFM is expected to vanish [Nicklas 2003]. Another important issue in the investigation of SC in the $Ce_nRh_mIn_{3n+2m}$ family is the magnitude of T_c . The T_c values for Ce_2RhIn_8 presented in [Nicklas 2003], taken at the onset of the SC transition in $\rho(T)$, can be considered an upper limit, a bulk SC state being reached probably at substantially lower temperatures. Indeed, our measurements of the heat capacity under pressure up to $p \approx 1.65$ GPa, do not show any evidence of SC down to $T = 0.35$ K. Moreover, in order to detect the pressure-induced SC state, measurements of a.c. susceptibility under pressure were also performed on the samples in the same setup (total mass of ≈ 0.4 g) as used for the specific-heat measurements. At $p \approx 1.65$ GPa, $\chi_{a.c.}(T)$ data down to $T = 50$ mK do not show any diamagnetic signal, indicating that no SC was established in any sample down to this temperature.

Application of a magnetic field leads to a very rich $B - T$ phase diagram at ambient pressure (see figure 3.17), but leaves the AFM phase transition temperature, T_N , nearly unchanged up to the highest magnetic field of $B = 8$ T accessible in our measurements. This behavior seems to change little upon increasing pressure. The multiple magnetic phase transitions seen in magnetic field below T_N at $p = 0$ GPa (figure 3.15) merge and are gradually suppressed with increasing pressure, leading, at high enough pressure, to the presence of only the AFM phase transition even at $B = 8$ T. On the other hand, the transition temperature $T_N(p, B)$ from the paramagnetic to the AFM state remains nearly unaffected by application of a magnetic field $B \leq 8$ T over the whole measured pressure range $p \leq 1.65$ GPa. Figure 3.22 shows as an example the effect of $B = 8$ T in comparison to $B = 0$ T on the low-temperature specific heat of Ce_2RhIn_8 for three different pressures. Compared to the data at ambient pressure, where several transitions are visible at $T < T_N$ and $B = 8$ T, at $p \approx 0.40$ GPa only one anomaly at $T < T_N$ can be detected at $B = 8$ T. At pressures $p \geq 0.67$ GPa, no additional phase transition is seen in magnetic field (see

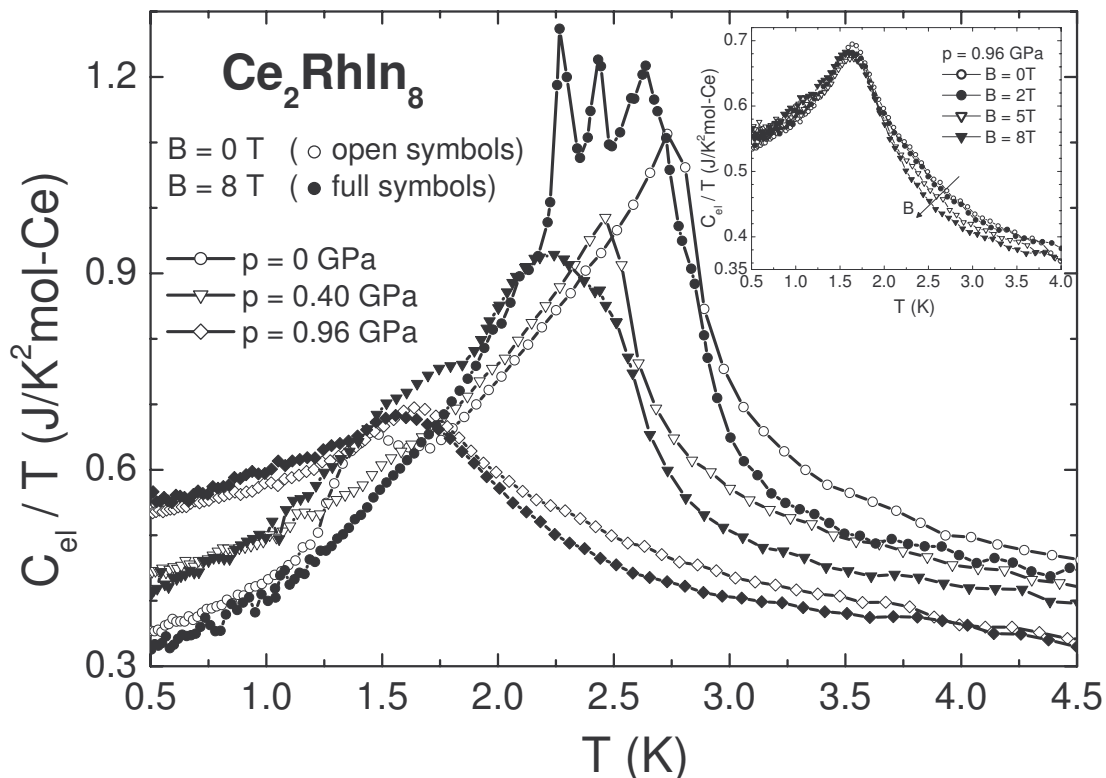


Figure 3.22: $C_{el}(T)/T$ versus T of Ce_2RhIn_8 at three different pressures at $B = 0$ T (open symbols) and $B = 8$ T (full symbols). As described in the text, in our setup part of the samples were oriented with $B \parallel (ab)$ while the other samples were placed with $B \parallel c$. At $p = 0$ GPa and $B = 8$ T several magnetic transitions are visible at $T < T_N$. At $B = 8$ T, for $p \approx 0.40$ GPa the multiple magnetic transitions merge in one transition at $T < T_N$, while for $p \approx 0.96$ GPa no anomalies, additional to that at T_N , can be seen. The inset shows the effect of magnetic field on $C_{el}(T)/T$ of Ce_2RhIn_8 at $p \approx 0.96$ GPa, a pressure where only T_N is observed.

$p \approx 0.96$ GPa data in figure 3.22). Remarkably, even with increasing pressure up to $p \approx 1.65$ GPa, where T_N is already suppressed to more than one third of its ambient-pressure value, the AFM phase transition at T_N remains nearly unchanged by the application of magnetic fields up to $B = 8$ T. Furthermore, the AFM phase transition anomaly sharpens in magnetic field over the entire measured pressure range. As already discussed earlier, our samples, specifically oriented with respect to the direction of the applied magnetic field (either $B \parallel c$ or $B \parallel (ab)$), should also yield information about the anisotropy of the AFM phase transition temperature, T_N , when magnetic fields $B \leq 8$ T are applied. Measurements in magnetic field do not show any detectable split at T_N over the whole measured pressured range ($p \leq 1.65$ GPa)

even at $B = 8$ T. Therefore, the unresolvably small anisotropy of T_N in $B \leq 8$ T seems to remain unchanged when increasing the pressure up to $p \approx 1.65$ GPa.

3.3.3 Discussion - Ce_2RhIn_8

We have studied the temperature, pressure and magnetic-field dependence of the low-temperature electronic specific heat of the HF AFM Ce_2RhIn_8 . We have observed that upon increasing pressure T_N is decreasing and its pressure dependence fits very well to the theoretical predictions for an itinerant 3D AFM ($T_N(p) \propto |p - p_c|^\gamma$, $\gamma = 2/3$ [Millis 1993]). This yields a critical pressure $p_c \approx 2.03$ GPa, a value situated in the region where in electrical-resistivity measurements the SC transition temperature, $T_c(p)$, was found to reach its maximum value [Nicklas 2003]. The second anomaly at T_{NL} , observed in Ce_2RhIn_8 at ambient pressure, which is attributed to a transition from an incommensurate to a commensurate magnetically ordered state, shifts to higher temperatures upon increasing the magnetic field and disappears rapidly with increasing pressure. This transition at T_{NL} shows hysteretic behavior and, therefore, appears to be a first-order phase transition. Additional magnetic-field-induced phase transitions detected at ambient pressure merge and gradually disappear with increasing pressure.

Regarding the strength of the AFM correlations, we find the AFM state in Ce_2RhIn_8 to be very robust against application of external magnetic field. Our heat-capacity measurements up to $B = 8$ T show almost no effect of the magnetic field on T_N even at our highest pressure of $p \approx 1.65$ GPa. Moreover, the phase transition at T_N sharpens in magnetic field in the entire measured pressure range. This robustness against applied magnetic field is also found in the related compound $CeRhIn_5$. The anisotropy of T_N as function of B (between $B \parallel c$ and $B \parallel a$) up to $B = 8$ T remains undetectably small in our measurements over the whole pressure range.

Our results also show that Ce_2RhIn_8 is approaching an AFM QCP upon increasing pressure. NFL behavior, observed in the system at $T > T_N$, stays unchanged by application of external magnetic fields up to $B = 8$ T and becomes more and more pronounced while increasing the pressure. The magnetic entropy obtained at T_N gradually decreases with increasing pressure (from $S_{el}(T_N) \approx 0.34R \ln 2$ per Ce at $p = 0$ GPa to $S_{el}(T_N) \approx 0.1R \ln 2$ per Ce at $p \approx 1.65$ GPa) showing the gradual reduction of the low-temperature ordered moment in Ce_2RhIn_8 due to increased Kondo screening of the f electrons of Ce by the conduction electrons. The electronic specific-heat coefficient, $C_{el}/T|_{T=4K}$, considered to be a measure of m^* , decreases with increasing pressure and becomes constant as the system is approaching the magnetic QCP. Assuming the possibility of magnetically mediated Cooper pairing in Ce_2RhIn_8 ,

the appearance of SC and the increase of T_c with pressure should be connected to a continuous decrease of m^* [Millis 1988, Moriya 1995, Lonzarich 1997, Mathur 1998]. This, however, is not observed in Ce_2RhIn_8 . Instead, the value of m^* is nearly pressure independent in the region where SC is expected to appear [Nicklas 2003]. However, the pronounced NFL behavior found upon approaching the AFM QCP may be considered to be responsible for the observed effective mass enhancement. At a fixed temperature well below T_N , C_{el}/T increases gradually with increasing pressure. However, for $p \leq 1.65$ GPa no evidence for a phase transition into the SC state is observed by our measurements of either the specific heat above $T = 0.35$ K or the susceptibility above $T = 0.05$ K.

These results lead us to conclude that Ce_2RhIn_8 , the $n = 2$ member of the $Ce_nRh_mIn_{3n+2m}$ family of HF AFMs, shows quantum critical behavior similar as it is observed in both the $n = 1$ and $n = \infty$ members, $CeRhIn_5$ and $CeIn_3$, respectively. Due to the crystal structure of Ce_2RhIn_8 , the physical properties of this compound are expected to be located somewhere in between those of $CeIn_3$ (3D) and $CeRhIn_5$ (more 2D like). We found that the pressure dependence of T_N in Ce_2RhIn_8 is typical for a 3D itinerant AFM. Electrical-resistivity measurements [Nicklas 2003] detected a relatively low value of T_c when compared to T_c observed in $CeRhIn_5$. Moreover, bulk SC was not observed in our measurements in the pressure range $p \leq 1.65$ GPa and down to $T \approx 50$ mK. Altogether, these findings suggest that the physical properties of Ce_2RhIn_8 are situated somewhat closer to those of the cubic (3D) $CeIn_3$. However, it is well known that the effect of disorder is detrimental to the appearance of SC and it leads to a decrease of the SC transition temperature as well. The residual resistivity of Ce_2RhIn_8 is one to two orders of magnitude larger than the very low values found for $CeIn_3$ and $CeRhIn_5$ [Nicklas 2003, Mathur 1998, Hegger 2000]. Therefore, the possibility of disorder as pair-breaking mechanism in Ce_2RhIn_8 should not be neglected. It is also worth mentioning that because of a more complex magnetic interaction between the Ce atoms due to the non-symmetric vicinity of each Ce atom, to consider Ce_2RhIn_8 just as the $n = 2$ member of the $Ce_nRh_mIn_{3n+2m}$ family of HF AFMs and to locate its physical properties in between those of the $n = \infty$ ($CeIn_3$ - 3D) and $n = 1$ ($CeRhIn_5$ - more 2D like) members might be too simple. However, in order to better understand the role of dimensionality on SC and AFM in this family of HF compounds and to learn more about the interplay between magnetism and SC in HF systems, measurements of the heat capacity of Ce_2RhIn_8 at higher pressures are needed. Moreover, whether a QCP exists or not in Ce_2RhIn_8 under pressure associated with the continuous or sudden vanishing of T_N upon increasing pressure is still an open question.

Chapter 4

The heavy-fermion antiferromagnet and superconductor CeCu_2Si_2

4.1 Short overview

CeCu_2Si_2 , discovered as the first HF SC [Steglich 1979], is a compound offering the chance to study a multitude of challenging physical properties. In the case of rare-earth-based HF systems, such as CeCu_2Si_2 , the low-temperature physical properties are dominated by their $4f$ electrons. The electronic configuration of Ce is $[\text{Xe}]4f^15d^16s^2$. In Ce-based intermetallic compounds the d and s electrons of the outer shells of Ce are hybridizing to form the conduction band. In a simple picture the $4f$ electron of Ce could either remain localized to the Ce atom, forming the Ce^{3+} state, or could become delocalized entering the conduction band, giving rise to the Ce^{4+} configuration. Therefore, it is obvious that the f electron of Ce is defining the magnetic Ce^{3+} or the non-magnetic Ce^{4+} state. At ambient pressure, the Ce ions of CeCu_2Si_2 are mostly in the Ce^{3+} configuration. This compound is a bulk SC below $T_c \approx 0.6$ K. It is well known in the classical BCS theory of SC that a very small amount of magnetic impurity suppresses the SC state. Surprising was therefore in 1979 the discovery of SC in CeCu_2Si_2 where one deals with a dense lattice of magnetic Ce^{3+} ions. Furthermore, it was found that the isostructural non-magnetic compound LaCu_2Si_2 is not a SC and already a small concentration of non-magnetic La^{3+} ions in $\text{Ce}_{1-x}\text{La}_x\text{Cu}_2\text{Si}_2$ is enough to destroy the SC state (e.g. $x \geq 0.1$) [Ahlheim 1988]. These clearly indicate that the SC state in CeCu_2Si_2 is not a conventional BCS-like state, where phonons mediate the formation of the Cooper pairs. However, the mechanism for the formation of the SC state in CeCu_2Si_2 is still not fully understood. Like in the materials discussed in the previous chapters, magnetic-fluctuation medi-

ated Cooper pairing is likely to occur. Besides its unconventional SC, $CeCu_2Si_2$ also shows a rather rich magnetic phase diagram upon cooling from room temperature. At high enough temperatures the $4f$ electrons of the Ce^{3+} ions have their full magnetic moment, the magnetic susceptibility showing the typical Curie-Weiss-like temperature dependence. While lowering the temperature the localized magnetic moments interact with the conduction electrons giving rise to the two major competing effects which take place in HF systems: the Kondo effect and the RKKY interaction (see section 1.1). The former one leads to the magnetic screening of the Ce^{3+} ions by the conduction electrons well below the Kondo temperature T_K (on-site effect), while the second one tries to establish AFM order due to the indirect exchange interaction of the neighboring f electrons via the conduction electrons (inter-site effect). As a resulting effect, an A/S -type crystal (for details about the different crystal types see section 4.2) of $CeCu_2Si_2$ at low temperatures shows the characteristics of a HF system, orders AFM with a very low magnetic moment and superconducts below a temperature which is slightly lower than T_N . Knowing that the low-temperature properties of $CeCu_2Si_2$ are mainly determined by the $4f$ electron of Ce and knowing that the system at ambient pressure is located close to a borderline between AFM and SC, one can imagine to tune the system from the $Ce^{3+|\delta|}$ ($|\delta| \ll 1$) valence state to an IV state with larger $|\delta|$ ($|\delta| < 1$). A suited tuning parameter has to be used to change the strength of the hybridization between the conduction electrons and the $4f$ electrons of Ce. Appropriate tuning parameters are the chemical doping on the Cu and/or Si site or externally applied hydrostatic pressure. Figure 4.1 shows a schematic phase diagram of CeT_2X_2 compounds (where $T = (Ni, Co, Cu, Ru, Au, Rh, \text{etc.})$ and $X = (Si, Ge)$), indicating the succeeding low-temperature physical properties which might appear while tuning the $4f$ electrons of Ce through different hybridization states.

In the following section we will focus on the description of the physical properties of $CeCu_2Si_2$ and some of the related compounds. The experimental results obtained from the specific-heat measurements under hydrostatic pressure on single-crystalline $CeCu_2Si_2$ will be presented in section 4.3. The chapter will be closed with a discussion.

4.2 Physical properties

$CeCu_2Si_2$ crystallizes in the tetragonal $ThCr_2Si_2$ structure ($I4/mmm$) (see figure 4.2). The single crystals are grown in aluminum-oxide crucibles by a modified Bridgman technique using Cu excess as flux medium [Jeevan 2007]. Powder X-ray diffraction patterns confirmed the proper tetragonal $ThCr_2Si_2$ structure with lattice parameters $a \approx 0.4099$ nm and $c \approx 0.9923$ nm at room temperature [Jeevan 2007].

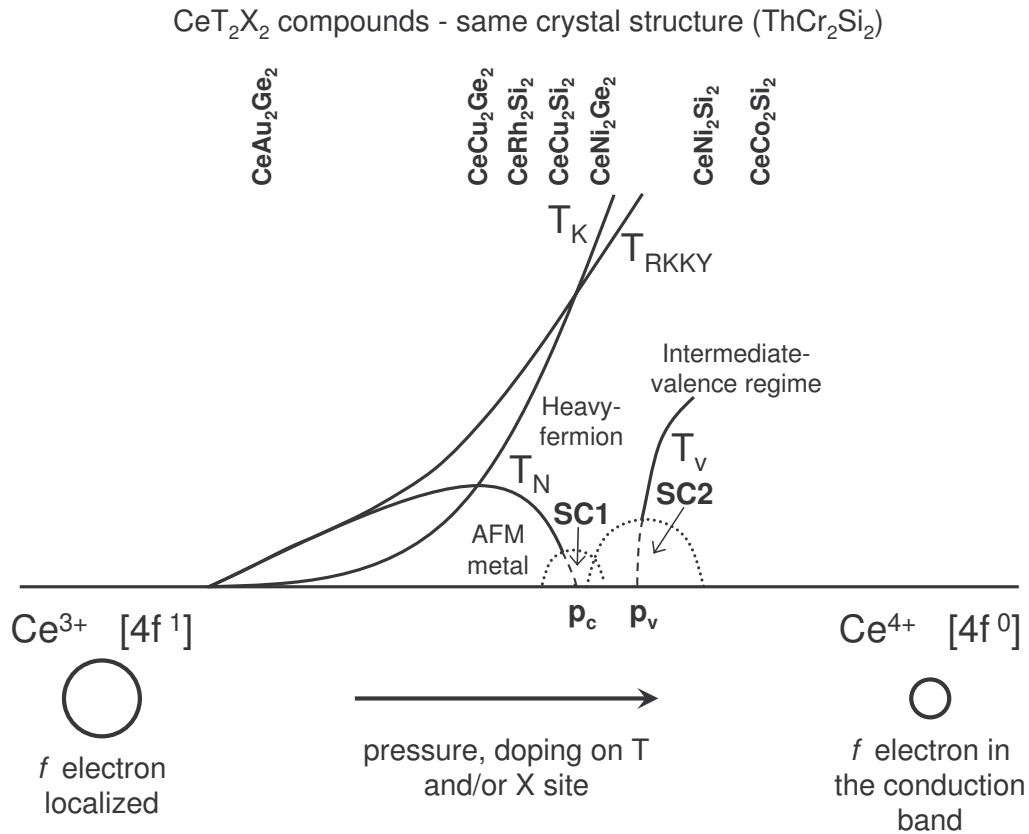


Figure 4.1: Schematic phase diagram of CeT₂X₂ compounds (where T = (Ni, Co, Cu, Ru, Au, Rh, etc.) and X = (Si, Ge)). The different compounds are placed in the phase diagram at the positions corresponding to their low-temperature properties at ambient pressure. The references corresponding to each compound are, in order from left to right: [Böhm 1988, Boer 1987, Quezel 1984, Steglich 1979, Knopp 1988, Sampathkumaran 1986, Dhar 1987].

Systematic investigations on the ternary chemical Ce-Cu-Si phase diagram revealed that in the narrow homogeneity range of the 1:2:2 phase, which allows for an exchange between Cu and Si atoms by not more than 1 at%, four different ground states exist [Modler 1995, Geibel priv. comm.] (see figure 4.3a). The four ground states are driven by a small difference in the hybridization of the 4*f* and the conduction electrons. Therefore, strong coupling induced by Cu excess leads to the formation of “*S*-type” superconducting samples. Cu-deficient samples (weak coupling) exhibit a magnetic phase - “*A* type”, while a higher Cu deficiency produces samples - “*X* type” - showing neither the *A*-phase nor superconductivity down to the lowest accessible temperature. In an intermediate range, in between the *S*- and the *A*-type samples, one finds so-called “*A/S*-type” CeCu₂Si₂ which exhibits an AFM phase transition at a

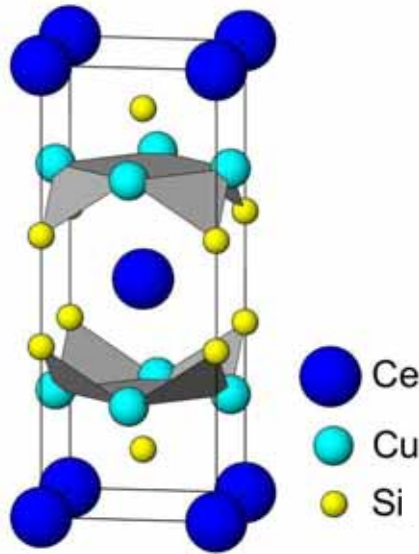


Figure 4.2: $ThCr_2Si_2$ structure of $CeCu_2Si_2$ ($I4/mmm$ group). Ce atoms are located in the body-centered tetragonal positions.

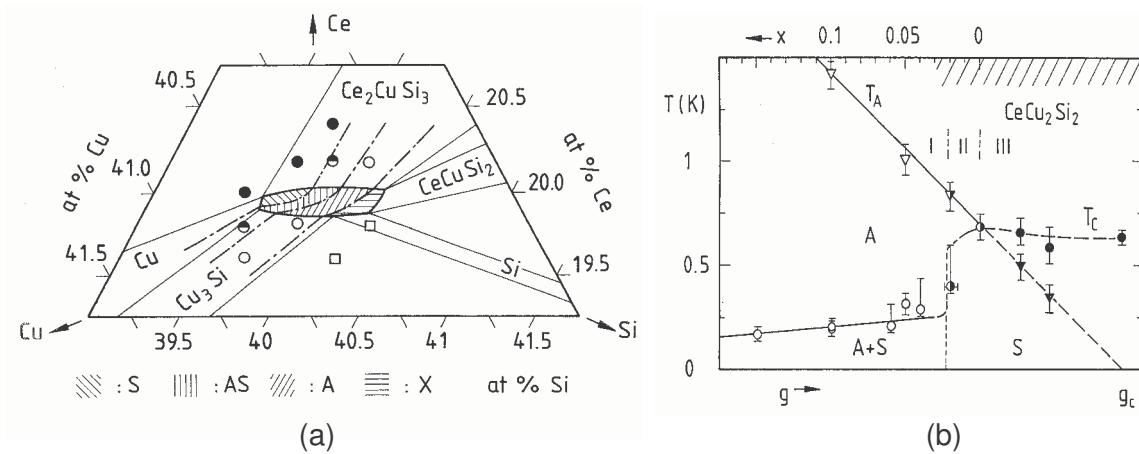


Figure 4.3: (a) Ternary chemical Ce-Cu-Si phase diagram in the vicinity of the homogeneity range of $CeCu_2Si_2$. The differently hatched areas indicate the four regions where the stoichiometric $CeCu_2Si_2$ with the four different ground-state properties (A , A/S , S , X) is formed. Figure taken from [Modler 1995, Geibel priv. comm.]. (b) Generic phase diagram of $CeCu_2Si_2$ combining data obtained from polycrystalline, pure and Ge-doped $CeCu_2(Si_{1-x}Ge_x)_2$. The undoped $CeCu_2Si_2$ ($x = 0$) is a stoichiometric 1-2-2 compound (see the four hatched regions in panel (a)). Sectors I, II and III indicate samples of type A , A/S and S , respectively. T_A represents the transition temperature to the AFM ordered state. The coupling constant g is shown on the abscissa and is assumed to be linear in $(1 - x)$. Figure taken from [Gegenwart 1998b, Steglich 2001].

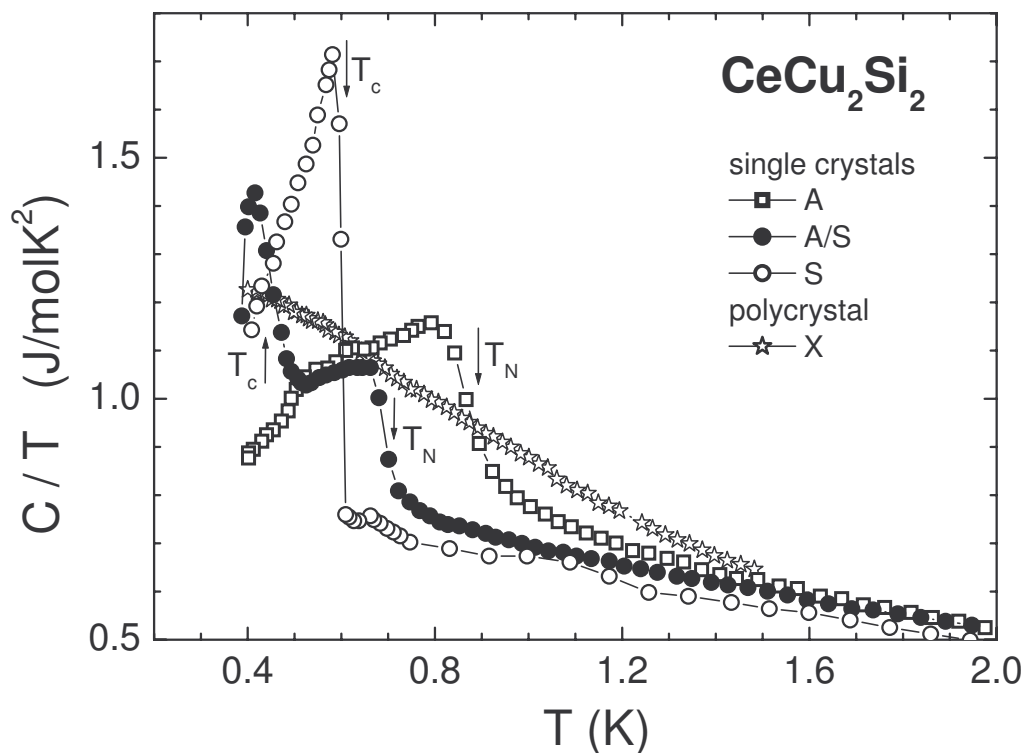


Figure 4.4: Specific-heat data on the four different types of CeCu_2Si_2 . The AFM (T_N), respectively the SC (T_c) transition temperatures, indicated by arrows, as well as their relative positions depending on the sample type, suggest the systematic evolution from A -, via A/S -, to S -type CeCu_2Si_2 . The X -type sample does not show any phase transition, neither to the A nor to the SC phase. The data for the A -, A/S - and S -type CeCu_2Si_2 are obtained on single-crystalline samples (data for the S -type crystal from [Jeevan 2007]), while the data for the X -type CeCu_2Si_2 were taken from a polycrystalline sample [Hellmann 1997].

transition temperature T_N and upon further cooling becomes superconducting at a SC transition temperature T_c ($T_c < T_N$). It is worth mentioning that the true stoichiometry point, with the most perfect crystallinity, is located within the A/S region of the phase diagram [Steglich 2001]. Furthermore, among the stoichiometric CeCu_2Si_2 , the A/S -type crystals show the lowest residual resistivities [Steglich 2001, Jeevan 2007]. With all the properties presented above, it is obvious that CeCu_2Si_2 is located just at the border of magnetism and SC, offering a good opportunity to study the low-temperature properties of HF systems. Figure 4.4 shows the heat-capacity data of the above-mentioned four different types of existing CeCu_2Si_2 compounds. The transition temperatures to the different ordered states are indicated in the figure. The X -type

samples are known to have the worst stoichiometry among all these stoichiometric samples. The other three types mainly differ by the hybridization strength between the $4f$ and conduction electrons (see figure 4.3b). In other words, upon applying a very small pressure of a few kilobars to an A -type sample one can shift gradually from an A - to the A/S - and further to the S -type behavior. The gradual decrease of the Néel temperature with increasing hybridization, accompanied by the appearance of SC, indicates the existence of a magnetic QCP but does not give a clear hint about the interplay of the two existing ground states in $CeCu_2Si_2$.

Extensive studies have been done in the past years to clarify the interplay between the magnetic phase and the HF SC phase in $CeCu_2Si_2$. Coexistence or competition between the two phases was for long time an open question. Isoelectronic doping of $CeCu_2Si_2$ with Ge on the Si site combined with application of hydrostatic pressure allows to study a broad range of the temperature - coupling strength phase diagram of $CeCu_2Si_2$. Application of hydrostatic pressure has the role of increasing the hybridization strength of the Ce $4f$ and the conduction electrons, while doping with Ge acts like negative pressure, reducing the hybridization strength and stabilizing the magnetic ground state. Although the chemical doping with Ge induces small atomic disorder in the system, the application of pressure on the two stoichiometric compounds $CeCu_2Ge_2$ and $CeCu_2Si_2$ leads to very similar temperature - coupling strength phase diagrams (see figure 4.5).

$CeCu_2Ge_2$ at ambient pressure shows an incommensurate (IC) AFM order with $T_N \approx 4.1$ K, magnetic ordering vector $Q \approx (0.28, 0.28, 0.53)$ and magnetic moment of $\mu_{ord} \approx 1.05 \mu_B$ per Ce site [Knopp 1989]. The nature of the A -phase in $CeCu_2Si_2$ was for a long time mysterious. Recently, large single crystals of $CeCu_2Si_2$ with well-defined ground-state properties became available [Jeevan 2007] facilitating neutron-diffraction experiments. Neutron-diffraction studies on Ge-substituted $CeCu_2(Si_{1-x}Ge_x)_2$ ($x \geq 0.25$) have shown that the magnetic order is the same as in pure $CeCu_2Ge_2$, with a continuous decrease of the magnetic moment upon decreasing the Ge concentration [Stockert 2005]. Stockert and coworkers have clarified in this way the origin of the A -phase of $CeCu_2Si_2$ as a magnetic phase evolving continuously from the magnetic phase of $CeCu_2Ge_2$. Therefore, the A -phase of $CeCu_2Si_2$ has been identified as an IC spin-density-wave (SDW) phase with the magnetic ordering vector $Q = (0.215, 0.215, 0.530)$ and with a low magnetic moment of about $\mu_{ord} \approx 0.1 \mu_B$ per Ce atom [Stockert 2004]. The ordering wave vector Q found in the experiment agrees well with the nesting vector of the FS sheets in $CeCu_2Si_2$ found by Zwicknagl *et al.* [Stockert 2004, Zwicknagl 1993] (see figure 4.6). Figure 4.6a shows the neutron-diffraction intensity in the reciprocal (hhl) plane at $T = 50$ mK and at $T = 1$ K,

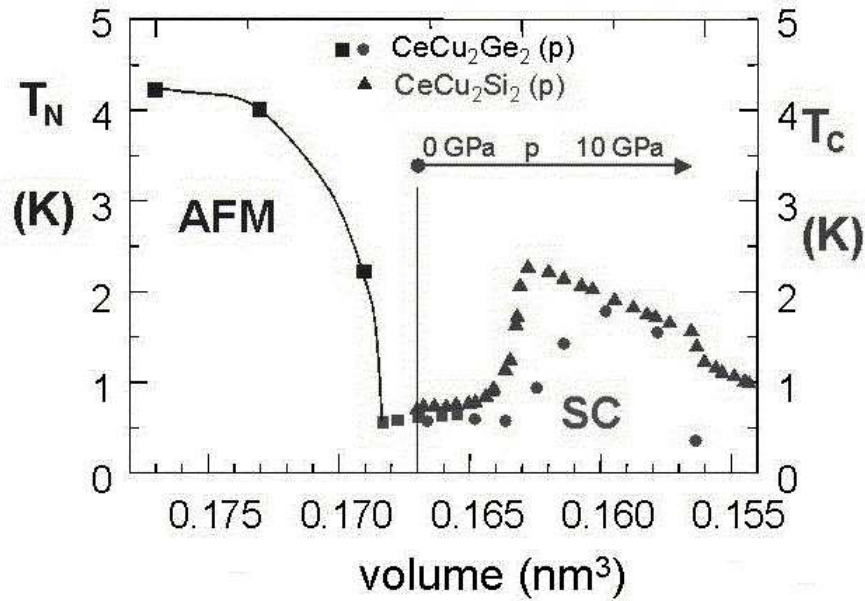


Figure 4.5: The temperature - volume, respectively pressure, phase diagram for polycrystalline CeCu_2Si_2 [Thomas 1996] and CeCu_2Ge_2 [Jaccard 1999]. The starting point of the arrow indicates the zero-pressure volume of CeCu_2Si_2 , while the length of it, as indicated in the figure, scales the pressure to the volume of the unit cell for both systems. As T_N is suppressed by pressure, CeCu_2Ge_2 shows similar SC properties as CeCu_2Si_2 . In both compounds SC continuously exists over a wide pressure range ($\Delta p \approx 10$ GPa).

corresponding to a temperature below and above the magnetic phase transition, respectively. The magnetic peak appears at $q = (0.215, 0.215, 1.470)$ corresponding to the above-mentioned IC SDW vector Q [Stockert 2004]. The main FS sheet, corresponding to the heavy QPs, obtained by renormalized band structure calculations [Zwicknagl 1993] is shown in figure 4.6c. The FS of the heavy electrons consists, additional to the small ellipsoidal pockets, of columns along the c direction with flat parts on the columns connected by a nesting vector Q (for details see also figure 4.6d). The strong nesting feature seen in the FS, suggesting the formation of a SDW ground state, together with the strong dependence of the topology of the FS on the f -level occupancy shown by Zwicknagl and Pulst [Zwicknagl 1993], suggests instabilities of the correlated LFL state at low temperatures. In good agreement with the experimentally obtained Q vector is also the calculated static magnetic susceptibility $\chi(q)$ shown in figure 4.6b [Stockert 2004, Thalmeier 2005a], which exhibits a maximum at $q = Q$. More than this, it was found in neutron-diffraction experiments that with lowering the temperature below T_N in A -type CeCu_2Si_2 , the propagation vector is temperature dependent and becomes smaller while the temperature is reduced to a

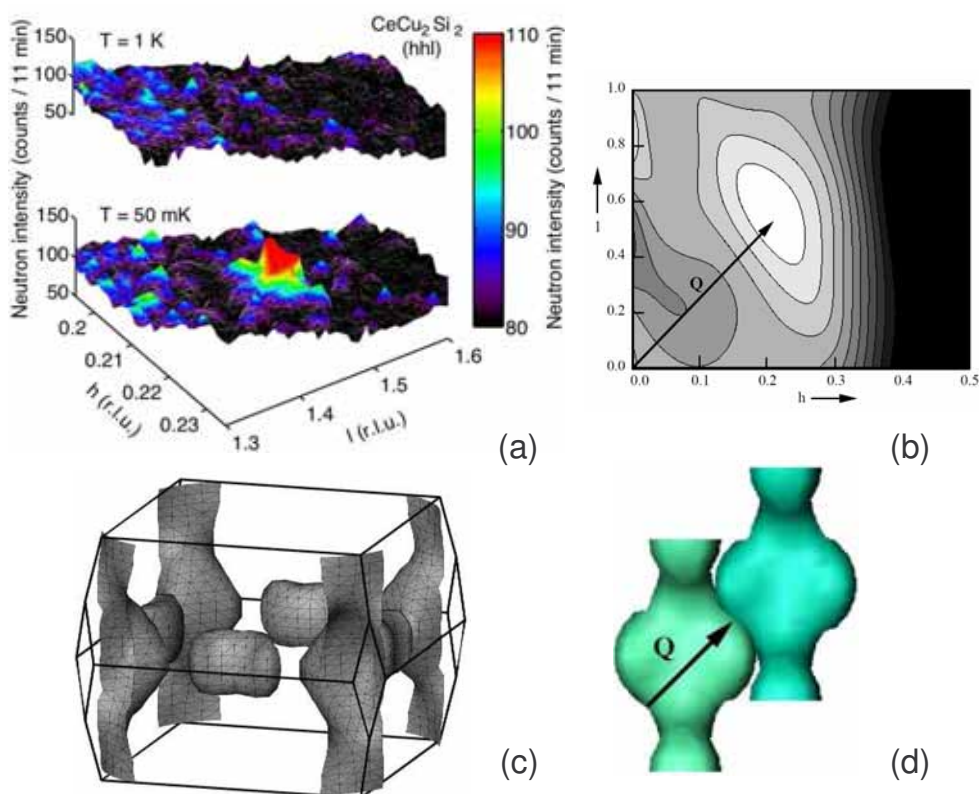


Figure 4.6: (a) Neutron-diffraction intensity map of the reciprocal plane (hhl) around $q = (0.215, 0.215, 1.470)$ in $CeCu_2Si_2$ at $T = 0.05$ K (below T_N) and at $T = 1$ K (above T_N). The resulting IC SDW vector is $Q = (0.215, 0.215, 0.530)$. Figure from [Stockert 2004]. (b) Contour map of the theoretically obtained static magnetic susceptibility, $\chi(q)$, at $T = 100$ mK (value increasing from dark to bright) in the reciprocal (hhl) plane in $CeCu_2Si_2$ [Stockert 2004, Thalmeier 2005a]. $\chi(q)$ shows its maximum at the same wave vector Q as obtained from neutron-diffraction experiments. (c) FS of the heavy QPs in $CeCu_2Si_2$ obtained by theoretical calculations using the renormalized band method [Zwicknagl 1993]. It consists of ellipsoids and modulated columns which are oriented parallel to the tetragonal axis. (d) Enlargement of the columns of the FS, showing their nesting property. The indicated nesting vector, Q , is in a good agreement with the ordering wave vector obtained by neutron-diffraction experiments. The nesting property of the FS confirms the IC SDW nature of the magnetic transition. Figures (b), (c) and (d) are taken from [Thalmeier 2005a].

temperature equal to roughly $T_N/2$ from where it remains constant down to low temperatures. This “lock-in” transition at about $T_N/2$, also visible in thermal-expansion and specific-heat measurements, is a first-order phase transition. Based on neutron-diffraction measurements, this anomaly was attributed to a transition to a probably commensurate low-temperature magnetic phase [Stockert 2004]. Furthermore, the isostructural compound $CeNi_2Ge_2$ - a HF located slightly on the non-magnetic side

of the magnetic QCP (see the schematic phase diagram shown in figure 4.1) and exhibiting NFL behavior at low temperatures in both the resistivity and the specific heat - exhibits, at roughly the same wave vector where the IC SDW in CeCu_2Si_2 was found, high-energy spin fluctuations which do not show any critical slowing down as the temperature is lowered to $T = 0$ K [Knopp 1988, Fåk 2000]. These fluctuations appear, nevertheless, to be related to the maximum of the static susceptibility and are probably not related to the NFL behavior, since the energy scale is too high. Low-energy spin fluctuations, possible to appear at some other competing wave vector, have not yet been observed in CeNi_2Ge_2 [Knopp 1988, Fåk 2000]. In conclusion, the whole family of $\text{CeCu}_2(\text{Si}_{1-x}\text{Ge}_x)_2$, with $0 \leq x \leq 1$, appears to show the existence of an AFM QCP at the same pressure where the AFM phase transition is tuned to $T_N = 0$ K.

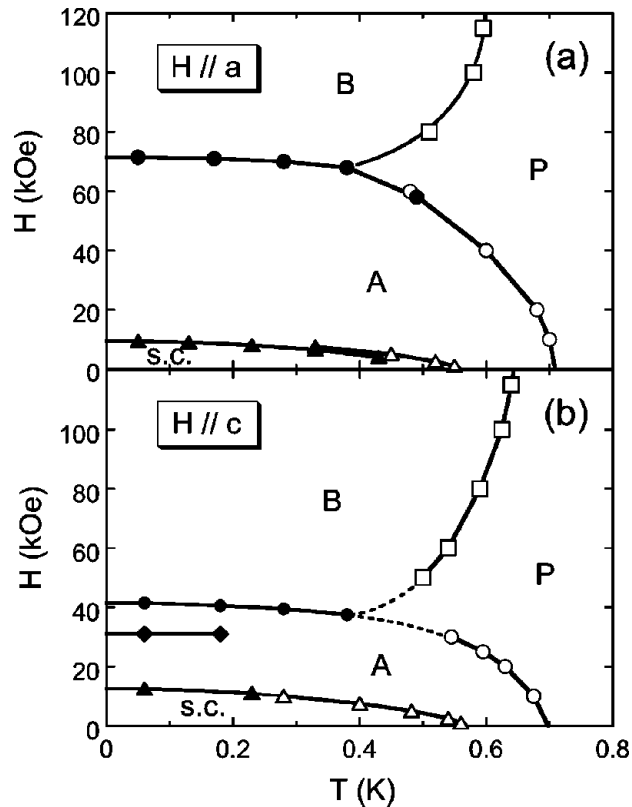


Figure 4.7: $B - T$ phase diagram of an A/S -type single crystal of CeCu_2Si_2 obtained by magnetization measurements at ambient pressure [Tayama 2003]. The upper (a) and the lower (b) figures show the phase diagram for $B \parallel a$ and $B \parallel c$, respectively.

The ground-state properties of CeCu_2Si_2 are strongly affected not only by the composition but also by the application of magnetic fields. Upon increasing the magnetic field, the AFM and SC phases are gradually suppressed and another

high-field phase, the so-called “ B -phase”, appears [Bruls 1994]. At ambient pressure, the low-temperature $B - T$ phase diagram of $CeCu_2Si_2$ is very rich and shows a certain anisotropy. Single-crystalline samples of $CeCu_2Si_2$ were studied in detail at ambient pressure and in magnetic field by specific-heat [Langhammer 2002], electrical-resistivity [Gegenwart 1998b], ultrasound [Bruls 1994], muon-spin-rotation [Feyerherm 1997], thermal-expansion [Lang 1999] and magnetization measurements [Tayama 2003]. In figure 4.7 the $B - T$ phase diagram for an A/S -type single crystal obtained by magnetization experiments is shown for B parallel to the two crystallographic directions a (a) and c (b) [Tayama 2003]. It is worth mentioning that the appearance of the magnetically-induced B -phase is not dependent on whether one is dealing with A -, A/S - or S -type samples. The nature of the B -phase is not yet completely understood, but it is believed to be magnetic in origin [Thalmeier 2005b, Stockert unpubl.]. However, there exists a theoretical suggestion related to the origin of the B -phase. The above-mentioned renormalized band structure calculations [Zwicknagl 1993] indicated that the topology of the FS sheets associated with the heavy QPs in $CeCu_2Si_2$ is strongly influenced by the occupancy of the f level. Reducing the occupancy of the f level from 95% by only $\sim 2\%$ implies a strong change in the FS topology, leading to a splitting of the FS sheets along the c direction [Zwicknagl 1993]. External magnetic field can strongly influence the f -level occupancy. Due to Zeeman splitting of the heavy QP bands, the structures of the QP density of states (DOS) are moved relative to the Fermi energy. The values of the critical magnetic fields for which the structures of the QP DOS meet the Fermi energy were estimated for B parallel to both the a and c direction by renormalized band structure calculations (B_{crit}^a , B_{crit}^c). It was found that the obtained values, $B_{crit}^a = 8$ T and $B_{crit}^c = 6.5$ T, are in good agreement with the experimentally obtained values for the magnetic field necessary to induce the B -phase in $CeCu_2Si_2$ of $B_{crit}^a(exp) \approx 7$ T and $B_{crit}^c(exp) \approx 4$ T, respectively. Therefore, it was suggested that the observed transition to the B -phase in $CeCu_2Si_2$ might be driven by a drastic topological change in the FS of the heavy QPs [Zwicknagl 1993]. Further experiments are in progress in order to shed light onto the nature of the B -phase.

Several Ce-based HF SCs (e.g. $CePd_2Si_2$ [Grosche 2001]) exhibit a generic phase diagram where the HF SC appears under a narrow “dome” centered around the AFM QCP, where the AFM ordering temperature is suppressed to $T_N = 0$ K. Two decades ago a broad SC region was found in the $T - p$ phase diagram of the two stoichiometric compounds $CeCu_2Si_2$ [Bellarbi 1984, Thomas 1993, Thomas 1996] and $CeCu_2Ge_2$ [Jaccard 1999] (see figure 4.5). This SC region extends well beyond the magnetic QCP and has its maximum at a pressure much higher than the critical pressure

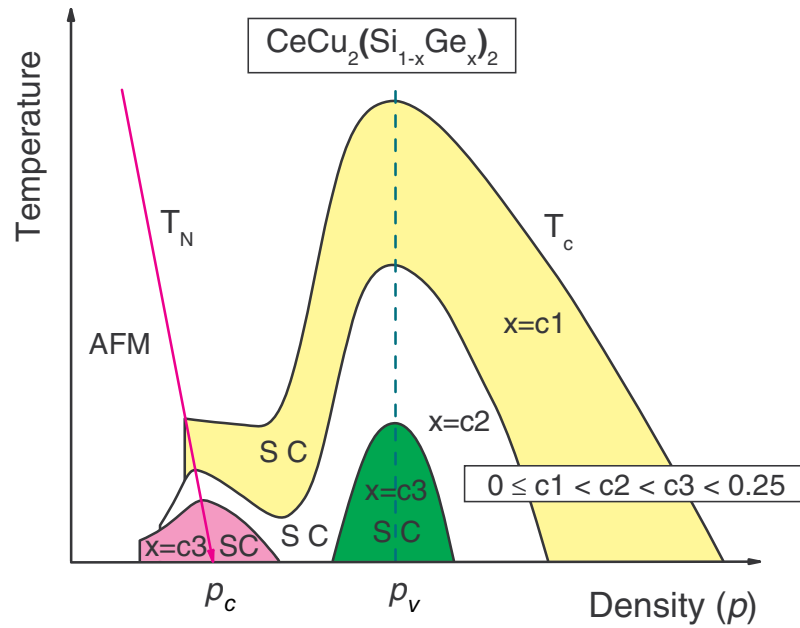


Figure 4.8: Schematic phase diagram of $\text{CeCu}_2(\text{Si}_{1-x}\text{Ge}_x)_2$ for low concentrations of Ge. As Si is replaced by low amounts of Ge, the single wide SC region existing in CeCu_2Si_2 starts to become weaker, showing first a minimum for a certain range of doping $c_1 < x < c_2$, collapsing then in two distinct regions for higher doping $c_2 < x < c_3$, and finally vanishes completely for a concentration of Ge of $x > 0.25$. The presented evolution of the SC is explained by the role of impurities, induced by chemical doping, in breaking the Cooper pairs. Figure taken from [Yuan 2004].

where the AFM QCP is supposed to be. Therefore, it was for a long time believed that CeCu_2Si_2 and CeCu_2Ge_2 do not fit into the “universal” phase diagram of the Ce-based HF SCs where the SC shows up in the region where the magnetic phase transition is tuned to zero temperature. However, it became clear that this anomalously shaped SC region and this unexpected maximum of T_c at high pressure in the two above-mentioned compounds is due to the presence of a weakly first-order valence transition of Ce [Yuan 2003]. High-pressure studies on the non-stoichiometric compounds $\text{CeCu}_2(\text{Si}_{1-x}\text{Ge}_x)_2$ ($x \neq 0, 1$), where non-magnetic disorder introduced by doping on the Si/Ge site plays a crucial role in destroying the Cooper pairs (see section 1.2.1 and table 1.1 - unconventional SC) and in reducing the SC transition temperature T_c (see also in equation 1.1 the dependence of T_c as function of ξ_0/l_{tr}), revealed the existence of two well separated SC regions in the $T - p$ phase diagram. Ge-substituted single crystals of $\text{CeCu}_2(\text{Si}_{1-x}\text{Ge}_x)_2$ with different but low Ge concentrations ($x = 0.01, 0.1$ and 0.25) were studied by resistivity measurements under pressure [Yuan 2004]. It was found that for $x = 0.01$, T_c shows a minimum around $p \approx 3$ GPa. With further increasing the Ge concentration to $x = 0.1$, which implies an

increase of the induced atomic disorder, the continuous SC region existing in the pure and slightly doped compounds breaks up into two disconnected SC domes. Furthermore, for $x = 0.25$ SC vanishes completely (see figure 4.8). The SC dome existing at low pressure is located around the AFM QCP (around p_c - see also figure 4.8), in good agreement with the observations for other Ce-based HF compounds, while the SC region at the high-pressure side is related to the existence of a low-temperature critical end point for the valence transition of Ce (at p_v - see also figure 4.8). However, in the two stoichiometric compounds CeCu₂Si₂ and CeCu₂Ge₂ the two SC regions seem to merge into a single wide SC region. In the following part we will focus on the SC region on the high-pressure side.

From the first discovery of this anomalously shaped SC region in the stoichiometric compound CeCu₂Si₂ [Bellarbi 1984] speculations arose concerning a correlation between the appearance of the maximum of T_c under pressure and a possible valence instability of the Ce ions. Therefore, a magnetic phase boundary and its interplay with SC were not the only physical peculiarities seen in the CeCu₂(Si_{1-x}Ge_x)₂ systems. Metallic Ce under pressure undergoes an isostructural phase transition, called the $\gamma - \alpha$ transition, which involves a volume collapse of $\sim 17\%$ at room temperature and $p \approx 0.8$ GPa [Koskenmaki 1978]. This transition was attributed to the instability of the $4f$ electrons, more precisely, to the delocalization of a fraction of the $4f^1$ electrons accompanied by a valence change. Analogous to the metallic Ce, increasing pressure in CeCu₂(Si_{1-x}Ge_x)₂ reduces the interatomic distances, leading to a transition from a nearly trivalent Ce^{3+ $|\delta|$} state ($|\delta| \ll 1$) with Kondo coupling to a Ce^{3+ $|\delta|$} state, where $0 \ll |\delta| < 1$, characteristic for an IV system, where the Ce ion fluctuates between the $4f^1$ and the $4f^0$ electronic configurations (see details in section 1.1.3). In addition to the mentioned $\gamma - \alpha$ transition in metallic Ce, there exists experimental evidence which hints at the possibility of a pressure-induced change of the valence of Ce in intermetallic CeCu₂(Si_{1-x}Ge_x)₂. At room temperature, CeCu₂Si₂ under pressure undergoes a first-order valence transition from a valence of Ce of about 3.10 to about 3.14 [Röhler 1988]. The observed valence change occurs at about the same pressure where the SC transition temperature is reaching its maximum value. Moreover, it was found by X-ray diffraction measurements that CeCu₂Ge₂ under pressure exhibits a volume discontinuity of about 2% at $T = 10$ K [Onodera 2002]. This anomaly was not detected at room temperature [Onodera 2002]. Since like in the case of elemental Ce no change of the crystal structure was observed to be associated with the volume collapse, a change of the Ce valence is considered to cause the observed volume discontinuity. Similar to the case of CeCu₂Si₂, the pressure where the volume collapse takes place in CeCu₂Ge₂ coincides with the pressure where a maximum of T_c is ob-

served in CeCu_2Ge_2 [Jaccard 1999]. It is worth mentioning that the above-described experimental evidences for a pressure-induced valence change of Ce in CeCu_2Si_2 and CeCu_2Ge_2 show a relatively weak change in the valence of Ce. Due to the fact that the maximum value of T_c is observed at the same pressure where the valence transition is detected for both CeCu_2Si_2 and CeCu_2Ge_2 , a connection between the presence of SC in the high-pressure region (far away from the AFM instability) and the valence change of Ce is suggestive.

Since the SC in $\text{CeCu}_2(\text{Si}_{1-x}\text{Ge}_x)_2$ ($0 \leq x \leq 1$ and x being in the range where SC is still formed) most likely has an unconventional nature over the whole range of pressure, it is also unlikely that in the SC state the formation of the Cooper pairs is mediated by phonons. Formation of Cooper pairs in a system implies the need of a certain amount of condensation energy necessary to overcome the mutual repulsion between electrons. In the case of HFs, where the charge carriers are heavy QPs, it is likely that the Cooper pairs are formed by the heavy QPs. Due to the strong difference existing in the energy and time scales between the conduction electrons in a simple metal and the heavy QPs in HF compounds it is very probable that also the condensation energies are very different (for details see table 1.1 in section 1.2.1). Therefore, appropriate conditions are needed for the formation of a SC state in HF systems. It was proposed that the strong (nearly) critical spin or valence fluctuations of the f electrons, which exist in HF systems close to a magnetic instability or to a weak valence transition with low-lying critical end point, may fulfill the needs for the formation of Cooper pairs [Monthoux 2001, Monthoux 2004] (see for details section 1.2.2). SC mediated by magnetic fluctuations in the low-pressure region, close to the AFM instability (around p_c), as well as SC mediated by strong (nearly critical) valence fluctuations in the high-pressure region (around p_v), is expected to form in the $\text{CeCu}_2(\text{Si}_{1-x}\text{Ge}_x)_2$ family of compounds. The SC pairing state in both of the above-mentioned situations has to be of non- s -wave type [Monthoux 2001, Monthoux 2004].

Still after nearly 30 years of intensive research focussing on the physical properties of CeCu_2Si_2 , many open questions are existing, giving a good motivation to scientists to further study this compound in order to get more insight into the interesting physics of HF systems. In the following part we will present our ambient-pressure, as well as pressure-dependent, experimental results obtained on A/S -type CeCu_2Si_2 .

4.3 Experimental results

We have performed specific-heat measurements under hydrostatic pressure on single-crystalline A/S -type CeCu_2Si_2 in the pressure range $0 \text{ GPa} \leq p < 2.1 \text{ GPa}$

and in the temperature range $0.26 \text{ K} \leq T \leq 7 \text{ K}$. The measurements were carried out utilizing a compensated quasiadiabatic heat-pulse technique in a single-shot ^3He evaporation cryostat equipped with a SC magnet providing a magnetic field up to $B = 8 \text{ T}$. The temperatures below the typical temperature achieved in the ^3He cryostat, of about $T \approx 0.35 \text{ K}$, were obtained by adiabatic demagnetization of the magnetic moments of Cu from the pressure cell. Simultaneously with the specific-heat measurements, the SC transition in $CeCu_2Si_2$ was monitored by a.c.-susceptibility measurements under pressure. For this purpose the coil used for determining the pressure, while detecting the evolution of the SC transition temperature of Sn placed inside of the pressure cell, was used. The resolution of the detecting coil is good enough to determine any SC transition (either from the pressure gauge - Sn - or from the sample), but detection of an AFM phase transition is not possible. Additional data points for the $B-T$ phase diagrams of $CeCu_2Si_2$ were obtained by monitoring the sample temperature while slowly sweeping the magnetic field (magnetocaloric effect, $T(B)$). For obtaining the above-mentioned pressure range, two types of pressure cells were used. Measurements at low pressures ($p < 1.1 \text{ GPa}$) were done in a CuBe piston-cylinder type pressure cell, while for the high-pressure range ($1.1 \text{ GPa} < p < 2.1 \text{ GPa}$) a double-layer Ni-Cr-Al/CuBe piston-cylinder type pressure cell was used. For the entire experiment Fluorinert FC72 was used as pressure transmitting medium. A more detailed description of the technique used is contained in Chapter 2. Due to the strong improvements in the last years concerning the growth of large single-crystalline $CeCu_2Si_2$ with well-defined ground-state properties [Deppe 2004, Jeevan 2007], a single piece of A/S -type $CeCu_2Si_2$ weighing about $m \approx 400 \text{ mg}$ and with dimensions of approximately $(11 \times 4 \times 4.5) \text{ mm}^3$ was used for the experiment. Using a large sample for the measurements under pressure made possible to have a unique well-defined orientation with respect to the magnetic field, $B \parallel c$, for the entire pressure range. Measurements of the electrical resistivity and specific heat at ambient pressure and various magnetic fields were also done in a Quantum Design PPMS with ^3He option on different samples prepared from the same batch from which the sample measured under pressure was taken. Concerning the quality of the samples used, a residual resistivity of $\rho_0 \approx 10 \mu\Omega\text{cm}$ has been measured at ambient pressure. The single-crystalline samples used in our experiments were prepared by H. S. Jeevan in the group of C. Geibel at MPI-CPfS, Dresden, Germany.

For the entire specific-heat data on $CeCu_2Si_2$ presented in this chapter ($p < 2.1 \text{ GPa}$), the electronic specific heat (C_{el}) is obtained by subtracting the ambient-pressure lattice specific heat of the isostructural non-magnetic reference compound $LaCu_2Si_2$ [Hellmann unpubl.]. Since we are not aware about any pressure-dependent

heat-capacity data of LaCu_2Si_2 , we have neglected the pressure dependence of the lattice heat capacity over the entire measured pressure range ($p < 2.1$ GPa) by using for the lattice contribution to the specific heat the ambient-pressure heat capacity of LaCu_2Si_2 (in the temperature range $0.26 \text{ K} \leq T \leq 7 \text{ K}$).

The pressure-dependent heat-capacity measurements on CeCu_2Si_2 were performed by measuring the sample encapsulated in the pressure cell (see details in Chapter 2). Therefore, in order to evaluate the errors introduced to the obtained data by the technique employed to perform the measurements, in figure 2.7 the pressure and temperature dependence of $C_{\text{sample}}/C_{\text{total}}$ obtained for CeCu_2Si_2 over the entire temperature and pressure range of our experiment ($0.26 \text{ K} \leq T \leq 7 \text{ K}$, $p < 2.1$ GPa) is presented. $C_{\text{sample}}/C_{\text{total}}$ signifies the contribution of the sample to the total measured heat capacity and represents the ratio between the heat capacity of the measured sample and the heat capacity of the complete ensemble consisting of the measured sample loaded in the pressure cell (see details in Chapter 2). In the temperature range $0.26 \text{ K} \leq T \leq 2 \text{ K}$, values of $C_{\text{sample}}/C_{\text{total}}$ ranging from $C_{\text{sample}}/C_{\text{total}} \approx 10\%$ at the highest pressure of our experiment, $p \approx 2.03$ GPa, to $C_{\text{sample}}/C_{\text{total}} \approx 64\%$ at ambient pressure were obtained. It is worth noting that the obtained values of $C_{\text{sample}}/C_{\text{total}}$ are rather good for this type of pressure-dependent specific-heat measurements and they prove the good accuracy of the absolute values of our specific-heat data obtained on CeCu_2Si_2 .

The remainder of this section is divided into three parts. The first two parts describe our main experimental results obtained under pressure on single-crystalline A/S -type CeCu_2Si_2 . In the first part, focusing on the interplay of AFM and SC in CeCu_2Si_2 , our data at ambient pressure, as well as at low pressures, are presented. In the second part the results obtained at higher pressures, away from the AFM instability, are described. Both of these parts contain at the beginning a short overview of some related experimental and theoretical results known from the literature. In the third part we interpret the afore-presented data. A study of the evolution of the SC properties in the different pressure regions is also contained in this part.

4.3.1 Interplay of antiferromagnetism and superconductivity in CeCu_2Si_2

Nowadays it is widely accepted that HF SC in the vicinity of an AFM ordered region is mediated by the existing magnetic fluctuations. However, the interplay of AFM and SC is a motivating subject for both experimentalists and theoreticians. In the SC state the gauge symmetry is broken, in the AFM state the spatial sym-

metries and possibly the spin-rotational and time-reversal symmetries are broken [Thalmeier 2005a]. Which of the two states is more favorable depends on the momentum and energy dependence of residual QP interactions and on the geometric properties of the FS and usually cannot be strictly predicted for real materials. The coexistence of the two ordering phenomena is well understood in those materials where they occur in different electronic subsystems which, in addition, are not coherently coupled (e.g. rare-earth borocarbides, RNi₂B₂C) [Thalmeier 2005a]. In the case of HF SCs, where both ordering phenomena (AFM and SC) are carried by the strongly correlated charge carriers, the situation is not yet clarified. Some experimental results obtained on CeCu₂Si₂ were in favor of the coexistence of AFM order and SC (e.g. [Kitaoka 2001, Kawasaki 2001, Kitaoka 2002, Koda 2002, Kitaoka 2005]), while others were supporting the picture of competition between AFM and SC in this compound (e.g. [Feyerherm 1997, Stockert 2004]). In addition, theoretical models exist in order to support either of the results.

Coexistence of AFM and SC in CeCu₂Si₂

Results obtained from muon-spin-rotation measurements performed on polycrystalline samples of CeCu₂Si₂ have suggested the microscopic coexistence of AFM and SC in CeCu₂Si₂ [Koda 2002]. Ambient-pressure, as well as pressure-dependent, Cu-NQR measurements on polycrystals of CeCu₂Si₂ [Ishida 1999, Kawasaki 2000, Kawasaki 2001] and slightly doped CeCu₂(Si_{1-x}Ge_x)₂ ($0 \leq x \leq 0.02$) [Kawasaki 2002, Kawasaki 2004] have identified two different behaviors of the nuclear spin-lattice relaxation rate, $1/T_1$, in the SC region located close to the magnetic QCP. Depending on pressure or composition, in the region where the AFM and SC transition temperatures are becoming equal ($T_N = T_c$) a systematic change of the temperature dependence of $1/T_1$ below T_c has been observed. By considering p_c^* the pressure where at $B = 0$ T $T_N = T_c$, it was found that for the pressure range $p \leq p_c^*$, where AFM order still exists in the system ($T_N > T_c$), $1/T_1(T) \propto T$ below T_c , suggesting an “exotic” type of gapless SC in this region. For pressures above p_c^* , where a transition to the AFM ordered state is not anymore detected, a $1/T_1(T) \propto T^3$ dependence below T_c was observed, a behavior which is typical for many HF systems and indicates a SC gap with line nodes. The appearance of $1/T_1(T) \propto T^3$ below T_c upon application of pressure, leads to the exclusion of the possibility that impurities would produce the $1/T_1(T) \propto T$ behavior observed below T_c in the low-pressure range in CeCu₂Si₂. These findings led the authors to consider that the “exotic” SC emerges below T_c , where AFM critical fluctuations remain active even below T_c . They argue in favor of the coexistence of AFM order and SC and of the existence of a common mechanism producing the “ex-

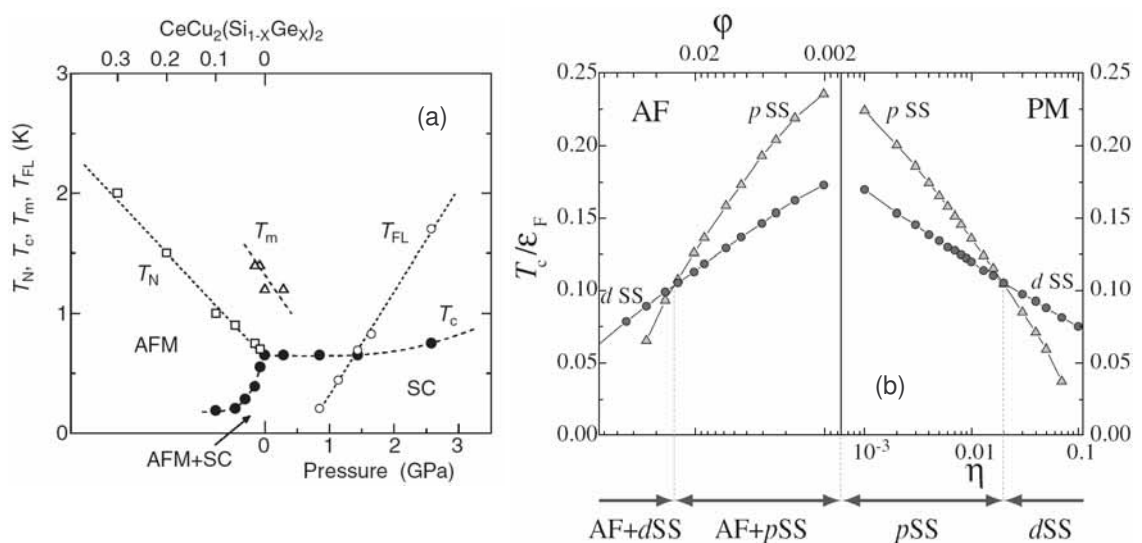


Figure 4.9: (a) T – p phase diagram obtained by NQR measurements on pure CeCu_2Si_2 and slightly doped $\text{CeCu}_2(\text{Si}_{1-x}\text{Ge}_x)_2$. T_N and T_c represent the AFM and SC transition temperatures. T_m represents the temperature below which the slowly fluctuating AFM spin waves develop, while T_{FL} denotes the temperature below which $1/(T_1(T)T)$ becomes constant (LFL behavior). Figure taken from [Kitaoka 2005]. (b) Theoretical prediction of the SC transition temperature near the AFM QCP. p SS and d SS are notations for p - and d -wave spin-singlet SC, respectively. φ and η are parameters used for representing the distance from the AFM QCP measured on the AFM and PM side, respectively. The p SS SC has gapless nature and is realized only near the QCP, while away from the QCP, on both the AFM and PM sides, the d SS SC with line nodes is present. Figure taken from [Fuseya 2003].

otic” SC and magnetism in CeCu_2Si_2 . It is worth mentioning that a behavior similar to that seen in CeCu_2Si_2 , consisting in a change of the $1/T_1(T)$ dependence below T_c from $1/T_1(T) \propto T$ on the AFM side of p_c^* to $1/T_1(T) \propto T^3$ at $p > p_c^*$, has been also observed in the pressure-induced SC state of CeRhIn_5 [Kawasaki 2003, Kitaoka 2005].

In support of the above-described experimental results, theoretical work was done by Fuseya and coworkers [Fuseya 2003]. Similar to the model used by Monthoux and Lonzarich [Monthoux 1999] in explaining the magnetically mediated Cooper pairing, the theoretical model of Fuseya and coworkers is based on a phenomenological treatment of the SC interactions in the vicinity of the AFM order [Fuseya 2003]. The realization of a gapless p -wave spin-singlet SC, mediated by AFM spin fluctuations, in the close vicinity of the AFM QCP, both on the paramagnetic as well as on the AFM side of the QCP, was suggested. With increasing distance from the AFM QCP, on each side of the QCP the formation of the “conventional” anisotropic d -wave spin-singlet SC with line nodes was proposed [Fuseya 2003]. For the spin-singlet p -wave symmetry

a SC gap function $\Delta_k^p \propto \sin(k_x a)$ or $\Delta_k^p \propto \sin(k_y a)$ was chosen [Fuseya 2003]. The $\Delta_k^d \propto (\cos(k_x a) - \cos(k_y a))$ gap function ($d_{x^2-y^2}$ type) was considered for the case of the d -wave type SC state [Fuseya 2003]. Apart from the gapless p -wave spin-singlet type SC state proposed for the close vicinity of the AFM QCP, the suggestion of a d -wave spin-singlet type Cooper pairing for the SC state near the AFM phase in $CeCu_2Si_2$ has been frequently made in other theoretical models considering the SC state as mediated by magnetic fluctuations (e.g. [Monthoux 2001]).

Figure 4.9 summarizes the main results of the experimental and theoretical works mentioned above. The $T-p$ phase diagram of $CeCu_2Si_2$ obtained by NQR measurements [Kawasaki 2002, Kitaoka 2005] is shown in figure 4.9a, while 4.9b presents the evolution of SC around the AFM QCP, obtained by the theoretical calculations performed by Fuseya *et al.* [Fuseya 2003]. As seen in panel (b) of figure 4.9, the gapless p -wave spin-singlet SC (p SS) is realized very close to the AFM QCP, while away from it the d -wave spin-singlet SC (d SS) is formed. The p SS state has the particular property of a gapless SC state and coexists with the AFM order, being probably generated by the same mechanism which generates AFM order. The d SS state is the common SC state observed in many HF SCs, exhibiting a gap function with line nodes [Fuseya 2003]. It was mentioned that a condition for the emergence of the p -wave singlet pairing is that the FS is not nested [Fuseya 2003]. However, it was considered by the authors that their theoretical model can be proposed to explain the “exotic” type of SC which coexists with the AFM order in $CeRhIn_5$ and $CeCu_2Si_2$, where the unusual behavior of the NQR relaxation rate below T_c , of $1/T_1(T) \propto T$, was detected on the AFM side of the QCP.

Next to the results of the theoretical model of Fuseya *et al.*, the interplay of AFM and SC in $CeCu_2Si_2$, as obtained from the NQR measurements described earlier, is depicted in the $T-p$ phase diagram shown in figure 4.9a. The presented data were obtained on pure as well as on Ge-doped $CeCu_2Si_2$ [Kawasaki 2002, Kitaoka 2005]. The area marked with the “AFM+SC” label corresponds to the region where $1/T_1(T) \propto T$ was observed in the SC state ($p < p_c^*$). On the right-hand side of this region, in the SC state at $p > p_c^*$, $1/T_1(T) \propto T^3$ below T_c was detected. The appearance of the different SC states with different symmetry types in the vicinity of an AFM QCP predicted theoretically [Fuseya 2003] and described in panel (b) of figure 4.9 seems to qualitatively explain the case of $CeCu_2Si_2$. However, the possible p SS state, meant to explain the experimentally observed unusual $1/T_1(T) \propto T$ dependence below T_c , was predicted to extend on both sides of the AFM QCP (see figure 4.9b). In the case of both compounds, $CeCu_2Si_2$ and $CeRhIn_5$, $1/T_1(T) \propto T$ below T_c was observed only on the AFM side of a possible QCP and in a pressure region limited to $p < p_c^*$.

Due to the presence of the SC state at low temperatures, the existence of an AFM QCP (in the SC phase) could not be experimentally observed in neither of the two compounds. However, the critical pressure, p_c , where the AFM QCP is supposed to be located, should be higher than the pressure p_c^* where $T_N = T_c$. In the case of CeCu₂Si₂ p_c^* and p_c seem to be relatively close to each other, while in CeRhIn₅ the two values are well separated [Shishido 2005, Knebel 2006, Park 2006] leading to a stronger discrepancy between the experimental findings and the theoretical estimation of Fuseya *et al.*. Anyhow, the possibility of the existence of two different SC states in the close vicinity of the AFM QCP in CeCu₂Si₂ (as well as in CeRhIn₅) can be considered. The critical AFM fluctuations, existing only in the vicinity of the AFM QCP, are supposed to produce the “exotic” (predicted to be gapless p -wave spin-singlet) SC state observed around the AFM QCP. This SC state seems to be robust against the critical AFM fluctuations. Once T_c becomes comparable to T_N , though those AFM critical fluctuations are still active also below T_c , the onset of magnetic order could be prevented by the existence of some SC fluctuations. However, when a magnetic field is applied to suppress SC, a phase transition from the SC to the AFM order is observed while increasing the magnetic field. This phase transition, from SC to AFM, was identified as first-order like by thermal-expansion measurements on CeCu₂Si₂ [Bruls 1994]. Application of pressure, necessary to suppress the AFM order, leads to the appearance of the typical HF d -wave SC with line-node gap [Fuseya 2003, Kitaoka 2005]. It was also suggested that the uniform coexistence of AFM and SC could produce the broadening of the SC phase transition seen in resistivity measurements on CeRhIn₅ under pressure [Hegger 2000] around the quantum critical region [Kitaoka 2005]. The presence of some fluctuations of the AFM order parameter or magnetic density fluctuations could induce the fluctuations of the SC order parameter, the latter leading then to the broadening of the phase transition. It was proposed that the SC state characterized by a broad phase transition and located in the close vicinity of the AFM order is not in the “conventional” regime with a SC gap around the Fermi level, but in a gapless regime [Kitaoka 2005]. It is worth mentioning that a broad phase transition into the SC state of CeRhIn₅ in the pressure region $p \leq p_c^*$ has been also observed by a.c.-susceptibility measurements [Kawasaki 2003, Knebel 2004]. A narrowing of the SC phase transition anomaly for $p > p_c^*$ has been also reported [Kawasaki 2003, Knebel 2004].

Using symmetry as a property which governs, and therefore can unify, different physical phenomena, an earlier phenomenological approach based on the SO(5) theory, constructed on the basis of quantum-field theory, unifying AFM and SC, also argues in favor of the coexistence, at microscopic level, of AFM and SC order in a certain

pressure/doping interval in $CeCu_2(Si_{1-x}Ge_x)_2$ [Zhang 1997, Hu 2000, Kitaoka 2001].

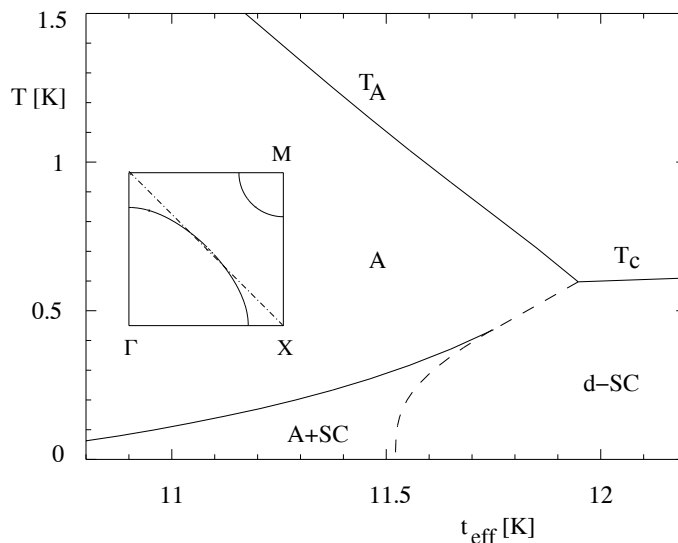


Figure 4.10: Phase diagram obtained by the 2D mean-field model described in the text. “A” denotes AFM SDW phase, “ d -SC” a SC phase with d_{xy} - symmetry and “A+SC” a phase with coexistence of SDW and d -SC. The dashed line represents a first-order phase transition, while the solid lines correspond to second-order phase transitions. t_{eff} represents the effective tight-binding hopping integral used in the model and it scales linearly with pressure (or doping with Ge, respectively). The inset shows the FS topology with two bands. The main FS sheet, around the Γ point, and the additional FS piece closed around the M point are shown. The dotted line in the inset shows the location where the constant SDW gap opens. Figure taken from [Steglich 2001].

Also arguing for the coexistent AFM and SC states in $CeCu_2Si_2$, a different theoretical approach based on a simplified 2D mean-field model for a SDW ground state competing with a d -wave SC state characterized by a d_{xy} symmetry was used in order to obtain the phase diagram shown in figure 4.10 [Steglich 2001]. It was speculated that not only the main columnar heavy FS sheets of $CeCu_2Si_2$ should be involved in the conduction but also the second, relatively small, FS pieces well separated from the former ones (two-band model) (see figure 4.6c and inset of figure 4.10 - ellipsoidal FS centered at point M in the reciprocal lattice). The second, nearly spherical, FS was supposed to contain approximately 13% of the charge carriers. The theoretical estimation, though based on a rather simple model, seems to offer a relatively good explanation for the experimentally obtained phase diagram shown in figure 4.3b. The main conclusions of the model are as follows: i) the phase transition from the AFM phase into the SC state is expected to be of first order in a certain region of the phase diagram (see dashed line in figure 4.10); ii) a SC gap function

with d_{xy} type symmetry is favored ($\Delta_k/\Delta_0 = \sin(k_x a)\sin(k_y a)$); iii) the constant SDW gap which opens below T_N along the dotted line seen in the inset of figure 4.10 leads to a gap only on part of the columnar FS (approximated to $\sim 40\%$ of the FS), allowing the remaining charge carriers to form a SC state coexisting with the magnetic phase at low temperatures. The charge carriers from the smaller FS pieces are only involved in the formation of the SC state. They are mainly responsible for the coexistent AFM and SC states because they remain unaffected by the SDW gap, making the coexistence of AFM and SC stable down to low hybridization strengths, i.e. in $\text{CeCu}_2(\text{Si}_{0.9}\text{Ge}_{0.1})_2$ [Steglich 2001].

Competition between AFM and SC in CeCu_2Si_2

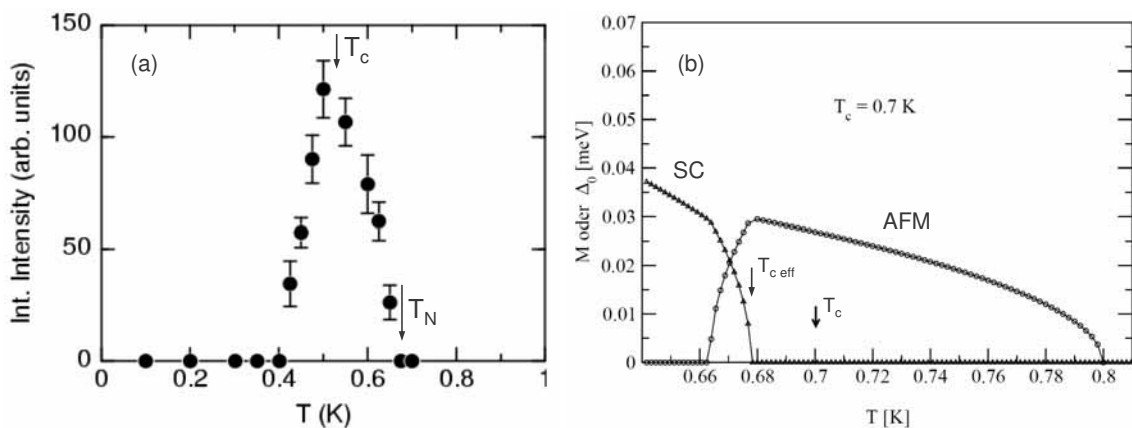


Figure 4.11: (a) Integrated neutron-diffraction intensity versus temperature of the AFM SDW satellite of the A/S -type CeCu_2Si_2 , corresponding to the ordering wave vector $Q \approx (0.215, 0.215, 0.530)$, proportional to the square of the AFM order parameter. Once SC sets in, the magnetic order parameter is continuously suppressed to zero. Figure taken from [Thalmeier 2005b]. (b) Temperature dependence of the AFM (M) and SC (Δ_0) order parameters calculated for the $\Delta_k \propto (\cos(k_x a) - \cos(k_y a))$ symmetry of the SC order parameter ($d_{x^2-y^2}$) for $T_N = 0.8$ K and $T_c = 0.7$ K. At T_N , M starts to increase. Upon further cooling, at T_c , first SC is suppressed by the magnetic order, until an effective transition temperature $T_{c,eff} < T_c$, from where, in a short temperature interval, M is completely suppressed and the SC order parameter is increasing to its full value. The temperature region where AFM and SC coexist is relatively narrow. Figure taken from [Neef 2004]. The estimations of the theoretical model (b) nicely agree with the experimental result obtained by neutron-diffraction measurements (a).

Most recent results obtained from neutron-scattering experiments [Stockert 2004, Thalmeier 2005b], together with recent theoretical calculations [Neef 2004], are supporting the picture where AFM and SC are competing in A/S -type CeCu_2Si_2 . Ev-

idence that AFM order and SC do not spatially coexist, but rather do compete, has been also shown by muon-spin-rotation and relaxation experiments performed on polycrystalline $CeCu_2Si_2$ [Feyerherm 1997].

A theoretical model, based on renormalized band structure calculations, has been used in order to try to elucidate the interplay of the AFM order and SC in $CeCu_2Si_2$ [Neef 2004]. The real FS, obtained on the basis of renormalized band structure calculations and used for the theory presented in the following, is depicted in figure 4.6c [Zwicknagl 1993]. It mainly consists of columns parallel to the tetragonal axis and small nearly spherical pockets. The topology of the FS suggests that the strongly correlated Fermi-liquid state should become unstable at low temperatures. The pronounced nesting features are responsible for the formation of a ground state with a spin-density modulation. As already mentioned in section 4.2, the topology of the main columnar sheet of the FS depends rather sensitively on the position of the Fermi energy and, hence, on the occupancy of the Ce f level. The model is based on mean-field approximation and is described in detail in [Neef 2004]. For the unconventional SC state, only the possible spin-singlet paired states, allowed for a tetragonal structure [Volovik 1985] (see also legend in figure 4.12, $S = 0$), were taken into account due to the Pauli limiting reported formerly in $CeCu_2Si_2$ [Rauchschwalbe 1982, Assmus 1984]. It was concluded that only for two allowed SC order parameters, namely $\Delta_k \propto k_x k_y (k_x^2 - k_y^2)$ and $\Delta_k \propto (\cos(k_x a) - \cos(k_y a))$, the experimentally seen A , A/S and S phases are possible to be realized. For the other order parameters taken in the calculations, it was shown that only the realization of the A -phase is possible. Figure 4.11b shows the temperature dependence of the AFM SDW (M) and SC (Δ_0) order parameters calculated for $T_N = 0.8$ K, $T_c = 0.7$ K and a SC order parameter with $\Delta_k \propto (\cos(k_x a) - \cos(k_y a))$ type symmetry ($d_{x^2-y^2}$ type). It can be seen that upon cooling, from T_N the AFM order parameter, M , starts to develop. Upon further cooling, at T_c SC is first suppressed by the magnetic order until an effective transition temperature $T_{c_{eff}} < T_c$, from where SC sets in, M starts to decrease and the SC order parameter, Δ_0 , develops. The region where AFM and SC coexist is very narrow and corresponds to a temperature interval of approximately 20 mK. Outside of the coexisting region, either only SC or only AFM exists in the system. It is worth mentioning, that in the case of the SC order parameter with $\Delta_k \propto k_x k_y (k_x^2 - k_y^2)$ type symmetry, the interplay of AFM and SC is developing in a similar manner like in the case of the $\Delta_k \propto (\cos(k_x a) - \cos(k_y a))$ symmetry. For the same transition temperatures, T_N and T_c , $T_{c_{eff}}$, where SC starts to develop, is smaller in the case of $\Delta_k \propto k_x k_y (k_x^2 - k_y^2)$ symmetry, while the value of Δ_0 is higher for the $\Delta_k \propto k_x k_y (k_x^2 - k_y^2)$ symmetry. Figure 4.11a shows the integrated neutron-diffraction

intensity of the SDW satellite as function of temperature, obtained on an A/S -type single crystal [Thalmeier 2005b]. It is visible that upon cooling, at T_N the integrated neutron-diffraction intensity, which is proportional to the square of the AFM order parameter, starts to increase. Upon further lowering the temperature, in the region where SC sets in, the integrated neutron-diffraction intensity drops to zero. The experimental findings are in good agreement with the theoretically obtained results, suggesting that in an A/S -type CeCu_2Si_2 , the AFM order coexists with SC in a very narrow temperature range below T_c , being then completely suppressed by the stable SC state. Moreover, muon-spin-rotation measurements performed on the same single crystal like the one used in the neutron-diffraction studies presented in figure 4.11a show no magnetic volume fraction at temperatures well below T_c ($T < 0.3$ K), confirming the above-described picture of competition of AFM and SC order in A/S -type CeCu_2Si_2 [Stockert 2006].

It is worth noting that in each of the theoretical models described above, only spin-singlet pairing states were taken into account due to the strong Pauli limitation suggested by experimental studies [Rauchschwalbe 1982, Assmus 1984]. Having in mind the different experimental results and theoretical approaches presented above, it seems important to carefully study the evolution of the SC properties of CeCu_2Si_2 in the very close vicinity of the AFM QCP.

Symmetry of the SC order parameter - theoretical concepts

Phase transitions with the appearance of a spontaneous symmetry breaking are characterized by order parameters. Many physical properties are directly determined by the symmetry of the order parameter. The possible types of order parameters are restricted by crystal symmetry. In the case of AFM order, the existence of magnetic order and the symmetry of its order parameter can be detected in neutron-diffraction experiments. The SC order parameter does not correspond to the expectation value of any classical observable. Therefore, its experimental detection is more difficult. Many experimental techniques offer information about physical properties obtained by averaging the SC gap function (Δ_k) over the whole FS (e.g. measurements of the specific heat), therefore, their interpretation is not always complete. In the case of conventional SC, characterized by a constant gap function ($\Delta_k = \Delta_0 = \text{const.}$ for any k), conventional techniques, like specific heat, are precisely determining the symmetry of the order parameter [Thalmeier 2005a]. For unconventional SCs with momentum-dependent gap functions ($\Delta_k \neq \text{const.}$, depending on k), for the precise determination of the positions of gap zeros, field-angle resolved measurement of specific heat and thermal conductivity in the SC state are appropriate to elucidate the symmetry of

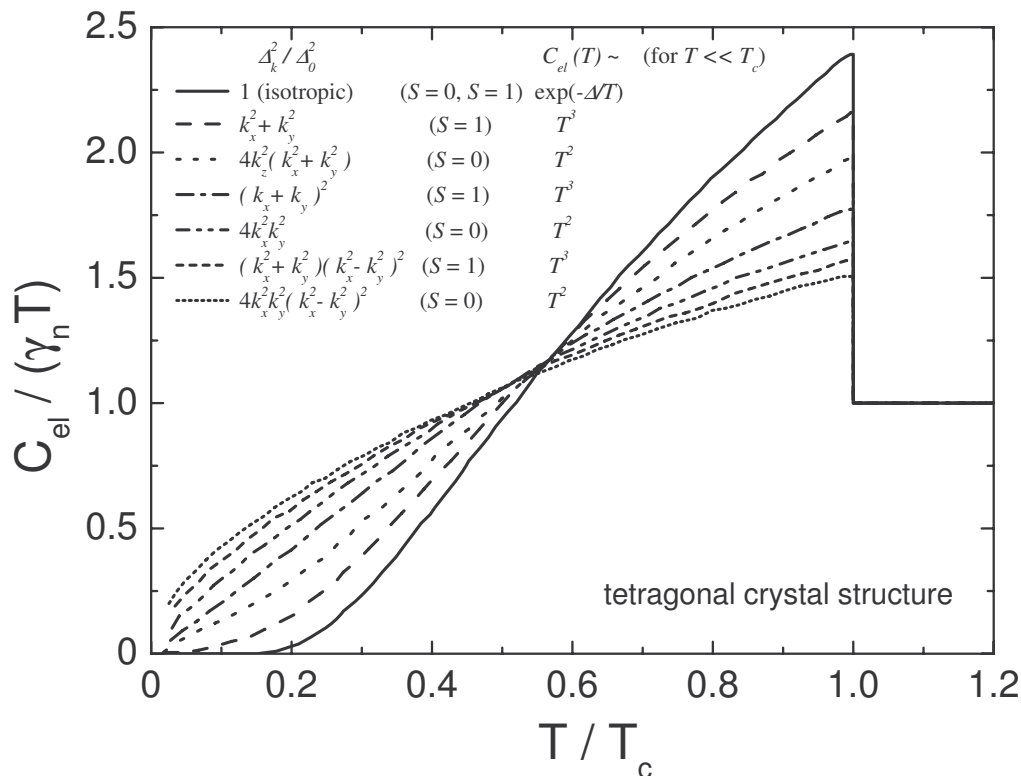


Figure 4.12: Calculated specific heat for all allowed SC gap symmetries in a system with tetragonal crystal structure. A single spherical FS was assumed for the calculations. The symmetry type of the SC gap function (given by Δ_k^2/Δ_0^2), the parity of the SC state (singlet - $S = 0$ or triplet - $S = 1$) and the expected power-law (respectively exponential) behavior of the electronic specific heat, $C_{el}(T)$, for temperatures $T \ll T_c$, are shown in the figure. The curves are taken from the work of Hasselbach *et al.* [Hasselbach 1993]. For their calculations, the SC gap symmetries presented in [Volovik 1985] were considered.

the order parameter. Several theoretical estimations, based on the BCS theory, were performed in order to model the temperature dependence of the SC gap function and of the electronic specific heat in the SC state for different possible symmetries of the SC order parameter (e.g. [Tachiki 1985, Volovik 1985, Hasselbach 1993]). It was proposed that in the case of triplet SC the type of zeros in the energy gap always correspond to points on the FS, whereas lines of zeros are possible in singlet pairing [Volovik 1985]. The heat capacity at low temperatures ($T \ll T_c$ - in order to have a nearly temperature-invariant gap function) $C_{el}(T) \propto T^2$ for gap functions having zeros on lines on the FS (singlet pairing) and $C_{el}(T) \propto T^3$ for gap functions having zeros on points on the FS (triplet pairing) [Volovik 1985]. In figure 4.12 the

calculated specific heat for all SC gap symmetries allowed to appear in a tetragonal crystal structure are shown [Hasselbach 1993]. The allowed SC gap symmetries presented in the work of Volovik and Gor'kov [Volovik 1985] have been considered in calculating the temperature dependence of the specific heat. A single spherical FS has been assumed when estimating the specific heat [Hasselbach 1993]. We will later use the above-calculated specific heat in order to try to estimate the possible order parameter symmetry for the broad SC region in CeCu_2Si_2 . The discrepancy between the spherical FS assumed to calculate the $C_{el}(T)$ presented in figure 4.12 and the more complex FS known for CeCu_2Si_2 has to be kept in mind.

In the following part we will focus on analyzing our experimental data at ambient pressure, as well as under finite pressure, on A/S -type CeCu_2Si_2 . This will offer us the possibility to extract information about the interplay of AFM and SC, as well as about the possible order parameter in the SC state and its evolution in the low-pressure range.

A/S -type CeCu_2Si_2 at ambient pressure

Ambient-pressure resistivity, a.c. susceptibility and electronic specific heat of our A/S -type CeCu_2Si_2 are shown in figure 4.13. The specific-heat and a.c.-susceptibility data are measured in the pressure cell, while resistivity data are taken on a small sample prepared from the same batch as the sample used for measurements in the pressure cell. Transition temperatures obtained from the different measurement techniques are marked by arrows. The inset shows the normalized resistivity at ambient pressure measured up to room temperature. Two consecutive maxima are visible in the high-temperature resistivity, at T^* and at T_{CEF} . The maximum at $T^* \approx 20$ K represents the onset of the coherent scattering of the conduction electrons due to the periodic Kondo lattice formed by the $4f$ electrons, while that at $T_{CEF} \approx 100$ K originates from the interplay of Kondo scattering and crystalline-electric-field (CEF) excitations. It should be noted that the current direction in the resistivity measurement is not known. However, when the current is applied in the (ab) plane or perpendicular to it, the high-temperature resistivity curves show quite a large anisotropy, increasing with decreasing temperature from T_{CEF} to T^* , both maxima being more pronounced in the case of $I \parallel (ab)$ [Holmes 2004a]. Furthermore, this anisotropy vanishes with increasing pressure at the same pressure where the two maxima merge, the QP-QP correlations become weak and the valence change is supposed to take place [Holmes 2004a].

Upon decreasing the temperature below $T = 1$ K, the A/S -type single crystal undergoes two consecutive phase transitions at ambient pressure, a first one at the

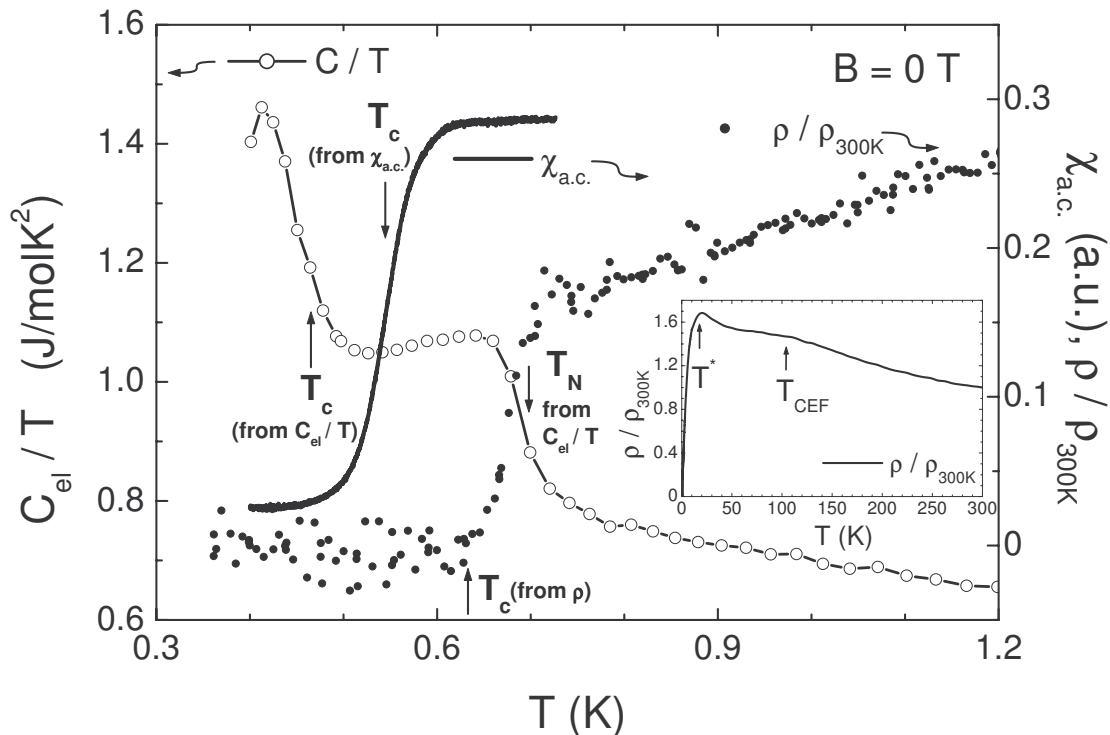


Figure 4.13: Low-temperature ambient-pressure properties of A/S -type single-crystalline $CeCu_2Si_2$ as $C_{el}(T)/T$, $\chi_{a.c.}(T)$ and $\rho(T)$ versus T are presented. Specific-heat and a.c.-susceptibility data were measured in the pressure cell, while resistivity data are taken in the PPMS on a small sample cut from a larger piece prepared from the same batch as the sample measured in the pressure cell. The inset shows the normalized resistivity up to $T = 300$ K. Arrows indicate the transition temperatures obtained from the different types of measurements.

Néel temperature, $T_N \approx 0.69$ K, to an IC AFM SDW type of order and a second one at a slightly lower temperature, marking the onset of SC at $T_c \approx 0.46$ K. The resistivity data shown in figure 4.13 are not accurate enough to resolve the transition to the AFM state due to its closeness to the SC transition, but the transition to the SC state is clearly determined at $T_c \approx 0.63$ K. A residual resistivity of $\rho_0 \approx 10 \mu\Omega\text{cm}$ has been obtained. A.c.-susceptibility data, similar to the heat-capacity data, show a quite broad transition into the SC state. The transition temperature, taken as the midpoint of a nearly 180 mK broad phase transition in $\chi_{a.c.}(T)$, $T_c \approx 0.545$ K, is in good agreement with the results from the other measurements. Due to the nearness of the two phase transitions, it is quite difficult to accurately separate them, but the shape and broadness of the phase transitions, both in specific heat and susceptibility, can be used as good measures for a further characterization of the system under pressure. The increased value of the electronic specific-heat coefficient at low temperatures

of $C_{el}/T \approx 0.73$ J/(molK²) taken at $T = 0.9$ K indicates the HF behavior of the system. A Kondo temperature of $T_K \approx 13$ K can be determined by analyzing the entropy of the system in the view of the single-impurity Kondo model which predicts in the case of a spin 1/2 system a total entropy of $S_{imp} = 0.5R \ln 2$ for a temperature $T \approx T_K/2$ [Desgranges 1982]. The obtained value is in fairly good agreement with the characteristic temperature determined from resistivity measurements, $T^* \approx 20$ K. At T_N , the entropy reaches a value of only $S_{el}(T_N) \approx 0.11R \ln 2$, in relatively good agreement with the low ordered magnetic moment of $\mu_{ord} \approx 0.1 \mu_B$ per Ce atom detected by neutron-diffraction experiments [Stockert 2004].

At ambient pressure, the A/S -type CeCu_2Si_2 shows for the case of the phase transition to the AFM ordered state at $B = 0$ T a ratio of $\Delta C/(\gamma T_N)|_{T=T_N} \approx 0.50$. Estimation of the $\Delta C/(\gamma_n T_c)|_{T=T_c}$ ratio in the case of the SC phase transition is more complex. Since the issue of competition or coexistence of the two ordered states, AFM and SC, in CeCu_2Si_2 is not yet completely clarified, for determining the jump height of $C_{el}(T)$ at the SC phase transition, as well as the $\Delta C/(\gamma_n T_c)|_{T=T_c}$ ratio, one has to consider both possibilities. The scenario of coexisting AFM and SC states in A/S -type CeCu_2Si_2 leads at ambient pressure to $\Delta C/(\gamma_n T_c)|_{T=T_c} \approx 0.79$ ($B = 0$ T). In this case, the value obtained by summing up the two ratios for the two phase transitions is $\Delta C/(\gamma T_N)|_{T=T_N} + \Delta C/(\gamma_n T_c)|_{T=T_c} \approx 1.29$. This value is close to that estimated by mean-field (e.g. BCS) theory, of $\Delta C/(\gamma T)|_{T=T_{order}} \approx 1.43$, where participation of the whole FS in the ordered state is considered. Considering the case where the AFM state is completely suppressed from the system at the temperature where the SC state is formed (competing AFM and SC), we obtain at $B = 0$ T $\Delta C/(\gamma_n T_c)|_{T=T_c} \approx 1.08$, a value slightly lower than the value of 1.43 known from mean-field theory. In both scenarios, due to the closeness in temperature of the AFM and SC phase transitions, the estimation of $\Delta C/(\gamma_n T_c)|_{T=T_c}$ for the SC phase transition is not very accurate.

Application of a magnetic field $B \parallel c$ leads to the slow destruction of the AFM phase, to the appearance of the B -phase (at T_B) and to a rapid suppression of the SC state (see figure 4.14). Figure 4.15 shows the $B - T$ phase diagram obtained at ambient pressure ($B \parallel c$). The values are taken from our measurements of specific heat, $C(T, B)$, a.c. susceptibility, $\chi_{a.c.}(T, B)$, and magnetocaloric effect, $T(B)$. The different lines used in the figure serve as guides to the eye. Due to our lowest temperature of $T \approx 0.35$ K which is accessible in high magnetic fields, the onset of the B -phase has been resolved only for $B = 8$ T (see figure 4.14). An estimated critical field of $B_c(0) \approx 4$ T is necessary to completely suppress AFM, while a much lower value of $B_{c2}(0) \approx 1.05$ T is needed to destroy SC in the system. The origin of the second phase line, appearing in the AFM phase and marked with T_{NL} , is not yet

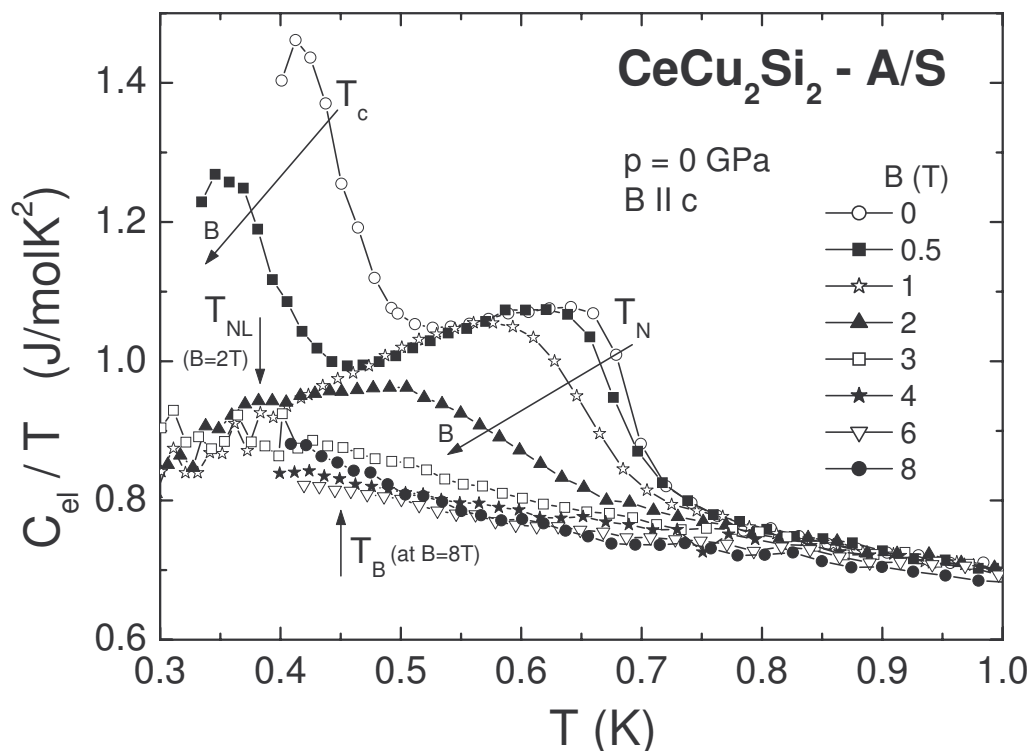


Figure 4.14: Effect of magnetic field on the low-temperature electronic specific heat of A/S -type $CeCu_2Si_2$ at ambient pressure.

clear. The data used to construct this phase line are taken from magnetocaloric measurements while specific-heat measurements do not clearly resolve this anomaly due to the closeness of the phase transition temperatures. In figure 4.14 a tiny anomaly indicated by an arrow at $T_{NL} \approx 0.39$ K can be seen at $B = 2$ T, an anomaly which could be associated to this phase line. However, the real shape and origin of the T_{NL} line in figure 4.15 is not clearly determined by our measurements. One possibility for the origin of this transition could be the first-order phase transition, reported in literature from thermal-expansion, specific-heat and neutron-scattering measurements [Stockert 2004] on an A -type $CeCu_2Si_2$ single crystal, attributed to a transition to a commensurate low-temperature magnetic phase [Stockert 2004] (see also section 4.2). However, this first-order phase transition to a commensurate magnetic phase, observed also in several Ge-doped $CeCu_2(Si_{1-x}Ge_x)_2$ compounds, is already visible at $B = 0$ T and was not detected by neutron-scattering experiments for A/S -type $CeCu_2Si_2$ at $B = 0$ T [Thalmeier 2005b, Stockert 2006]. These suggest that, if the origin of T_{NL} is a transition to the commensurate magnetic state, then the proposed

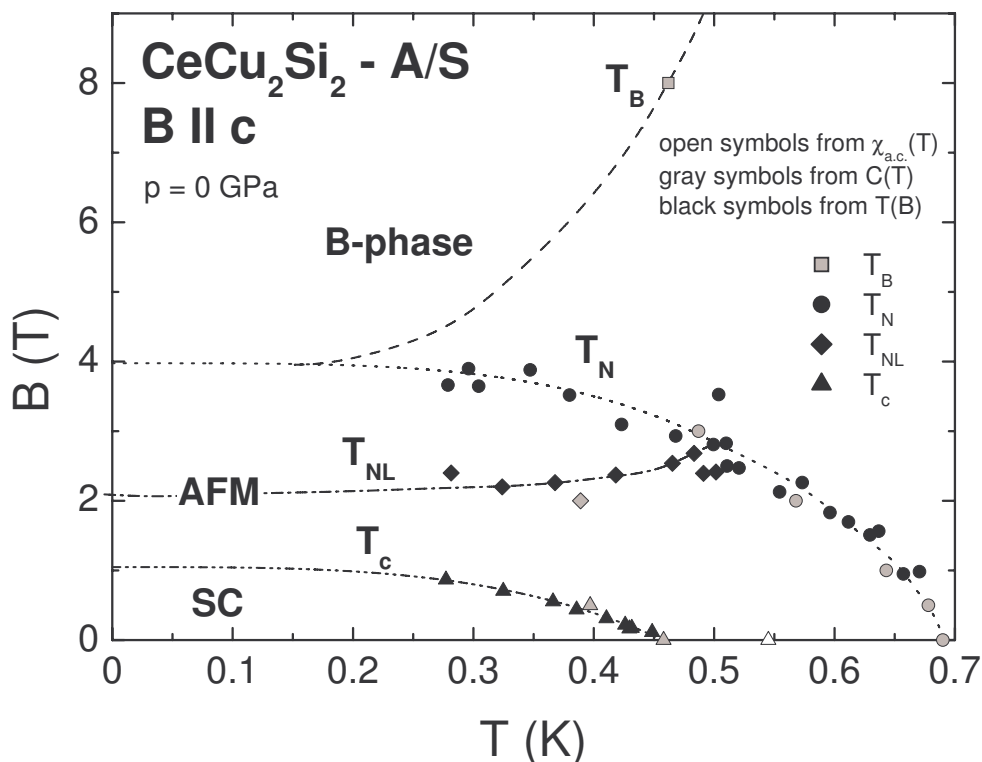


Figure 4.15: $B - T$ phase diagram ($B \parallel c$) of single-crystalline A/S -type $CeCu_2Si_2$ at ambient pressure. The lines are used as guides for the eyes.

shape of the T_{NL} phase line drawn in figure 4.15 needs to be modified. Unfortunately, this T_{NL} line cannot be followed clearly by our measurements at higher pressures due to the narrowing of the temperature range between the transition temperatures into the AFM and SC phases. Low-temperature magnetization measurements on single-crystalline A/S -type $CeCu_2Si_2$ have revealed in the case of $B \parallel c$ an additional phase line within the AFM phase in the ambient-pressure $B - T$ phase diagram [Tayama 2003]. Figure 4.7 shows the corresponding $B - T$ phase diagram obtained by magnetization measurements. For $B \parallel a$ (see figure 4.7a) no such phase line in the AFM phase was reported. This additional phase line was attributed to a first-order phase transition and was observed at temperatures lower than $T \leq 0.2$ K only [Tayama 2003]. For the case of $B \parallel a$, the phase transition from the AFM phase to the B -phase was reported to be of first order at low temperatures, while in the case of $B \parallel c$ the transition from the AFM phase to the B -phase was shown to be of second order and a first-order phase transition of yet unclear origin was detected within the AFM phase [Tayama 2003]. Since for the case of $B \parallel c$ no observation of

this phase transition at $T \geq 0.2$ K was reported [Tayama 2003], the possibility of the same origin for the phase line at T_{NL} obtained by our measurements and the phase line at $T \leq 0.2$ K reported from magnetization measurements should be considered with care. A more detailed analysis of the possible origin of the phase line at T_{NL} will be given in section 4.3.3.

A/S-type $CeCu_2Si_2$ at low pressures

Application of low pressure on the A/S-type $CeCu_2Si_2$ single crystal leads to a rapid shift of the AFM phase transition to lower temperatures, with a slope of $dT_N/dp \approx -1.17$ K/GPa, and to a strong increase of the SC transition temperature ($dT_c/dp \approx 2.33$ K/GPa for $p \leq 0.06$ GPa). A small pressure of about $p \approx 0.06$ GPa is enough to shift the two phase transitions very close to each other to $T_N \approx 0.62$ K and $T_c \approx 0.60$ K. Further increasing pressure leads to a much slower increase of the SC transition temperature. Once T_c becomes larger than T_N the presence of the AFM order cannot be detected anymore, except by application of a magnetic field high enough to suppress SC in the system. Figure 4.16 shows the low-temperature $B = 0$ T electronic specific heat in the pressure range $0 \text{ GPa} \leq p \leq 0.4 \text{ GPa}$. This pressure range was chosen to emphasize the interplay of the two basic phenomena, AFM and SC, in A/S-type $CeCu_2Si_2$. Very small steps in pressure were used in order to follow the rapid changes taking place and to try to solve the controversial question about the coexistence or competition of the two phenomena in this material. Parallel to the specific-heat measurements we have detected the SC transition of $CeCu_2Si_2$ by a.c.-susceptibility measurements. In figure 4.17 the evolution of the SC phase transition, namely of its temperature and of its width, is presented as seen from a.c.-susceptibility measurements. The symbols in the two figures, 4.16 and 4.17, are chosen to be the same for a given value of pressure.

The surprisingly rapid evolution of the physical properties under pressure gives rise to a broad phase transition anomaly in the specific heat at $p \approx 0.06$ GPa, including both phase transitions AFM and SC, with $T_N > T_c$. An additional tiny increase in pressure to $p \approx 0.09$ GPa already leads to the crossing of the two phase lines, $T_c > T_N$. The phase transition anomaly seen in specific heat becomes sharp and represents only the transition to the SC state. For temperatures below $T_c \approx 0.61$ K no further anomaly corresponding to the entrance into the AFM phase can be resolved at this pressure, indicating that AFM is expelled once SC has been established. Application of a magnetic field of $B = 2$ T (see figure 4.18), higher than the critical field needed to suppress SC at this pressure, shows that the system enters the AFM phase at $T_N \approx 0.4$ K. The electronic specific heat displayed in figure 4.18 for $p \approx 0.09$ GPa

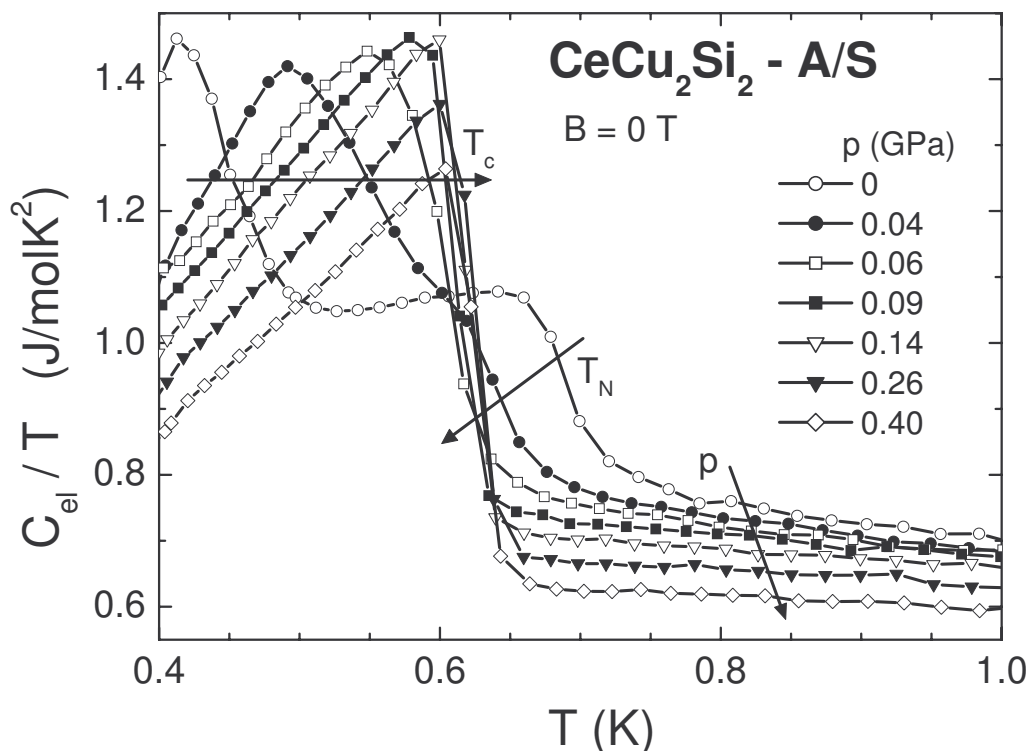


Figure 4.16: Low-temperature electronic specific heat of *A/S*-type CeCu_2Si_2 measured at zero magnetic field and very low pressures, $0 \text{ GPa} \leq p \leq 0.4 \text{ GPa}$.

shows the evolution of the SC phase transition as function of magnetic field. T_c is gradually shifted to lower temperatures upon increasing the magnetic field. The phase transition seen for $B = 2 \text{ T}$ has been identified as a transition to the AFM phase. Since measurements of specific heat solely can only identify the existence of a phase transition without elucidating its origin, we have simultaneously measured the a.c. susceptibility of the system in magnetic field. As seen in the inset of figure 4.18, for $B = 1.5 \text{ T}$ one can easily detect the SC phase transition in the a.c.-susceptibility measurements, but already at $B = 2 \text{ T}$ no indication for a transition to a SC state is visible down to the lowest measured temperature of $T = 0.26 \text{ K}$. Therefore, the phase transition in the $B = 2 \text{ T}$ specific heat occurring at a temperature of $T \approx 0.40 \text{ K}$ is due to the onset of the AFM phase. Moreover, it is becoming clear that while lowering the temperature, once SC is established in the system ($T_c > T_N$) the AFM order is expelled. This is in contrast to the situation existing at lower pressures, when upon cooling first the AFM order appears in the system ($T_N > T_c$) followed by the entrance into the SC state. The reappearance of the AFM order and its gradual suppression to

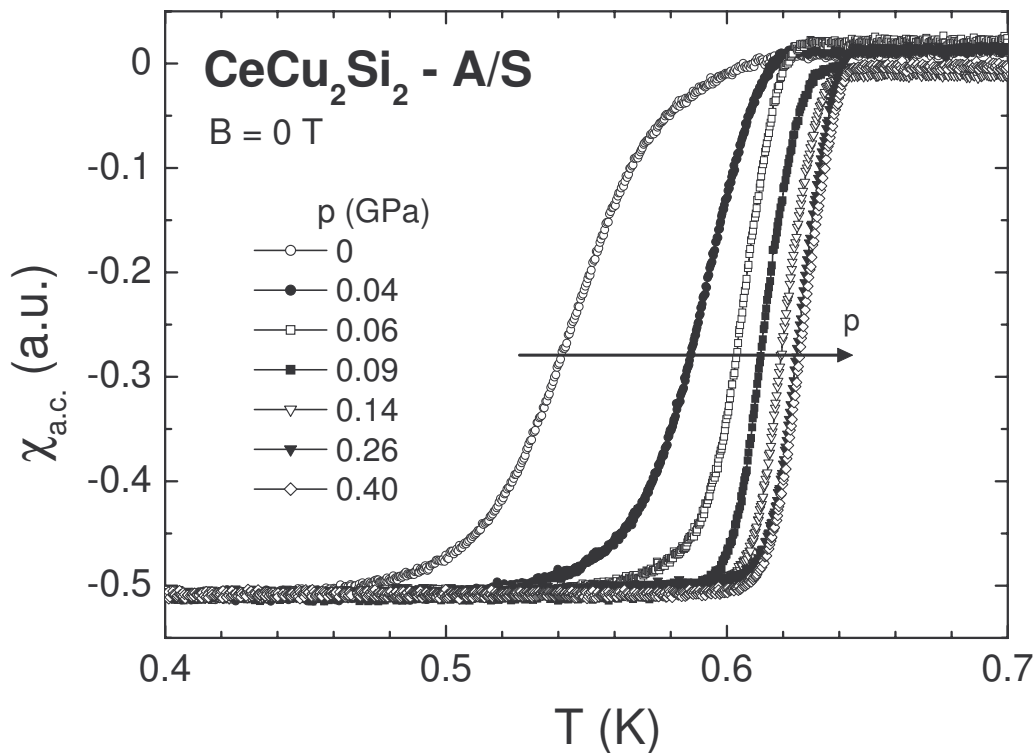


Figure 4.17: Low-temperature a.c. susceptibility of A/S -type CeCu_2Si_2 measured at $B = 0$ T in the pressure range $0 \text{ GPa} \leq p \leq 0.4 \text{ GPa}$. The pressure values, as well as the symbols corresponding to the different pressures, are the same as those used in the case of the specific-heat data shown in figure 4.16.

$T_N = 0$ K once SC is destroyed by a magnetic field lead to the following conclusions: i) AFM is expelled once SC is stabilized ($T_c > T_N$) in CeCu_2Si_2 (for $p \leq p_c$, where p_c represents the critical pressure where at $B = 0$ T the AFM phase transition is suppressed to $T_N = 0$ K); and ii) magnetic-field and pressure-induced QCPs should exist.

Figure 4.19 presents the low-temperature $T - p$ phase diagram obtained by specific-heat and a.c.-susceptibility measurements at $B = 0$ T. By extrapolating the obtained $T_N(p)$ to lower pressures, the $T_N(p)$ and $T_c(p)$ phase lines are expected to meet at the pressure $p_c^* \approx 0.07$ GPa ($T_N(p_c^*) = T_c(p_c^*)$). At $B = 0$ T, the $p < p_c^*$ pressure region is characterized by $T_c < T_N$. Above p_c^* , T_c becomes larger than T_N and T_N is not detectable anymore at zero magnetic field. Due to the proximity in temperature of the AFM and SC phase transitions, the objective interpretation of the specific heat data is difficult. A.c.-susceptibility measurements, detecting only the SC phase transition in this setup, are a good tool to have a closer look inside the

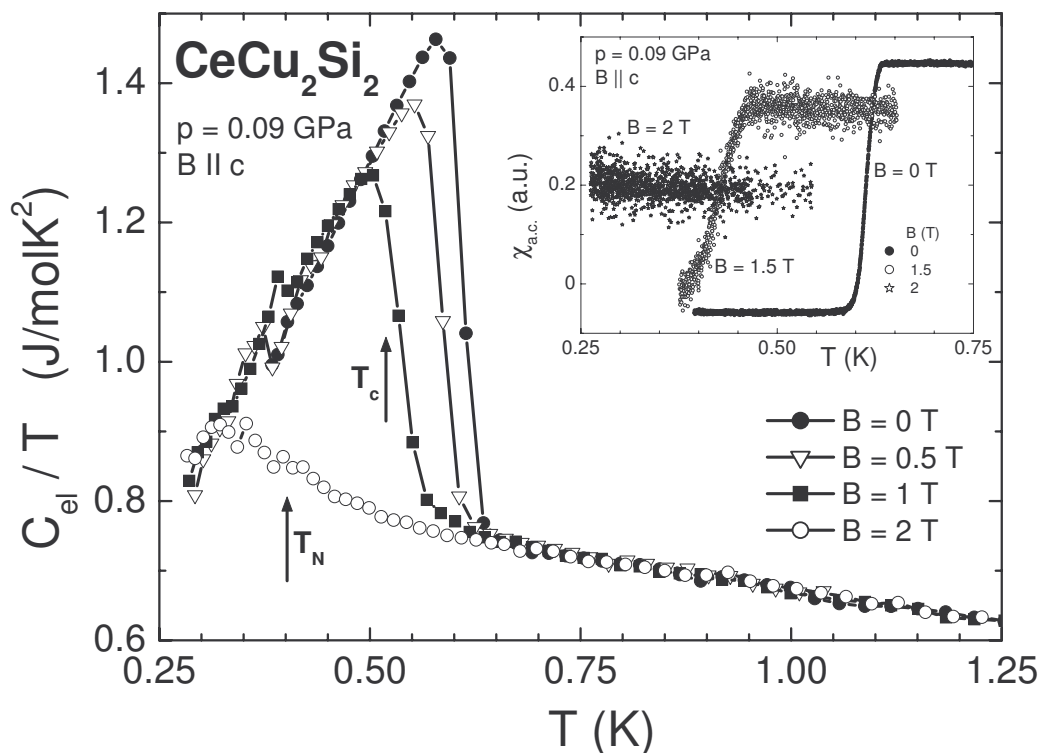


Figure 4.18: Low-temperature specific heat of CeCu_2Si_2 at $p \approx 0.09$ GPa in different magnetic fields, $B = (0, 0.5, 1, 2)$ T. The evolution of the SC transition temperature in magnetic field, $B = (0, 1.5, 2)$ T, measured by a.c. susceptibility is shown in the inset. $\chi_{a.c.}(T)$ at $B = 2$ T does not show any transition to a SC state down to $T \approx 0.26$ K, suggesting that the transition seen in $C_{el}(T)/T$ at $B = 2$ T corresponds to a transition to the AFM ordered state.

measured physical phenomena. In figure 4.19 the width of the SC phase transition, possible to be detected by the a.c susceptibility measurements only, is shown by the error bars. T_c (from $\chi_{a.c.}(T)$) is taken at the midpoint of the phase transition anomaly, while the error bars are constructed as the distance from T_c to the onset (T_c^+) and to the full transition (T_c^-), respectively. It is seen that the width of the phase transition is very large in the low-pressure range (e.g. $\Delta T \approx 180$ mK at $p = 0$ GPa) where AFM is present above T_c and is gradually decreasing upon increasing the pressure until the pressure where at $B = 0$ T AFM is not detected anymore ($p \approx p_c^*$). With further increasing the pressure (above p_c^*) the transition width stays more or less constant at a strongly reduced value of about $\Delta T \approx 50$ mK (see also figure 4.17). The broadening of the SC phase transition seems to be intrinsic to the studied system and cannot be attributed to any pressure inhomogeneity in the setup, due to the fact

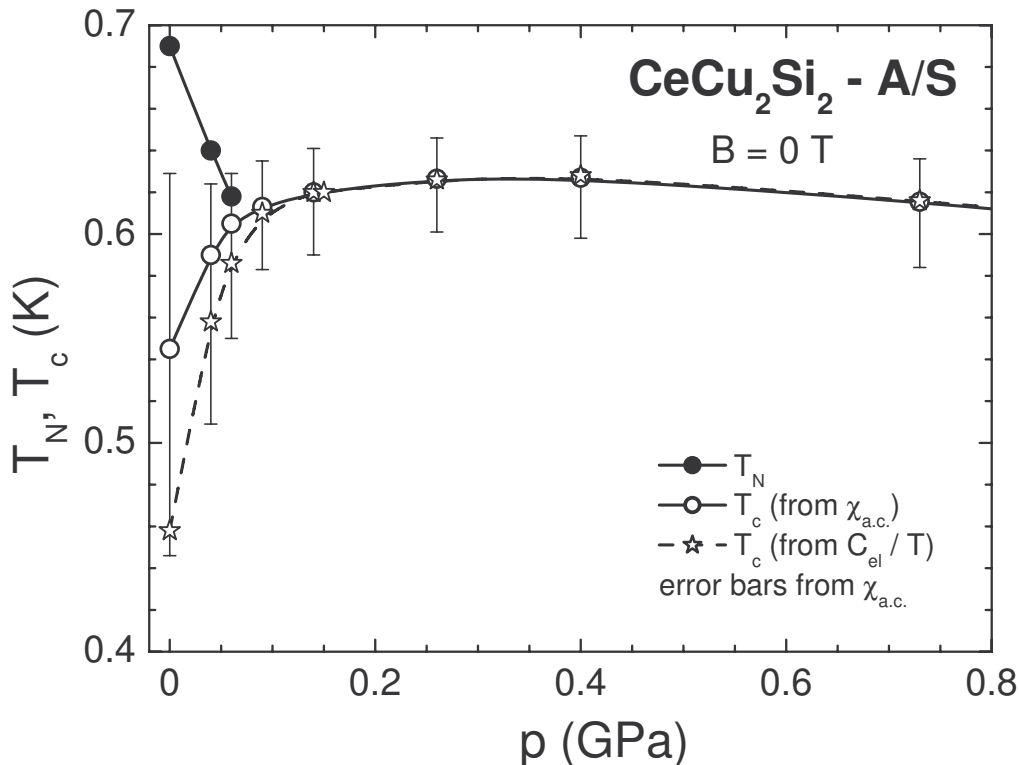


Figure 4.19: Low-pressure $T - p$ phase diagram of A/S -type $CeCu_2Si_2$ at $B = 0$ T. AFM and SC transition temperatures (T_N, T_c) obtained from specific heat ($C_{el}(T)/T$) and T_c obtained from a.c.-susceptibility ($\chi_{a.c.}(T)$) measurements are presented. The error bars shown for T_c determined from $\chi_{a.c.}(T)$ are obtained as the distance from the onset, at T_c^+ , respectively from the full transition, at T_c^- , to the midpoint of the transition at T_c .

that it is largest at ambient pressure and is decreasing upon increasing pressure. In the pressure region where the AFM transition precedes SC upon cooling, T_c taken from specific-heat measurements is always lower than that detected by $\chi_{a.c.}(T)$. In this pressure range, due to the closeness of the two phase transitions the entropy-balance technique used to determine the transition temperatures from $C_{el}(T)/T$ is not very accurate. However, once the AFM order is expelled by SC the accuracy in determining T_c is very good, the SC transition being very sharp up to the highest pressure achieved in our experiment. As a particular feature of the interplay of AFM and SC in A/S -type $CeCu_2Si_2$ one can mention that at $B = 0$ T the presence of the AFM order in the system leads to the broadening of the SC phase transition, the broadest SC transition being observed at ambient pressure. Once AFM is expelled at $B = 0$ T by increasing pressure ($T_N < T_c$) the SC phase in the system becomes

more stable, the SC phase transition anomaly showing no additional broadening over the entire measured pressure range, suggesting that the broadening of the SC phase transition in A/S -type CeCu_2Si_2 is due to the presence of the AFM order. Similar results have been reported for the pressure-induced SC state of CeRhIn_5 [Hegger 2000, Kawasaki 2003, Knebel 2004]. A broad phase transition from the AFM to the SC state in the pressure region $p \leq p_c^*$ where both AFM and SC are observable at $B = 0$ T has been detected by a.c.-susceptibility [Kawasaki 2003, Knebel 2004] and by electrical-resistivity [Hegger 2000] measurements. The broad phase transition in the low-pressure SC state, in the vicinity of the AFM order, is replaced by a narrower SC phase transition in the pressure region $p > p_c^*$ [Hegger 2000, Kawasaki 2003, Knebel 2004]. Moreover, like in the case of our results on A/S -type CeCu_2Si_2 , the same type of evolution of the SC transition temperature depending on the type of the measurements has been observed in CeRhIn_5 . For A/S -type CeCu_2Si_2 we do not observe any significant difference between T_c obtained from $C_{el}(T)/T$ or $\chi_{a.c.}(T)$ measurements at pressures $p > p_c^*$. On the other hand, at $p \leq p_c^*$, $T_c(\text{from } \chi_{a.c.}) > T_c(\text{from } C_{el}/T)$ and the difference between the two values for T_c is gradually decreasing with increasing pressure (see figure 4.19). A similar behavior has been reported for CeRhIn_5 under pressure [Knebel 2006], further suggesting a similarity of the interplay between AFM and SC in these two compounds.

Concerning the interplay of AFM and SC in CeCu_2Si_2 , the $\Delta C/(\gamma T)|_{T=T_c, T_N}$ ratio is an interesting quantity. As described in more detail in the case of the results obtained on A/S -type CeCu_2Si_2 at ambient pressure, the accuracy in estimating $\Delta C/(\gamma T)|_{T=T_c, T_N}$ is strongly reduced by the narrow distance in temperature between the AFM and SC phase transitions. However, for the AFM phase transition $\Delta C/(\gamma T_N)|_{T=T_N}$ can be more precisely determined, while for the case of the SC phase transition the value of $\Delta C/(\gamma T_c)|_{T=T_c}$ is much stronger affected by the narrowing of the distance between T_N and T_c . Application of pressure is therefore even leading to the increase of the errors in determining the $\Delta C/(\gamma T)|_{T=T_c, T_N}$ ratios. Moreover, the coexistence or competition of the two ordered states, AFM and SC, also has to be considered for the SC phase transition when estimating $\Delta C/(\gamma T_c)|_{T=T_c}$. In a similar manner as described earlier for the $p = 0$ GPa data on A/S -type CeCu_2Si_2 , the values of $\Delta C/(\gamma T)|_{T=T_c, T_N}$ have been determined also for pressures $p < p_c^*$ where AFM and SC are both detectable by specific-heat measurements at $B = 0$ T ($p \approx 0.04$ GPa and $p \approx 0.06$ GPa). Table 4.1 contains the values of $\Delta C/(\gamma T_N)|_{T=T_N}$ and $\Delta C/(\gamma T_c)|_{T=T_c}$ obtained at $B = 0$ T on A/S -type CeCu_2Si_2 for pressures $p = 0$ GPa, $p \approx 0.04$ GPa and $p \approx 0.06$ GPa, respectively. The $\Delta C/(\gamma T_c)|_{T=T_c}$ values shown in the third column are obtained by considering the coexistence of the AFM and SC states down to

lowest temperatures, while the values shown in the fourth column were estimated by considering that at T_c the AFM order is completely replaced by SC (competition). Either by looking to the sum of $\Delta C/(\gamma T_N)|_{T=T_N} + \Delta C/(\gamma_n T_c)|_{T=T_c}$ (where the value of $\Delta C/(\gamma_n T_c)|_{T=T_c}$ is taken for the scenario of coexisting AFM and SC states) or separately to each value of the $\Delta C/(\gamma T)|_{T=T_c, T_N}$ ratios, one can observe that independent of the pressure the obtained values are smaller than that obtained by mean-field (e.g. BCS) theory, $\Delta C/(\gamma T)|_{T=T_{order}} \approx 1.43$. In the case of the phase transition from the paramagnetic to the AFM ordered state, the value of $\Delta C/(\gamma T_N)|_{T=T_N} \approx 0.50$ obtained at $p = 0$ GPa is slightly decreasing upon increasing pressure up to $p \approx 0.06$ GPa. At higher pressures a phase transition to the AFM ordered state cannot be detected anymore at $B = 0$ T. Assuming that different parts of the FS are implied either in the AFM or in the SC state and that therefore the two states coexist down to the lowest temperatures, the mentioned sum of $\Delta C/(\gamma T_N)|_{T=T_N} + \Delta C/(\gamma_n T_c)|_{T=T_c}$ indeed shows, for $p \leq 0.06$ GPa, values close to the theoretical value of 1.43. In this case, the ratio between $\Delta C/(\gamma T_N)|_{T=T_N}$ and $\Delta C/(\gamma T_N)|_{T=T_N} + \Delta C/(\gamma_n T_c)|_{T=T_c}$, which could be considered as an estimate for the percentage of the FS implied in the formation of the AFM state, is gradually decreasing with increasing pressure, from about 0.39 at ambient pressure to about 0.36 at $p \approx 0.06$ GPa. Though slightly lower than the values of $\Delta C/(\gamma T_N)|_{T=T_N} + \Delta C/(\gamma_n T_c)|_{T=T_c}$ considered for the case where the AFM and SC states are supposed to coexist, the values of $\Delta C/(\gamma_n T_c)|_{T=T_c}$ estimated for the competing AFM and SC orders (assuming that the AFM state is destroyed at the temperature where the SC state is formed, leading to the fact that only the SC state survives below T_c) are also comparable to the theoretical value of 1.43. Based on these results and also by considering the relatively large errors in obtaining all these values, it is difficult to decide in favor of either of the scenarios of coexisting or competing AFM and SC orders in $CeCu_2Si_2$. Concerning the SC state at $p > p_c^*$, an analysis of the $\Delta C/(\gamma_n T_c)|_{T=T_c}$ ratio obtained up to the highest pressure of our experiment, $p \approx 2.03$ GPa, will be done later.

The overall interplay of magnetic order and SC in A/S -type $CeCu_2Si_2$ is shown in the four panels of figure 4.20. The pressure is increasing gradually in small steps from the top to the bottom panel ($p = (0, 0.04, 0.06, 0.09)$ GPa). Pressure and magnetic field have a similar effect of destroying the AFM order. In the case of SC pressure is stabilizing the SC state, while magnetic field is destroying it. AFM order is strongly suppressed by the application of pressure, while in contrast to SC it is relatively robust against application of magnetic field. T_N and T_c for $B = 0$ T are indicated in the figure by arrows. Where the two phase transitions are very close to each other in temperature, making their separation in $C(T)/T$ difficult, the $\chi_{a.c.}(T)$ data were

p (GPa)	$\Delta C/(\gamma T_N) _{T=T_N}$	$\Delta C/(\gamma_n T_c) _{T=T_c}$ (AFM and SC coexisting)	$\Delta C/(\gamma_n T_c) _{T=T_c}$ (AFM and SC competing)
0	0.50	0.79	1.08
≈ 0.04	0.45	0.77	1.25
≈ 0.06	0.47	0.83	1.12

Table 4.1: $\Delta C/(\gamma T_N)|_{T=T_N}$ and $\Delta C/(\gamma_n T_c)|_{T=T_c}$ obtained for A/S -type CeCu_2Si_2 at $B = 0$ T. The different pressure values are indicated in the first column. In order to determine $\Delta C/(\gamma_n T_c)|_{T=T_c}$, coexistence (third column), respectively competition (fourth column), of the AFM and SC states were considered.

used for a more precise determination of the relative position of the phase transitions.

The effect of magnetic field ($B \parallel c$) on the low-pressure $T - p$ phase diagram of A/S -type CeCu_2Si_2 is presented in figure 4.21. The AFM phase is detectable in the system only when, for certain values of p and B , T_N is larger than T_c . For the pressure values ($p > p_c^*$) where AFM order does not appear at $B = 0$ T above T_c , the detection of the AFM phase is only possible in magnetic fields high enough to suppress SC. In figure 4.21 it is emphasized that for a certain value of B the measured $T_N(p)$ phase line never crosses the $T_c(p)$ phase line. The spin-fluctuation theory predicts that T_N vanishes near the critical pressure p_c as $T_N(p) \propto |p - p_c|^\gamma$ with $\gamma = 2/3$ for a 3D itinerant AFM [Millis 1993] (see details in section 1.2.2). In order to estimate the critical pressure p_c where T_N is suppressed to $T_N = 0$ K, we have fitted our data of $T_N(p)$ at $B = 0$ T with the theoretically expected dependence for an itinerant 3D AFM, of $T_N(p) \propto |p - p_c|^{2/3}$. A critical pressure of $p_c(B = 0 \text{ T}) \approx 0.39$ GPa was obtained. The extrapolation of the fit to low temperatures is shown by a dashed line in figure 4.21. The same procedure has been used for the $T_N(p)$ data at different values of the applied magnetic field ($B = (0.5, 1, 2)$ T). The obtained values of the critical pressure, p_c , for each value of B are indicated in figure 4.21. The dashed lines, corresponding to the $T_N(p)$ curves obtained for various values of B , are extrapolations of the corresponding fits. Remarkable is that at $B = 0$ T, the obtained value of $p_c(B = 0 \text{ T}) \approx 0.39$ GPa coincides with the pressure where $T_c(p)$ obtained for $B = 0$ T is reaching its maximum value of $T_c \approx 0.628$ K, a result in good agreement with the predictions of the theory of AFM spin-fluctuation mediated SC [Millis 1993, Nakamura 1996, Lonzarich 1997, Mathur 1998, Monthoux 1999] (for details see section 1.2.2). As mentioned earlier, the evolution of T_c under pressure and in magnetic field ($B \parallel c$) is also presented in figure 4.21. The relatively low values of T_c at $B = 2$ T are not very precisely detected due to the fact that the transitions seen in the specific-heat data and a.c.-susceptibility measurements are not complete at

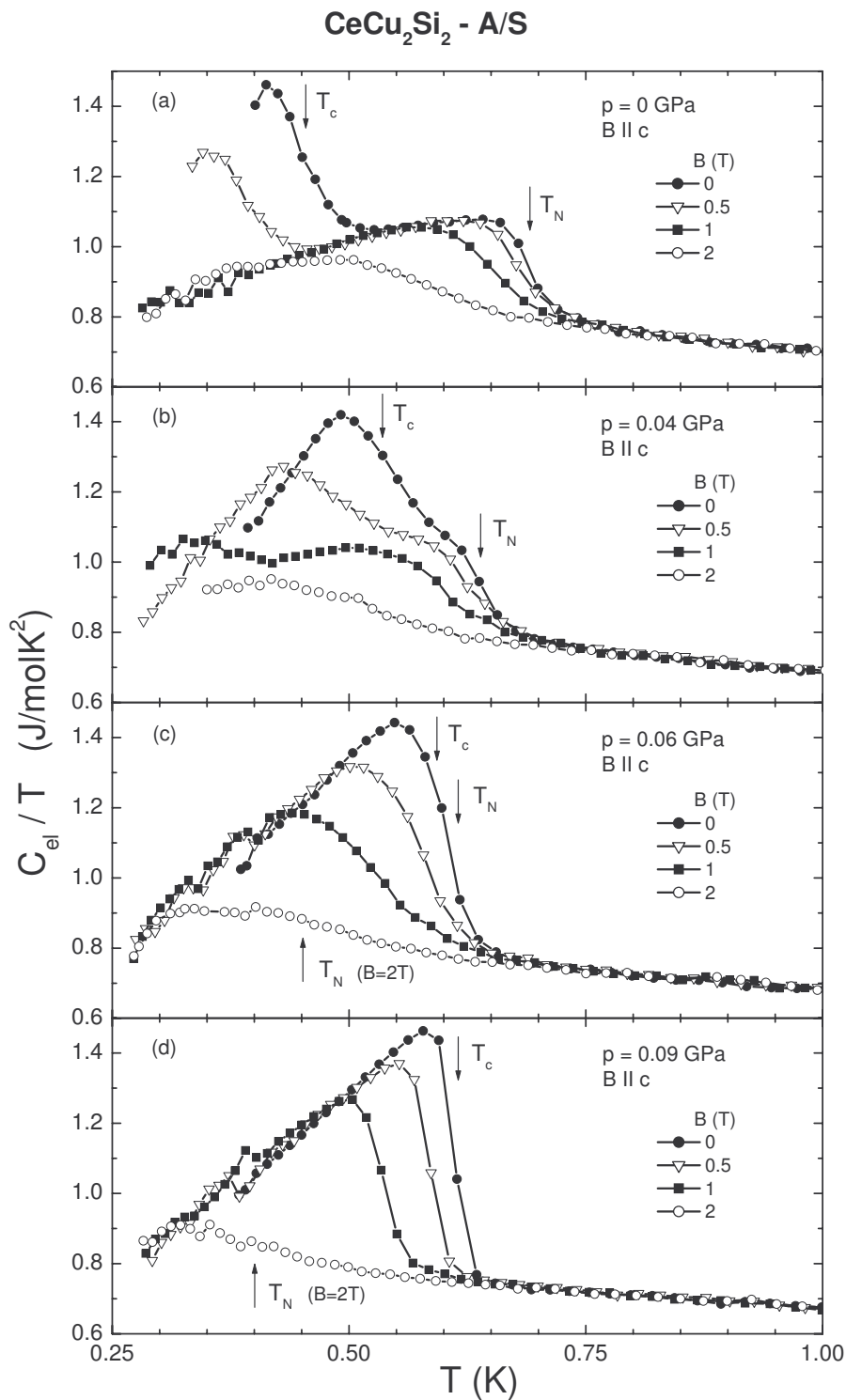


Figure 4.20: $C_{el}(T)/T$ versus T of A/S-type $CeCu_2Si_2$ in low magnetic fields, $B = (0, 0.5, 1, 2)$ T ($B \parallel c$), and at four different pressures. The pressure values are increasing from the top to the bottom panel, as indicated in the figure. The evolution of T_N and T_c as function of magnetic field and pressure can be followed.

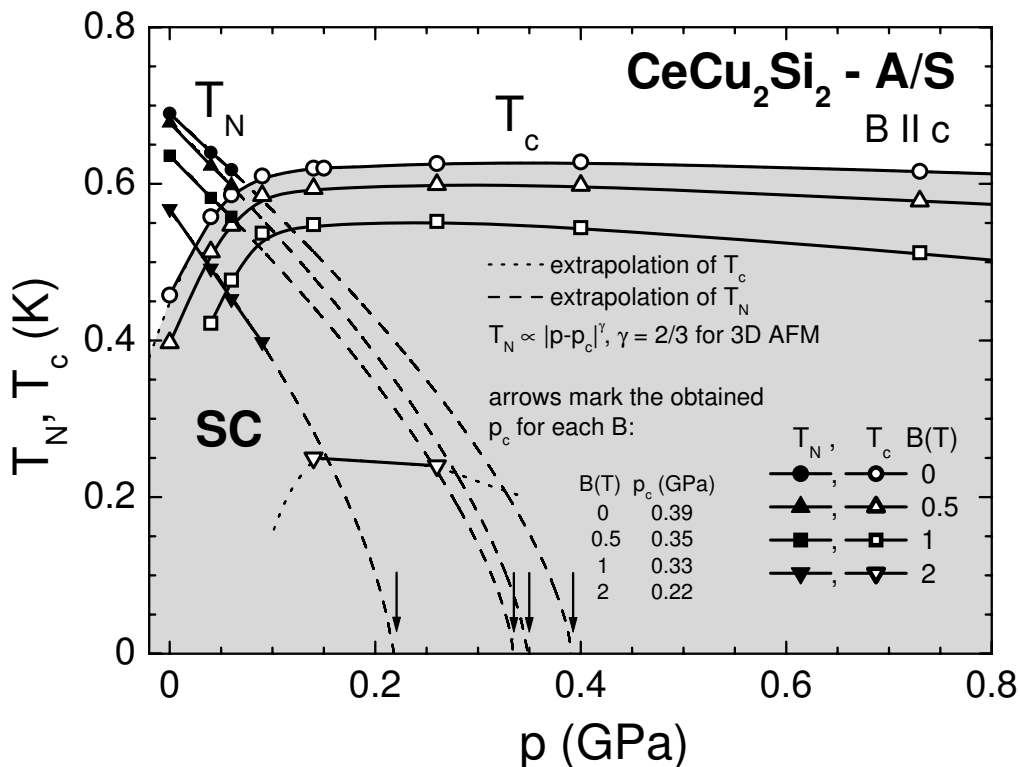


Figure 4.21: Effect of magnetic field ($B \parallel c$) on the low-pressure $T - p$ phase diagram of A/S -type CeCu_2Si_2 . Full symbols are used to represent T_N , while open symbols mark T_c . The values of B and the corresponding symbol types are shown in the figure. Dotted lines are used to extrapolate T_c and they are only serving as guiding lines. For each value of B , the dashed line is constructed by extrapolating the curve obtained by fitting the existing $T_N(p)$ data by using $T_N(p) \propto |p - p_c|^{2/3}$, with p_c as fitting parameter. The values of p_c corresponding to each B are indicated in the figure (see arrows and the table containing $p_c(B)$).

the lowest accessible temperature of $T = 0.26$ K. In a.c.-susceptibility measurements performed at $B = 2$ T, the onset of the SC transition is clearly detectable only for two pressure values, $p \approx 0.14$ GPa and $p \approx 0.26$ GPa, proving the SC origin of the phase transition seen in the $C(T)/T$ measurements. For values of $p \leq 0.09$ GPa and $p \geq 0.4$ GPa, no transition to the SC state (for $T \geq 0.26$ K) could be observed by $\chi_{a.c.}(T)$ measurements at $B = 2$ T (see for example $p \approx 0.09$ GPa shown in figure 4.18, where the anomaly seen in $C(T)/T$ at low temperatures at $B = 2$ T does not correspond to the formation of a SC state but is due to the entrance to the AFM ordered state). The dotted line used to extrapolate the $T_c(p)$ curve for $B = 2$ T is not obtained experimentally and serves only as guide to the eyes. Similar to the case

of $B = 0$ T, the maximum value of $T_c(p)$ for $B = 2$ T is expected in the pressure interval $0.14 \text{ GPa} \leq p \leq 0.26 \text{ GPa}$, in the vicinity of the critical pressure obtained for $B = 2$ T of $p_c(B = 2 \text{ T}) \approx 0.22 \text{ GPa}$. A similar finding, that the value of p_c obtained (by fitting the experimental data with $T_N(p) \propto |p - p_c|^{2/3}$) for a certain value of B is situated in the pressure region where the experimentally obtained $T_c(p)$ for the corresponding B is reaching its maximum value, holds also for the case of $B = 0.5$ T and $B = 1$ T. Therefore, it seems that the afore-mentioned prediction of the theory of AFM spin-fluctuation mediated SC made for the case of $B = 0$ T [Millis 1993, Nakamura 1996, Lonzarich 1997, Mathur 1998, Monthoux 1999] is valid also for the case when a magnetic field $B \neq 0$ T (in our case $B \parallel c$) is applied to the system. These results also hint at a strong connection between the mechanisms leading to the formation of both ordered phases in $CeCu_2Si_2$, AFM and SC. A similar study for the case of $B \parallel (ab)$ could help to shed more light onto the relation between AFM and SC in $CeCu_2Si_2$ and the mechanism inducing the unconventional SC state in $CeCu_2Si_2$.

By assuming the same $B_{c2}(T)$ dependence (see equation 4.2) for the whole pressure range, the maximum value of the upper critical field, $B_{c2}(0)$, seems to be obtained at $p \in [0.14, 0.26]$ GPa. With further increasing pressure, $B_{c2}(0)$ seems to decrease. A more detailed analysis of the pressure dependence of the effect the magnetic field has on SC in $CeCu_2Si_2$ will be presented later.

The low-pressure ($0 \text{ GPa} \leq p \leq 0.09 \text{ GPa}$) $B - T$ phase diagram ($B \parallel c$) illustrating the interplay between magnetism and SC in A/S -type $CeCu_2Si_2$ is shown in figure 4.22. The AFM phase transition is detected by specific-heat measurements, while the SC transition temperatures are taken from specific-heat ($C(T, B)$), a.c. susceptibility ($\chi_{a.c.}(T, B)$) and adiabatic temperature versus magnetic field scans ($T(B)$). In order to estimate the $T \rightarrow 0$ K values of the critical field for the AFM ordered state, $B_c(0)$, and of the upper critical field for SC, $B_{c2}(0)$, we have fitted the experimentally determined $T_N(B)$ and $T_c(B)$ curves for each pressure value.

$$B_c(T) = B_c(0) \left[1 - \left(\frac{T}{T_N} \right)^n \right] \quad (4.1)$$

for AFM order and

$$B_{c2}(T) = B_{c2}(0) \left[1 - \left(\frac{T}{T_c} \right)^n \right] \quad (4.2)$$

for SC were used as fitting functions. As free fitting parameters $B_c(0)$ ($B_{c2}(0)$) and n for the AFM (SC) transition were chosen, while for T_N and T_c the values obtained from specific-heat measurements at $B = 0$ T were used as fixed values. In the case of SC, the continuous lines shown in figure 4.22 represent the obtained fits. For

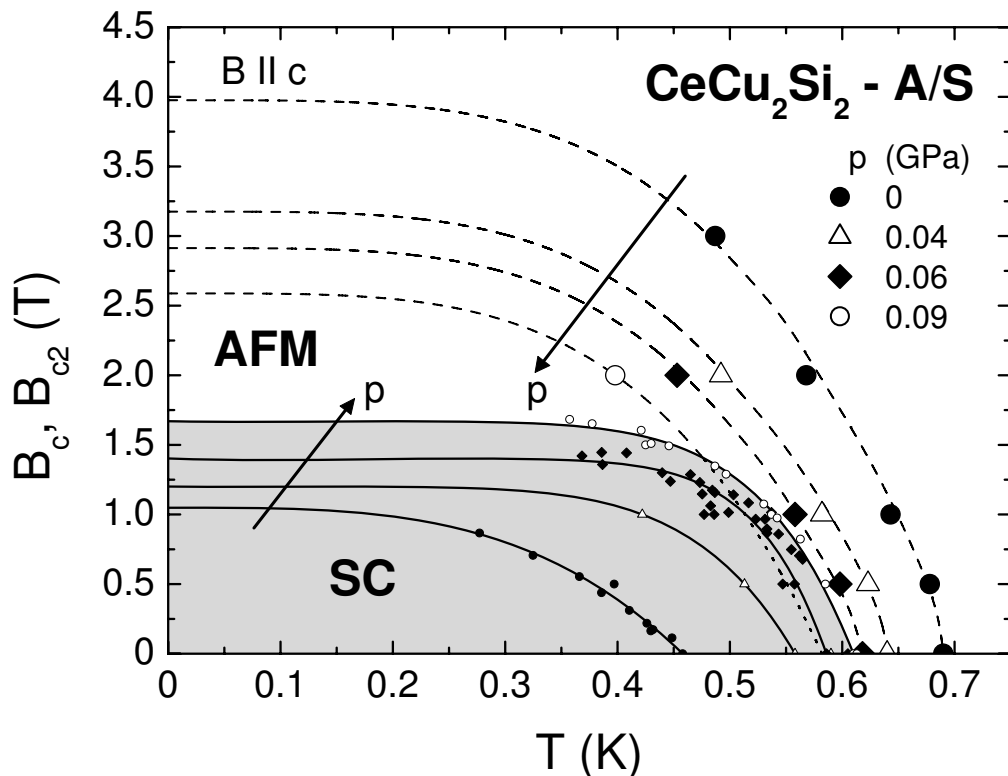


Figure 4.22: Low-pressure, $0 \text{ GPa} \leq p \leq 0.09 \text{ GPa}$, $B - T$ phase diagram ($B \parallel c$) of A/S -type CeCu_2Si_2 . For the SC state, continuous lines are corresponding to the fits done to the obtained $B_{c2}(T)$ data, according to equation 4.2. In the case of the transition to the AFM ordered state, the dashed lines in the high-temperature region, where the data points are shown, are guides for the eyes. The corresponding dashed lines in the low-temperature region, where no experimental data are available, were obtained by extrapolating the fits done to the $B_c(T)$ data by using equation 4.1 to low temperatures. The dotted line in the SC phase, not detectable experimentally due to the suppression of AFM by SC, corresponds to the extension of the fit obtained for $B_c(T)$ for $p \approx 0.09 \text{ GPa}$ (see text for details). The arrows indicate the direction of increasing pressure.

the AFM state, the dashed lines used to describe the low-temperature dependencies of B_c , in the region where no experimental data for $B_c(T)$ are available, were constructed by extrapolating the fits obtained on the existing data by using equation 4.1. However, the obtained fits underestimate the initial slope of $B_c(T)$ (at T_N). Therefore, the dashed lines shown on the high-temperature side of the phase diagram depicted in figure 4.22, where experimental data for $B_c(T)$ exist, are just drawn to guide the eyes. Due to the low number of data points, the fits used for $B_c(T)$ are considered only as guidance for the critical field curves. However, for ambient

pressure more data exist also from magnetocaloric measurements, $T(B)$ (see figure 4.15), and the obtained fit, together with the obtained $B_c(0)|_{p=0\text{GPa}} \approx 4$ T, is in very good agreement with other experimental results (cf. the results of magnetization measurements shown in figure 4.7b). The fits obtained for the data shown in figure 4.22 for $B_c(T)$ for the next three pressures ($p \approx (0.04, 0.06, 0.09)$ GPa) are taken by using only one free fitting parameter, namely $B_c(0)$, and fixing the exponent n to the value obtained for the ambient-pressure data. As also indicated by the arrows in figure 4.22, AFM is gradually suppressed with increasing pressure, while SC is stabilized. Application of magnetic field causes a relatively moderate suppression of the AFM phase transition, leading to an estimate of the critical field at $p = 0$ GPa of $B_c(0)|_{p=0\text{GPa}} \approx 4$ T. This critical field is gradually decreasing upon increasing pressure, leading to $B_c(0)|_{p \approx 0.09\text{GPa}} \approx 2.6$ T. Already at this pressure of $p \approx 0.09$ GPa, the AFM transition at $B = 0$ T cannot be detected anymore since it is expelled by the SC state (see also figure 4.18). Therefore, the dotted line used in the SC phase is not detectable experimentally and represents the extension of the fit obtained for $B_c(T)|_{p \approx 0.09\text{GPa}}$. The second phase line visible at ambient pressure inside the AFM phase (not shown in figure 4.22; see figure 4.15 for details), detected in our measurements only by adiabatic $T(B)$ scans, cannot be followed anymore at higher pressures because the AFM and SC phase transitions are coming too close to each other in temperature/magnetic field. In the case of SC, though T_c is strongly increased by increasing the pressure, the magnetic field destroys SC much more rapidly than it destroys AFM. At ambient pressure, the data shown for the SC transition reveal $B_{c2}(0)|_{p=0\text{GPa}} \approx 1.05$ T, a value which is gradually increasing with increasing pressure, reaching $B_{c2}(0)|_{p \approx 0.09\text{GPa}} \approx 1.67$ T. Unfortunately, due to the restricted temperature range of our measurements ($T > T_{min} = 0.26$ K) the interplay of magnetism and SC at lower temperatures and higher pressures ($p > 0.09$ GPa), the real shape of the critical field curves for both AFM and SC transitions and the existence of magnetic-field and pressure-induced QCPs cannot be precisely determined.

The appearance of the field-induced B -phase (at T_B), at ambient pressure seen only for $B = 8$ T ($B \parallel c$), shifts to lower temperatures upon increasing pressure. In the limits of our setup, it is still partly detectable at $p \approx 0.04$ GPa and $B = 8$ T and completely disappears from our experimental window at higher pressures. The decrease of T_B at $B = 8$ T with increasing pressure to $p \approx 0.04$ GPa hints at pressure-induced shifting of the B -phase in the $B - T$ phase diagram to higher values of the magnetic field. Since the AFM phase is moved by application of pressure towards lower values of B in the $B - T$ phase diagram of A/S -type $CeCu_2Si_2$, a complete separation of the AFM and B -phase in the $B - T$ plane might appear under

application of pressure for $B \parallel c$. Upon increasing pressure, a shift of the critical field where the B -phase appears at $T = 0$ K, $B_{crit}^{B-phase}(0)$, to lower values of B , accompanied by a narrowing in temperature of the region of the B -phase in the $B-T$ phase diagram, could also be considered as a possible scenario. However, electrical-resistivity measurements on polycrystalline samples of CeCu_2Si_2 have shown a gradual splitting of the AFM and B -phase at $T \approx 0$ K when going from the A - to A/S - and then to the S -type polycrystals [Gegenwart 1998a]. As mentioned at the beginning of section 4.2, a systematic shift from A - to A/S - and further to S -type CeCu_2Si_2 can be seen as pressure is applied to the system (see for details figure 4.3). It was shown that in the case of the A/S -type polycrystalline sample the critical magnetic field necessary to suppress the AFM phase to $T_N = 0$ K, $B_c(0)$, and the critical field necessary for the appearance of the B -phase at $T = 0$ K, $B_{crit}^{B-phase}(0)$, are coinciding [Gegenwart 1998a]. In the case of the S -type polycrystalline sample the AFM and the B -phase were found to be well separated in the $B-T$ phase diagram (AFM in this S -type sample appears at $B > B_{c2}$), $B_c(0)$ being shifted to lower values while $B_{crit}^{B-phase}(0)$ being moved to higher values of B compared to the case of A/S -type CeCu_2Si_2 [Gegenwart 1998a]. Therefore, our results related to the evolution of the B -phase with increasing pressure seem to be in good agreement with the evolution of the B -phase observed by systematically shifting from polycrystalline A/S -type CeCu_2Si_2 to polycrystalline S -type CeCu_2Si_2 . Thus, a pressure-induced splitting of the AFM and B -phase at $T = 0$ K in the $B \parallel c$ $B-T$ phase diagram of A/S -type CeCu_2Si_2 from $B_c(0) \approx B_{crit}^{B-phase}(0)$ at ambient pressure to $B_c(0) < B_{crit}^{B-phase}(0)$ at higher values of p is suggested (with $B_c(0)$ decreasing and $B_{crit}^{B-phase}(0)$ increasing upon increasing pressure). For a more precise study of the evolution of the B -phase and of the AFM – B -phase interface (where exists) with increasing pressure, pressure experiments at lower temperatures are needed.

Application of both magnetic field and pressure lead to a gradual suppression of AFM order in A/S -type CeCu_2Si_2 . In the case when T_N is continuously suppressed to $T_N = 0$ K (QCP), quantum critical fluctuations are expected to occur. Even though $T = 0$ K is not reachable experimentally, strong deviations from the typical LFL behavior (NFL) are observed already at higher temperatures around the QCP (see for details section 1.3). The extrapolations of the $T_N(B, p)$ phase lines, presented in figures 4.21 and 4.22, to $T_N = 0$ K mark the expected AFM QCPs in A/S -type CeCu_2Si_2 ($B \parallel c$). In order to follow the pressure and magnetic-field dependence of the expected line of AFM QCPs, we have summarized the values of critical pressure (p_c) and critical magnetic field obtained by the above-mentioned extrapolations to $T_N(B, p) = 0$ K in a plot shown in figure 4.23. In this plot, the data are presented in

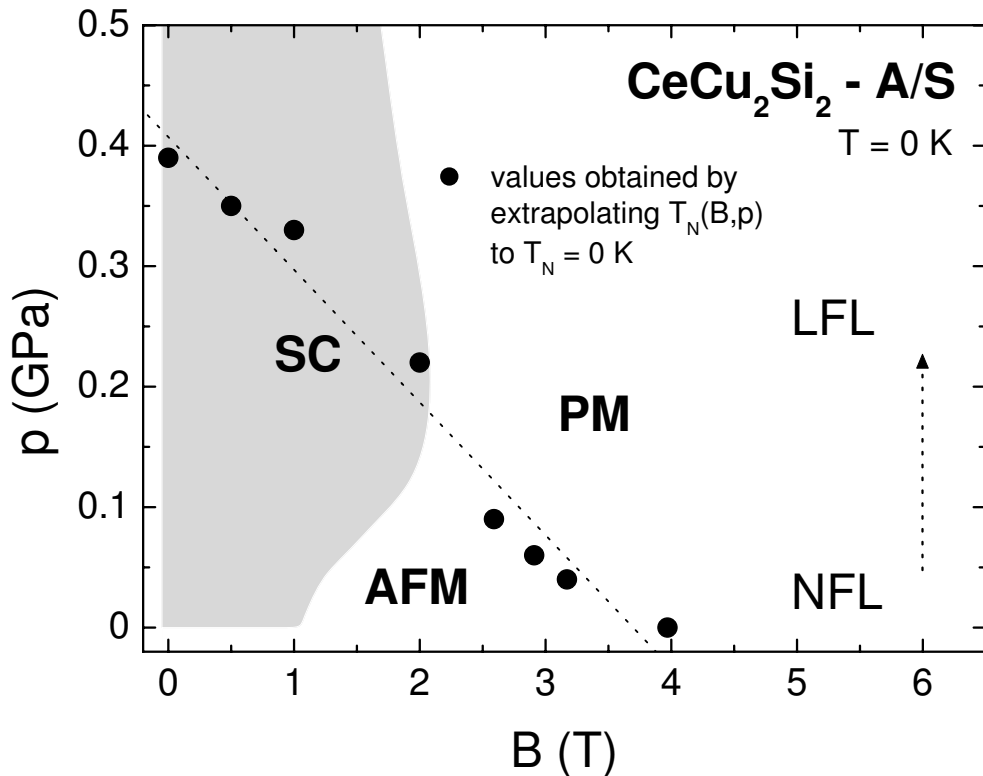


Figure 4.23: $p - B$ phase diagram of A/S -type CeCu_2Si_2 for $T = 0$ K and $B \parallel c$. Closed circles represent the (p, B) points obtained by extrapolating the $T_N(p, B)$ data to $T_N(p, B) = 0$ K. The extrapolations of $T_N(p, B)$ shown in figures 4.21 and 4.22 were used. The dashed line serves as a guiding line. The gray area, marked by “SC”, indicates the $p - B$ region where the system is expected to be in the SC state at $T = 0$ K ($B \parallel c$) (drawn by using the estimated $B_{c2}(0)$ as function of p). “AFM” and “PM” mark the regions where the system is supposed to be AFM or PM at $T = 0$ K. The arrow is located at $B = 6$ T and indicates the direction of increasing pressure.

a $p - B$ plane at $T = 0$ K. The full circles mark the estimated AFM QCPs ($B \parallel c$). The dashed line is used to schematically show the evolution of the AFM quantum critical region in A/S -type CeCu_2Si_2 . As seen in this figure, at ambient pressure $B \approx 4$ T is the critical field needed for a complete suppression of the AFM phase transition to $T_N = 0$ K. Increase of pressure leads to a gradual decrease of the critical field necessary to suppress T_N to $T_N = 0$ K. At $p \approx 0.4$ GPa the critical field is $B \approx 0$ T. The gray area in figure 4.23 represents the region where CeCu_2Si_2 is in the SC state at $T = 0$ K. We have constructed this region by using the pressure dependence of the estimated upper critical fields at $T = 0$ K, $B_{c2}(0)(p)$. The border of this region is delineated by the corresponding $p(B_{c2}(0))$. The regions where the

system is in the AFM or PM state at $T = 0$ K are marked in the figure by “AFM” and “PM”, respectively. As mentioned earlier, for any value of magnetic field and pressure, we do not detect the presence of a phase transition to the AFM ordered state below the temperature where SC has already set in (we have never seen any anomaly at T_N when T_N is expected to be smaller than T_c). Therefore, the existence of AFM QCPs in the region where SC is present at $T = 0$ K (gray area) is improbable. However, the AFM QCPs estimated to be located outside of the gray region in figure 4.23 are very likely to exist and, therefore, should be observable. Any fixed value of B larger than the critical field of $B \approx 4$ T obtained for $p = 0$ GPa (e.g. $B = 6$ T, marked by the arrow in figure 4.23) is located closest to the line of AFM QCPs at ambient pressure. Upon increasing pressure, the distance from that value of B to the line of QCPs is gradually increasing. In order to provide evidence for the existence of the estimated pressure and magnetic-field-induced AFM QCPs in A/S -type CeCu_2Si_2 ($B \parallel c$) we expect that at any fixed magnetic field, slightly higher than the critical field of $B \approx 4$ T obtained for $p = 0$ GPa, the increase of pressure would lead to a gradual shift from NFL to LFL behavior.

As suggested by the arrow in figure 4.23, the magnetic field of $B = 6$ T, where no phase transition can be detected over the whole measured pressure and temperature range, was used to follow the change from NFL to LFL properties. Figure 4.24 shows the evolution of the electronic specific heat at $B = 6$ T as function of pressure, on a \sqrt{T} temperature scale. At ambient pressure, $C_{el}(T)/T$ increases as $\Delta C_{el}(T)/T \propto -\sqrt{T}$, showing a clear deviation from the prediction of the LFL theory (for details see table 1.2 for 3D AFM). Upon increasing pressure, the \sqrt{T} dependence of $C_{el}(T)/T$ becomes less and less pronounced, until $C_{el}(T)/T \approx \text{const.}$ at sufficiently high pressure ($p \approx 1$ GPa). At $B = 6$ T, the deviation from the LFL behavior at low pressures indicates the proximity of the system to a QCP, while at higher pressures (away from the QCP) LFL behavior is recovered. Variation of both pressure and magnetic field can be used to move along the line of AFM QCPs. As suggested by figure 4.23, with increasing pressure the estimated magnetic-field and pressure-induced QCPs shift to lower values of B . The data presented in figure 4.24 clearly show that increase of pressure stabilizes the LFL state, a result expected for a system which is gradually driven away from the line of QCPs. These results argue in favor of the existence of the line of AFM QCPs suggested in figure 4.23. Since in the SC region no AFM can be detected, the QCPs shown in the gray area of figure 4.23 are unlikely to exist.

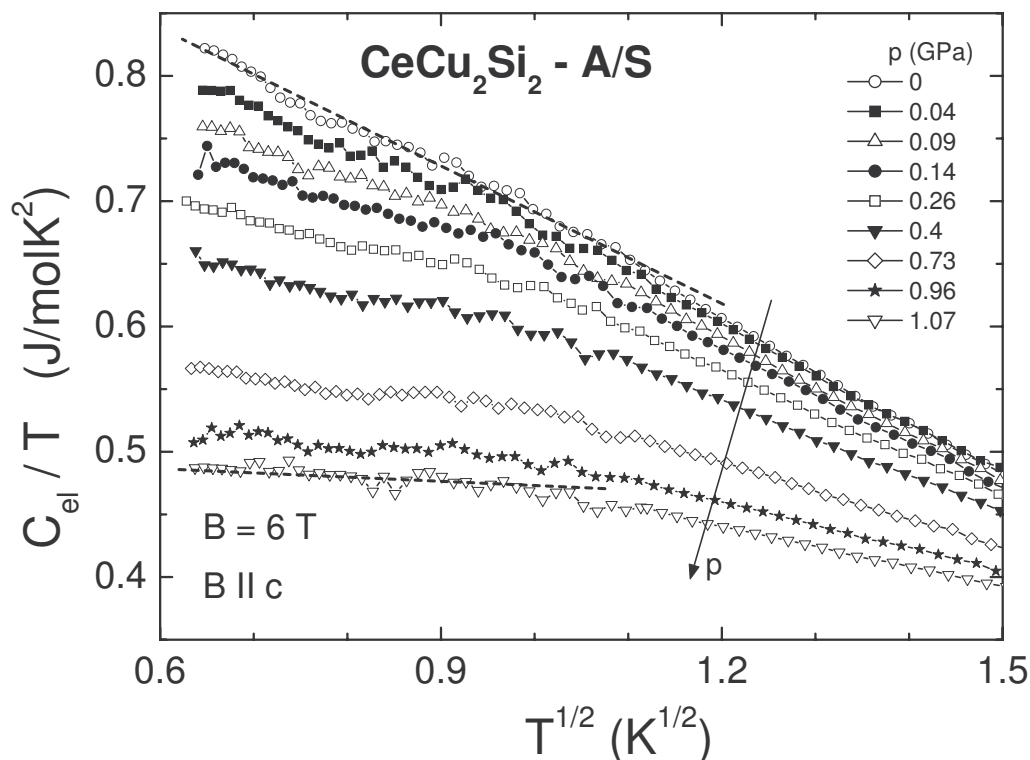


Figure 4.24: Effect of pressure on the specific heat of A/S -type $CeCu_2Si_2$ taken at $B = 6$ T ($B \parallel c$). The data are presented as function of \sqrt{T} . The shown temperature range corresponds to 0.36 K $\leq T \leq 2.25$ K. The dotted lines are linear fits, in \sqrt{T} , to the data ($\Delta C_{el}(T)/T \propto -\sqrt{T}$).

4.3.2 Superconductivity in the high-pressure range

As already mentioned in section 4.2, $CeCu_2Si_2$ shows a rather unconventional temperature - hybridization strength phase diagram. SC, supposed to exist under a “dome” centered around the AFM QCP, is indeed extending much further away from the magnetic instability. Therefore, magnetic fluctuations, most likely responsible for SC in the region located around the AFM QCP, are not very likely to induce SC in the region far away from the magnetic fluctuations. In analogy with metallic Ce [Koskenmaki 1978], an isostructural volume discontinuity associated with the valence change of Ce is expected to take place in intermetallic Ce-based compounds too. With increasing pressure, the $4f$ electron of the Ce atom is transferred to the conduction band. Strong valence fluctuations between the $4f^1$ and $4f^0$ configurations, if they exist at low enough temperatures, might eventually cause SC far from the magnetic region. In the case of Ce-based HF compounds, the partial delocaliza-

tion of the $4f$ electron, perhaps mediating the formation of Cooper pairs, replaces the HF state by an IV state. The transition from the HF to the IV state usually is a first-order phase transition accompanied by a symmetry-conserving collapse of the unit-cell volume. The isostructural $\gamma - \alpha$ transition, involving a volume collapse of about 17%, takes place in metallic Ce at room temperature and $p \approx 0.8$ GPa [Koskenmaki 1978]. CeCu_2Ge_2 , the isostructural relative of CeCu_2Si_2 , shows a volume discontinuity of about 2% at $T = 10$ K, at the same pressure where the SC transition temperature reaches its maximum value [Onodera 2002]. Röhler *et al.* [Röhler 1988] have shown that CeCu_2Si_2 undergoes a first-order valence transition at room temperature, at about the same pressure where T_c shows its maximum value. The above-mentioned experimental evidences (also briefly described in section 4.2) strongly hint at the involvement of nearly critical valence fluctuations in the formation of SC in Ce-based HF systems. Valence-fluctuation mediated Cooper pairing is a subject of recent theoretical work. A short introduction to a phenomenological model explaining both, spin- and valence-fluctuation mediated SC, is given in section 1.2.2 [Monthoux 1999, Monthoux 2004]. In the following part we will briefly introduce the theoretical approach of Onishi and Miyake [Onishi 2000], where a microscopic model was implied in order to explain the formation of SC in the vicinity of a valence instability.

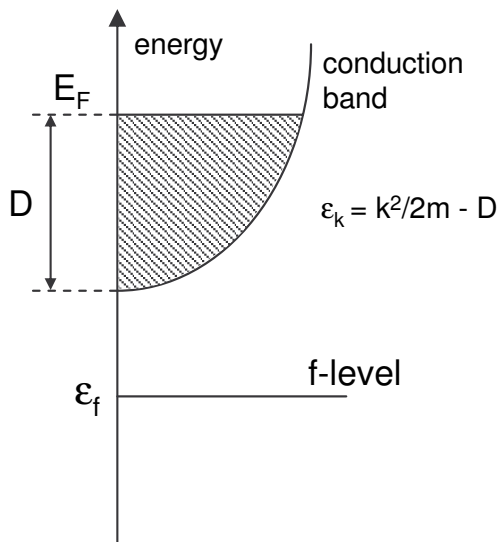


Figure 4.25: Schematic representation of the energy levels as used in the theoretical model of Onishi and Miyake [Onishi 2000]. With increasing pressure the energy of the f level, ϵ_f , shifts towards the Fermi energy, E_F . D represents the conduction bandwidth.

A valence transition does not break any spatial symmetry but is strongly coupled

to the volume. Therefore, a pressure-induced valence transition is very likely to exist in many systems. In the case of Ce-based HF systems, where the valence transition is generated by the expulsion of the $4f$ electron of Ce into the conduction band, a strong Coulomb repulsion between the conduction electrons and the f electrons raising from this transition could strongly enhance the valence fluctuations, leading in this way to the formation of a SC state [Onishi 2000]. Onishi and Miyake have elaborated a microscopic theory, where the strong Coulomb repulsion between the f and conduction electrons, U_{fc} , was additionally introduced in the periodic Anderson model. The model is based on the following Hamiltonian:

$$H = \sum_{k\sigma} (\epsilon_k - \mu) c_{k\sigma}^\dagger c_{k\sigma} + \epsilon_f \sum_{k\sigma} f_{k\sigma}^\dagger f_{k\sigma} + U_{ff} \sum_i n_{i\uparrow}^f n_{i\downarrow}^f + V \sum_{k\sigma} (c_{k\sigma}^\dagger f_{k\sigma} + \text{h.c.}) + U_{fc} \sum_{i\sigma\sigma'} n_{i\sigma}^f n_{i\sigma'}^c, \quad (4.3)$$

where $f_{k\sigma}$, $c_{k\sigma}$ ($f_{k\sigma}^\dagger$, $c_{k\sigma}^\dagger$) are the annihilation (creation) operators for the f and conduction electrons with wave vector k and spin index σ . U_{fc} denotes the $f - c$ Coulomb interaction, while U_{ff} is the on-site Coulomb repulsion between the f electrons. V represents the hybridization matrix element between the conduction electrons and the f electrons, μ is the chemical potential and ϵ_f denotes the energy of the f level relative to the Fermi level (see figure 4.25). $n_{i\uparrow}^f$, $n_{i\downarrow}^f$, $n_{i\sigma}^f$ and $n_{i\sigma'}^c$ are particle number operators. The first two terms represent the energy of the conduction electrons and of the f electrons, respectively. The third term is associated to the on-site correlation energy. The fourth term takes into account the hybridization of the f and conduction electrons, while the fifth term is the extra term introduced to the extended periodic Anderson Hamiltonian, incorporating the short-range repulsive Coulomb interaction between the conduction electrons and the f electrons. Increase of pressure leads to an increase of V and a shift of the f level, ϵ_f , towards the Fermi energy. When $\epsilon_f + \langle n_f \rangle U_{fc} \simeq E_F$ (where n_f represents the number of f electrons per site), the $4f^1$ and $4f^0$ states are nearly degenerate giving rise to valence fluctuations. Therefore, the introduction of U_{fc} produces a rapid charge transfer of the f electrons to the conduction band. The associated fluctuations can produce an attractive interaction in the d -wave channel, leading to SC [Onishi 2000]. SC was investigated within the weak-coupling theory. The SC transition temperature, T_c , calculated by the use of the slave-boson and large- N expansion approach, was shown to have a finite value only for the d -wave pairing. The variation of T_c as function of ϵ_f (which practically represents pressure) estimated for the d -wave SC channel is shown in figure 4.26 for different values of the interaction potential U_{fc} [Onishi 2000]. For convenience, values of T_c and ϵ_f are normalized to D , where D represents the conduction bandwidth. T_c versus ϵ_f displays a sharp maximum at the

same point where n_f starts to show a rapid decrease. The increase of U_{fc} leads to a more pronounced maximum in T_c , as well as to a more dramatic, more and more first-order-like valence change (more drastic drop of n_f). In the region where n_f has decreased enough, T_c is strongly suppressed. As another important result of this model, one should mention that the scattering processes of $(f, f) \rightarrow (f, c)$ and $(f, c) \rightarrow (f, f)$, in which the valence of f electrons is changed directly, play the most important role in the formation of Cooper pairs. Moreover, the estimation of the Sommerfeld coefficient, γ , of the electronic specific heat leads to the relation $\gamma \propto (T_K)^{-1}$ ($T_K \propto (\bar{\epsilon}_f - \mu)$). The γ versus T_K curves show a universal behavior, lying on the same line independent of the value of U_{fc} . It was shown that the enhanced scattering due to valence fluctuations is nearly independent of the momentum transfer, q , for $q \lesssim 3k_F/2$, indicating that the valence change is a local phenomenon. This model has several shortcomings, e.g. a simplified, single spherical FS is used for the conduction band and the spin fluctuations which exist near the AFM QCP are neglected. The real change in n_f across the valence transition will be certainly much less than theoretically estimated. Therefore, in real systems only the overall behavior and not the absolute numbers must be taken in consideration (usually n_f does not drop below 0.8 - 0.85 in the case of Ce-based intermetallic compounds [Malterre 1996]).

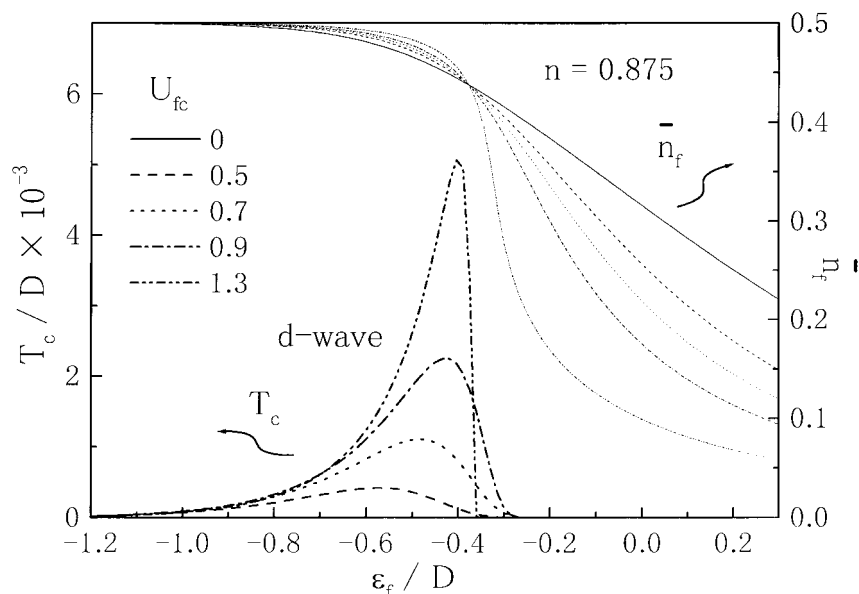


Figure 4.26: T_c dependence for a d -wave SC as function of the f -level position ϵ_f for different Coulomb interaction potentials U_{fc} . Values are normalized to the conduction bandwidth, D . The right axis shows the associated variation of the valence, n_f . \bar{n}_f represents the number of f electrons per site and spin ($\bar{n}_f = n_f/2$). Figure taken from [Onishi 2000].

Miyake and Maebashi [Miyake 2002] predicted that the existence of critical valence fluctuations in Ce-based HF systems causes an enhancement of the residual resistivity, ρ_0 , in the region of valence instabilities, p_v . This enhancement of ρ_0 is expected to be much stronger than that seen around the magnetic QCP [Miyake 2002]. Experimental evidence for a strong increase of ρ_0 around the critical pressure, p_v , can indeed be seen in measurements of the electrical resistivity under pressure in $CeCu_2Ge_2$ [Jaccard 1999] and $CeCu_2Si_2$ [Holmes 2004b]. A linear temperature dependence of the electrical resistivity and an enhancement of the electronic specific-heat coefficient, γ , in the vicinity of p_v were found experimentally [Holmes 2004b]. A theoretical explanation for the observed behavior is given in the same paper [Holmes 2004b]. However, a small shift of the maximum of γ to a pressure lower than the critical pressure where the maxima of ρ_0 and T_c are found was predicted [Holmes 2004b].

In the strongly correlated limit, the effective mass of the heavy electrons is drastically changed due to the gradual delocalization of the $4f^1$ electrons of Ce under the effect of pressure, leading to a less correlated state. The effective mass will be reduced according to:

$$\frac{m^*}{m} = \frac{1 - n_f/2}{1 - n_f}, \quad (4.4)$$

when n_f , the number of localized f electrons per Ce atom, is significantly reduced below its Kondo-limit value, $n_f \lesssim 1$ [Rice 1986]. According to the change of the effective mass of the heavy QPs (respectively of γ , $\gamma \propto m^*$), the A coefficient of the T^2 term to the resistivity ($\rho = \rho_0 + AT^2$, $A \propto \gamma^2$) and the Kadowaki-Woods ratio, A/γ^2 , should also decrease across the valence transition. The Kadowaki-Woods ratio is expected to change through the valence transition from a strongly to a weakly correlated limit [Kadowaki 1986, Miyake 1989]:

$$\gamma = \gamma_{band} + \gamma_{corr}; \quad (4.5)$$

in the strongly correlated limit, $\gamma_{corr} \gg \gamma_{band}$:

$$\frac{A}{\gamma^2} \approx \frac{A}{(\gamma_{corr})^2} \approx 1.0 \times 10^{-5} \mu\Omega\text{cm}(\text{molK/mJ})^2, \quad (4.6)$$

in the weakly correlated region, $\gamma_{corr} < \gamma_{band}$:

$$\frac{A}{\gamma^2} = \frac{A}{(\gamma_{band} + \gamma_{corr})^2} \ll \frac{A}{(\gamma_{corr})^2} \approx 1.0 \times 10^{-5} \mu\Omega\text{cm}(\text{molK/mJ})^2. \quad (4.7)$$

Figure 4.27 presents the experimental results obtained by measurements of electrical resistivity and a.c. calorimetry under pressure on $CeCu_2Si_2$ done by Holmes *et al.* [Holmes 2004b] together with data from electrical-resistivity measurements under

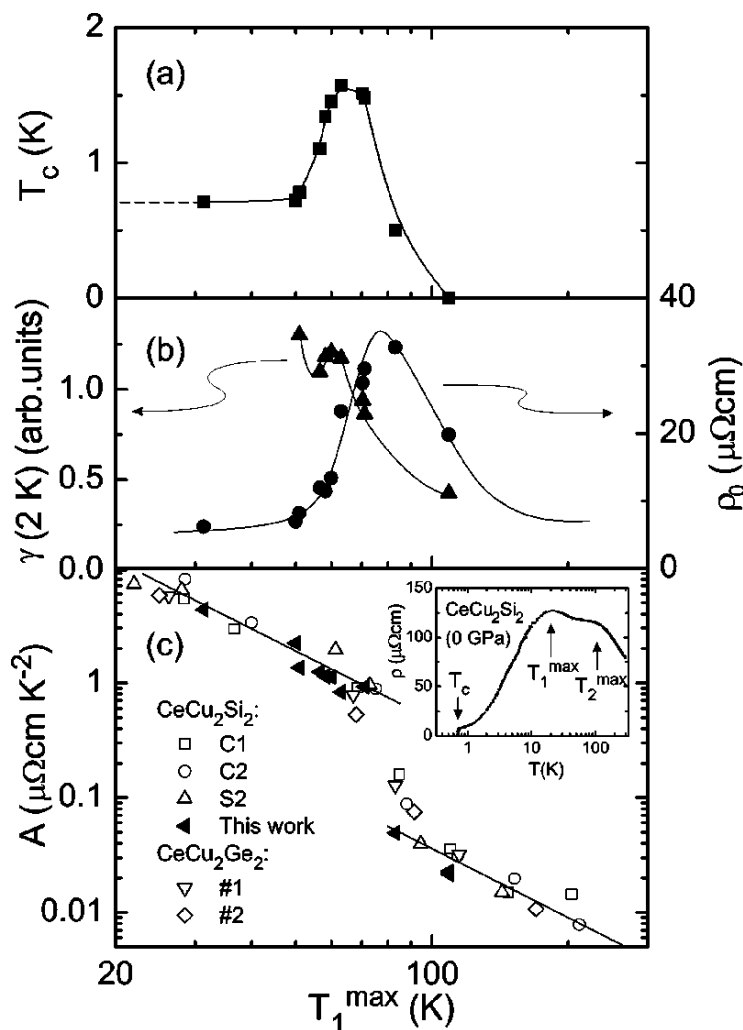


Figure 4.27: (a) - T_c , (b)-left axis - electronic specific-heat coefficient, γ , (b)-right axis - residual resistivity, ρ_0 , and (c) - A coefficient of the T^2 term to the resistivity ($\rho = \rho_0 + AT^2$) as function of logarithm of T_1^{max} , the characteristic temperature of the system, for CeCu_2Si_2 and CeCu_2Ge_2 (only in panel (c)). The inset shows the way how T_1^{max} is defined. The straight lines in (c) mark the expected scaling, $A \propto (T_1^{max})^{-2}$. The maximum of T_c coincides with the start of the region where the scaling relation of A is broken, while the maximum in ρ_0 is situated at the middle of the collapse of A . The maximum of γ is situated at a lower T_1^{max} . The pressure is increasing as $\log(T_1^{max})$. Figure taken from [Holmes 2004b] (for data on CeCu_2Ge_2 see [Jaccard 1999]).

pressure on CeCu_2Ge_2 from [Jaccard 1999]. The abscissa shows the coherence temperature, T_1^{max} , taken from the low-temperature maximum in resistivity (see inset panel (c)) on a logarithmic scale, a scale which corresponds to an approximately linear increase of pressure from left to right. A maximum of T_c , ρ_0 and γ , respectively, a drastic reduction of the A coefficient, marking also a change of the value of the

Kadowaki-Woods ratio, A/γ^2 , ($T_1^{max} \propto T_K \propto \gamma^{-1}$), are accompanying the valence instability in $CeCu_2Si_2$ and $CeCu_2Ge_2$ under pressure.

H. Kontani [Kontani 2004] has derived a generalized Kadowaki-Woods ratio for the case of systems where the f -orbital degeneracy, N , takes values $N \geq 2$. It was shown that, depending on N :

$$\frac{A}{\gamma^2} = \frac{1.0 \times 10^{-5}}{\frac{1}{2}N(N-1)} \mu\Omega\text{cm}(\text{molK/mJ})^2 \quad (N \geq 2). \quad (4.8)$$

The second maximum in the temperature-dependent electrical resistivity, observed in the high-temperature region and marked by T_2^{max} in the inset of figure 4.27c, is attributed to the excited CEF levels. Pressure-dependent electrical-resistivity measurements performed on $CeCu_2Ge_2$ have shown that at $p \geq 7$ GPa, a strong increase of T_1^{max} ($T_1^{max} \propto T_K$) with increasing pressure is accompanied by a slight decrease of T_2^{max} ($T_2^{max} \propto \Delta_{CEF}$) [Jaccard 1999]. At the pressure p_v where $T_c(p)$ exhibits its maximum value, most likely associated to a valence change of the Ce atom, the two maxima observed in $\rho(T)$ merge into a single maximum which is further increasing upon increasing pressure [Jaccard 1999]. At this pressure, due to the fact that the system crosses the region where $T_K \approx \Delta_{CEF}$, a change of the ground-state degeneracy from $N = 2$ (for $T_K < \Delta_{CEF}$) to the full $N = 6$ -fold degeneracy of the $J = 5/2$ $4f^1$ multiplet (for $T_K > \Delta_{CEF}$) is expected. According to relation 4.8, a change of the f -orbital degeneracy from $N = 2$ (at $p < p_v$) to $N = 6$ (at $p > p_v$) implies a strong reduction of the Kadowaki-Woods ratio at p_v , in good agreement with the sharp drop of A/γ^2 at p_v found in the case of $CeCu_2Si_2$ [Holmes 2004b] and $CeCu_2Ge_2$ [Jaccard 1999] under pressure (see figure 4.27c).

Our measurements of the specific heat under pressure show that application of pressure on single-crystalline A/S -type $CeCu_2Si_2$ leads to a rapid suppression of the AFM order and to a steep increase of the SC transition temperature from its ambient-pressure value to $T_c \approx 0.628$ K at about $p \approx 0.4$ GPa. Upon further increasing pressure T_c decreases slightly up to $p \approx 1.5$ GPa, from where it starts to increase again, marking the entrance into the second (high-pressure) SC region. Figure 4.28 shows the overall behavior of the $B = 0$ T specific heat, for the pressure range $0 \text{ GPa} \leq p < 2.1 \text{ GPa}$. Two distinct SC regions, corresponding to the vicinity of the AFM (region SC1 - low- p region) and valence (region SC2 - high- p region) instability, respectively, are expected to exist in $CeCu_2Si_2$. As the border between these two SC regions we chose the pressure $p \approx 1.5$ GPa at which $T_c(p)$ has its minimum value at $B = 0$ T. Since the SC1 region, located in the vicinity of the magnetic instability, was already discussed in the previous part, in the following we will focus on the SC properties of $CeCu_2Si_2$ in the SC2 region. The detailed evolution of the electronic

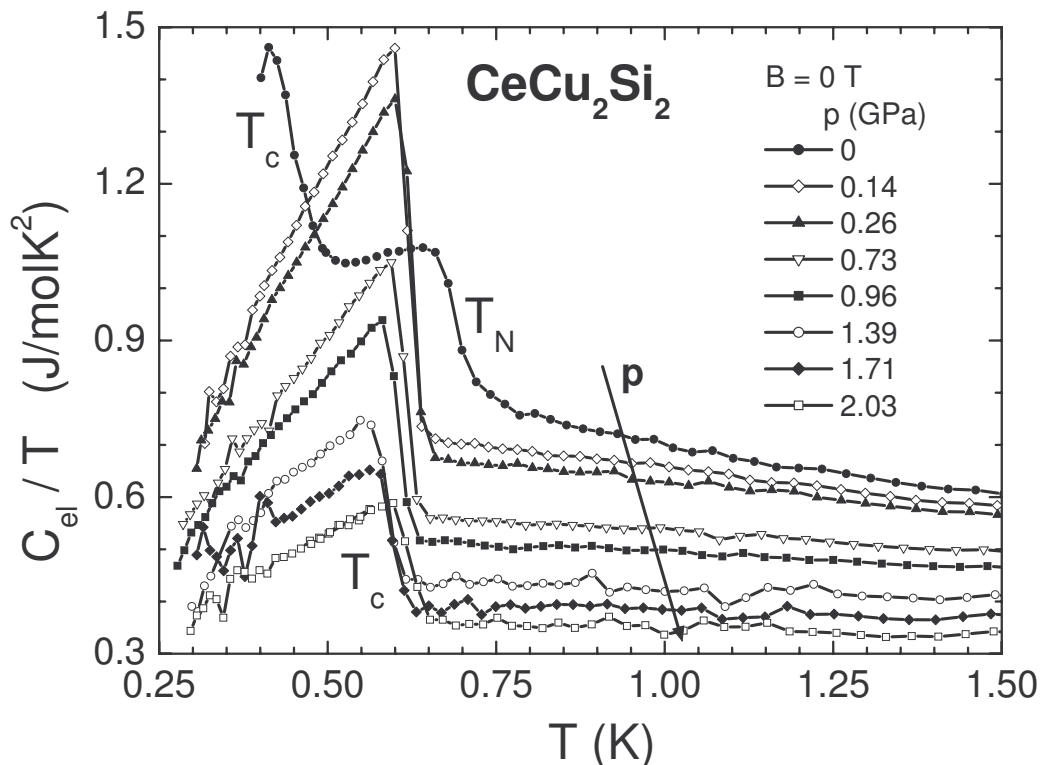


Figure 4.28: Low-temperature $C_{el}(T)/T$ versus T of A/S -type CeCu_2Si_2 at $B = 0$ T for different pressures covering completely the measured pressure range, $0 \text{ GPa} \leq p \leq 2.1 \text{ GPa}$. The visible anomalies correspond to the SC phase transitions, except in the curve corresponding to $p = 0$ GPa, where also the AFM phase transition (T_N), at a temperature higher than T_c is seen. The arrow marks the direction of increasing pressure.

specific heat and of the SC transition in the SC2 region, where T_c is continuously increasing upon application of pressure, can be seen in figure 4.29. With increasing pressure, C_{el}/T taken just above the transition temperatures (e.g. at $T = 0.9$ K) is continuously decreasing. The data at pressures above $p = 1.1$ GPa were collected in a double-layer pressure cell, having the advantage of reaching higher pressures but with the disadvantage of a higher addenda and of a smaller volume available for the sample (for details see Chapter 2). Therefore, for the pressure range $1.1 \text{ GPa} < p < 2.1 \text{ GPa}$ a smaller piece ($m \approx 340$ mg) was cut from the original single crystal ($m \approx 393$ mg) used in the measurements at pressures below $p = 1.1$ GPa. Though the heat capacity of the measured sample in the $1.1 \text{ GPa} < p < 2.1 \text{ GPa}$ pressure range was strongly reduced in comparison to the heat capacity of the loaded cell, the resolution of the measurement still remained in an acceptable range (for details about the accuracy of

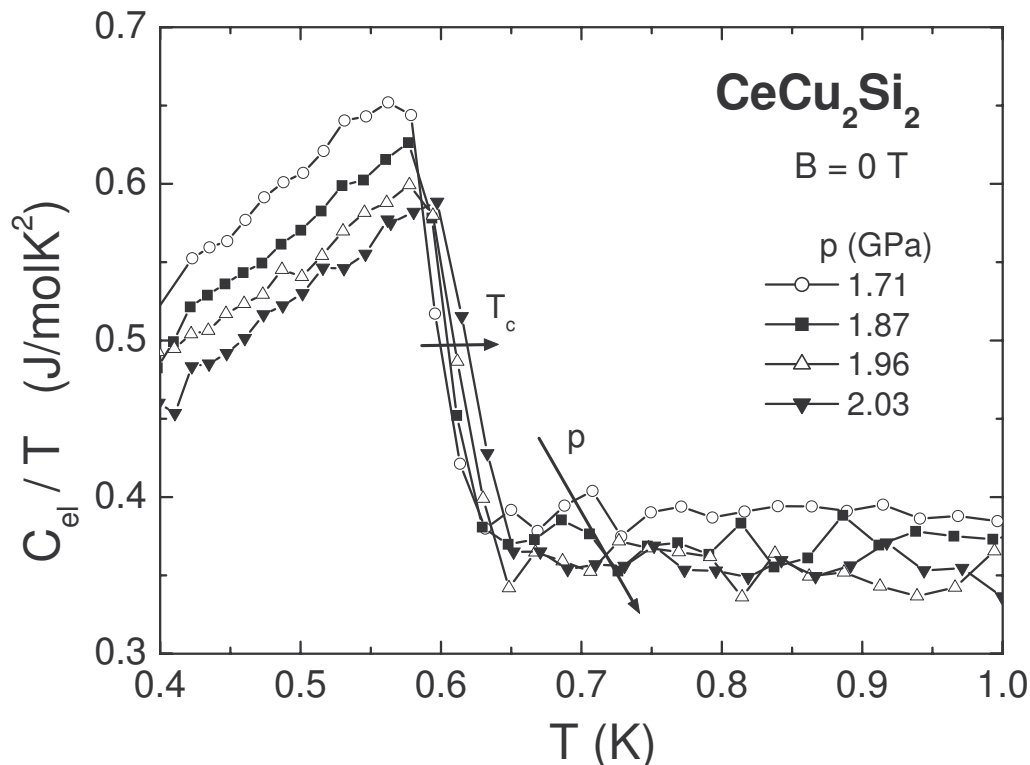


Figure 4.29: Low-temperature $C_{el}(T)/T$ versus T of A/S -type $CeCu_2Si_2$ at $B = 0$ T for different pressures corresponding to the high-pressure SC region, SC2.

the measurements see figure 2.7). Therefore, accurate absolute values of the specific heat, but with slightly increased scattering, were obtained. The SC phase transition is clearly detectable and is very sharp proving the good hydrostatic conditions in the pressure cell even at these high pressure values. The a.c.-susceptibility data displaying the SC phase transition are shown in figure 4.30. The data taken at $p \approx 1.39$ GPa (dashed line) are used as a reference for the width of the phase transition anomaly obtained for the pressures below $p \approx 1.5$ GPa (region - SC1). It can be seen that there is no apparent broadening of the SC transition when going from the region SC1 to the region SC2.

The application of magnetic field leads to a suppression of the SC phase transition in a more rapid manner than observed in the low-pressure range. Though the value of T_c at $B = 0$ T does not change much in the pressure region starting from where the AFM transition is suppressed at $B = 0$ T ($p \geq p_c^*$), already $B = 1$ T shifts T_c to only 69% of its $B = 0$ T value in the case of $p \approx 1.96$ GPa, in comparison to 83% for the case of $p \approx 0.73$ GPa. As an example, figure 4.31 shows the effect of

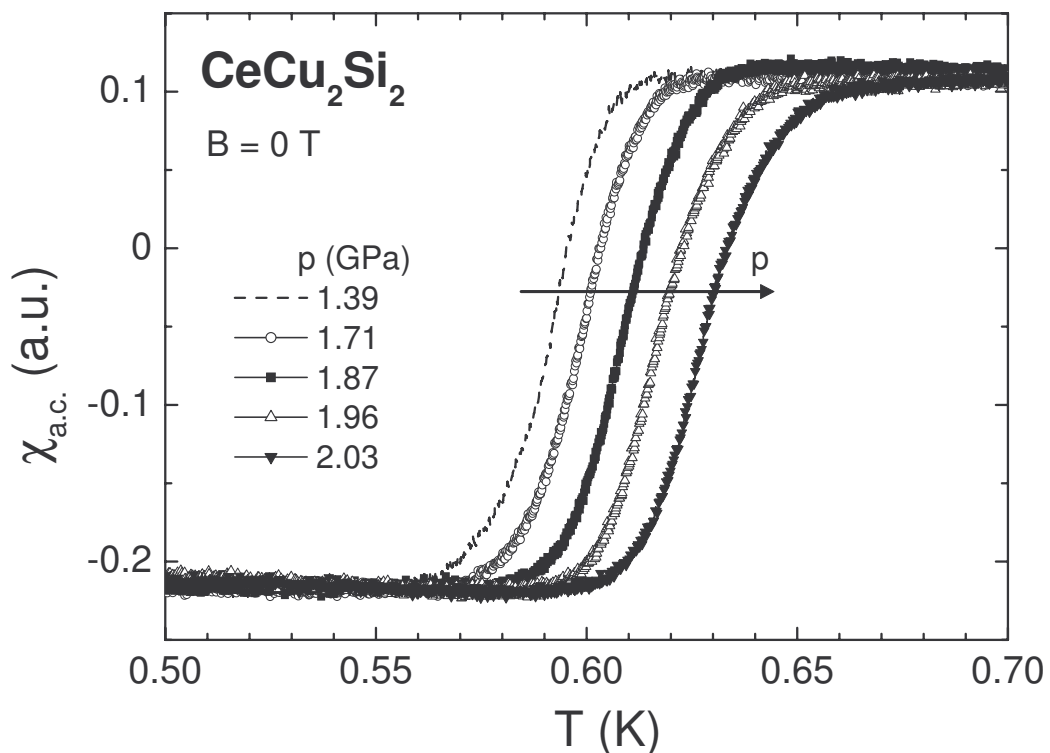


Figure 4.30: Low-temperature $\chi_{a.c.}(T)$ versus T of A/S -type CeCu_2Si_2 at $B = 0$ T, for pressures as indicated in the figure. The last four pressure curves ($p \approx (1.71, 1.87, 1.96, 2.03)$ GPa - shown by symbols) are depicting the transitions to the SC state in region SC2 and are corresponding to the same values of pressures as used for $C_{el}(T)/T$ shown in figure 4.29. As explained in the text, the curve at $p \approx 1.39$ GPa, drawn by the dashed line, is used as reference for the width of the SC phase transition anomaly.

applied magnetic field ($B \parallel c$) on the SC phase transition for $p \approx 1.96$ GPa. Upon increasing B , once the SC phase transition cannot be followed anymore in our experimental window, no other anomaly can be detected in $C_{el}(T)/T$ up to $B = 8$ T. The system shows LFL behavior in the normal state ($C_{el}(T)/T \approx \text{const.}$) in the whole pressure range corresponding to the high-pressure SC region, SC2 ($p \leq 2.03$ GPa). The evolution of $C_{el}(T)/T$ in the pressure range $1.5 \text{ GPa} < p < 2.1 \text{ GPa}$ is shown in figure 4.32 for $B = 2$ T, a magnetic field sufficiently high to suppress SC in this pressure range. Despite of the increased scattering of the data (as explained before), it is still clearly detectable that the value of C_{el}/T taken at a certain temperature continuously decreases upon increasing pressure. Furthermore, for each pressure $C_{el}(T)/T$ stays temperature independent ($C_{el}(T)/T \approx \text{const.}$) below $T \approx 1$ K, indicating LFL

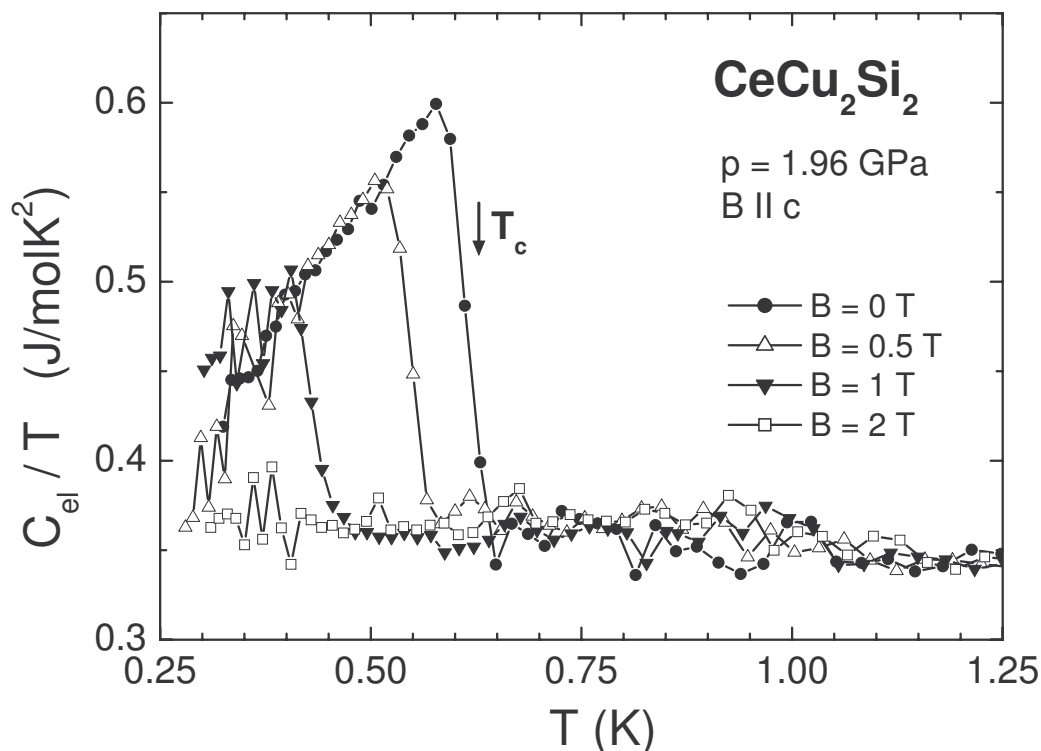


Figure 4.31: Magnetic-field dependence ($B \parallel c$, $B \leq 2$ T) of the low-temperature $C_{el}(T)/T$ of $CeCu_2Si_2$ at $p \approx 1.96$ GPa. The values of B are indicated in the figure. The observed phase transition anomalies correspond to the transitions to the SC state.

behavior in this pressure range.

4.3.3 Comparison of the evolution of the superconducting properties in the different pressure regimes

Figure 4.33 displays the evolution of magnetism and SC under pressure in single-crystalline A/S -type $CeCu_2Si_2$ as obtained by specific-heat and a.c.-susceptibility measurements under hydrostatic pressure and in magnetic field $B \parallel c$. $T_N(p)$ obtained from specific-heat measurements and its extrapolation to $T_N(p_c) = 0$ K (described in section 4.3.1) are shown only for $B = 0$ T, while $T_c(p)$ determined from $C_{el}(T)$ and $\chi_{a.c.}(T)$ are shown for $B = (0, 0.5, 1)$ T. The critical pressure, $p_c \approx 0.39$ GPa, and the pressure $p \approx 1.5$ GPa separating the low-pressure (SC1) from the high-pressure (SC2) SC region are indicated in the figure. Upon increasing pressure at $B = 0$ T, $T_N(p)$ decreases rapidly while $T_c(p)$ quickly increases reaching a maximum value of

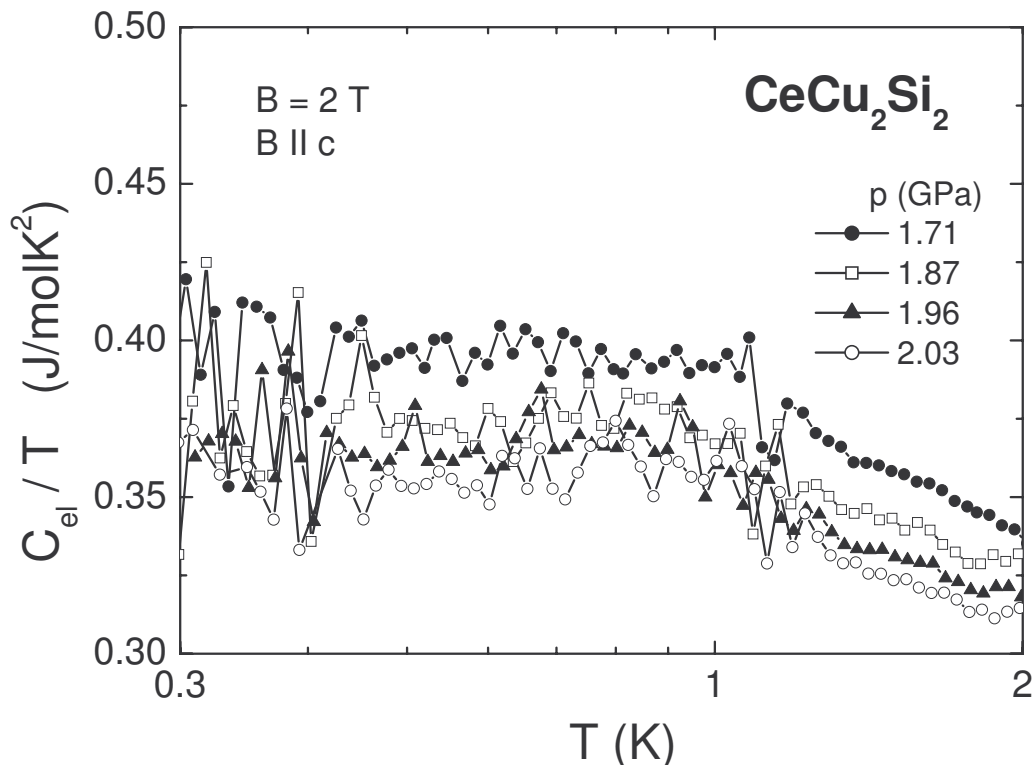


Figure 4.32: Temperature dependence of the low-temperature C_{el}/T of CeCu_2Si_2 obtained for $B = 2$ T, $B \parallel c$, at different pressures. The values of p and the corresponding symbols are indicated in the figure.

$T_c \approx 0.628$ K at about $p_c \approx 0.39$ GPa. Following a slight decrease up to $p \approx 1.5$ GPa, $T_c(p)$ increases again, marking the entrance into the SC2 region. T_c in this region is suppressed much stronger by a magnetic field than in the SC1 region (see data at $B = 0.5$ T and $B = 1$ T in figure 4.33). In addition, with increasing B , the minimum of $T_c(p)$ shifts to higher pressures.

The effect of a magnetic field $B \parallel c$ on the SC in A/S -type CeCu_2Si_2 is shown in figure 4.34 for the whole pressure range $0 \text{ GPa} \leq p \leq 2.1$ GPa. The lines are obtained by fitting the data by using the function described in equation 4.2. For each pressure, the fitting procedure was carried out with $B_{c2}(0)$ and n as variables, while T_c was fixed to the value of $T_c|_{B=0\text{T}}$ obtained at $B = 0$ T from specific-heat measurements. The values obtained for $B_{c2}(0)$ are used as estimates for the upper critical fields and are presented as function of pressure in figure 4.35c. Due to the limited temperature range accessible in our measurements (down to approximately $0.4T_c$), the errors for the determined upper critical fields are relatively large, but a still good estimation of the overall pressure dependence of $B_{c2}(0)$ can be obtained.

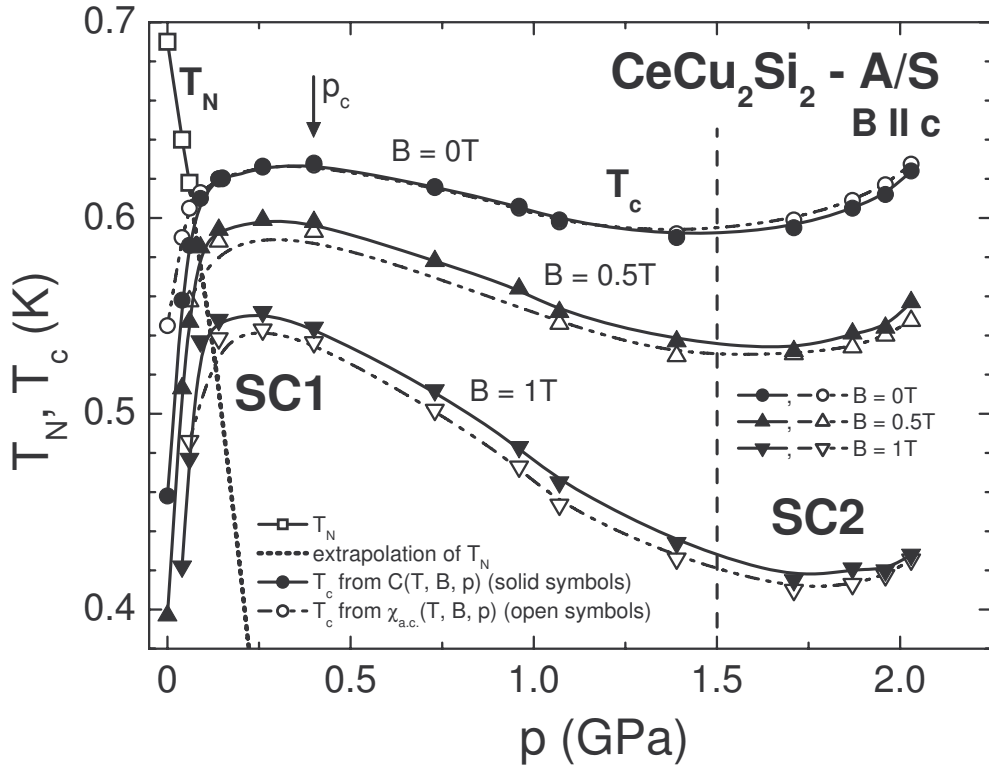


Figure 4.33: Evolution of AFM and SC in single-crystalline A/S -type $CeCu_2Si_2$ under hydrostatic pressure. Variation of T_N under pressure and its extrapolation to $T_N \rightarrow 0$ K (dotted line) are shown only for $B = 0$ T. The estimated critical pressure is indicated by the arrow at $p_c \approx 0.39$ GPa. The evolution of T_c determined from specific-heat (solid symbols) and a.c.-susceptibility (open symbols) measurements is shown for $B = (0, 0.5, 1)$ T ($B \parallel c$). The vertical dashed line indicates, at $p \approx 1.5$ GPa, the estimated border between the low-pressure (SC1), respectively the high-pressure (SC2) SC regions.

The initial slope of the upper critical field, $dB_{c2}(T)/dT|_{T=T_c}$, was calculated for each pressure from the derivative of the function (cf. equation 4.2) used for fitting the experimental $B_{c2}(T)$ data. Accordingly:

$$\left. \frac{dB_{c2}(T)}{dT} \right|_{T=T_c} \text{ (from fit)} = -\frac{B_{c2}(0)n}{T_c}, \quad (4.9)$$

with $B_{c2}(0)$ and n obtained from the fitting procedures. As mentioned earlier, for T_c , the value obtained from the $B = 0$ T $C_{el}(T)/T$ data was taken. We have chosen this way to estimate the initial slope of the upper critical field, due to the fact that $CeCu_2Si_2$ has a relatively low $B_{c2}(0)$ over the whole measured pressure range and our experimental data both from specific-heat and from $\chi_{a.c.}$ measurements are available

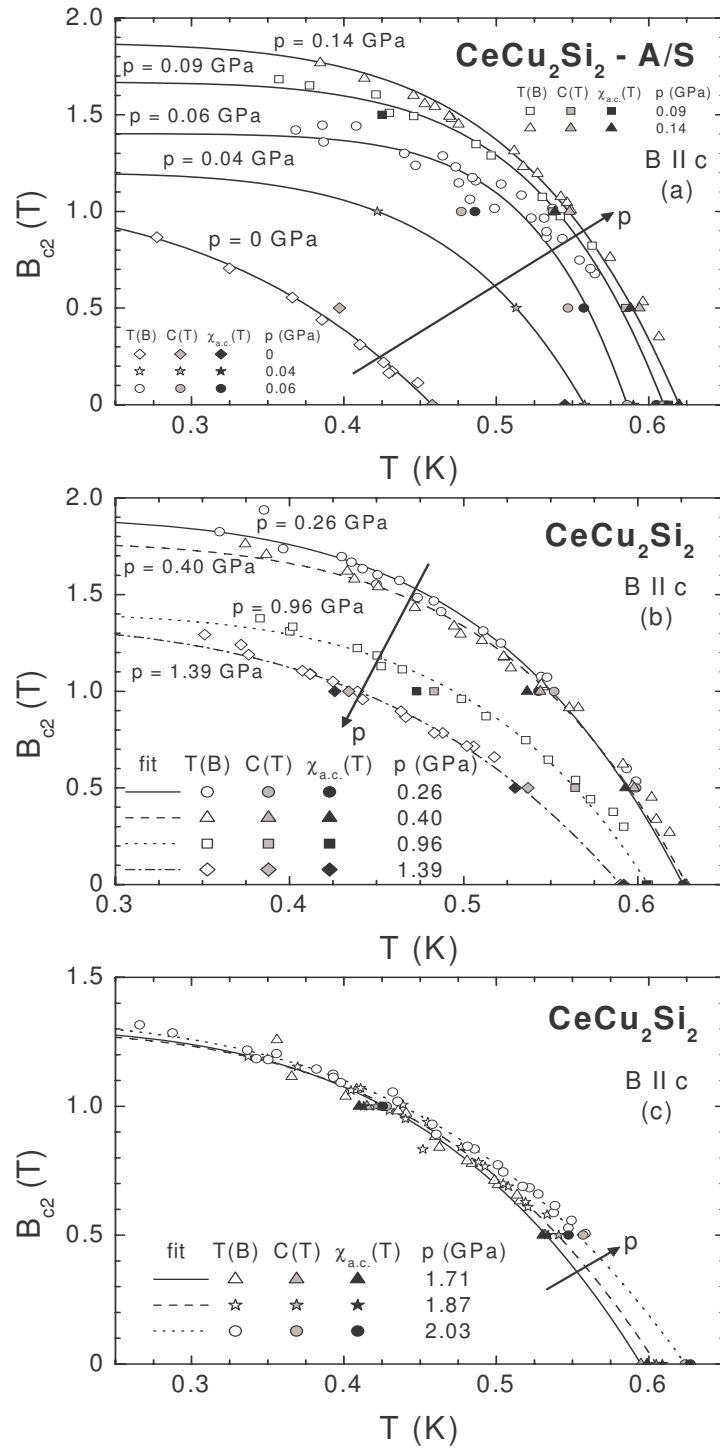


Figure 4.34: $B_{c2}(T)$ versus T for different pressures for A/S -type $CeCu_2Si_2$ for $B \parallel c$. The open symbols represent the data from adiabatic $T(B)$ scans, the gray symbols are used for the values obtained from specific-heat measurements and the black symbols correspond to data from a.c.-susceptibility measurements. The lines correspond to the fits obtained by using the function described in equation 4.2.

only for $B \geq 0.5$ T. However, as a lower estimate for $dB_{c2}(T)/dT|_{T=T_c}$ we have also calculated this value from specific-heat data by using values of T_c obtained at $B = 0$ T and $B = 0.5$ T:

$$\left. \frac{dB_{c2}(T)}{dT} \right|_{T=T_c} \text{ (from } C/T) = \frac{(0 - 0.5)T}{T_c|_{B=0T} - T_c|_{B=0.5T}}. \quad (4.10)$$

The full symbols in figure 4.35b display $(-dB_{c2}(T)/dT|_{T=T_c})$ versus pressure obtained for $B \parallel c$ by using equation 4.9. For comparison, the pressure dependence of $(-dB_{c2}(T)/dT|_{T=T_c})$ calculated by using equation 4.10 is shown by open circles. The absolute value of the initial slope of the upper critical field for $B \parallel c$ shows a rapid increase under pressure up to $p \approx 0.06$ GPa to $(-dB_{c2}(T)/dT|_{T=T_c}) \approx 22.9$ T/K, from where it decreases gradually with increasing pressure. At $p \approx 2.03$ GPa $(-dB_{c2}(T)/dT|_{T=T_c}) \approx 8.4$ T/K, a value close to the value detected at ambient pressure of $(-dB_{c2}(T)/dT|_{T=T_c}) \approx 7.8$ T/K. Except for the steep increase of $(-dB_{c2}(T)/dT|_{T=T_c})$ at very low pressures ($p \leq 0.06$ GPa; $p < p_c^*$), which is similar to the increase of T_c in this pressure region, $(-dB_{c2}(T)/dT|_{T=T_c}) \propto m^*$ is characterizing the system for pressures $p \geq 0.09$ GPa ($p > p_c^*$). In the dirty-limit approximation $(-dB_{c2}(T)/dT|_{T=T_c}) \propto \gamma_n \rho_n$ was predicted by Orlando *et al.* [Orlando 1979], with γ_n being the normal-state electronic specific-heat coefficient and ρ_n the low-temperature normal-state electrical resistivity. Using this dirty-limit approximation for $p \geq 0.09$ GPa, we find a nearly pressure-independent $\rho_n \approx 30 \mu\Omega\text{cm}$. A very light tendency of ρ_n to decrease upon increasing pressure has been found for the mentioned pressure range. Since we have measured a value of $\rho_n \approx 12 \mu\Omega\text{cm}$ at ambient pressure, the value of $\rho_n \approx 30 \mu\Omega\text{cm}$ estimated for higher pressures appears to be too high. It might be possible that the dirty-limit approximation is not the most appropriate.

As mentioned earlier, the upper critical field, $B_{c2}(0)$, was estimated for each pressure by fitting the data with the function described by equation 4.2. The pressure dependence of $B_{c2}(0)$ over the whole measured pressure range is displayed in figure 4.35c for $B \parallel c$. The magnetic field couples to the orbital motion of the charge carriers, yielding an orbital-limiting field, $B_{orb}(0)$, defined by:

$$B_{orb}(0) = h^*(0)T_c \left| \frac{dB_{c2}(T)}{dT} \right|_{T=T_c}, \quad (4.11)$$

where $h^*(0)$ ranges from 0.69 in the dirty limit ($l_{tr}/\xi_0 \ll 1$) to 0.73 in the clean limit ($l_{tr}/\xi_0 \gg 1$), with l_{tr} and ξ_0 representing the mean-free path and the SC coherence length, respectively [Helfand 1966]. The Pauli limit, $B_{Pauli}(0)$, estimated by Yang and Sondhi [Yang 1998] for a SC with $d_{x^2-y^2}$ symmetry is given by:

$$B_{Pauli}(0)|_{d_{x^2-y^2}} = \frac{0.56}{\mu_B} \Delta_0 = (1.78 \text{ T/K}) T_c, \quad \Delta_0 = 2.14 k_B T_c, \quad (4.12)$$

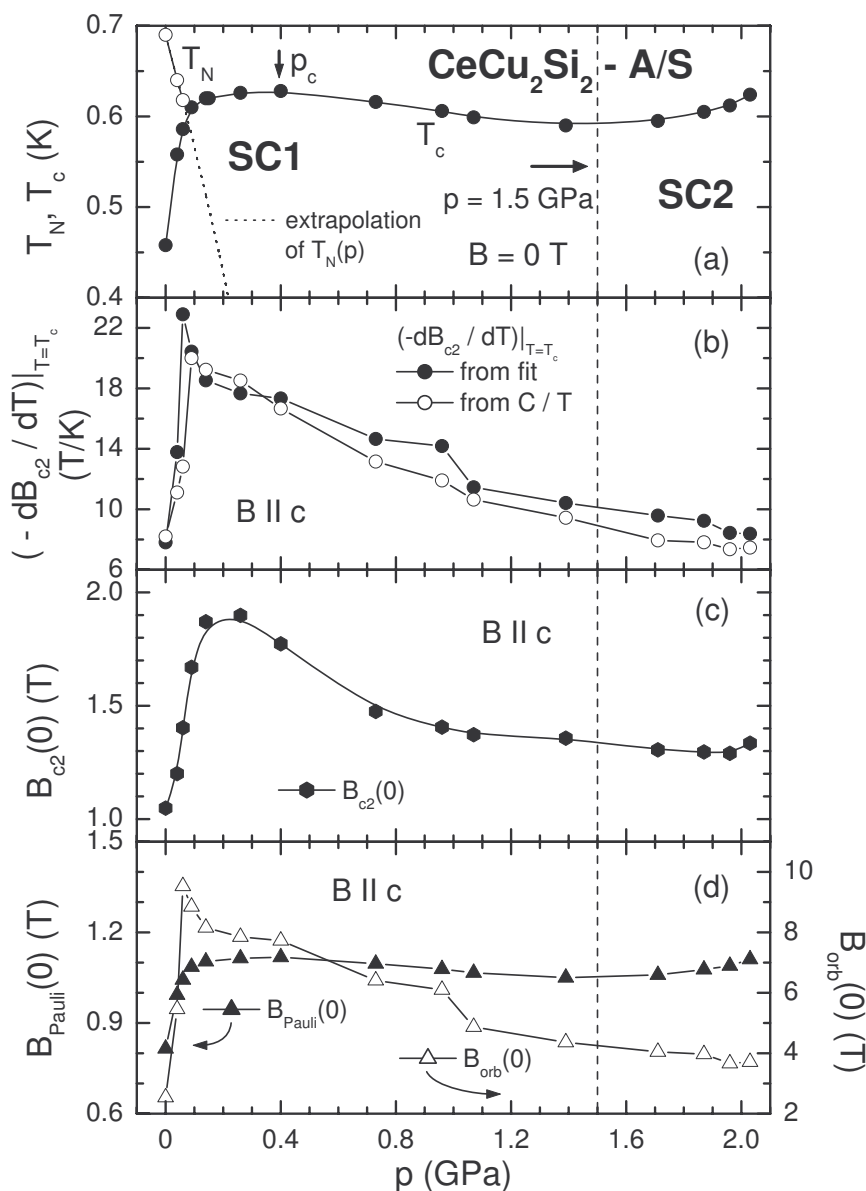


Figure 4.35: (a) T_N and T_c versus pressure obtained at $B = 0$ T for A/S -type CeCu_2Si_2 . The dotted line describes the extrapolation of $T_N(p)$ to $T_N = 0$ K. The critical pressure, $p_c \approx 0.39$ GPa, is indicated by an arrow. The estimated border line between the two SC regions, SC1 and SC2, at $p = 1.5$ GPa is marked over all panels by the vertical dashed line. (b) Pressure dependence of the initial slope of the upper critical field, as $(-dB_{c2}(T)/dT)|_{T=T_c}$ versus p ($B \parallel c$). Full circles show the values obtained by utilizing equation 4.9, while the open symbols describe the values estimated by using equation 4.10 (for details see text). (c) Pressure dependence of the estimated upper critical field - $B_{c2}(0)$ ($B \parallel c$). (d) Pauli-limiting field - $B_{Pauli}(0)$ (left axis - full triangles) and the orbital-limiting field - $B_{orb}(0)$ (right axis - open triangles) versus pressure ($B \parallel c$).

while for the s -wave SC Clogston [Clogston 1962] proposed:

$$B_{Pauli}(0)|_s = \frac{1}{\sqrt{2}\mu_B} \Delta_0 = (1.84 \text{ T/K}) T_c, \quad \Delta_0 = 1.76 k_B T_c. \quad (4.13)$$

Although the symmetry of the SC order parameter is not known, we have estimated the $B_{Pauli}(0)$ for the case of $d_{x^2-y^2}$ symmetry. For calculating $B_{orb}(0)$ we have used for $h^*(0)$ an intermediate value in between the clean and dirty limit of $h^*(0) = 0.71$. For $dB_{c2}(T)/dT|_{T=T_c}$ the values calculated from the fits were used. Figure 4.35d contains the pressure dependence of $B_{Pauli}(0)$ (left axis) and $B_{orb}(0)$ (right axis). For $p < 2.1$ GPa, the values of the Pauli-limiting field are slightly lower than the estimated values for the upper critical field ($B_{Pauli}(0) < B_{c2}(0)$), while the values of the orbital-limiting field are 3 to 4 times higher than $B_{c2}(0)$. These results suggest that in A/S -type $CeCu_2Si_2$ the upper critical field is strongly Pauli limited over the entire pressure range of our measurements, $p < 2.1$ GPa. This indicates that in this pressure range the Cooper pairs in A/S -type $CeCu_2Si_2$ are most likely in a spin-singlet state.

In order to try to estimate the SC order parameter in A/S -type $CeCu_2Si_2$ and its evolution under pressure we have normalized the specific-heat data at $B = 0$ T and compared them with the normalized specific heat calculated theoretically for different order parameters [Volovik 1985, Hasselbach 1993]. In these calculations a single spherical FS was considered [Hasselbach 1993]. A more detailed description of the theoretical estimation was done in section 4.3.1 (see also figure 4.12). Figure 4.36 shows the $B = 0$ T normalized specific-heat data under pressure of A/S -type $CeCu_2Si_2$ together with the theoretically determined data for all SC order parameters allowed for tetragonal symmetry. The figure presents the data as $C_{el}(T)/(\gamma_n T)$ versus T/T_c , where γ_n is $C_{el}/T|_{T=T_c^+}$ in the normal state (right at T_c). The three panels in figure 4.36 refer to different pressure ranges, the calculated curves being the same in all three panels. The symmetry type of the SC gap (Δ_k^2/Δ_0^2), the singlet ($S = 0$) or triplet ($S = 1$) character of the SC state, as well as the expected $C_{el}(T)$ dependence at very low temperatures ($T \ll T_c$), are indicated in the legend of panel (b). The low-pressure data of panel (b), where both AFM and SC anomalies are present in $C_{el}(T)/T$, are not very precise, due to the low accuracy in determining T_c and γ_n . The above-mentioned theoretical estimation is more precise at low temperatures, because there the SC gap function is nearly temperature independent. Therefore, to accurately establish the SC order parameter, experimental data at low temperatures are needed. Our measurements are available only down to approximately $0.5T_c$. Therefore, our results could give just a hint about the character of the SC order parameter. However, the evolution of the SC order parameter under pressure can be determined better.

Except for the data at very low pressures ($p \leq 0.06$ GPa, $p < p_c^*$), we observe a $\Delta C_{el}(T)/T \propto T$ dependence in the SC state at $B = 0$ T over the entire pressure range of our measurements (0.09 GPa $\leq p \leq 2.03$ GPa, $p > p_c^*$). For $p \leq 0.06$ GPa, due to the presence of the AFM phase transition at $T_N > T_c$ and to the yet unclarified type of interplay between AFM and SC, as well as due to the low number of data below T_c , we cannot estimate the $C_{el}(T)/T$ dependence at $T < T_c$. The linear temperature dependence of $C_{el}(T)/T$ in the SC state of CeCu₂Si₂ suggests an unconventional SC gap function with line nodes [Volovik 1985]. Formation of a spin-singlet type SC state in CeCu₂Si₂ (0.09 GPa $\leq p \leq 2.03$ GPa, $p > p_c^*$) is thus concluded [Volovik 1985] (see also introductory part of section 4.3.1). This agrees with the strong Pauli limiting of the upper critical field observed over the entire range of pressure measured, which also suggests a spin-singlet SC state in A/S -type CeCu₂Si₂.

Along with the normalized specific-heat data shown in figure 4.36, the normalized upper critical field curves $B_{c2}(T)/T_c$ versus T/T_c are presented for different pressures in the three panels of figure 4.37. The two figures (4.36 and 4.37) show a clear similarity in the evolution of SC as function of pressure. Two outstanding groups of data under pressure can be observed in both, normalized specific-heat and normalized upper critical field data, both of them presented in panels (a) of figures 4.36 and 4.37. The normalized specific-heat data in the pressure range 0.09 GPa $\leq p \leq 0.4$ GPa scale to a single curve located in the vicinity of the theoretically calculated data for the SC gap symmetries characterized by $\Delta_k^2/\Delta_0^2 \propto k_x^2 + k_y^2$ (triplet pairing, $S = 1$) and $\Delta_k^2/\Delta_0^2 \propto 4k_z^2(k_x^2 + k_y^2)$ (singlet pairing, $S = 0$). For the high-pressure range, 1.71 GPa $\leq p \leq 2.03$ GPa, the measured data scale as well to one curve, that is in the vicinity of the curves theoretically estimated for SC with gap symmetries $\Delta_k^2/\Delta_0^2 \propto (k_x + k_y)^2$ (triplet pairing, $S = 1$) and $\Delta_k^2/\Delta_0^2 \propto 4k_x^2k_y^2$ (singlet pairing, $S = 0$). The data at very low pressures ($p < p_c^*$) shown in figure 4.36b are located between these two groups. At intermediate pressures, starting from $p \approx 0.73$ GPa, the experimental curves are located in between the other two groups and they shift systematically with increasing pressure from the group at lower pressures to the group at high pressures (see figure 4.36c). A similar behavior can be detected from the normalized upper critical field ($B \parallel c$) under pressure presented in figure 4.37. A clear difference in the SC properties seems to exist between the low, 0.09 GPa $\leq p \leq 0.4$ GPa, and high, 1.71 GPa $\leq p \leq 2.03$ GPa, pressure ranges. This strongly suggests different SC order parameters in the SC regions below (SC1) and above (SC2) $p = 1.5$ GPa. The intermediate-pressure region, from $p \approx 0.73$ GPa to $p \approx 1.39$ GPa, (figures 4.36c and 4.37c) may be explained by a superposition of two distinct SC domes, with two different order parameters, existing in the regions around

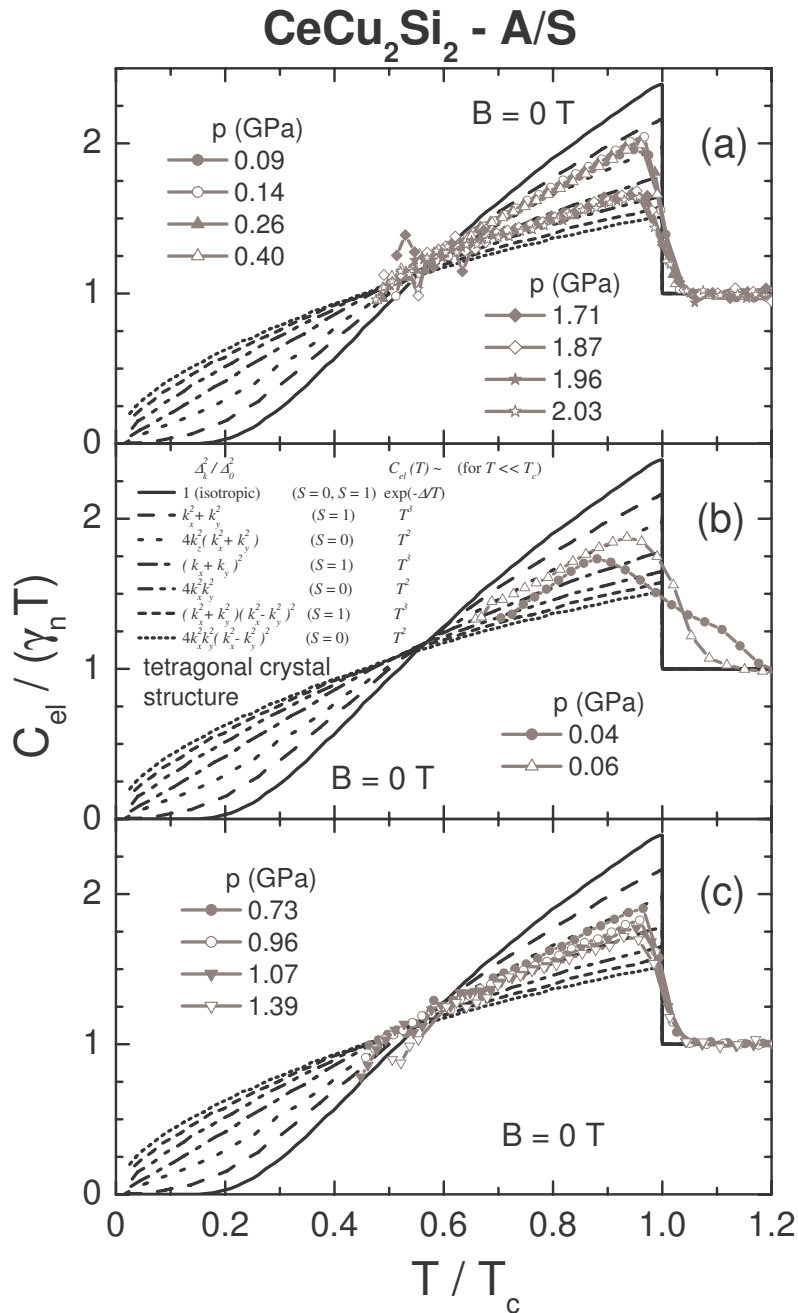


Figure 4.36: Calculated specific heat for different SC gap symmetries allowed for a tetragonal crystal structure (black lines) compared with the experimental data for A/S -type $CeCu_2Si_2$ under pressure (gray symbols). Calculated curves are the same in each of the three panels and were already presented in figure 4.12 [Volovik 1985, Hasselbach 1993]. The corresponding symmetry type of the SC gap function, the parity of the SC state and the expected low-temperature ($T \ll T_c$) behavior of $C_{el}(T)$ are indicated in panel (b). For the experimental data, the different pressures and the corresponding symbols are shown in each panel of the figure. Data at low pressures, presented in panel (b), at $T/T_c > 1$ show the presence of the AFM phase transition.

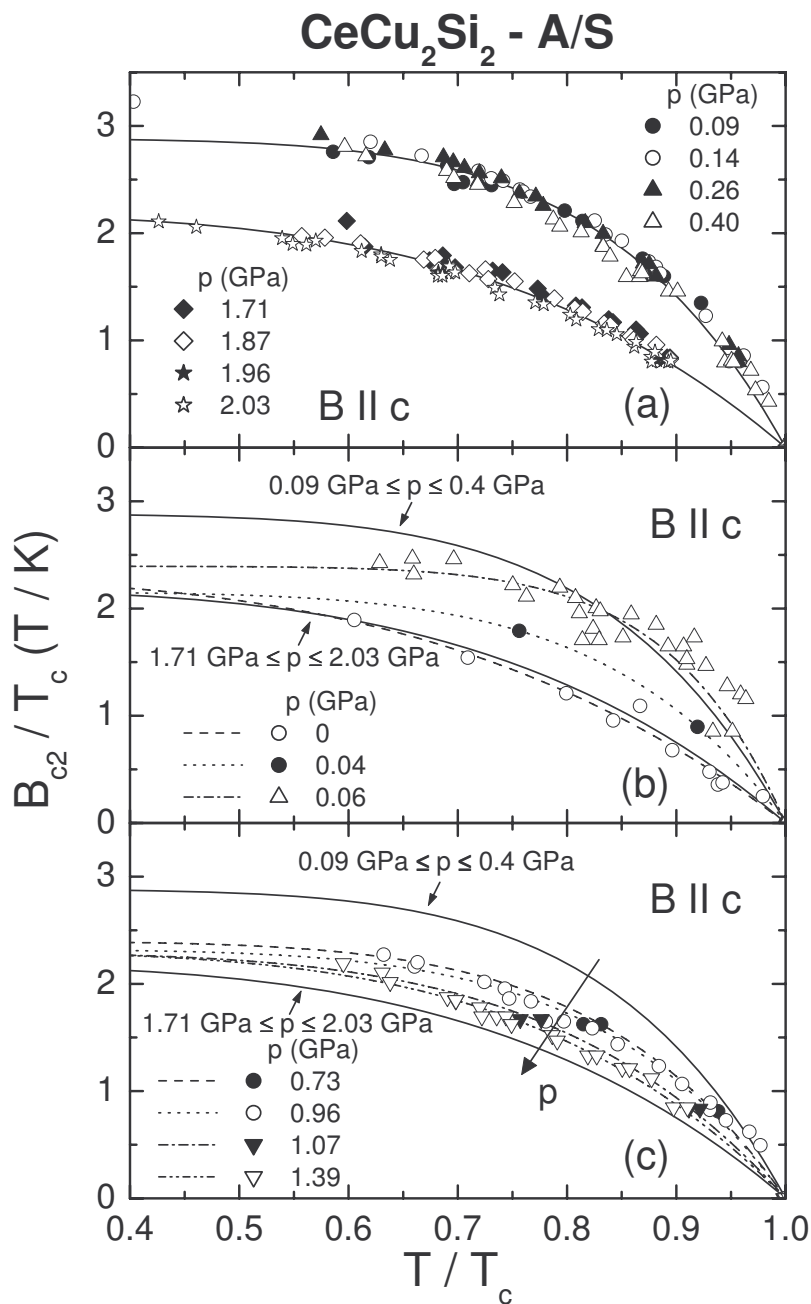


Figure 4.37: $B_{c2}(T)/T_c$ versus T/T_c for different pressures obtained for A/S -type CeCu_2Si_2 , $B \parallel c$. Lines are guides to the eyes and correspond to the curves obtained by fitting the data by use of equation 4.2. For reference, the two continuous lines from panel (a) are reproduced in (b) and (c) (also as continuous lines). The corresponding pressure ranges where the respective lines were used in panel (a) are indicated next to each line.

the magnetic (p_c) respectively valence (p_v) instabilities. This finding is in good agreement with the experimental studies on doped $\text{CeCu}_2(\text{Si}_{1-x}\text{Ge}_x)_2$ ($x \neq 0, 1$), where due to pair breaking caused by alloying-derived atomic disorder, two separated SC

regions (around p_c and around p_v) were observed [Yuan 2003, Yuan 2004] (for details, see section 4.2 and figure 4.8). Reducing the atomic disorder in the undoped compounds, $CeCu_2Si_2$ and $CeCu_2Ge_2$, the two SC domes become broader in temperature and pressure, leading to their merging into a single wide SC region where a clear separation of them is difficult. Concerning the mechanisms which lead to the formation of Cooper pairs, it was suggested that magnetic and valence fluctuations could be responsible for mediating SC in the SC1 and SC2 regions, respectively. Theoretical calculations by Monthoux and Lonzarich suggest the $d_{x^2-y^2}$ spin-singlet Cooper pair state as being most robust for both the magnetic and the valence-fluctuation mediated SC [Monthoux 2004] (for a more detailed description see section 1.2.2). By the theoretical considerations of K. Miyake, the $d_{x^2-y^2}$ spin-singlet SC state for the SC1 region and the d_{xy} spin-singlet SC state for the SC2 region were suggested as being the most favorable ones [Miyake priv. comm.].

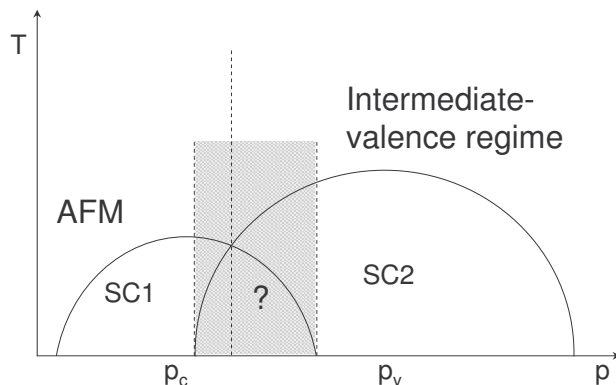


Figure 4.38: Schematic $T - p$ phase diagram describing the unusual SC state observed in the HF compounds $CeCu_2Si_2$ and $CeCu_2Ge_2$.

Figure 4.38 schematically depicts the $T - p$ phase diagram expected for the pure compounds $CeCu_2Si_2$ and $CeCu_2Ge_2$. At low pressures, in the vicinity of the AFM fluctuations, SC is formed in a region centered around p_c (SC1). In this region, AFM spin fluctuations are supposed to mediate the formation of Cooper pairs. At higher pressures, centered around p_v and close to the IV regime, a second SC region (SC2) is expected to exist. In this region, valence fluctuations are supposed to be responsible for the formation of SC. The hatched area in the figure describes the region where the two distinct SC domes (SC1 and SC2) overlap. The minimum of $T_c(p)$ is suggested by the dashed line inside the hatched area. In the case of our measurements on $CeCu_2Si_2$ this line was estimated to be at $p = 1.5$ GPa. Due to the different mechanisms supposed to mediate the formation of Cooper pairs, one may expect different SC properties (in particular, SC order parameters) to exist in

the regions SC1 and SC2. When different SC properties exist in the two SC regions, then this should be clearly observable in the pressure regions outside the hatched area. The situation in the intermediate region (hatched area) is probably more complicated. Different scenarios could be considered for this intermediate area: i) a clear separation of the two SC regions with a phase transition (probably first order) from the SC1 to the SC2 region; ii) a crossover region where both pairing mechanisms are mixed together; iii) a uniform region with the same SC properties everywhere, independent of the different pairing mechanisms. In this latter case no differences are expected to be observed between the SC properties in the SC1 and SC2 regions located outside the hatched area.

As described above, our results clearly reveal different thermodynamic properties in the two SC regions SC1 and SC2. The transition from one SC region to the other one seems to happen smoothly, suggesting the possibility of a more complicated SC state due to the overlapping of the two SC domes. Since the thermodynamic properties in the intermediate-pressure region (hatched area in figure 4.38) do correspond neither to those observed in the region SC1 nor to those in the region SC2, but rather indicate a crossover-like behavior between the two regions (see figures 4.36 and 4.37), the action of both types (AFM spin and valence) of fluctuations in forming the Cooper pairs in the intermediate region may be assumed. Considering the theoretical proposal by K. Miyake [Miyake priv. comm.] of two different SC order parameters in the two distinct SC regions SC1 and SC2, i.e. of $d_{x^2-y^2}$ type symmetry in SC1 and of d_{xy} type symmetry in SC2, the changes observed in the thermodynamic properties displayed in figures 4.36 and 4.37 may be well explained. In their theoretical calculations for the shape of $C_{el}(T)$ at temperatures $T < T_c$ Hasselbach and coworkers [Hasselbach 1993] assumed a single spherical FS. This prevents them from distinguishing between $C_{el}(T)$ corresponding to the $d_{x^2-y^2}$ or d_{xy} type symmetry. However, the real FS of CeCu₂Si₂ is not spherical and is multisheeted (see figure 4.6c). Therefore, an exact correspondence to the theoretical data shown in figure 4.36 is not expected. Due to the strong Pauli limiting of the upper critical field, the possibility of a spin-triplet SC state in CeCu₂Si₂ can be excluded for the entire pressure range of our measurement ($p < 2.1$ GPa). It is worth noting that indeed by looking to figure 4.36a, if we eliminate the possibility of a spin-triplet SC state, in the high-pressure SC region ($1.71 \text{ GPa} \leq p \leq 2.03 \text{ GPa}$) the experimental data fit best to the theoretical curve calculated for the SC state with d_{xy} type symmetry.

As suggested by figures 4.36b and 4.37b, for the pressure region where at $B = 0 \text{ T}$ T_N exceeds T_c , $p \leq p_c^* \approx 0.07 \text{ GPa}$, a SC state different from that seen in the pressure region $0.09 \text{ GPa} \leq p \leq 0.4 \text{ GPa}$ (where $p > p_c^*$) might be expected. The

yet unclear type of interplay between AFM and SC makes it difficult to interpret our data. Due to the reduced temperature range of our measurements and the proximity in temperature of the AFM and SC phase transitions for $p < p_c^*$, our heat-capacity data cannot provide sufficient information concerning the SC state. However, the normalized upper critical field data presented in figure 4.37b are more reliable in this pressure range and indeed show a behavior hinting at different SC states in the pressure ranges below and above p_c^* . Moreover, as depicted by the error bars in figure 4.19, the width of the SC phase transition, detected by our $\chi_{a.c.}(T)$ measurements, also shows different values for the pressure ranges below and above p_c^* . A broad SC phase transition with its width gradually decreasing upon increasing pressure characterizes the system in the pressure region $p \leq p_c^*$, while a narrow, nearly pressure-independent width of the SC phase transition is observed at $p > p_c^*$. These results suggest the possibility that at p_c^* a borderline between two different SC states (SC at $p < p_c^*$ and SC at $p_c^* < 0.09 \text{ GPa} \leq p \leq 0.4 \text{ GPa}$), characterized by different SC properties and possibly by different SC order parameters, may exist in A/S -type $CeCu_2Si_2$. However, in the low-pressure region, $p < p_c^*$, where a transition to the AFM ordered state is detected at temperatures above T_c , no scaling of $B_{c2}(T)/T_c$ versus T/T_c can be observed (see figure 4.37b).

As briefly described in the beginning of section 4.3.1, Cu-NQR measurements under pressure on pure and slightly Ge-doped $CeCu_2Si_2$ suggest different SC properties on the magnetic and the non-magnetic sides of p_c^* [Ishida 1999, Kawasaki 2000, Kawasaki 2001, Kawasaki 2002, Kawasaki 2004, Kitaoka 2005]. In order to support the results obtained by the Cu-NQR measurements, the theoretical work of Fuseya *et al.* [Fuseya 2003] (see section 4.3.1 and figure 4.9) suggests that different SC states with different SC symmetries could be present in the region near the AFM QCP. A gapless p -wave spin-singlet SC (pSS) was proposed for the close vicinity of the AFM QCP (at p_c), on both the magnetic and the PM side of the QCP. With further departing from the AFM QCP an anisotropic d -wave spin-singlet SC state (dSS) was proposed for both sides of the AFM QCP. Both types of SC states were supposed to be mediated by AFM spin fluctuations. A broadening of the SC phase transition in the vicinity of the AFM QCP due to fluctuations of the SC order parameter, fluctuations induced by the AFM fluctuations existing in the system, was also proposed [Fuseya 2003, Kitaoka 2005]. However, the other theoretical approaches presented in section 4.3.1 predict the same symmetry of the SC order parameter over the whole pressure range close to the AFM QCP, namely the d_{xy} type [Steglich 2001] (figure 4.10) or the $\Delta_k \propto (\cos(k_x a) - \cos(k_y a))$ type ($d_{x^2-y^2}$) [Neef 2004] (figure 4.11) spin-singlet order parameters.

Based on our experimental results, it is not possible to clearly define the type of the SC order parameters for the broad SC region observed in A/S -type CeCu_2Si_2 . However, we can suggest that a succession of different SC states occurs with increasing pressure. On the low-pressure side, at $p < p_c^*$, the SC state seems to be different from the SC state at $p_c^* < 0.09 \text{ GPa} \leq p \leq 0.4 \text{ GPa}$. The presence of the AFM ordered state above T_c , as well as the interplay between AFM and SC, could be responsible for the observed difference. However, AFM fluctuations are most likely to mediate the SC pair formation in both of the mentioned SC states. With further increasing pressure, two distinct SC regions, one on the low-pressure side, $0.09 \text{ GPa} \leq p \leq 0.4 \text{ GPa}$, and another on the high-pressure side, $1.71 \text{ GPa} \leq p \leq 2.03 \text{ GPa}$, have been observed. The evolution of the thermodynamic properties suggests that different SC properties exist in the mentioned pressure regions. Moreover, the existence of different types of SC order parameters in the two SC regions is proposed. The main difference between these two SC states could be the different mechanisms implied in the formation of Cooper pairs. AFM spin fluctuations in the low-pressure and valence fluctuations in the high-pressure range could be considered responsible for the formation of the SC states. In the intermediate-pressure region, $0.73 \text{ GPa} \leq p \leq 1.39 \text{ GPa}$, a crossover region from the low-pressure to the high-pressure SC region is expected, where the two distinct SC regions are apparently overlapping. In this pressure region, AFM spin and valence fluctuations might interfere in forming the SC state.

The temperature of the adiabatically isolated pressure cell loaded with the A/S -type CeCu_2Si_2 crystal was monitored while the magnetic field was slowly changed, resulting in different $T(B)$ curves. The crossing of different phase lines is marked by a change of the otherwise nearly constant slope obtained in $T(B)$. Therefore, at the phase transitions, a step-like change is seen in $dT(B)/dB$. The transition temperatures are deduced from the maximum in the second derivative of $T(B)$, $d^2T(B)/dB^2$. The same experiment (meaning the same adiabatic conditions and the same sweeping rate for the magnetic field) carried out with the empty pressure cell in the investigated temperature and magnetic-field range of $T \in [0.26, 0.65] \text{ K}$ and $B \in [0.2, 8] \text{ T}$ gives an almost linear $T(B)$ with $dT(B)/dB \approx 0.028 \text{ K/T}$ when the magnetic field is decreased. Hence, in the case of the pressure cell loaded with the sample, the contribution to $T(B)$ coming from the pressure cell gives only a constant offset in the measured $dT(B)/dB$, which is eliminated in the second derivative. Figure 4.39 shows the data (as B versus T) obtained while crossing the phase line separating the SC state from the normal state in the case of $p \approx 0.40 \text{ GPa}$ ($B \parallel c$). The open symbols in the figure are corresponding to the transition points (T, B_{c2}) obtained from the maximum in $d^2T(B)/dB^2$. The dashed line corresponds to the fit obtained for the

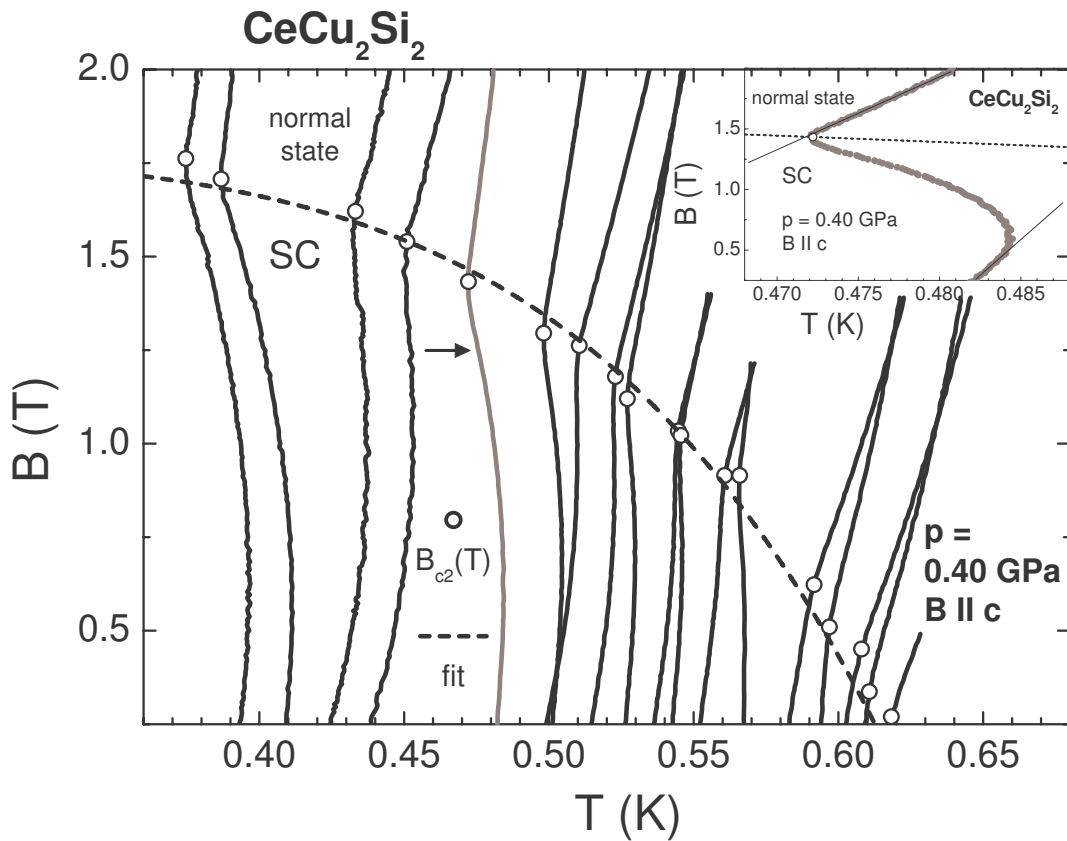


Figure 4.39: Adiabatic $B(T)$ curves of $CeCu_2Si_2$ at $p \approx 0.40$ GPa, for $B \parallel c$. The data are collected on the complete ensemble formed by the pressure cell loaded with the sample. The open symbols represent the transition points obtained for each curve from the maximum in $d^2T(B)/dB^2$. The fitting curve for the temperature dependence of the upper critical field (obtained by using equation 4.2), delimiting the normal state from the SC state, is represented by the dashed line. The gray curve, marked by an arrow, is shown in detail in the inset. The solid lines in the inset are guides to the eyes.

temperature dependence of the upper critical field by using equation 4.2. The gray curve, marked by an arrow, is shown in detail in the inset. Upon decreasing magnetic field, the temperature of the complete ensemble of pressure cell and sample is decreasing linearly (see the upper solid line in the inset), mainly due to the contribution of the pressure cell. When the phase line between the normal and the SC state - marked by the dotted line in the inset - is reached, the temperature of the system starts to rapidly increase until the phase transition is completed. Afterwards the temperature decreases again linearly in the region deep in the SC phase (see the lower solid line in the inset). The phase transition from the normal to the SC state is accompanied by a strong increase in temperature. The real value of the temperature increase due

to the phase transition taking place in the sample is higher than the value seen in the figure due to the fact that the pressure cell is absorbing part of the heat implied in the phase transition. The first and second derivatives of $T(B)$ obtained for four of the curves presented in figure 4.39 are shown in figure 4.40 (see the inset for the corresponding four $B(T)$ curves). Each of these curves, as well as the corresponding derivatives, are marked with labels *a* to *d*. As depicted in figure 4.40, the inflection point of the step-like transition visible in the first derivative (left axis) gives a maximum in the second derivative (right axis). The maxima obtained for the presented data are marked in the figure by arrows and correspond to the phase transitions at $B_{c2}(T)$ shown by open circles in the inset of the figure.

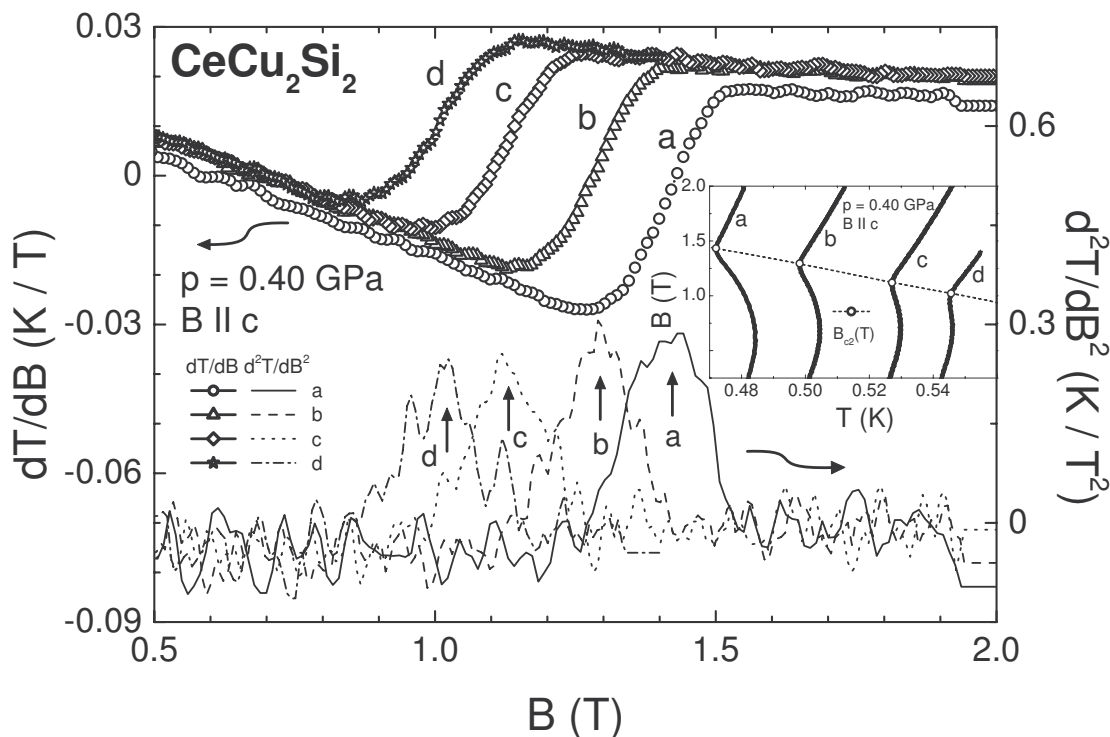


Figure 4.40: $dT(B)/dB$ versus B (left axis) and $d^2T(B)/dB^2$ versus B (right axis) from $T(B)$ ($B \parallel c$) obtained at $p \approx 0.40$ GPa on CeCu_2Si_2 . For $T(B)$ four data sets from figure 4.39 are used. They are shown in detail, as $B(T)$, in the inset of the figure. The arrows, indicating the maxima in the second derivatives, mark the estimated transition points (the corresponding values of T and B_{c2} are shown by open circles in the inset). The dotted line in the inset represents the border between the normal and the SC state.

The real temperature variation of the sample, $T_{\text{sample}}(B)$, in the pressure cell is not accurately determined due to the fact that the sample is in very good thermal contact to the pressure cell and, therefore, only the final temperature of the com-

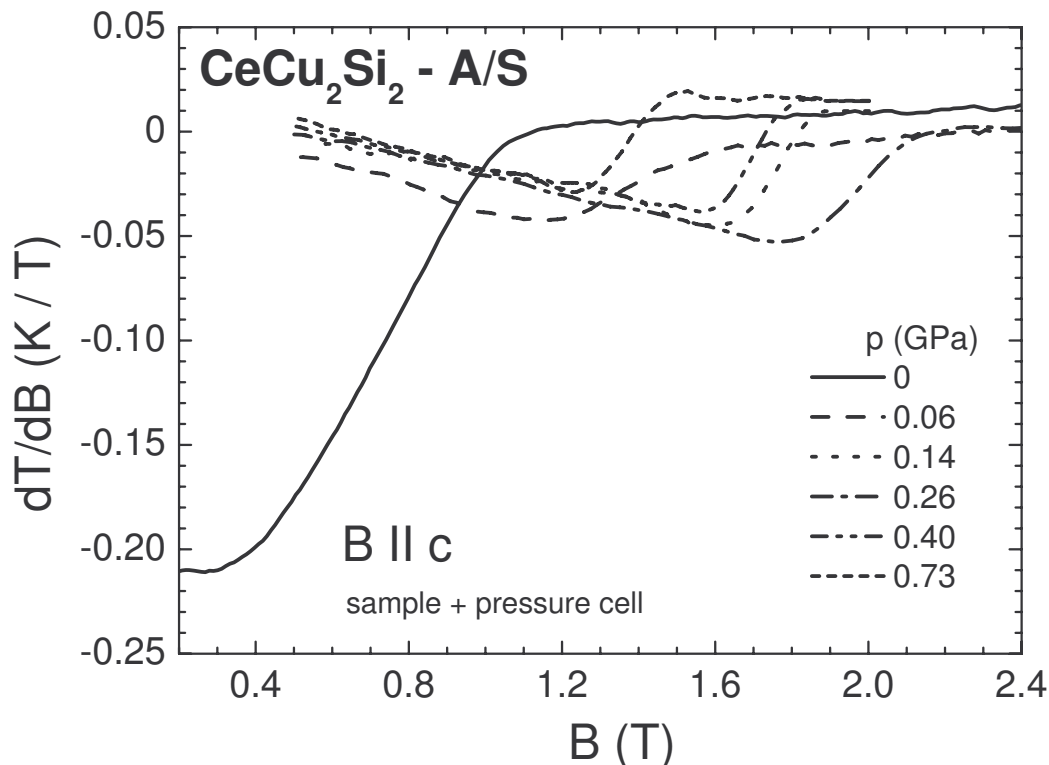


Figure 4.41: $dT(B)/dB$ versus B ($B \parallel c$) at different pressures for A/S -type $CeCu_2Si_2$. The data are obtained on the complete ensemble formed by the pressure cell loaded with the sample. For comparison, for each pressure the data correspond to a SC transition temperature of $\approx (0.6 \div 0.7) T_c(p)|_{B=0T}$.

plete ensemble can be measured (sample and pressure cell are both independently changing their temperature when the magnetic field is varied). Consequently, our experimental data include not only the data obtained from the bare sample, but they also contain the contribution of the pressure cell, which in the case of $dT(B)/dB$ is a constant positive value. Although the sample is measured together with the pressure cell, by looking to the value of the jump height of dT/dB through the step-like phase transition to (or from) the SC state, $\Delta\left(\frac{dT}{dB}\right)|_{B_{c2}}$, we can eliminate the constant contribution to $dT(B)/dB$ due to the pressure cell. $\Delta\left(\frac{dT}{dB}\right)|_{B_{c2}}$ is estimated as the difference between dT/dB at B_{c2} before and after the phase transition. Therefore, we can use the value of $\Delta\left(\frac{dT}{dB}\right)|_{B_{c2}}$ as a measure characterizing only the phase transition taking place in the sample and being independent of the pressure cell in which the sample is contained. As seen in figure 4.40, for a certain pressure (here $p \approx 0.4$ GPa), with lowering the upper critical field, B_{c2} , the value of $\Delta\left(\frac{dT}{dB}\right)|_{B_{c2}}$ at the $B_{c2}(T)$ phase line separating the normal and the SC states is gradually decreasing in the region of

our measurements. For different pressures, a comparison of the size of the step in $dT(B)/dB$ at the $B_{c2}(T)$ phase line, $\Delta\left(\frac{dT}{dB}\right)\Big|_{B_{c2}}$, also accounting for the amount of entropy implied in the phase transition, is shown in figure 4.41. All the data presented in this figure correspond to SC transition temperatures of $\approx (0.6 \div 0.7) T_c(p)|_{B=0T}$. It is worth noting that, depending on the pressure and temperature (and correspondingly magnetic-field) range, the phase transition into the SC state can start from either an AFM or a PM state. The phase transition anomalies represented in figure 4.41 (recorded upon lowering B) correspond to transitions from the AFM to the SC state for $p \leq 0.06$ GPa and to transitions from the PM to the SC state for $p \geq 0.14$ GPa. A considerable difference in $\Delta\left(\frac{dT}{dB}\right)\Big|_{B_{c2}}$ is visible between data at ambient pressure, where $\Delta\left(\frac{dT}{dB}\right)\Big|_{B_{c2}} \approx 0.2$ K/T, and data at higher pressures, $p \geq 0.06$ GPa, where $\Delta\left(\frac{dT}{dB}\right)\Big|_{B_{c2}} \approx 0.06$ K/T. Unfortunately adiabatic $T(B)$ data at pressures between $p = 0$ GPa and $p \approx 0.06$ GPa are not available. However, as also seen in figure 4.41, independent of whether the phase transition takes place from the AFM to the SC state, as in the case of the data at $p \approx 0.06$ GPa, or from the PM to the SC state, as in the case of the data at $p \geq 0.14$ GPa, all data at $p \geq 0.06$ GPa show a similar behavior. They imply a much smaller $\Delta\left(\frac{dT}{dB}\right)\Big|_{B_{c2}}$ when entering the SC phase compared to that in the case of $p = 0$ GPa (about 3 times smaller). Since the heat capacity of the pressure cell is not changing drastically in the investigated pressure and temperature range, the data suggest the possibility of the existence of an extra entropy at the AFM to SC phase transition in magnetic field at ambient pressure, hinting at the possibility of a first-order character of the phase transition. Consistent with the data presented in figure 4.41 for $p = 0$ GPa, over the entire magnetic-field range where we have performed adiabatic $T(B)$ scans at $p = 0$ GPa, $B \gtrsim 0.3$ T, the obtained values for $\Delta\left(\frac{dT}{dB}\right)\Big|_{B_{c2}}$ are much higher compared to the values of $\Delta\left(\frac{dT}{dB}\right)\Big|_{B_{c2}}$ obtained under similar conditions at $p \geq 0.6$ GPa. Moreover, in the case of $p \approx 0.09$ GPa and $p \approx 0.14$ GPa, with decreasing temperature, the step-like phase transition seen in $dT(B)/dB$ crosses a tri-critical point (in the $B - T$ plane) separating the region where the observed phase transitions correspond to transitions from the PM to the SC state (higher T) from the region where transitions from the AFM to the SC state are detected (lower T). It is worth mentioning that no obvious difference in the values of $\Delta\left(\frac{dT}{dB}\right)\Big|_{B_{c2}}$ has been observed while crossing the tri-critical point, suggesting that no significant change in $\Delta\left(\frac{dT}{dB}\right)\Big|_{B_{c2}}$ exists in the case of CeCu_2Si_2 while crossing from the AFM - SC phase line to the PM - SC phase line. Taking into account the above-presented results for $B \parallel c$ on A/S -type CeCu_2Si_2 it is most likely that the considerable difference between $\Delta\left(\frac{dT}{dB}\right)\Big|_{B_{c2}}$ obtained in the case of entering the SC state at ambient pressure compared to higher values of pressure ($p \geq 0.06$ GPa) (see

figure 4.41) is due to a first-order character of the phase transition from the AFM to the SC state in magnetic field at ambient pressure. No hint for a first-order phase transition, neither in the case of the AFM to SC nor in the case of the PM to SC phase transitions, has been observed by the $T(B)$ scans, except for the case of the measurements at ambient pressure.

In A -type $CeCu_2Si_2$ a first-order phase transition, marking the transition from the IC to a commensurate AFM state (“lock-in” transition) was detected by several different types of measurements performed at ambient pressure ([Stockert 2004] and references therein; see also the second phase transition anomaly, below T_N , in $C(T)/T$ of the A -type single crystal shown in figure 4.4). Ambient-pressure neutron-scattering measurements on A/S -type single-crystalline $CeCu_2Si_2$ (prepared from the same batch as the samples used in our experiments) do not show any evidence for this so-called “lock-in” transition at $B = 0$ T [Thalmeier 2005b, Stockert 2006]. Moreover, a disappearance of the magnetic-scattering intensity (see figure 4.11), as well as of the magnetic volume fraction, once SC develops in the system was reported for $B = 0$ T [Thalmeier 2005b, Stockert 2006]. Our measurements of adiabatic $T(B)$ curves at ambient pressure on A/S -type $CeCu_2Si_2$ detect for $B \parallel c$ an additional phase transition (within the AFM phase), marked by T_{NL} (see figure 4.15). Unfortunately, neither its origin nor the complete shape of the $T_{NL}(B)$ phase line can be determined by our measurements. Moreover, an anomaly in $C_{el}(T)/T$ in the AFM phase at $p = 0$ GPa and $B = 2$ T ($B \parallel c$) is observed at a transition temperature which lies on the $T_{NL}(B)$ line determined by the magnetocaloric, $T(B)$, measurements (see figures 4.14 and 4.15). A similar phase line, due to a first-order phase transition, has been observed for $B \parallel c$ by magnetization measurements performed on single-crystalline A/S -type $CeCu_2Si_2$ (see figure 4.7b) [Tayama 2003]. Therefore, it is possible that the phase transition at T_{NL} observed at ambient pressure in A/S -type $CeCu_2Si_2$ ($B \parallel c$) represents a “lock-in” transition marking the entrance into a commensurate AFM phase. However, clear evidence for the origin of the observed phase transition at T_{NL} is still missing. At pressures $p \geq 0.04$ GPa we do not detect (neither below nor above T_c) any sign for a possible transition inside the AFM phase which might correspond to T_{NL} . If we assume that the phase transition at T_{NL} corresponds to the transition from an IC to a commensurate AFM ordered state, it is likely that the appearance (or absence) of the “lock-in” transition in already AFM ordered $CeCu_2Si_2$ is strongly related to the formation of SC. It is probable that, in the case of any $CeCu_2Si_2$ sample which orders AFM, the presence of this phase transition from the IC to the commensurate AFM order is restricted by the formation of the SC state. Independent of pressure or magnetic field, the transition from the

IC to the commensurate AFM state to exist seems to require a T_c which is lower than the temperature where the “lock-in” transition takes place. Indeed, we do not detect any phase transition below T_c , indicating that it is unlikely for the “lock-in” transition to appear in the SC phase. This behavior is similar to our finding that, when cooling below the temperature where SC is stabilized in A/S -type CeCu_2Si_2 , independent of the applied pressure or magnetic field, we never observe a transition into the AFM ordered state. Independent of p or B , the relative distance between T_N and T_c ($T_N > T_c$) seems to play an important role in the appearance of the “lock-in” transition. Guided by the distance between T_N and T_c , it could be speculated that a transition from an IC to a commensurate AFM phase before the system enters the SC state is very unlikely to take place in the pressure range $p \geq 0.04$ GPa (at least in the temperature range of our measurements, $T \geq 0.26$ K), but it is very probable to occur in the case of A/S -type CeCu_2Si_2 at ambient pressure. Therefore, from our measurements the presence of a transition from the IC to a commensurate AFM state should be considered at $p = 0$ GPa. Since the “lock-in” transition to the commensurate AFM ordered state seen in A -type CeCu_2Si_2 (as well as in other HF AFM compounds changing their order from IC to commensurate) is a first-order phase transition ([Stockert 2004] and references therein), one can expect that the “lock-in” transition, once existing in case of A/S -type CeCu_2Si_2 , should be also of first order.

Our measurements of the heat capacity employing the compensated quasiadiabatic heat-pulse technique, a technique which implies that measurements can be done only on increasing temperature, do not allow us to verify the existence of a hysteretic effect as indication for the first-order character of a phase transition. Therefore, measurements of the specific heat for different magnetic fields, $B \parallel c$, on several single crystals of A/S -type CeCu_2Si_2 grown in the same batch as the sample measured in the pressure cell were performed at ambient pressure with a relaxation-time technique in a Quantum Design PPMS. This technique allows measurements to be performed in both directions upon cooling and upon warming the system, offering the chance to detect hysteretic behavior. As an example, the electronic specific heat obtained at ambient pressure on one of the A/S -type CeCu_2Si_2 single crystals is shown in figure 4.42 for $B = 0$ T and $B = 0.2$ T ($B \parallel c$). As indicated by the arrows, the full symbols represent the data taken on increasing, while the open symbols show the data obtained on decreasing temperature. Upon lowering the temperature, from slightly below T_N a clear hysteretic behavior can be observed in both panels. The hysteretic behavior seems to be present down to the lowest temperature of our measurements of $T \approx 0.36$ K. At this lowest temperature the SC phase transition is not yet completed for both values of B shown in figure 4.42. Independent of the value of B ,

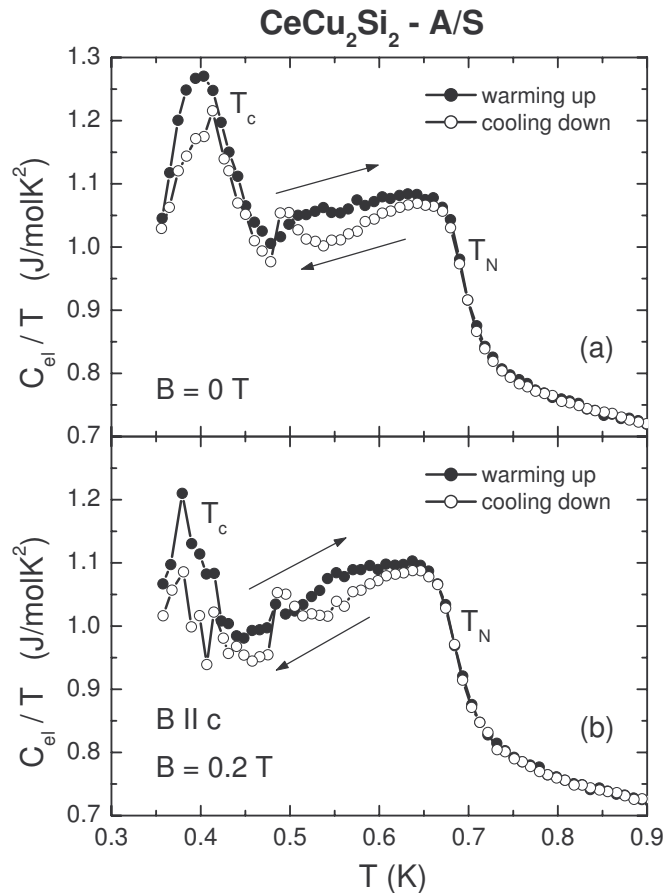


Figure 4.42: Ambient-pressure $C_{el}(T)/T$ of A/S -type single-crystalline $CeCu_2Si_2$ for $B = 0$ T, panel (a), and $B = 0.2$ T ($B \parallel c$), panel (b). Measurements have been performed in a Quantum Design PPMS, upon warming (full circles) and upon cooling (open circles) the system. For both values of B , hysteretic behavior can be observed for $T < T_N$.

the hysteretic behavior observed in the broad temperature range from slightly below T_N down to the lowest temperature of our measurements suggests that the phase transition from the AFM to the SC state is of first order. However, the possibility of a first-order type “lock-in” transition taking place somewhere between T_N and T_c should not be neglected. The magnetocaloric measurements, where in magnetic field we detect the additional transition at T_{NL} between T_N and T_c , in good agreement with the measurements presented in figure 4.42, also hint at the first-order type of the phase transition from the AFM to the SC state. Suggested by the high value of $\Delta(\frac{dT}{dB})|_{B_{c2}}$ at the SC phase transition at ambient pressure, that is about three times larger than the value observed at higher pressures, and by the fact that the hysteretic behavior found in the ambient-pressure $C_{el}(T)/T$ measurements is present down to

temperatures below T_c , it seems likely that the phase transition from the AFM to the SC state in A/S -type CeCu_2Si_2 at ambient pressure, independent of whether the “lock-in” transition is present or not, is of first order. Moreover, this finding seems to hold for $B = 0$ T, as well as for non-zero values of the magnetic field ($B \parallel c$). In correlation with the steep increase of T_c with p at very low pressures, with a maximum value at ambient pressure of $dT_c/dp|_{p=0\text{GPa}} \approx 2.5$ K/GPa (at $B = 0$ T), we have seen that the AFM to SC phase transition in A/S -type CeCu_2Si_2 seems to be of first order only at ambient pressure (at $B = 0$ T as well as at $B \neq 0$ T, $B \parallel c$). In addition, we find the AFM to SC phase transition to become either of second order or weakly first-order like already at small finite pressure, where dT_c/dp is substantially reduced compared to the ambient-pressure value. The very broad SC phase transition anomaly detected by our $\chi_{a.c.}(T)$ measurements at ambient pressure and the gradual narrowing of the SC phase transition anomaly upon slightly increasing pressure (see figures 4.17 and 4.19) could also support the above-discussed findings. However, the strong AFM fluctuations present at very low pressures in the close vicinity of the SC phase could also induce the observed broadening of the SC phase transition anomaly.

It should be noted that from our measurements on CeCu_2Si_2 we could not elucidate whether the AFM ordered state exists or not in the system once SC has formed, neither for the case when $T_N > T_c$ nor for the case when T_N is supposed to be smaller than T_c . Therefore, while presenting our data, over the entire chapter, we do not exclude the possibility that AFM order could exist below T_c .

The low-temperature entropy of CeCu_2Si_2 is continuously decreasing upon increasing pressure, as expected for Ce-based HF systems. The evolution of the $B = 0$ T entropy versus temperature for different pressures, measured in A/S -type CeCu_2Si_2 is shown in figure 4.43. The Kondo temperature, T_K , of the system can be roughly estimated from specific-heat measurements based on the single-impurity Kondo model for spin $S = 1/2$ systems [Desgranges 1982] as about twice the temperature where the entropy reaches the value of $S(T_K/2) = 0.5R \ln 2$. The open symbols in the inset of figure 4.43 show the estimated T_K over the measured pressure range. With increasing pressure, the strength of the hybridization between the Ce $4f$ electrons and the conduction electrons increases and causes an increase of T_K . Due to the fact that our measurements were performed only up to $T = 7$ K, the estimation of T_K had to be done by extrapolating the obtained $S_{el}(T)$ curves to higher temperatures. Thus, the accuracy in determining T_K is not very high especially in the high-pressure region. In the same theoretical work of Desgranges and Schotte [Desgranges 1982] mentioned above, it was proposed that T_K can be also estimated from the low-temperature specific heat, i.e. $T_K \approx R\pi/(3\gamma)$, where γ represents C_{el}/T as $T \rightarrow 0$ K. The full symbols

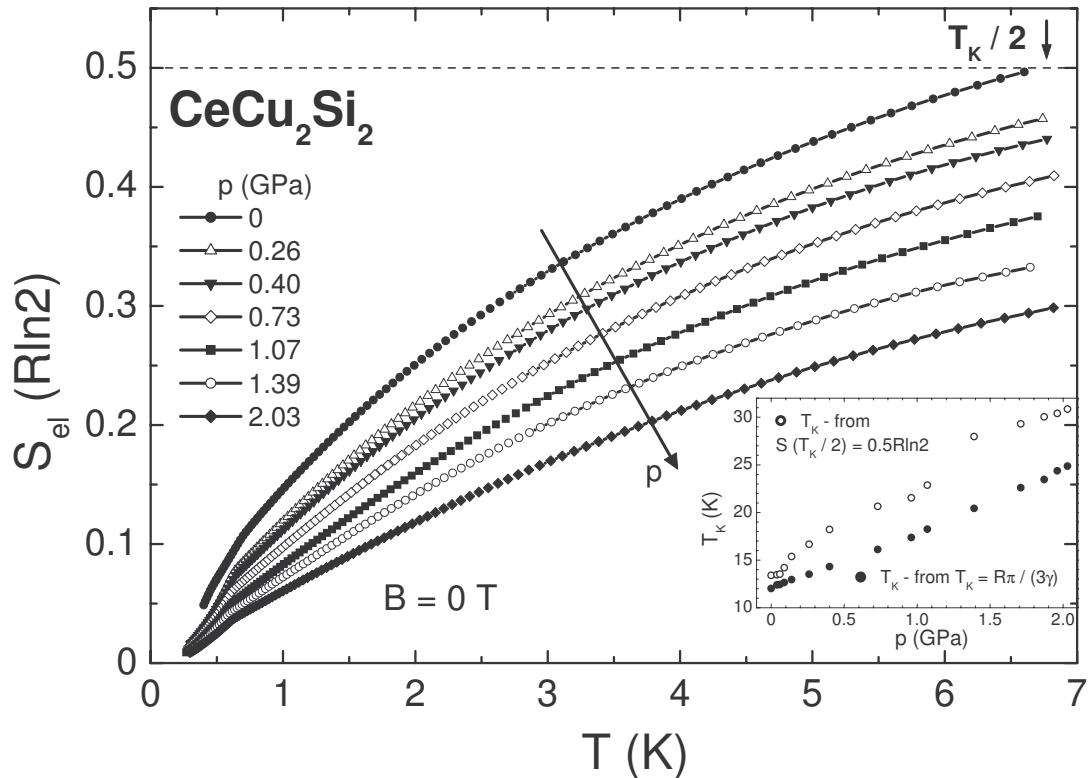


Figure 4.43: Evolution of the low-temperature entropy of $CeCu_2Si_2$ under pressure for $B = 0$ T. The value of $S = 0.5R \ln 2$ is marked by the dashed line and represents the entropy which according to the single-impurity Kondo model for spin $S = 1/2$ systems should be obtained at about $T_K/2$ [Desgranges 1982]. The same model predicts that $T_K \approx R\pi/(3\gamma)$, where γ represents the value of C_{el}/T taken at $T \rightarrow 0$ K [Desgranges 1982]. The inset contains the variation with pressure of the estimated Kondo temperatures, T_K . Open symbols show the values of T_K obtained by using the high-temperature entropy of the system - $S(T_K/2) = 0.5R \ln 2$ -, while the full circles correspond to the values of T_K calculated by using $T_K \approx R\pi/(3\gamma)$. For γ the experimentally obtained values of C_{el}/T taken at $T = 0.9$ K, $C_{el}/T|_{T=0.9K}$, have been considered.

in the inset of figure 4.43 show the values of T_K obtained by using the above-mentioned relation. Due to the presence of the AFM and/or SC states at low temperatures at $B = 0$ T, we have used for γ the values of C_{el}/T taken at $T = 0.9$ K, a temperature exceeding any transition temperature over the entire measured pressure range ($T_N, T_c < 0.9$ K for $p < 2.1$ GPa). As seen in the inset of figure 4.43, the values of T_K obtained in both ways are in quite good agreement at low values of p . As expected, at higher pressure values the discrepancy between the two curves is increasing and probably the values of T_K obtained by using the relation depending on the low-

temperature values of C_{el}/T are more reliable. The overall pressure dependence of T_K , independent of the way T_K was estimated, shows a pressure-induced increase of T_K , a behavior expected for Ce-based HF systems.

As mentioned already, the effect of pressure on Ce-based HF compounds is to increase the hybridization strength between the $4f$ electrons and the conduction electrons. Sufficiently high pressure causes a partial delocalization of the $4f$ electrons, replacing the HF state by an IV state. The transition from the HF to the IV state might be of first order accompanied by a symmetry-conserving collapse of the unit-cell volume [Röhler 1988]. As described in the introductory part of section 4.3.2, the evolution of m^* , the effective mass of the QPs, is a good measure of such a transition (see equation 4.4). m^* can be obtained from the Sommerfeld coefficient, γ , of the electronic specific heat ($m^* \propto \gamma$; $C_{el}(T) = \gamma T$ in metals - see equation 1.5). Due to the fact that at $B = 0$ T, the SC state is present in CeCu₂Si₂ at low temperatures over the entire pressure range of our measurements, we need to estimate the Sommerfeld coefficient, γ , from specific-heat measurements at temperatures $T > T_c$. In addition, the AFM ordered state at low pressures has to be considered. Therefore, in order to be above any transition temperature (either T_N or T_c) over the whole studied pressure range (in the PM state), we have chosen the value of C_{el}/T at $T = 0.9$ K, $C_{el}/T|_{T=0.9K}$, to estimate γ ($C_{el}/T|_{T=0.9K} \approx \gamma \propto m^*$). In figure 4.44b, the variation with pressure of the electronic specific-heat coefficient taken at $T = 0.9$ K, $C_{el}/T|_{T=0.9K}$, is shown. Our experiments reveal that for the low-pressure range, $p \leq 1.5$ GPa, $C_{el}/T|_{T=0.9K}$ decreases with $d \ln(C_{el}/T|_{T=0.9K})/dp \approx -0.373$ /GPa while for the high-pressure region $1.5 \text{ GPa} \leq p \leq 2.1 \text{ GPa}$ $d \ln(C_{el}/T|_{T=0.9K})/dp \approx -0.303$ /GPa. The reduction of $d \ln(C_{el}/T|_{T=0.9K})/dp$ at $p \approx 1.5$ GPa, right in the region where the SC transition temperature starts to increase, might indicate a smooth transition from the HF state to a metallic state with an increased electronic density of states. As seen in figures 4.36, 4.37 and 4.44b, the occurrence of a broad region of SC with different electronic properties in different pressure regions supports the existence of two distinct pairing mechanisms in the two SC regions merging to one in CeCu₂Si₂. As concluded from figures 4.36a and 4.37a, the existence of different order parameters for the different SC regions could be expected too.

As briefly described earlier, for A/S -type CeCu₂Si₂ at $B = 0$ T the low-temperature dependence of the electronic specific heat in the SC state ($T < T_c$) has also been studied. For pressures $p \leq 0.06$ GPa where the AFM state is still detected in our measurements at $B = 0$ T the estimation of the $C_{el}(T)$ dependence below T_c cannot be done accurately due to the yet unclear type of the interplay between the AFM and the SC states (coexistence or competition). For this pressure

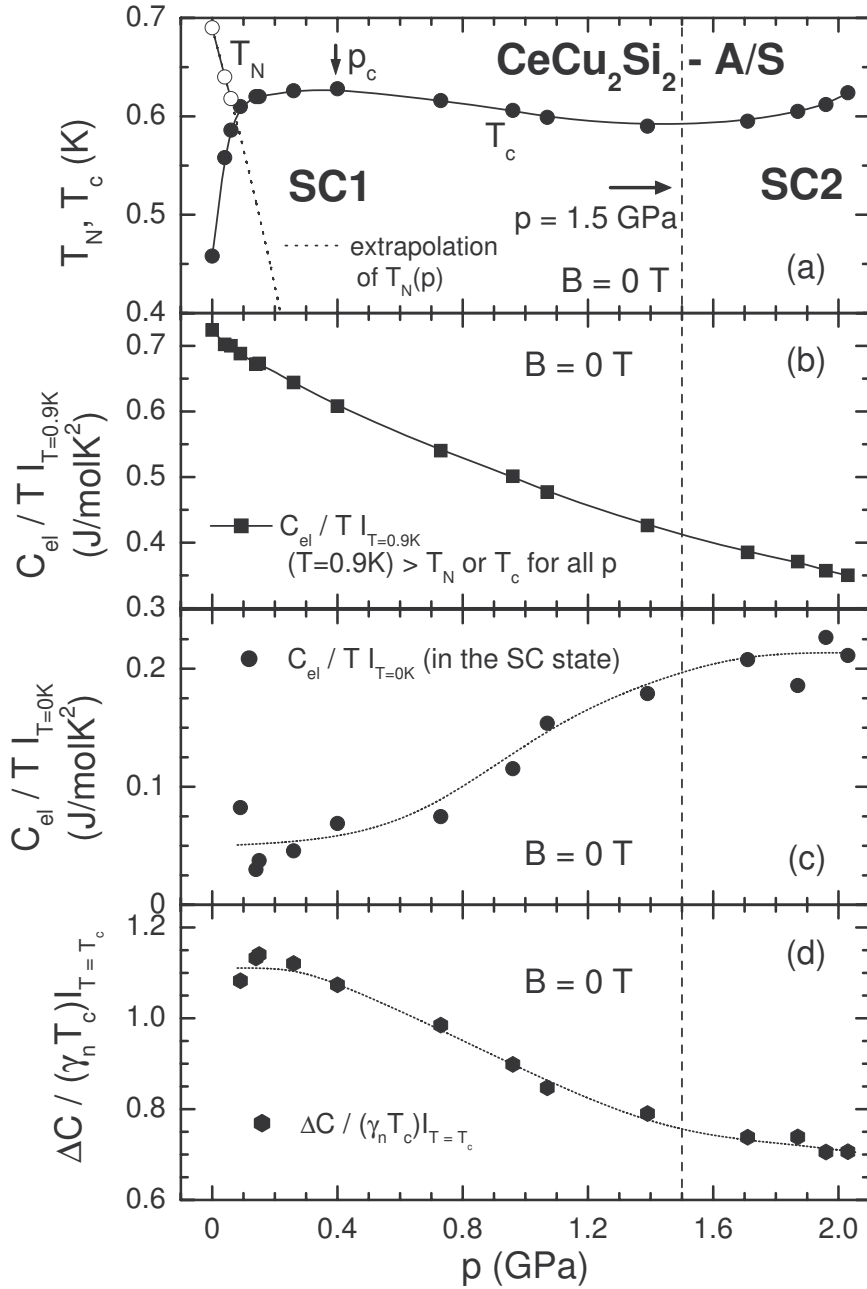


Figure 4.44: Pressure dependence of different physical properties of A/S -type $CeCu_2Si_2$ obtained at $B = 0$ T ($p < 2.1$ GPa). The estimated border line between the two SC regions, at $p = 1.5$ GPa, is marked over all panels by the vertical dashed line. (a) T_N and T_c versus pressure obtained from specific-heat measurements. The dotted line describes the extrapolation of $T_N(p)$ to $T_N = 0$ K. The obtained critical pressure, $p_c \approx 0.39$ GPa, is indicated by an arrow. (b) C_{el}/T taken at $T = 0.9$ K, as $C_{el}/T|_{T=0.9K}$ versus pressure. (c) C_{el}/T estimated at $T = 0$ K, in the SC state, as $C_{el}/T|_{T=0K}$ versus pressure. (d) $\Delta C / (\gamma_n T_c)|_{T=T_c}$ versus pressure.

range the narrow temperature interval below T_c obtained by our experiment also limits the possibilities to study $C_{el}(T)$ at $T < T_c$. For $0.09 \text{ GPa} \leq p \leq 2.03 \text{ GPa}$ $C_{el}(T)/T$ in the SC state shows a linear temperature dependence, $\Delta C_{el}(T)/T \propto T$, down to the lowest temperatures of our measurements. It is worth noting that in this pressure range, $C_{el}(T)$ data down to $T \approx 0.5T_c$ are available. We have estimated the expected C_{el}/T for $T = 0 \text{ K}$, $C_{el}/T|_{T=0\text{K}}$, by extrapolating the obtained linear temperature dependencies of $C_{el}(T)/T$ (for $T < T_c$) to $T = 0 \text{ K}$. The effect of pressure on $C_{el}/T|_{T=0\text{K}}$ is shown in panel (c) of figure 4.44. The values of $C_{el}/T|_{T=0\text{K}}$, ranging from about $C_{el}/T|_{T=0\text{K}} \approx 0.05 \text{ J}/(\text{molK}^2)$ in the low-pressure region ($0.09 \text{ GPa} \leq p \leq 0.40 \text{ GPa}$) to about $C_{el}/T|_{T=0\text{K}} \approx 0.2 \text{ J}/(\text{molK}^2)$ in the high-pressure side ($1.71 \text{ GPa} \leq p \leq 2.03 \text{ GPa}$), show a smooth crossing from the region at low p with nearly pressure-independent values of $C_{el}/T|_{T=0\text{K}}$ to the region at high p , where $C_{el}/T|_{T=0\text{K}}$ is also almost pressure independent. A SC with a completely gapped FS should exhibit $C_{el}/T|_{T=0\text{K}} = 0 \text{ J}/(\text{molK}^2)$. Over the mentioned pressure range, the relatively low, but non-zero values of $C_{el}/T|_{T=0\text{K}}$ in the SC state of CeCu_2Si_2 suggest the possibility that at $T = 0 \text{ K}$ on a small fraction of the FS a SC gap does not exist. The variation with pressure of the ratio between $C_{el}/T|_{T=0\text{K}}$ and $C_{el}/T|_{T=0.9\text{K}}$ could hint at the pressure dependence of the fraction of the FS that does not form a SC gap. However, due to the fact that in our measurements we do not know the real $C_{el}(T)$ dependence at very low temperatures (we measured only down to $T \approx 0.5T_c$), a precise estimation of the fraction of ungapped FS cannot be done.

The $\Delta C/(\gamma_n T_c)|_{T=T_c}$ ratio at $B = 0 \text{ T}$ exhibits in the case of A/S -type CeCu_2Si_2 values ranging from $\Delta C/(\gamma_n T_c)|_{T=T_c} \approx 1.1$ at $p \approx 0.09 \text{ GPa}$ to $\Delta C/(\gamma_n T_c)|_{T=T_c} \approx 0.7$ at $p \approx 2.03 \text{ GPa}$, the highest pressure achieved in our measurements. The values of $\Delta C/(\gamma_n T_c)|_{T=T_c}$ obtained in this pressure range ($0.09 \text{ GPa} \leq p \leq 2.03 \text{ GPa}$), similar to those observed at lower pressures, $p \leq 0.06 \text{ GPa}$ (see table 4.1), are all smaller than the value known from the BCS theory of $\Delta C/(\gamma_n T_c)|_{T=T_c} \approx 1.43$. As already suggested by the normalized electronic specific heat presented in the panels (a) and (c) of figure 4.36, $\Delta C/(\gamma_n T_c)|_{T=T_c}$ shows a nearly pressure-independent value of about $\Delta C/(\gamma_n T_c)|_{T=T_c} \approx 1.1$ in the low-pressure range $0.09 \text{ GPa} \leq p \leq 0.40 \text{ GPa}$. Similar to this behavior, in the high-pressure region, $1.71 \text{ GPa} \leq p \leq 2.03 \text{ GPa}$, a nearly pressure-independent value of $\Delta C/(\gamma_n T_c)|_{T=T_c} \approx 0.7$ is found. For the intermediate-pressure range, $0.73 \text{ GPa} \leq p \leq 1.39 \text{ GPa}$, values showing a smooth transition from the low- to the high-pressure region are observed.

The behavior of the thermodynamic properties of A/S -type CeCu_2Si_2 presented in figure 4.44 shows that while crossing from the SC region at low pressures (SC1)

to that at high pressures (SC2) an observable, but not abrupt change was detected in any of the presented physical properties. Moreover, a smooth crossover from the region where SC exists in the vicinity of strong AFM spin fluctuations (SC1) to the high-pressure SC region (SC2) dominated by valence fluctuations is observed.

4.4 Discussion

We have studied the pressure ($p < 2.1$ GPa) and magnetic-field ($B \leq 8$ T) dependence of the low-temperature ($0.26 \text{ K} \leq T \leq 7 \text{ K}$) electronic specific heat of the ambient-pressure HF AFM and SC, $CeCu_2Si_2$. Low-temperature a.c.-susceptibility and magnetocaloric measurements have been performed as well. The experiments were carried out on an A/S -type $CeCu_2Si_2$ single crystal, with the magnetic field oriented $B \parallel c$. As a result of a strong interaction between the Kondo and the RKKY type interactions, HF behavior, shown by a large electronic specific-heat coefficient $C_{el}/T \approx 0.73 \text{ J}/(\text{molK}^2)$ at $T = 0.9 \text{ K}$, as well as AFM order, is present at low temperatures and ambient pressure. Moreover, at temperatures lower than the temperature where the system orders AFM, $T_N \approx 0.69 \text{ K}$, a SC state is formed below $T_c \approx 0.46 \text{ K}$. We have seen that, as expected for Ce-based HF compounds, the application of pressure leads to the suppression of T_N . In the case of $CeCu_2Si_2$, this is accompanied by a rapid increase of T_c . A very small pressure of $p_c^* \approx 0.07 \text{ GPa}$ leads to $T_N(p) = T_c(p)$. At pressures $p > p_c^*$ and $B = 0 \text{ T}$ only the phase transition to the SC state can be observed by our measurements and no phase transition anomaly which could mark the entrance into the AFM ordered state can be detected neither below nor above T_c . Both ordered states, AFM and SC, are suppressed by the application of magnetic field. While SC is rapidly destroyed by an external magnetic field, the AFM ordered state is much more robust against it. As a result, at $p > p_c^*$, for certain values of p and B , T_N becomes larger than T_c and, therefore, both phase transitions to the AFM and to the SC state can be observed in $CeCu_2Si_2$. A phase transition anomaly marking the entrance into the AFM ordered state has been observed by our measurements at $p > p_c^*$ only when a magnetic field sufficiently high to suppress SC was applied. The rapid increase of T_c at low pressures holds only for $p \leq p_c^*$. At pressures above p_c^* , where no phase transition to the AFM state is observed at $B = 0 \text{ T}$, T_c is only slightly increasing further with increasing pressure. A maximum value of T_c is detected at $p \approx 0.4 \text{ GPa}$. Upon increasing the pressure further one observes a slight decrease of T_c , until a minimum of $T_c(p)$ is obtained at $p \approx 1.5 \text{ GPa}$. Above $p \approx 1.5 \text{ GPa}$, T_c starts to increase again with increasing pressure. The borderline between the SC state in the pressure region around the AFM instability, SC1, and the SC state in

the high-pressure region, SC2, in the vicinity of a valence instability of Ce has been assumed to be at about the pressure $p = 1.5$ GPa where $T_c(p)$ has its minimum value.

In the relatively broad SC region studied by our measurements, different SC properties have been identified. The two main SC regions reported in literature [Yuan 2003], supposed to be distinct due to the different mechanisms implied in the formation of the Cooper pairs, have been observed in our measurements by a difference in the measured thermodynamic properties. In the SC1 state, SC is likely to be mediated by AFM spin fluctuations. In the high-pressure SC state, marked by SC2, valence fluctuations are expected to mediate the formation of Cooper pairs. Distinct scaling laws of $C_{el}(T)/(\gamma_n T)$ versus T/T_c and of $B_{c2}(T)/T_c$ versus T/T_c in these two different SC regions have been observed. Therefore, the existence of different SC order parameters in the two SC regions is suggested by our measurements. This agrees with the different mechanisms supposed to be implied in the formation of the two distinct SC states in CeCu₂Si₂ (e.g. [Monthoux 2001, Monthoux 2004]). Based on the experimental results and corroborated by theoretical considerations, a possible change of the SC order parameter in CeCu₂Si₂, from the $d_{x^2-y^2}$ type in the vicinity of the AFM ordered state (SC1) to d_{xy} type in the vicinity of a state characterized by valence instability (SC2), has been discussed. Aside from the physical properties characterizing the SC states of CeCu₂Si₂ in the two distinct SC regions, the SC state in the crossover region between the AFM and the valence instability has been also studied. We have seen no abrupt change in any of the measured physical properties on going from the region SC1 to region SC2. However, the transition from one SC region to the other is clearly distinguishable in almost all measured physical properties. The electronic specific-heat coefficient, $C_{el}/T|_{T=0.9K}$, considered an estimate of the effective mass of the QPs, is continuously decreasing over the entire pressure range of our measurements. However, a change in the rate how $C_{el}/T|_{T=0.9K}$ is decreasing with increasing pressure is observed at the pressure where the borderline between the SC1 and the SC2 regions has been considered. The upper critical field, $B_{c2}(0)$, shows as well a remarkable, but continuous decrease when crossing from region SC1 to region SC2. Therefore, a smooth crossover region, characterized by a SC state where probably both AFM spin and valence fluctuations are acting, is likely. An overlap of the two distinct SC domes seems to be favored instead of a sharp transition when pressure is driving CeCu₂Si₂ from the AFM HF state at low pressures to the IV state at high pressures. The proximity of the system to the rather low-lying critical end point (at p_v) of the first-order valence transition is another important issue. $C_{el}(T)$ at $p > 1.5$ GPa shows LFL behavior up to the highest pressure of our experiment. This finding suggests that at the highest pressure of our measurement

of $p \approx 2.03$ GPa, $CeCu_2Si_2$ is still located relatively far below p_v , in good agreement with the fact that larger values of T_c and a maximum of $T_c(p)$ (supposed to be at p_v) are expected at higher pressures. However, the above-described LFL behavior also suggests that in the mentioned pressure range $CeCu_2Si_2$ is located far away from the AFM quantum critical fluctuations as well. Offering information about the strength of the SC coupling, the $\Delta C/(\gamma_n T_c)|_{T=T_c}$ ratio was found to show values below $\Delta C/(\gamma_n T_c)|_{T=T_c} \approx 1.43$ known from the BCS theory of SC in the entire studied pressure range. Moreover, the high-pressure SC region (SC2) is characterized by substantially lower values of $\Delta C/(\gamma_n T_c)|_{T=T_c}$ compared to those seen in the low-pressure SC region (SC1).

The results obtained by the measurements at very low pressures are very important concerning the interplay of AFM and SC in A/S -type $CeCu_2Si_2$. A detailed study of the physical properties of A/S -type $CeCu_2Si_2$, for which the pressure was increased in very small steps, has been performed at low pressures in order to learn more about the intimate interplay of the two ordering phenomena, AFM and SC. At ambient pressure, the phase transition from the AFM to the SC state at $B = 0$ T was found by our measurements to be most likely of first order. This is also suggested by the maximum value of the slope of $T_c(p)$ of $dT_c(p)/dp|_{p=0\text{GPa}} \approx 2.5$ K/GPa, as well as by the largest width (in temperature) of the SC phase transition anomaly observed in a.c.-susceptibility measurements. By help of magnetocaloric measurements we have seen that the probably first-order character of the AFM to SC phase transition seems to hold also for the case of $B \neq 0$ T. However, already a slight increase in pressure leads to a different situation. No hint for a first-order type phase transition from the AFM to the SC state has been found anymore at finite pressures, $p \geq 0.06$ GPa. The width of the phase transition anomaly detected by a.c.-susceptibility measurements, as well as the value of $dT_c(p)/dp$, is drastically decreasing with increasing pressure already at very small values of p . These findings suggest that the first-order type of the AFM to SC phase transition in $CeCu_2Si_2$ can be related to the way SC develops in this system, namely to the high value of $dT_c(p)/dp$. It was found that the broad phase transition to the SC state observed in the $\chi_{a.c.}(T)$ measurements is related to the presence of the AFM state in the system. At pressures $p < p_c^*$, the width of the SC phase transition detected in the $\chi_{a.c.}(T)$ measurements ($B = 0$ T) decreases strongly with increasing pressure, while at $p \geq p_c^*$ it is very small and remains almost pressure independent. The SC state in the region $p \leq p_c^*$ was found to be different from that in the slightly higher pressure region, $p > p_c^*$, though the formation of SC in both cases is supposed to be mediated by the AFM spin fluctuations. However, whether different SC order parameters cause the observed difference or the fact that

AFM order is present at temperatures higher than the temperature where the system becomes SC is not yet clear. No observable change in the SC phase transition was found by magnetocaloric measurements while crossing the region where SC is formed from either the PM or the AFM state.

An unconventional nature of the SC state in CeCu₂Si₂ is suggested for the entire pressure range of our measurements. The $B = 0$ T electronic specific-heat coefficient, $C_{el}(T)/T$, in the SC state shows a linear temperature dependence at $0.5T_c < T < T_c$ for all values of $p \geq p_c^*$, suggesting an unconventional SC state characterized by a SC gap function with line nodes. Unfortunately, in the narrow pressure range of $p < p_c^*$, the temperature dependence of $C_{el}(T)/T$ could not be determined in the SC state. The upper critical field was found to be strongly Pauli limited over the entire pressure range of our experiment, indicating the formation of spin-singlet SC in CeCu₂Si₂ at least for pressures $p < 2.1$ GPa. Concerning the mechanisms implied in the formation of the unconventional SC state, evidence for a relation between the AFM fluctuations and SC in the SC region at low pressures (SC1) has been found. Due to the limitation in pressure, the relatively large distance to p_v does not allow us to carefully study the relation between SC and the valence fluctuations supposed to mediate SC in this pressure region. At $B = 0$ T, extrapolation of $T_N(p)$ to $T_N = 0$ K has led to a critical pressure $p_c \approx 0.39$ GPa, a value which coincides with the pressure at which $T_c(p)$ exhibits its maximum value. This observation is in good agreement with the prediction of the theory of AFM spin-fluctuation mediated SC [Millis 1993, Nakamura 1996, Lonzarich 1997, Mathur 1998, Monthoux 1999] and suggests the possible role of AFM in the formation of the SC state in this pressure region. Moreover, our measurements in magnetic field $B \parallel c$ have shown that this theoretical prediction that was made for $B = 0$ T only is also observed at $B \neq 0$ T. This fact suggests that the two phenomena, AFM and SC, are intimately correlated in CeCu₂Si₂. Similar measurements for the case of $B \parallel (ab)$ could help to better understand the relation between AFM and SC in CeCu₂Si₂. Altogether, these findings are in strong favor for AFM spin fluctuations being essential for the formation of the low-pressure SC state in CeCu₂Si₂.

The complete and smooth suppression of the AFM state in HF systems leads to the occurrence of an AFM QCP. Application of pressure, as well as of magnetic field, both lead to the suppression of the AFM order in a Ce-based compound. We have studied the simultaneous effect of pressure and magnetic field on the AFM state in CeCu₂Si₂. The existence of a line of AFM QCPs as function of p and B has been predicted for the low-pressure region of CeCu₂Si₂. The existence of a QCP, as well as its observation, is hindered in CeCu₂Si₂ by the presence of SC at low temperatures. A

p – B phase diagram at $T = 0$ K has been constructed, in which the expected ground-state properties of CeCu₂Si₂ are summarized (see figure 4.23). It was shown that the line of AFM QCPs located outside of the SC state at $T = 0$ K very likely exists in CeCu₂Si₂. NFL behavior, characteristic to the vicinity of a QCP, has been observed in the low-temperature specific-heat measurements in the pressure and magnetic-field region where the AFM QCPs were predicted. Upon departing from this predicted line of QCPs, a low-temperature state described by LFL behavior has been observed. The coexistence or competition of AFM and SC states being not yet completely clarified, a clear statement about the ground state of CeCu₂Si₂ as function of p and B is difficult to make for the region where SC is present. While a phase transition to the SC state is always detected at low temperatures in a certain pressure and magnetic-field range, a phase transition anomaly marking the onset of AFM order is observable in A/S -type CeCu₂Si₂ only if $T_N > T_c$, suggesting the robustness of the SC state. Contrary to the SC state which is always identified the presence or absence of AFM order in the SC state of CeCu₂Si₂, independently whether AFM is supposed to set in at $T_N < T_c$ or is already formed at $T_N > T_c$, is still an open question. Accordingly, whether the AFM QCPs, predicted to be located in the SC phase at $T = 0$ K, really exist or not is not yet clear.

In this chapter we have shown that CeCu₂Si₂ under pressure indeed displays a sequence of different physical properties at low temperatures. As function of pressure, the $4f$ state of the Ce ion defines the ground-state properties of CeCu₂Si₂. As also suggested by the observed continuous increase of the Kondo temperature with increasing pressure, the AFM HF state of CeCu₂Si₂ at low pressures is replaced by an IV state at higher pressures. However, SC seems to be present as a ground state of CeCu₂Si₂ over a very broad pressure range enriching even further the fascinating T – p phase diagram of CeCu₂Si₂. As function of pressure, we have identified different SC regions in CeCu₂Si₂. We have observed different SC properties characteristic to each SC region and we have seen that the different SC states are strongly related to the specific (AFM/valence) instabilities existing in the respective regions. Heat-capacity measurements at even higher pressures would be very useful to have a better access to the region where SC occurs in the vicinity of the valence instability of Ce. Extending the measurements to lower temperatures, where the number of degrees of freedom become more limited and quantum critical phenomena eventually occur, would help as well.

Chapter 5

Summary

The interplay of antiferromagnetism and superconductivity in three Ce-based HF compounds, CeCoIn₅, Ce₂RhIn₈ and *A/S*-type CeCu₂Si₂, has been studied. Pressure is an ideal tool to tune a system through different ground states without introducing additional disorder in the system as in the case of doping. Low-temperature specific-heat, a.c.-susceptibility and magnetocaloric measurements under pressure have been performed in order to investigate the evolution of the ground-state properties of the mentioned HF systems. The experiments were carried out in the temperature range $0.26 \text{ K} \leq T \leq 7 \text{ K}$ and in magnetic fields up to $B = 8 \text{ T}$. Single-crystalline samples have been used for all the experiments. To generate hydrostatic pressures up to $p \approx 2.1 \text{ GPa}$, two different piston-cylinder type pressure cells have been used, a single-layer cell made entirely from CuBe and a double-layer pressure cell made from Ni-Cr-Al and CuBe. The latter one was developed in this work and used for the first time for heat-capacity measurements.

CeCoIn₅ and Ce₂RhIn₈ belong to the same family of HF compounds Ce_{*n*}T_{*m*}In_{3*n*+2*m*}, (T: Co, Rh, Ir). The members of this family exhibit a variety of unconventional physical properties, such as unconventional superconductivity or quantum critical behavior, and have been in the focus of extensive research in the last years. Since they present a layered structure, similar to the structure of high- T_c cuprate SCs, the role of the electronic dimensionality in the formation of a SC state was one of the subjects motivating scientists to study this family of compounds.

CeCoIn₅ is an ambient-pressure HF SC with $T_c \approx 2.26 \text{ K}$. At $B = 0 \text{ T}$, application of pressure leads to the increase of $T_c(p)$ up to $p \approx 1.4 \text{ GPa}$ where a maximum value of $T_c \approx 2.63 \text{ K}$ is observed. Upon further increasing the pressure, T_c decreases. The effective mass of the QPs, m^* , estimated from the specific-heat coefficient, C/T at $T = 3 \text{ K}$, decreases continuously upon increasing pressure. In good agreement with the pressure-induced decrease of m^* , the Kondo temperature, T_K , continuously increases with increasing pressure. Such a behavior is well known and

is always expected in Ce-based HF systems because the pressure induces an increase of the hybridization strength between the Ce $4f$ and the conduction electrons. In accordance with the predictions of the theory of AFM spin-fluctuation mediated SC [Millis 1988, Lonzarich 1997, Mathur 1998], $T_c \propto T_{sf} \propto 1/m^*$ dependence has been found over the entire pressure range of our measurements ($p < 1.5$ GPa). The observed logarithmic increase of $C(T)/T$ in the normal state at $p = 0$ GPa was found to become weaker with increasing pressure suggesting that pressure moves the system away from a QCP. The AFM spin-fluctuation theory predicts that at $B = 0$ T a maximum value of $T_c(p)$ is obtained at the critical pressure where $T_N(p)$ is suppressed to $T_N = 0$ K [Millis 1993, Nakamura 1996, Lonzarich 1997, Mathur 1998, Monthoux 1999]. We have shown that this prediction is observed in CeCoIn₅ not only for $B = 0$ T but also for non-zero values of the magnetic field ($B \parallel c$) suggesting that SC in CeCoIn₅ is mediated by AFM spin fluctuations. We have also provided evidence for the unconventional nature of the SC state of CeCoIn₅ for the entire range of pressures studied.

At ambient pressure, Ce₂RhIn₈ orders AFM at $T_N \approx 2.99$ K. The occurrence of a SC state at $p \approx 1.6$ GPa was concluded from electrical-resistivity measurements under pressure [Nicklas 2003]. We observed that T_N shifts to lower temperatures with increasing pressure. The pressure dependence of T_N was found to follow the theoretical predictions for an itinerant 3D AFM, $T_N(p) \propto |p - p_c|^{2/3}$ [Millis 1993], with a critical pressure $p_c \approx 2.03$ GPa. In the temperature ($T \geq 0.26$ K) and pressure ($p \leq 1.65$ GPa) range of our measurements we did not find any indication for bulk superconductivity. Moreover, our a.c.-susceptibility measurements up to $p \approx 1.65$ GPa and down to $T = 0.05$ K did not show any transition to a SC state. For Ce₂RhIn₈ measured at $p = 0$ GPa and $B \leq 8$ T, the anisotropy of $T_N(B)$ is very small and T_N is nearly independent of B . This behavior was found not to change up to the highest pressure of our experiment, suggesting the robustness of the AFM state in Ce₂RhIn₈ against application of magnetic field. The effective mass of the QPs, estimated from C_{el}/T at $T = 4$ K, decreases with increasing pressure up to $p \approx 1.5$ GPa, from where it remains nearly pressure independent, suggesting that in the pressure range where SC is supposed to set in the dependence $1/m^* \propto T_c$ does not hold for Ce₂RhIn₈. The observed pressure dependence of T_N suggests that Ce₂RhIn₈ shows a behavior typical for a 3D itinerant AFM. This finding, together with the relatively low values of T_c observed by the electrical-resistivity measurements under pressure [Nicklas 2003] and with the fact that no SC has been found in our measurements, led us to conclude that among the three members of the Ce_{*n*}Rh_{*m*}In_{*3n+2m*} family of HF AFMs, Ce₂RhIn₈ shows a stronger similarity to the cubic CeIn₃ than to CeRhIn₅.

A/S-type CeCu_2Si_2 displays both states, AFM and SC, already at ambient pressure ($T_N \approx 0.69$ K and $T_c \approx 0.46$ K). AFM is rapidly suppressed by the application of pressure while SC survives over the entire pressure range of our experiment, $p < 2.1$ GPa. Two main SC regions have been observed by our measurements, one in the low-pressure region (SC1) close to the AFM ordered state and a second one in the high-pressure region (SC2) in the vicinity of a region where a valence change of Ce is supposed to take place. We have found that the thermodynamic properties of CeCu_2Si_2 in the two SC regions behave differently. This finding supports the proposal that different mechanisms are mediating the formation of the SC states existing in the two distinct regions (AFM spin fluctuations in the region SC1 and valence fluctuations in the region SC2). We have shown that the SC state is unconventional over the entire range of pressures studied. A smooth crossover region with a SC state in which probably both types of fluctuations (AFM spin and valence) are acting was proposed for the region located between SC1 and SC2. We have argued that different SC order parameters are likely to exist in the two SC regions. By increasing the pressure in very small steps we were able to carefully study the low-pressure region where AFM and SC are strongly interacting. In the whole pressure and magnetic-field ranges studied, for fixed values of p and B , we have detected a phase transition to the AFM state only when $T_N > T_c$. A phase transition to the AFM state was never observed at temperatures below T_c . A SC region with unusual properties has been found for $p < p_c^*$, with p_c^* representing the pressure where at zero magnetic field $T_N(p) = T_c(p)$. Moreover, we have found strong evidence from different types of measurements that the AFM to SC phase transition in *A/S*-type CeCu_2Si_2 is of first order at ambient pressure. We suggest that the first-order character of the phase transition could be related to the large slope $T_c(p)$ shows at ambient pressure. We have found in CeCu_2Si_2 , similar to the case of CeCoIn_5 , that at a given value of B , $T_c(p)$ reaches its maximum value at the critical pressure where $T_N(p)$ for the respective B is suppressed to $T_N = 0$ K (measurements were done for $B \parallel c$). The observed behavior has been predicted by the AFM spin-fluctuation theory, however only for $B = 0$ T [Millis 1993, Nakamura 1996, Lonzarich 1997, Mathur 1998, Monthoux 1999]. We have shown that in the case of *A/S*-type CeCu_2Si_2 this holds also for $B \neq 0$ T ($B \parallel c$). Evidence for the existence of pressure and magnetic-field-induced QCPs in *A/S*-type CeCu_2Si_2 has also been provided by our measurements.

Low-temperature specific-heat measurements under pressure have been proven to be an ideal tool to investigate the peculiar ground-state properties of HF systems. In this thesis, we were able to identify common characteristics of the compounds studied, suggesting similar underlying physical principles. Measurements to lower

temperatures and higher pressures are highly desirable to further elucidate the fascinating properties of this class of materials.

Bibliography

- [Ahlheim 1988] U. Ahlheim, M. Winkelmann, P. van Aken, C. D. Bredl, F. Steglich and G. R. Stewart, *J. Magn. Magn. Mater.*, 76&77, 520 (1988).
- [Anderson 1981] P. W. Anderson, in "Valence fluctuations in solids", North-Holland, Amsterdam, p. 451 (1981).
- [Andrei 1980] N. Andrei, *Phys. Rev. Lett.*, 45, 379 (1980).
- [Aoki 2004] H. Aoki, T. Sakakibara, H. Shishido, R. Settai, Y. Ōnuki, P. Miranovic and K. Machida, *J. Phys.: Condens. Matter*, 16, L13 (2004).
- [Assmus 1984] W. Assmus, M. Herrmann, U. Rauchschwalbe, S. Riegel, W. Lieke, H. Spille, S. Horn, G. Weber, F. Steglich and G. Cordier, *Phys. Rev. Lett.*, 52, 469 (1984).
- [Bao 2000] W. Bao, P. G. Pagliuso, J. L. Sarrao, J. D. Thompson, Z. Fisk, J. W. Lynn and R. W. Erwin, *Phys. Rev. B*, 62, R14621 (2000), *Phys. Rev. B*, 63, 219901(E) (2001) and *Phys. Rev. B*, 67, 099903 (2003).
- [Bao 2001] W. Bao, P. G. Pagliuso, J. L. Sarrao, J. D. Thompson, Z. Fisk and J. W. Lynn, *Phys. Rev. B*, 64, 020401(R) (2001).
- [Bardeen 1957] J. Bardeen, L. N. Cooper and J. R. Schrieffer, *Phys. Rev.*, 108, 1175 (1957).
- [Bellarbi 1984] B. Bellarbi, A. Benoit, D. Jaccard, J. M. Mignot and H. F. Braun, *Phys. Rev. B*, 30, 1182 (1984).
- [Benoit 1980] A. Benoit, J. X. Boucherle, P. Convert, J. Flouquet, J. Palleau and J. Schweizer, *Solid State Commun.*, 34, 293 (1980).
- [Bednorz 1986] J. G. Bednorz and K. A. Müller, *Z. Phys. B*, 64, 189 (1986).

- [Bianchi 2002] A. Bianchi, R. Movshovich, N. Oeschler, P. Gegenwart, F. Steglich, J. D. Thompson, P. G. Pagliuso and J. L. Sarrao, *Phys. Rev. Lett.*, 89, 137002 (2002).
- [Bianchi 2003a] A. Bianchi, R. Movshovich, C. Capan, P. G. Pagliuso and J. L. Sarrao, *Phys. Rev. Lett.*, 91, 187004 (2003).
- [Bianchi 2003b] A. Bianchi, R. Movshovich, I. Vekhter, P. G. Pagliuso and J. L. Sarrao, *Phys. Rev. Lett.*, 91, 257001 (2003).
- [Bickers 1987] N. E. Bickers, D. L. Cox and J. W. Wilkins, *Phys. Rev. B*, 36, 2036 (1987).
- [Boer 1987] F. R. de Boer, J. C. P. Klaasse, P. A. Veenhuizen, A. Bohm, C. D. Bredl, U. Gottwick, H. M. Mayer, L. Pawlak, U. Rauchschwalbe, H. Spille and F. Steglich, *J. Magn. Magn. Mater.*, 63&64, 91, 1987.
- [Böhm 1988] A. Böhm, R. Caspary, U. Habel, L. Pawlak, A. Zuber, F. Steglich and A. Loidl, *J. Magn. Magn. Mater.*, 76&77, 150, 1988.
- [Bruls 1994] G. Bruls, B. Wolf, D. Finsterbusch, P. Thalmaier, I. Kouroudis, W. Sun, W. Assmus, B. Lüthi, M. Lang, K. Gloos, F. Steglich and R. Modler, *Phys. Rev. Lett.*, 72, 1754 (1994).
- [Christianson 2004] A. D. Christianson, E. D. Bauer, J. M. Lawrence, P. S. Riseborough, N. O. Moreno, P. G. Pagliuso, J. L. Sarrao, J. D. Thompson, E. A. Goremychkin, F. R. Trouw, M. P. Hehlen and R. J. McQueeney, *Phys. Rev. B*, 70, 134505 (2004).
- [Clogston 1962] A. M. Clogston, *Phys. Rev. Lett.*, 9, 266 (1962).
- [Coleman 2001] P. Coleman, C. Pépin, Q. M. Si and R. Ramazashvili, *J. Phys.: Condens. Matter*, 13, R723 (2001).
- [Coleman 2002] P. Coleman, *Lectures on the Physics of Highly Correlated Electron Systems VI*, Editor F. Mancini, American Institute of Physics, New York, 79 (2002).
- [Coqblin 1969] B. Coqblin and J. R. Schrieffer, *Phys. Rev.*, 185, 847 (1969).
- [Cornelius 2001] A. L. Cornelius, P. G. Pagliuso, M. F. Hundley and J. L. Sarrao, *Phys. Rev. B*, 64, 144411 (2001).

- [Deppe 2004] M. Deppe, Ph.D thesis, TU Dresden (2004).
- [Desgranges 1982] H. U. Desgranges and K. D. Schotte, *Phys. Lett.*, 91A, 240 (1982).
- [Desgranges 1985] H. U. Desgranges and J. W. Rasul, *Phys. Rev. B*, 32, 6100 (1985).
- [Desgranges 1987] H. U. Desgranges and J. W. Rasul, *Phys. Rev. B*, 36, 328 (1987).
- [Dhar 1987] S. K. Dhar, E. V. Sampathkumaran, J. Ray and G. Chandra, *Phys. Rev. B*, 36, 785 (1987).
- [Doniach 1977] S. Doniach, *Physica B*, 91, 231 (1977).
- [Eiling 1981] A. Eiling and J. S. Schilling, *J. Phys. F: Metal Phys.*, 11, 623 (1981).
- [Eremets 1996] M. Eremets, *High pressure experimental methods*, Oxford University Press (1996).
- [Fåk 2000] B. Fåk, J. Flouquet, G. Lapertot, T. Fukuhara and H. Kadowaki, *J. Phys.: Condens. Matter*, 12, 5423 (2000).
- [Feyerherm 1997] R. Feyerherm, A. Amato, C. Geibel, F. N. Gygax, P. Hellmann, R. H. Heffner, D. E. MacLaughlin, R. Müller-Reisener, G. J. Nieuwenhuys, A. Schenk and F. Steglich, *Phys. Rev. B*, 56, 699 (1997).
- [Fisher 2002] R. A. Fisher, F. Bouquet, N. E. Phillips, M. F. Hundley, P. G. Pagliuso, J. L. Sarrao, Z. Fisk and J. D. Thompson, *Phys. Rev. B*, 65, 224509 (2002).
- [Fujiwara 1980] H. Fujiwara, H. Kadomatsu and K. Tohma, *Rev. Sci. Instrum.*, 51, 1345 (1980).
- [Fulde 1964] P. Fulde and R. A. Ferrell, *Phys. Rev.*, 135, A550 (1964).
- [Fuseya 2003] Y. Fuseya, H. Kohno and K. Miyake, *J. Phys. Soc. Jpn.*, 72, 2914 (2003).
- [Gegenwart 1998a] P. Gegenwart, Ph.D thesis, TU Darmstadt (1998).
- [Gegenwart 1998b] P. Gegenwart, C. Langhammer, C. Geibel, R. Helfrich, M. Lang, G. Sparn, F. Steglich, R. Horn, L. Donnevert, A. Link and W. Assmus, *Phys. Rev. Lett.*, 81, 1501 (1998).
- [Gegenwart 2002] P. Gegenwart, J. Custers, C. Geibel, K. Neumaier, T. Tayama, K. Tenya, O. Trovarelli and F. Steglich, *Phys. Rev. Lett.*, 89, 056402 (2002).

- [Geibel priv. comm.] C. Geibel, private communications.
- [Grin 1979] Y. N. Grin, Y. P. Yarmolyuk and E. I. Gladyshevskii, *Sov. Phys. Crystallogr.* 24, 137 (1979).
- [Grosche 1996] F.M. Grosche, S.R. Julian, N.D. Mathur and G.G. Lonzarich, *Physica B*, 223-224, 50 (1996).
- [Grosche 2001] F. M. Grosche, I. R. Walker, S. R. Julian, N. D. Mathur, D. M. Freye, M. J. Steiner and G. G. Lonzarich, *J. Phys.: Condens. Matter*, 13, 2845 (2001).
- [Hasselbach 1993] K. Hasselbach, J. R. Kirtley and J. Flouquet, *Phys. Rev. B*, 47, 509 (1993).
- [Hegger 2000] H. Hegger, C. Petrovic, E. G. Moshopoulou, M. F. Hundley, J. L. Sarrao, Z. Fisk and J. D. Thompson, *Phys. Rev. Lett.*, 84, 4986 (2000).
- [Helfand 1966] E. Helfand and N. Werthamer, *Phys. Rev.*, 147, 288 (1966).
- [Hellmann 1993] P. Hellmann, Diploma thesis, TH Darmstadt (1993).
- [Hellmann 1997] P. Hellmann, Ph.D thesis, TU Darmstadt (1997).
- [Hellmann unpubl.] P. Hellmann, unpublished.
- [Hertz 1976] J. A. Hertz, *Phys. Rev. B*, 14, 1165 (1976).
- [Holmes 2004a] A. T. Holmes, Ph.D thesis, University of Geneva (2004).
- [Holmes 2004b] A. T. Holmes, D. Jaccard and K. Miyake, *Phys. Rev. B*, 69, 024508 (2004).
- [Hu 2000] J. P. Hu and S. C. Zhang, *Phys. Rev. B*, 62, R791 (2000).
- [Ishida 1999] K. Ishida, Y. Kawasaki, K. Tabuchi, K. Kashima, Y. Kitaoka, K. Asayama, C. Geibel and F. Steglich, *Phys. Rev. Lett.*, 82, 5353 (1999).
- [Izawa 2001] K. Izawa, H. Yamaguchi, Y. Matsuda, H. Shishido, R. Settai and Y. Ōnuki, *Phys. Rev. Lett.*, 87, 057002 (2001).
- [Jaccard 1999] D. Jaccard, H. Wilhelm, K. Alami-Yadri and E. Vargoz, *Physica B*, 259-261, 1 (1999).
- [Jeevan 2007] H. S. Jeevan, Ph.D thesis, TU Dresden, to be published (2007).

- [Jourdan 1999] M. Jourdan, M. Huth and H. Adrian, *Nature*, 398, 47 (1999).
- [Kadowaki 1986] K. Kadowaki and S. Woods, *Solid State Commun.*, 58, 507 (1986).
- [Kamerlingh 1911] H. Kamerlingh Onnes, *Comm. Phys. Lab. Univ. Leiden*, 122&124 (1911).
- [Kawasaki 2000] Y. Kawasaki, K. Ishida, T. Mito, C. Thessieu, G.-q. Zheng, Y. Kitaoka, K. Asayama, C. Geibel and F. Steglich, *Physica B*, 281&282, 14 (2000).
- [Kawasaki 2001] Y. Kawasaki, K. Ishida, T. Mito, C. Thessieu, G.-q. Zheng, Y. Kitaoka, C. Geibel and F. Steglich, *Phys. Rev. B*, 63, 140501(R) (2001).
- [Kawasaki 2002] Y. Kawasaki, K. Ishida, K. Obinata, K. Tabuchi, K. Kashima, Y. Kitaoka, O. Trovarelli, C. Geibel and F. Steglich, *Phys. Rev. B*, 66, 224502 (2002).
- [Kawasaki 2003] S. Kawasaki, T. Mito, Y. Kawasaki, G.-q. Zheng, Y. Kitaoka, D. Aoki, Y. Haga and Y. Ōnuki, *Phys. Rev. Lett.*, 91, 137001 (2003).
- [Kawasaki 2004] Y. Kawasaki, K. Ishida, S. Kawasaki, T. Mito, G.-q. Zheng, Y. Kitaoka, C. Geibel and F. Steglich, *J. Phys. Soc. Jpn.*, 73, 194 (2004).
- [Kitaoka 2001] Y. Kitaoka, K. Ishida, Y. Kawasaki, O. Trovarelli, C. Geibel and F. Steglich, *J. Phys.: Condens. Matter*, 13, L79 (2001).
- [Kitaoka 2002] Y. Kitaoka, Y. Kawasaki, T. Mito, S. Kawasaki, G.-q. Zheng, K. Ishida, D. Aoki, Y. Haga, R. Settai, Y. Ōnuki, C. Geibel and F. Steglich, *J. Phys. Chem. Solids*, 63, 1141 (2002).
- [Kitaoka 2005] Y. Kitaoka, S. Kawasaki, T. Mito and Y. Kawasaki, *J. Phys. Soc. Jpn.*, 74, 186 (2005).
- [Knebel 2004] G. Knebel, M-A Méasson, B. Salce, D. Aoki, D. Braithwaite, J. P. Brison and J. Flouquet, *J. Phys.: Condens. Matter*, 16, 8905 (2004).
- [Knebel 2006] G. Knebel, D. Aoki, D. Braithwaite, B. Salce and J. Flouquet, *Phys. Rev. B*, 74, 020501(R) (2006).
- [Knopp 1988] G. Knopp, A. Loidl, R. Caspary, U. Gottwick, C. D. Bredl, H. Spille, F. Steglich and A. P. Murani, *J. Magn. Magn. Mater.*, 74, 341 (1988).

- [Knopp 1989] G. Knopp, A. Loidl, K. Knorr, L. Pawlak, M. Duczmal, R. Caspary, U. Gottwick, H. Spille, F. Steglich and A. P. Murani, *Z. Phys. B: Condens. Matter*, 77, 95 (1989).
- [Koda 2002] A. Koda, W. Higemoto, R. Kadono, Y. Kawasaki, K. Ishida, Y. Kitaoka, C. Geibel and F. Steglich, *J. Phys. Soc. Jpn.*, 71, 1427 (2002).
- [Kohori 2001] Y. Kohori, Y. Yamato, Y. Iwamoto, T. Kohara, E. D. Bauer, M. B. Maple and J. L. Sarrao, *Phys. Rev. B*, 64, 134526 (2001).
- [Kondo 1964] J. Kondo, *Prog. Theor. Phys.*, 32, 37 (1964).
- [Kontani 2004] H. Kontani, *J. Phys. Soc. Jpn.*, 73, 515 (2004).
- [Koskenmaki 1978] D. C. Koskenmaki and K. A. Gschneidner, Jr., *Handbook on the Physics and Chemistry of Rare Earth*, North Holland Publishing Company, Amsterdam (1978).
- [Kumar 2004] R. S. Kumar, A. L. Cornelius and J. L. Sarrao, *Phys. Rev. B*, 70, 214526 (2004).
- [Landau 1956] L. D. Landau, *Sov. Phys. JETP*, 3, 920 (1956).
- [Landau 1957] L. D. Landau, *Sov. Phys. JETP*, 5, 101 (1957).
- [Landau 1959] L. D. Landau, *Sov. Phys. JETP*, 8, 70 (1959).
- [Lang 1999] M. Lang, P. Gegenwart, R. Helfrich, M. Köppen, F. Kromer, C. Langhammer, C. Geibel, F. Steglich, J. S. Kim and G. R. Stewart, *Electron Correlations and Materials Properties*, Kluwer Academic, Dordrecht, MA/Plenum, New York, 153 (1999).
- [Langhammer 2002] C. Langhammer, Ph.D thesis, TU Dresden (2002).
- [Larkin 1965] A. I. Larkin and Y. N. Ovchinnikov, *Pis'ma Zh. Eksp. Teor. Fiz.*, 47, 1136 (1964), [*Sov. Phys. JETP*, 20, 762 (1965)].
- [Lawrence 1980] J. M. Lawrence and S. M. Shapiro, *Phys. Rev. B*, 22, 4379 (1980).
- [Leggett 1997] A. J. Leggett, in *Electron*, Ed. by M. Springford, Cambridge University Press (1997) and references therein.
- [Llobet 2004] A. Llobet, J. S. Gardner, E. G. Moshopoulou, J.-M. Mignot, M. Nicklas, W. Bao, N. O. Moreno, P. G. Pagliuso, I. N. Goncharenko, J. L. Sarrao and J. D. Thompson, *Phys. Rev. B*, 69, 024403 (2004).

- [Llobet unpublished] A. Llobet, W. Bao, N. O. Moreno, J. L. Sarrao, J. D. Thompson and J. W. Lynn (unpublished).
- [Lonzarich 1997] G. G. Lonzarich, in *Electron*, Ed. by M. Springford, Cambridge University Press (1997) and references therein.
- [Löhneysen 1994] H. v. Löhneysen, T. Pietrus, G. Portisch, H. G. Schlager, A. Schröder, M. Sieck and T. Trappmann, *Phys. Rev. Lett.*, **72**, 3262 (1994).
- [Maehira 2003] T. Maehira, T. Hotta, K. Ueda and A. Hasegawa, *J. Phys. Soc. Jpn.*, **72**, 854 (2003).
- [Maeno 1994] Y. Maeno, H. Hashimoto, K. Yoshida, S. Nishizaki, T. Fujita, J. G. Bednorz and F. Lichtenberg, *Nature*, **372**, 532 (1994).
- [Maki 1964] K. Maki and T. Tsuneto, *Prog. Theor. Phys.*, **31**, 945 (1964).
- [Malinowski 2003] A. Malinowski, M. F. Hundley, N. O. Moreno, P. G. Pagliuso, J. L. Sarrao and J. D. Thompson, *Phys. Rev. B*, **68**, 184419 (2003).
- [Malterre 1996] D. Malterre, M. Grioni and Y. Baer, *Adv. Phys.*, **45**, 299 (1996).
- [Mathur 1998] N. D. Mathur, F. M. Grosche, S. R. Julian, I. R. Walker, D. M. Freye, R. K. W. Haselwimmer and G. G. Lonzarich, *Nature*, **394**, 39 (1998).
- [Meissner 1933] W. Meissner and R. Ochsenfeld, *Naturwissenschaften*, **21**, 787 (1933).
- [Miclea 2006a] C. F. Miclea, M. Nicklas, D. Parker, K. Maki, J. L. Sarrao, J. D. Thompson, G. Sparn and F. Steglich, *Phys. Rev. Lett.*, **96**, 117001 (2006).
- [Miclea 2006b] C. F. Miclea, Ph.D thesis, TU Dresden (2006).
- [Millis 1988] A. J. Millis, S. Sachdev and C. M. Varma, *Phys. Rev. B*, **37**, 4975 (1988).
- [Millis 1993] A. J. Millis, *Phys. Rev. B*, **48**, 7183 (1993).
- [Miyake priv. comm.] K. Miyake, private communications.
- [Miyake 1989] K. Miyake, T. Matsuura and C. M. Varma, *Solid State Commun.*, **71**, 1149 (1989).
- [Miyake 2002] K. Miyake and H. Maebashi, *J. Phys. Soc. Jpn.*, **71**, 1007 (2002).

- [Modler 1995] R. Modler, M. Lang, C. Geibel, C. Schank, R. Müller-Reisener, P. Hellmann, A. Link, G. Sparn, W. Assmus and F. Steglich, *Physica B*, 206&207, 586 (1995).
- [Monthoux 1999] P. Monthoux and G. G. Lonzarich, *Phys. Rev. B*, 59, 14598 (1999).
- [Monthoux 2001] P. Monthoux and G. G. Lonzarich, *Phys. Rev. B*, 63, 054529 (2001).
- [Monthoux 2004] P. Monthoux and G. G. Lonzarich, *Phys. Rev. B*, 69, 064517 (2004).
- [Moriya 1995] T. Moriya and T. Takimoto, *J. Phys. Soc. Jpn.*, 64, 960 (1995).
- [Movshovich 2001] R. Movshovich, M. Jaime, J. D. Thompson, C. Petrovic, Z. Fisk, P. G. Pagliuso and J. L. Sarrao, *Phys. Rev. Lett.*, 86, 5152 (2001).
- [Muramatsu 2003] T. Muramatsu, T. C. Kobayashi, K. Shimizu, K. Amaya, D. Aoki, Y. Haga and Y. Ōnuki, *Physica C*, 388-389, 539 (2003).
- [Nakamura 1996] S. Nakamura, T. Moriya and K. Ueda, *J. Phys. Soc. Jpn.*, 65, 4026 (1996).
- [Neef 2004] M. Neef, Diploma thesis, TU Braunschweig (2004).
- [Nicklas priv. comm.] M. Nicklas, private communications.
- [Nicklas 2001] M. Nicklas, R. Borth, E. Lengyel, P. G. Pagliuso, J. L. Sarrao, V. A. Sidorov, G. Sparn, F. Steglich and J. D. Thompson, *J. Phys.: Condens. Matter*, 13, L905 (2001).
- [Nicklas 2003] M. Nicklas, V. A. Sidorov, H. A. Borges, P. G. Pagliuso, C. Petrovic, Z. Fisk, J. L. Sarrao and J. D. Thompson, *Phys. Rev. B*, 67, 020506(R) (2003).
- [Oeschler 2003] N. Oeschler, P. Gegenwart, M. Lang, R. Movshovich, J. L. Sarrao, J. D. Thompson and F. Steglich, *Phys. Rev. Lett.*, 91, 076402 (2003).
- [Onishi 2000] Y. Onishi and K. Miyake, *J. Phys. Soc. Jpn.*, 69, 3955 (2000).
- [Onodera 2002] A. Onodera, S. Tsuduki, Y. Onishi, T. Watanuki, K. Ishida, Y. Kitaoka and Y. Onuki, *Solid State Commun.*, 123, 113 (2002).
- [Orlando 1979] T. P. Orlando, E. J. McNiff, Jr., S. Foner and M. R. Beasley, *Phys. Rev. B*, 19, 4545 (1979).
- [Ott 1983] H. R. Ott, H. Rudigier, Z. Fisk and J. L. Smith, *Phys. Rev. Lett.*, 50, 1595 (1983).

- [Paglione 2003] J. Paglione, M. A. Tanatar, D. G. Hawthorn, E. Boaknin, R. W. Hill, F. Ronning, M. Sutherland, L. Taillefer, C. Petrovic and P. C. Canfield, *Phys. Rev. Lett.*, 91, 246405 (2003).
- [Park 2006] T. Park, F. Ronning, H. Q. Yuan, M. B. Salamon, R. Movshovich, J. L. Sarrao and J. D. Thompson, *Nature*, 440, 65 (2006).
- [Petrovic 2001a] C. Petrovic, P. G. Pagliuso, M. F. Hundley, R. Movshovich, J. L. Sarrao, J. D. Thompson, Z. Fisk and P. Monthoux, *J. Phys.: Condens. Matter*, 13, L337 (2001).
- [Petrovic 2001b] C. Petrovic, R. Movshovich, M. Jaime, P. G. Pagliuso, M. F. Hundley, J. L. Sarrao, Z. Fisk and J. D. Thompson, *Europhys. Lett.*, 53, 354 (2001).
- [Pham 2006] L. D. Pham, T. Park, S. Maquilon, J. D. Thompson and Z. Fisk, *Phys. Rev. Lett.*, 97, 056404 (2006).
- [Quezel 1984] S. Quezel, J. Rossat-Mignod, B. Chevalier, P. Lejay and J. Etourneau, *Solid State Commun.*, 49, 685 (1984).
- [Rajan 1983] V. T. Rajan, *Phys. Rev. Lett.*, 51, 308 (1983).
- [Rauchschwalbe 1982] U. Rauchschwalbe, W. Lieke, C. D. Bredl, F. Steglich, J. Aarts, K. M. Martini and A. C. Mota, *Phys. Rev. Lett.*, 49, 1448 (1982).
- [Rice 1986] T. M. Rice and K. Ueda, *Phys. Rev. B*, 34, 6420 (1986).
- [Ronning 2005] F. Ronning, C. Capan, A. Bianchi, R. Movshovich, A. Lacerda, M. F. Hundley, J. D. Thompson, P. G. Pagliuso and J. L. Sarrao, *Phys. Rev. B*, 71, 104528 (2005).
- [Ronning 2006] F. Ronning, C. Capan, E. D. Bauer, J. D. Thompson, J. L. Sarrao and R. Movshovich, *Phys. Rev. B*, 73, 064519 (2006).
- [Röhler 1988] J. Röhler, J. Klug and K. Keulerz, *J. Magn. Magn. Mater.*, 76&77, 340 (1988).
- [Sachdev 1999] S. Sachdev, *Quantum Phase Transitions*, Cambridge University Press (1999).
- [Sampathkumaran 1986] E. V. Sampathkumaran and R. Vijayaraghavan, *Phys. Rev. Lett.*, 56, 2861 (1986).
- [Sarma 1963] G. Sarma, *J. Phys. Chem. Solids*, 24, 1029 (1963).

- [Sato 2001] N. K. Sato, N. Aso, K. Miyake, R. Shiina, P. Thalmeier, G. Varelogiannis, C. Geibel, F. Steglich, P. Fulde and T. Komatsubara, *Nature*, 410, 340 (2001).
- [Satoh 1993] K. Satoh, Y. Fujimaki, I. Umehara, J. Itoh, Y. Ōnuki and M. Kasaya, *Physica B*, 186-188, 658 (1993).
- [Schröder 2000] A. Schröder, G. Aeppli, R. Coldea, M. Adams, O. Stockert, H. v. Löhneysen, E. Bucher, R. Ramazashvili and P. Coleman, *Nature*, 407, 351 (2000).
- [Settai 2001] R. Settai, H. Shishido, S. Ikeda, Y. Murakawa, M. Nakashima, D. Aoki, Y. Haga, H. Harima and Y. Ōnuki, *J. Phys.: Condens. Matter*, 13, L627 (2001).
- [Shishido 2002] H. Shishido, R. Settai, D. Aoki, S. Ikeda, H. Nakawaki, N. Nakamura, T. Iizuka, Y. Inada, K. Sugiyama, T. Takeuchi, K. Kindo, T. C. Kobayashi, Y. Haga, H. Harima, Y. Aoki, T. Namiki, H. Sato and Y. Ōnuki, *J. Phys. Soc. Jpn.*, 71, 162 (2002).
- [Shishido 2005] H. Shishido, R. Settai, H. Harima and Y. Ōnuki, *J. Phys. Soc. Jpn.*, 74, 1103 (2005).
- [Si 2001] Q. Si, S. Rabello, K. Ingersent and J. L. Smith, *Nature*, 413, 804 (2001).
- [Sidorov 2002] V. A. Sidorov, M. Nicklas, P. G. Pagliuso, J. L. Sarrao, Y. Bang, A. V. Balatsky and J. D. Thompson, *Phys. Rev. Lett.*, 89, 157004 (2002).
- [Steglich 1979] F. Steglich, J. Aarts, C. D. Bredl, W. Lieke, D. Meschede, W. Franz and H. Schäfer, *Phys. Rev. Lett.*, 43, 1892 (1979).
- [Steglich 2001] F. Steglich, P. Gegenwart, C. Geibel, P. Hinze, M. Lang, C. Langhammer, G. Sparn, T. Tayama, O. Trovarelli, N. Sato, T. Dahm and G. Varelogiannis, *More is different - fifty years of condensed matter physics*, Princeton University Press, Chapter 13, p. 191 (2001).
- [Stewart 1984] G. R. Stewart, Z. Fisk, J. O. Willis and J. L. Smith, *Phys. Rev. Lett.*, 52, 679 (1984).
- [Stewart 2001] G. R. Stewart, *Rev. Mod. Phys.*, 73, 797 (2001).
- [Stockert 2004] O. Stockert, E. Faulhaber, G. Zwircknagl, N. Stüsser, H. S. Jeevan, M. Deppe, R. Borth, R. KÜchler, M. Loewenhaupt, C. Geibel and F. Steglich, *Phys. Rev. Lett.*, 92, 136401 (2004).

- [Stockert 2005] O. Stockert, M. Deppe, E. Faulhaber, H. S. Jeevan, R. Schneider, N. Stüsser, C. Geibel, M. Loewenhaupt and F. Steglich, *Physica B*, 359-361, 349 (2005).
- [Stockert 2006] O. Stockert, D. Andreica, A. Amato, H. S. Jeevan, C. Geibel and F. Steglich, *Physica B*, 374-375, 167 (2006).
- [Stockert unpubl.] O. Stockert, unpublished.
- [Sun 1994] G. F. Sun, K. W. Wong, B. R. Xu, Y. Xin and D. F. Lu, *Phys. Lett. A*, 192, 122 (1994).
- [Tachiki 1985] M. Tachiki, M. Nakahara and R. Teshima, *J. Magn. Magn. Mater.*, 52, 161 (1985).
- [Tayama 2002] T. Tayama, A. Harita, T. Sakakibara, Y. Haga, H. Shishido, R. Settai and Y. Ōnuki, *Phys. Rev. B*, 65, 180504(R) (2002).
- [Tayama 2003] T. Tayama, M. Lang, T. Lühmann, F. Steglich and W. Assmus, *Phys. Rev. B*, 67, 214504 (2003).
- [Tayama 2005] T. Tayama, Y. Namai, T. Sakakibara, M. Hedo, Y. Uwatoko, H. Shishido, R. Settai and Y. Ōnuki, *J. Phys. Soc. Jpn.*, 74, 1115 (2005).
- [Thalmeier 2005a] P. Thalmeier and G. Zwicknagl, *Handbook on the Physics and Chemistry of Rare Earths*, Vol. 34, Ed. by K. A. Gschneidner, Jr., J.-C. G. Bünzli and V. K. Pecharsky, 135 (2005).
- [Thalmeier 2005b] P. Thalmeier, G. Zwicknagl, O. Stockert, G. Sparn and F. Steglich, "Frontiers in Superconducting Materials", A. Narlikar (Ed.), Springer Verlag, Berlin (2005).
- [Thomas 1993] F. Thomas, J. Thomasson, C. Ayache, C. Geibel and F. Steglich, *Physica B*, 186-188, 303 (1993).
- [Thomas 1996] F. Thomas, C. Ayache, I. A. Fomine, J. Thomasson and C. Geibel, *J. Phys.: Condens. Matter*, 8, L51 (1996).
- [Thompson priv. comm.] J. D. Thompson, private communications.
- [Thompson 2001] J. D. Thompson, R. Movshovich, Z. Fisk, F. Bouquet, N. J. Curro, R. A. Fisher, P. C. Hammel, H. Hegger, M. F. Hundley, M. Jaime, P. G. Pagliuso, C. Petrovic, N. E. Phillips and J. L. Sarrao, *J. Magn. Magn. Mater.*, 226-230, 5 (2001).

- [Thompson 2003] J. D. Thompson, M. Nicklas, A. Bianchi, R. Movshovich, A. Llobet, W. Bao, A. Malinowski, M. F. Hundley, N. O. Moreno, P. G. Pagliuso, J. L. Sarrao, S. Nakatsuji, Z. Fisk, R. Borth, E. Lengyel, N. Oeschler, G. Sparn and F. Steglich, *Physica B*, 329-333, 446 (2003).
- [Trovarelli 2000] O. Trovarelli, C. Geibel, S. Mederle, C. Langhammer, F. M. Grosche, P. Gegenwart, M. Lang, G. Sparn and F. Steglich, *Phys. Rev. Lett.*, 85, 626 (2000).
- [Ueda 2004] T. Ueda, H. Shishido, S. Hashimoto, T. Okubo, M. Yamada, Y. Inada, R. Settai, H. Harima, A. Galatanu, E. Yamamoto, N. Nakamura, K. Sugiyama, T. Takeuchi, K. Kindo, T. Namiki, Y. Aoki, H. Sato and Y. Ōnuki, *J. Phys. Soc. Jpn.*, 73, 649 (2004).
- [Uwatoko 2002] Y. Uwatoko, S. Todo, K. Ueda, A. Uchida, M. Kosaka, N. Mori and T. Matsumoto, *J. Phys.: Condens. Matter*, 14, 11291 (2002).
- [Volovik 1985] G. E. Volovik and L. P. Gor'kov, *Zh. Eksp. Teor. Fiz.* 88, 1412 (1985).
- [Walker 1997] I. R. Walker, F. M. Grosche, D. M. Freye and G. G. Lonzarich, *Physica C*, 282-287, 303 (1997).
- [Walker 1999] I. R. Walker, *Rev. Sci. Instrum.*, 70, 3402 (1999).
- [Wilson 1975] K. G. Wilson, *Rev. Mod. Phys.*, 47, 773 (1975).
- [Yang 1998] K. Yang and S. L. Sondhi, *Phys. Rev. B*, 57, 8566 (1998).
- [Yuan 2003] H. Q. Yuan, F. M. Grosche, M. Deppe, C. Geibel, G. Sparn and F. Steglich, *Science*, 302, 2104 (2003).
- [Yuan 2004] H. Q. Yuan, F. M. Grosche, M. Deppe, C. Geibel, G. Sparn and F. Steglich, *New J. Phys.*, 6, 132 (2004).
- [Zhang 1997] S. C. Zhang, *Science*, 275, 1089 (1997).
- [Zwicknagl 1993] G. Zwicknagl and U. Pulst, *Physica B*, 186-188, 895 (1993).

Acknowledgments

First of all, I would like to express my gratitude to Prof. Dr. Frank Steglich for his constant support and guidance during these years.

I would like to thank Dr. Michael Nicklas for his patience in reading the thesis and for his useful comments and advises. Without his help the completion of this thesis would have been nearly impossible. I thank him as well for helping in taking care of many administrative formalities during the last years.

I am especially indebted to Dr. Günter Sparn for his guidance, competent supervision and kindness from the beginning of my work in Dresden. He was introducing me to the fascinating field of high-pressure physics.

For preparing and supplying the samples investigated in this thesis I would like to thank Dr. P. G. Pagliuso, Dr. N. O. Moreno, Dr. John L. Sarrao, Prof. Dr. Joe D. Thompson, Hirale S. Jeevan and Dr. Christoph Geibel.

I acknowledge valuable discussions with Dr. Kazumasa Miyake, Prof. Dr. Joe D. Thompson, Dr. Peter Thalmeier and Dr. Christoph Geibel.

The work in the high-pressure group was always pleasant. The interesting scientific discussions and the useful sharing of experiences in how to solve technical problems made our group meetings valuable. I thank to all present and former members of this group.

I would like to thank Robert Borth and Christoph Klausnitzer for their technical assistance and permanent help in solving different problems.

I would like to acknowledge the administrative staff of our institute. I am especially thankful to the members of the guest department for their help and kindness. I acknowledge the support of our workshop as well.

I would like to thank to my colleagues, Dr. Corneliu Miclea and Dr. Huiqiu Yuan for the pleasant time I have had sharing the office with them. I especially would like to thank to Dr. Corneliu Miclea for reading through the thesis.

I would like to thank to my colleagues and friends which have contributed to a pleasant period in Dresden, especially to my former colleague Dr. Stefan Mederle for being a nice colleague and a good friend over these years. Many people have helped

in making enjoyable my time in the last years. Chatting with Dr. Gabriel Dionicio, Dr. Corneliu Miclea, Dr. Takeshi Nakanishi, Monica Macovei, Dr. Micha Deppe, Dr. Michael Nicklas, Hirale S. Jeevan, Dr. Julia Ferstl, Dr. Adriana Sanchez was always funny and relaxing.

I owe my deepest thanks to my parents and my family. My friends from home, though they have been far from me in this period, they have always supported me.

I apologize if I forgot to mention someone. To all who have helped in any way in making this thesis possible, thank you very much.

The financial support from the Max Planck Society and DFG (SFB463) is acknowledged.

Author's declaration

I declare that the work described in this dissertation was carried out in accordance with the regulations of the Dresden University of Technology. No part of this work has been submitted previously for a degree or other qualification at this or any other university. The research reported herein is original, except where specific reference is acknowledged to the work of others. All the research was carried out under the supervision of Prof. Dr. Frank Steglich at the Max Planck Institute for Chemical Physics of Solids.

Edit Lengyel
Dresden, Germany
June 6th, 2007



Versicherung

Hiermit versichere ich, dass ich die vorliegende Arbeit ohne unzulässige Hilfe Dritter und ohne Benutzung anderer als der angegebenen Hilfsmittel angefertigt habe; die aus fremden Quellen direkt oder indirekt übernommenen Gedanken sind als solche kenntlich gemacht. Die Arbeit wurde bisher weder im Inland noch im Ausland in gleicher oder ähnlicher Form einer anderen Prüfungsbehörde vorgelegt.

Die vorliegende Dissertation wurde unter der Betreuung von Prof. Dr. Frank Steglich am Max-Planck-Institut für Chemische Physik fester Stoffe in Dresden angefertigt. Ich erkenne die Promotionsordnung an.

Edit Lengyel
Dresden, Deutschland
6. Juni 2007

